Quantifying Isothermal Solidification Kinetics during Transient Liquid Phase Bonding using Differential Scanning Calorimetry

by

Michael Lawrence Kuntz

A thesis
presented to the University of Waterloo
in fulfillment of the
thesis requirements for the degree of
Doctor of Philosophy
In
Mechanical Engineering

Waterloo, Ontario, Canada, 2006

© Michael Lawrence Kuntz 2006

I hereby declare that I am the sole author of this thesis. This is a true copy of the thesis, including any required final revisions, as accepted by my examiners.

I understand that my thesis may be made electronically available to the public.

Abstract

The problem of inaccurate measurement techniques for quantifying isothermal solidification kinetics during transient liquid phase (TLP) bonding in binary and ternary systems; and resulting uncertainty in the accuracy of analytical and numerical models has been addressed by the development of a new technique using differential scanning calorimetry (DSC). This has enabled characterization of the process kinetics in binary and ternary solid/liquid diffusion couples resulting in advancement of the fundamental theoretical understanding of the mechanics of isothermal solidification.

The progress of isothermal solidification was determined by measuring the fraction of liquid remaining after an isothermal hold period of varying length. A 'TLP half sample', or a solid/liquid diffusion couple was setup in the sample crucible of a DSC enabling measurement of the heat flow relative to a reference crucible containing a mass of base metal. A comparison of the endotherm from melting of an interlayer with the exotherm from solidification of the residual liquid gives the fraction of liquid remaining. The Ag-Cu and Ag-Au-Cu systems were employed in this study. Metallurgical techniques were used to compliment the DSC results.

The effects of sample geometry on the DSC trace have been characterized. The initial interlayer composition, the heating rate, the reference crucible contents, and the base metal coating must be considered in development of the experimental parameters. Furthermore, the effects of heat conduction into the base metal, baseline shift across the initial melting endotherm, and the exclusion of primary solidification upon cooling combine to systematically reduce the measured fraction of liquid remaining. These effects have been quantified using a modified temperature program, and corrected using a universal factor. A comparison of the experimental results with the predictions of various analytical solutions for isothermal solidification reveals that the moving interface solution can accurately predict the interface kinetics given accurate diffusion data.

The DSC method has been used to quantify the process kinetics of isothermal solidification in a ternary alloy system, with results compared to a finite difference model for interface motion. The DSC results show a linear relationship between the interface position and the square root of the isothermal hold time. While the numerical simulations do not agree well with the experimental interface kinetics due to a lack of accurate thermodynamic data, the model does help develop an understanding of the isothermal solidification mechanics. Compositional shift at the solid/liquid interface has been measured experimentally and compared with predictions. The results show that the direction of tie-line shift can be predicted using numerical techniques. Furthermore, tie-line shift has been observed in the DSC results.

This study has shown that DSC is an accurate and valuable tool in the development of parameters for processes employing isothermal solidification, such as TLP bonding.

Acknowledgements

I would like to sincerely thank my supervisors, Dr. Norman Zhou and Dr. Stephen Corbin. I appreciate the freedom they have given me to pursue my academic interests, as well as the guidance and insight that they provided when needed. I am grateful for the opportunity to have worked with them during the period of this study.

I would also like to thank my friends who have supported me throughout the years. I have learned so much about myself from each and every one of you. Special thanks to the many students and co-workers with whom I have shared so much, especially: Andy Punkari, Ryan Clemmer, Youngae Kwon, Troy D'Hondt, Laura Mammoliti, and Scott Finlayson. You have made this an enjoyable journey.

This work has been supported by Materials and Manufacturing Ontario (MMO), an Ontario Centre of Excellence (OCE), and the Natural Sciences and Engineering Research Council of Canada (NSERC). Other financial support from the University of Waterloo is gratefully acknowledged.

For my wife Julie, who was there for me every step of the way.

And for my parents, who have made everything possible through their everlasting support.

...How can a person know if he does not learn? How can he learn without teachers? O stupid and idle gossip of the ignorant! An enemy of nature is the one who despises knowledge: the longing for knowledge lies within human nature...The danger lies not in knowledge, but in the abuse of knowledge.

St. John of Capistrano 1386-1456

Letter on Study to the Friars of the Observance

Table of Contents

List of Tables

List of Figures

1. Introduction

1.1. TLP Bonding Background

Transient liquid phase (TLP) bonding [1] is a material joining process that produces a high quality bond at the interface of the parts to be joined [2]. TLP bonding, which is also known as diffusion brazing [3], is a brazing or soldering variation; and, as such it depends on the formation of a liquid at the faying surfaces by an interlayer that melts at a temperature lower than that of the substrate. TLP bonding, however, is distinguished from other brazing processes by the re-solidification of this liquid at a constant temperature. The interlayer is rich in a melting point depressant and upon heating through the eutectic temperature; the interlayer will either melt or react with the base metal to form a liquid. During an isothermal hold above the melting temperature of the interlayer, the melting point depressant (solute) is removed from the liquid phase through extensive long range diffusion into the base metal (solvent). The resulting solid/liquid interfacial motion via epitaxial growth of the substrate is termed "isothermal solidification" [2]. A homogeneous bond between the substrates is formed when isothermal solidification is complete, which is when the two solid/liquid interfaces meet at the joint centerline.

Upon completion of the TLP bonding process, the re-melt temperature of the bond is similar to the base metal. This melting point shift differentiates TLP bonding from high temperature brazing and makes it attractive for applications requiring elevated service temperatures. In traditional brazing processes solidification is induced by cooling, resulting in a heterogeneous bond. Isothermal solidification proceeds via epitaxial growth of the substrate, and, when followed with an appropriate homogenization will result in a bond microstructure similar to the bulk material [2].

Since the microstructure and hence mechanical properties of the bond tend to match the base material, TLP bonding shows great potential for joining materials that are not easily joined by conventional fusion welding processes [1,2,4,5,6,7,8]. TLP bonding has been considered for the manufacturing and repair of aerospace and land based turbine blades [5,6,9], and other applications requiring high joint strength at elevated temperatures. Additionally, TLP bonding has been suggested for the joining of medical implant components and microelectronic packaging [10]. The isothermal solidification mechanism makes TLP bonding attractive for joining MMC (metal matrix composite) [11,12], SMA (shape memory alloy) [13], single crystal [4,9] and intermetallic materials [14].

1.2. Problem

There is significant potential for the application of the TLP bonding process, especially in circumstances that require high quality joints in materials with low weldability. There are, however, several feasibility issues related to the practical application of TLP bonding technology. First, TLP bonding is a diffusion controlled process and as a result, the process time is usually on the order of hours. The optimized process schedule is one that reduces the overall process time for an acceptable level of quality. Second, development of process parameters for TLP bonding is a tedious task. Typically, trial and error techniques require the metallurgical preparation and examination of joint cross sections. The width of the liquid after the isothermal hold period is then estimated using manual measurements of the solidified eutectic phase; however, the results are often erroneous. Third, analytical models that predict the time required for the completion of isothermal solidification have been developed; however, they are considered inaccurate, especially in polycrystalline samples and complicated alloy systems where one or more phases can form at the interface. Finally, model accuracy can be increased with the use of numerical models. These models are very complicated and require skill that is often beyond the reach of those who would use them to develop TLP bonding schedules. A reliable method for quantifying isothermal solidification kinetics is required.

A method using differential scanning calorimetry (DSC) to measure the process kinetics of isothermal solidification during the TLP sintering process in binary alloy systems has been developed by Corbin and Lucier [15]. TLP sintering is similar to TLP bonding in the mechanism of isothermal solidification of a melting point depressant rich liquid phase. In the sintering process, the liquid completely surrounds spherical particles whereas in the case of TLP bonding, solidification occurs on a planar interface. Nevertheless, it is expected that the DSC method can be applied to TLP bonding; however, the geometrical differences between TLP bonding and TLP sintering are expected to significantly affect the DSC results. These effects need to be characterized before DSC can be used to accurately quantify the solid/liquid interface kinetics during isothermal solidification.

The majority of the efforts devoted to predicting and measuring the process kinetics of isothermal solidification have been developed for binary systems, i.e. one solute. In most real applications, the order of the material system is at least ternary or higher. The effect of alloying with an additional solute element is to complicate the isothermal solidification process and has been the subject of many recent studies. The ternary case lends itself to numerical modeling techniques, and several authors have presented sophisticated numerical models to predict the solid/liquid interface kinetics; however, very little empirical evidence has been provided to support assumptions on which these models are based.

The predicted interface kinetics generated from numerical models deviate significantly from the limited amount of experimental data that is available (§ 2.5.3). The lack of agreement with

measured results is not surprising since reliable phase diagram information and diffusion data is rarely available for ternary systems. Since the accuracy of the model output is dependent upon the availability of accurate data, an accurate empirical approach for developing process parameters is still required.

1.3. Objectives

1. The isothermal solidification stage during TLP bonding is analogous to a bi-phase diffusion couple. A preliminary objective is to develop an experimental approach for measuring the interface kinetics in a solid/liquid diffusion couple using the DSC method. The effects of the diffusion couple geometry are expected to manifest error in the DSC results. In order to accurately characterize the interface kinetics, the root cause of these effects must be thoroughly investigated and quantified.
2. Compare the experimentally measured interface kinetics in a solid/liquid diffusion couple using the DSC method with the predictions generated from various analytical models to validate the DSC method.
3. Apply the DSC method to isothermal solidification in ternary alloy systems. Validate the experimental approach and use the measured kinetics of interface motion to evaluate the science that the models for isothermal solidification in ternary alloy systems are based on.
4. Use the accurate experimental data for interface kinetics in ternary alloy systems along with simple models for interface motion to predict the direction of tie line shift at the solid/liquid interface during the progression of isothermal solidification and compare the prediction with experimentally measured results.

1.4. Justification, Criteria and Constraints

A reliable method for accurately characterizing the interface kinetics during isothermal solidification has the potential to reduce process parameter development time for the application of TLP bonding. The value of accurate empirical data is amplified when accurate predictions cannot be generated using available models, e.g. when reliable diffusion or phase boundary data is not available, and in complicated cases such as higher order systems or when additional phases form at the solid/liquid interface. The expected impact of efficient process parameter development is streamlined process optimization and increased adoption of the TLP bonding process in suitable applications. Similar results can be expected in other material processing applications that employ bi-phase diffusion controlled interactions.

The materials selected for the experimental work in this study must be suitable for isothermal solidification at temperatures within reason according to the limits of the DSC

equipment. The barriers to interfacial interactions between the liquid and solid phases, such as impurities and oxide layers must be minimized. The material system selected must satisfy this criteria; furthermore, the interlayer composition and thickness must result in interface kinetics that are sufficiently fast to be measured with good resolution within a reasonable time frame.

This study is constrained to the binary and ternary cases in order to limit the complexity of the resulting analysis. Furthermore, the formation of intermediate phases at the solid/liquid interface (e.g. intermetallics) will not be considered.

2. Literature Review

2.1. Transient Liquid Phase (TLP) Bonding

2.1.1. Historical Development

What is perhaps the most comprehensive description of the evolutionary development of diffusion controlled joining processes in the presence of a liquid is given in two parts by MacDonald and Eagar [7,16]. Historical references show that the use of a transient interlayer can be traced back to ancient times. In fact, the technology has been dated to 2500 BC in the ornamentation on King Tutankhamen's gold dagger [17]. Centuries later, a hallmark of Etruscan art is the joining of decorative gold beads to gold articles using the process known as 'granulation'. Reference to this process is made in the eighth century *Mappae Clavicula* [18] or the *Little Key to Medieval Arts*. Recipes for granulation are given in the twelfth century *De Re Deversis Artibus* [19] by Theophilus. Benvenuto Cellini [20], a Renaissance Italian goldsmith describes granulation in his notebooks as the joining of small gold balls on to an article of gold using a copper oxide paint interlayer with tallow or glue to hold the balls in place before joining and act as a flux. A reducing flame is used to heat the piece allowing the copper to form a eutectic with the gold. The joint is homogenized in the flame resulting in an invisible diffusion bonded joint (i.e. no solder fillet is visible at the interface). With the advent of modern technologies, the painstaking granulation process was abandoned and the techniques were fundamentally lost.

The modern reinvention of the granulation process is credited to Littledale by the granting of a patent [21]; however, it is accepted that Wilm and Treskow synchronistically discovered a practical means of achieving granulation based on theory proposed by Wagner in 1913 [22]. In the modern iteration of this technique, the parts to be joined were cemented together with a mixture of oxide, fish glue, and water. The fish glue is a source of carbon, which serves to reduce the oxide at elevated temperatures. The metallic component then forms a liquid interlayer in-situ through reaction with the base material.

As MacDonald and Eagar [16] point out, the first application of the transient liquid interlayer process was based on an isomorphous azeotropic system; however, modern applications utilize binary eutectic alloy systems. Recent development efforts have moved away from decorative jewellery and been focused on joining of high temperature materials such as titanium and nickel base superalloys [7]. The direction of future work will include small scale joining applications such as microelectronics and medical implant devices.

Gale and Butts [23] point out that the naming convention for the process known as TLP bonding is not universally accepted. In fact, the process has been referred to by a number of titles. The earliest account of the modern industrial application of TLP bonding technology is given by Lynch et al. who called the process they used to join titanium using a nickel-copper interlayer 'eutectic brazing' [24]. Owczarski et al. joined dissimilar metals Zircaloy 2 to 304 stainless steel without an interlayer [25]. A liquid interlayer was formed in-situ and the process was termed 'eutectic bonding'. The 'solid-liquid interdiffusion bonding' (SLID) process was introduced by Bernstein and Bartholomew [10,26], who produced experimental bonds on electrical components using the ternary Ag-In-Sn system. In this variation, isothermal solidification was not completed, however, successive bonds were produced at decreasing temperatures and the high temperature exposure helped homogenize the joint.

The 1970's was a decade of TLP bonding process development in the aerospace industry. Hoppin and Berry [27] of General Electric Aircraft Engine Group used 'activated diffusion bonding' (ADB) for joining superalloys (including René 80) using a Ni-based eutectic interlayer. Wu [28] describes the Nor-Ti-Bond process developed by Wells and Mikus [29] of Northrop in which resistance heating is used to melt an electrolytically deposited copper interlayer to join titanium structural shapes followed by a heat treatment. Niemann and Garrett at MacDonnell Douglas developed 'eutectic bonding' for joining boron-aluminum composites with a copper interlayer [30]. In 1974 the term 'transient liquid phase' (TLP) bonding was coined and copyrighted by a group at Pratt and Whitney after a process patented by Owczarski et al. [31]. Using the TLP bonding process, Duvall et al. [32] joined Udimet 700 using a Ni-Co interlayer and later found that near base metal properties could be achieved in a number of superalloys [1]. TLP bonding is the most widely recognized name for the process described here.

There are yet other variants of the TLP bonding process which are known by their individual names. 'Liquid interface diffusion' (LID) was developed to bond honeycomb sandwich structures using Cu-Ni interlayers [33]. 'Transient insert metal bonding' (TILM) was developed by Nakao et al. [34,35] and was later modified to include powder at the interface [36]; this process variant is also known as wide-gap TLP bonding. New technologies are also evolving, such as 'temperature gradient transient liquid phase' (TG-TLP) bonding [37,38], where a temperature gradient is imposed across the interface to decrease the length of the isothermal solidification stage.

The nomenclature of this process and all of its variants is a confusing issue. The most widely recognized name of 'TLP bonding' is itself controversial because of the copyright issue surrounding it. The American Welding Society (AWS) has attempted to resolve the issue by applying the moniker 'diffusion brazing' (DFB, or DB) [3].

2.1.2. Process Description

The TLP bonding process has been described in detail by a number of sources. Duvall et al. [1] describe 5 steps in the mechanism of bond formation by isothermal solidification. The first step is heating to the bonding temperature and subsequent melting of the interlayer. Step 2 is defined as the dissolution of the base metal by the liquid. Step 3 is isothermal solidification, which is completed at step 4. The final step is homogenization of the excessive solute at the bond line. Zhou et al. [2] condensed the description given by Duvall et al. to 3 discrete stages: base metal dissolution, isothermal solidification, and homogenization. Tuah-Poku et al. [39] expanded the first stage (base metal dissolution) into two stages: dissolution of the interlayer, and homogenization of the liquid (by additional base metal dissolution).

MacDonald and Eagar [16] added an initial stage (stage 0) to account for the heating time from room temperature to just before the onset of liquation in the interlayer. This is in response to the loss of solute during heating of the joint reported by Niemann and Garrett [30] during TLP bonding of Al-B using an electroplated Cu interlayer. They found that when heating from room temperature is very slow, insufficient liquid forms at the interface due to diffusion of solute into the base metal. The four subsequent stages as identified by MacDonald and Eagar [16] are: dissolution, widening, isothermal solidification, and homogenization.

Zhou et al. [2] reclassified TLP bonding into four discrete stages. Stage 1 is the heating stage (stage 0 from MacDonald and Eagar [16]). Stages 1 and 2 from MacDonald and Eagar [16] were combined by Zhou et al. [2] into stage 2: dissolution and widening, which is further subdivided into stage 2-I (heating from melting point to bonding temperature) and stage 2-II (isothermal dissolution at the bonding temperature). Stage 3: isothermal solidification, and stage 4: homogenization follows the convention of the previous authors.

In this study, the classification system according to Zhou et al. [2] is followed. The initial conditions (i.e. joint at room temperature, before heating begins) is referred to as stage 0.

2.1.3. Initial Conditions

Initially, the base metal substrates are brought into intimate contact with a thin interlayer placed between the faying surfaces. The joint is assembled at room temperature. The interlayer contains a melting point depressant (MPD) solute and is usually added in the form of a thin foil [23]. The MPD can also be added in a powder form [6,40,41] or as a coating (sputter or thermal spray) [42]. If the simple eutectic shown in Figure 2-1 is considered, it can be shown that the bulk composition of the interlayer can be tailored to melt at the eutectic temperature, or can shift in-situ, through reaction with the base metal to form liquid. MacDonald and Eagar have catalogued the differences between the two process variants: the type-I process, which employs a pure interlayer; and the type-II process, which employs an interlayer composition near the liquidus composition at the bonding temperature [7]. In

practice, any composition between these two boundaries may be used in the interlayer, however, the type-II interlayer is most commonly used. This facilitates a reduction of the overall process time by reducing the solute to be diffused from the interface.

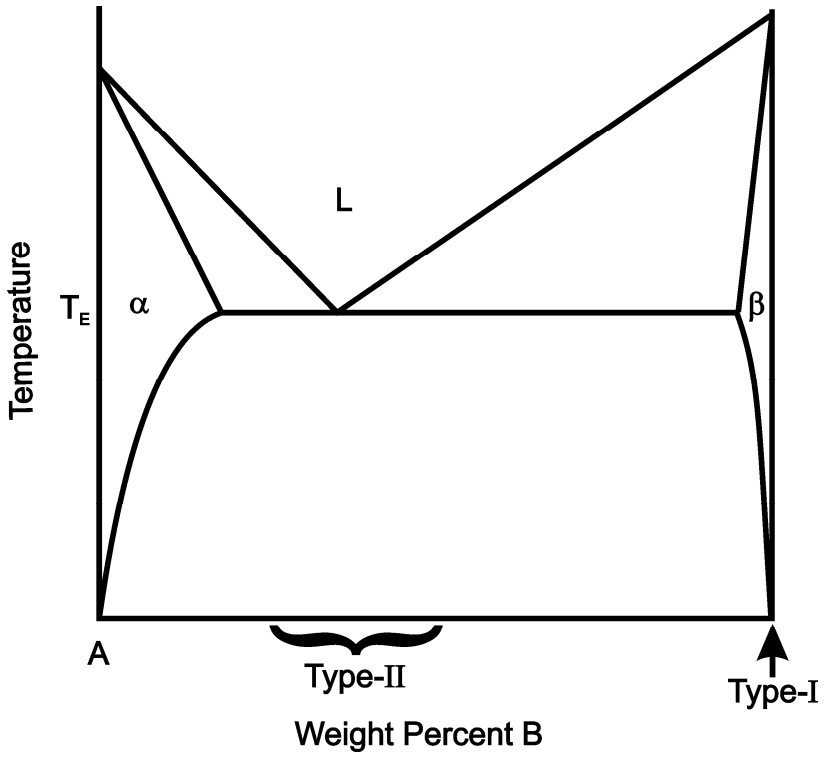

Figure 2-1: Binary phase diagram schematic showing the composition of a Type-I (pure) interlayer, and the hypothetical compositional range for a Type-II interlayer as described by MacDonald and Eagar [7].

It is important to note that a eutectic system is not requisite of isothermal solidification; in fact, isothermal solidification will occur in any system with a base metal that will form a low melting point phase and has solubility of the MPD solute.

The initial thickness of the interlayer also has a profound impact on the process kinetics throughout the stages of TLP bonding. Thus, the two major concerns of the interlayer are the initial thickness or width, W_o; and the initial composition, C_F, given as the compositional fraction of B, where the element B is the MPD solute. Point 0 in Figure 2-2 shows the initial compositional profile of solute across the TLP bond joint assembly in the special type-II case of a eutectic interlayer. The type-I case of a pure interlayer will be discussed in § 2.1.6 below.

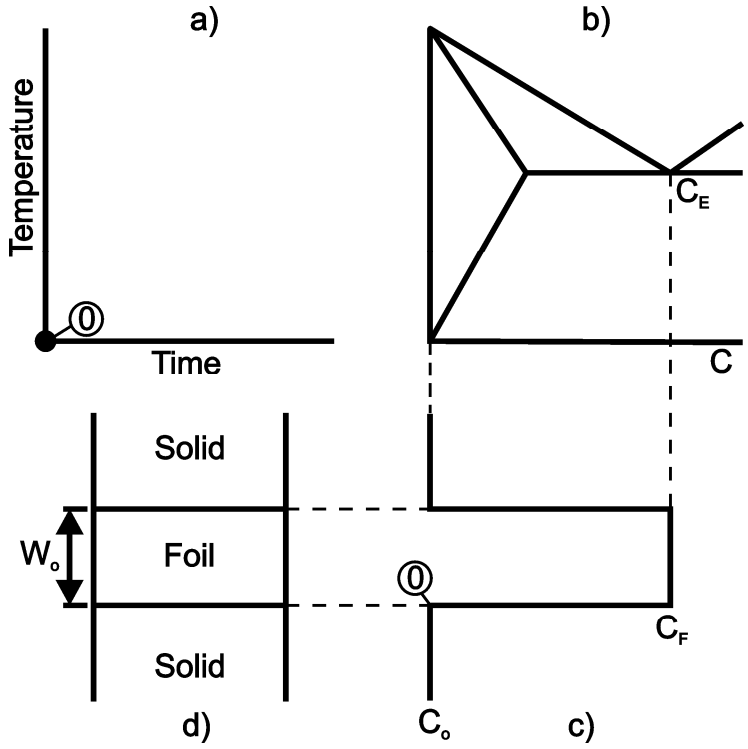

Figure 2-2: TLP bonding process initial conditions a) temperature profile, b) phase diagram schematic, c) composition profile across the joint, and d) joint schematic.

The TLP Bonding process has been broken down into four discrete stages [2,11,16,39]. These four stages are: 1. heating; 2. dissolution and widening; 3. isothermal solidification; and 4. homogenization. Each of these stages has been examined in detail. In the ensuing description, the focus is on the special case of a eutectic interlayer since this is the easiest treatment, however, the off-eutectic variant will also be discussed.

2.1.4. Heating Stage

During the heating stage, the entire assembly is heated, usually in a furnace, from room temperature to just below the eutectic temperature, shown as point 1 in Figure 2-3 a). An inert atmosphere or vacuum is usually used to protect the joint from oxidation at elevated temperatures. As the assembly is heated, some solid state diffusion between the interlayer and base material occurs. The magnitude of the interaction depends on a number of factors including surface condition (i.e. roughness, cleanliness, etc.), and pressure exerted normal to the interface (high pressure will help to flatten the asperities and improve surface contact). The exchange results in a typical diffusion couple compositional profile as shown in Figure 2-3 c). The extent of diffusion is expected to be small in most cases; however, the amount of mass

transferred during the heating stage will also depend upon the eutectic temperature and the heating rate as well as the diffusivities of the elements [2].

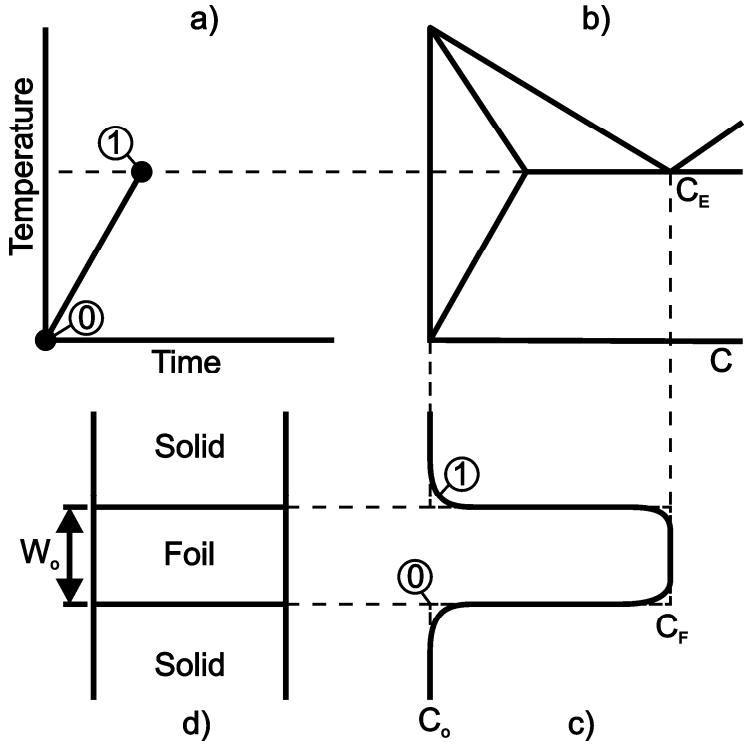

Figure 2-3: TLP bonding process heating stage a) temperature profile, b) phase diagram schematic, c) composition profile across the joint, and d) joint schematic.

A longer heating stage will result in more diffusion of the solute (MPD) into the base material. If the heating stage is too long because the heating rate is too low, the maximum composition of solute in the interlayer may dip below the solidus composition at the bonding temperature (T_b) and no liquid will form upon further heating [11]. This problem will be most severe with very thin interlayers and low solute concentrations. Li et al. [43] found that decreasing the heating rate from 5 to 1 K/s resulted in a need to increase the interlayer thickness from 0.6 to 2 μm to achieve acceptable bonds in alumina metal matrix composites using a copper interlayer.

There is a case where the bulk composition of the interlayer is initially below the liquidus composition, $C_{L\alpha}$, at T_b. This will result in incomplete melting of the interlayer with a bulk composition in the two-phase region. Only a limited discussion of this case has been found in the literature [43], however, it is expected that the result will be similar to the wide gap TLP bonding variation that will be discussed further below. Clearly, it is important to control the heating rate during the heating stage of TLP bonding.

2.1.5. Dissolution and Widening Stage

As the assembly is heated past the eutectic temperature, the eutectic interlayer will melt and wet the base metal at the faying surface. Reference to the binary phase diagram schematic in Figure 2-4 b) shows that the composition of the liquid just above point 1 will be eutectic. Conversely, the composition of the solid at the solid/liquid interface will be at the limit of solid solubility. Additional heating of the assembly above the eutectic temperature will cause widening of the liquid zone. Figure 2-4 shows that with an increase in temperature above point 1, the equilibrium composition of both the liquid and the solid at the interface will track along the solidus and liquidus phase boundaries, respectively. To maintain equilibrium at the solid/liquid interface, the base metal is dissolved by the liquid resulting in a widening of the liquid zone due to conservation of solute mass. Since diffusion in the liquid phase is relatively fast (orders of magnitude higher than in the solid state), the MPD solute is swiftly transported across the liquid width to the solid/liquid interface where dissolution of the base metal occurs rapidly [44]. The liquid width is at a maximum (W_{max}) at the peak, or bonding temperature, where the liquid composition is at $C_{L\alpha}$ as shown in Figure 2-4 b). It is important to note, however, that the time at which the maximum liquid width is reached does not necessarily coincide with the time at which the bonding temperature is reached. The kinetics of dissolution depend on a number of factors including solute diffusivity and heating rate such that widening of the liquid will continue some time after the bonding temperature is reached until a steady state is achieved following the equilibrium phase diagram schematic as shown in Figure 2-4 [45].

2.1.6. Type-I Interlayer

In the case of a type-I (pure) interlayer, eutectic melting will initiate at the base metal/interlayer interface where, through diffusion, there will be a thin band that is at the eutectic composition [7]. The liquid will grow from each interface through dissolution of both the interlayer and the base metal; diffusional transport of solute from the interlayer to the base metal is required for this to occur. The resulting diffusion couple is shown in Figure 2-5. Dissolution is complete when the entire interlayer has been consumed by the liquid phase.

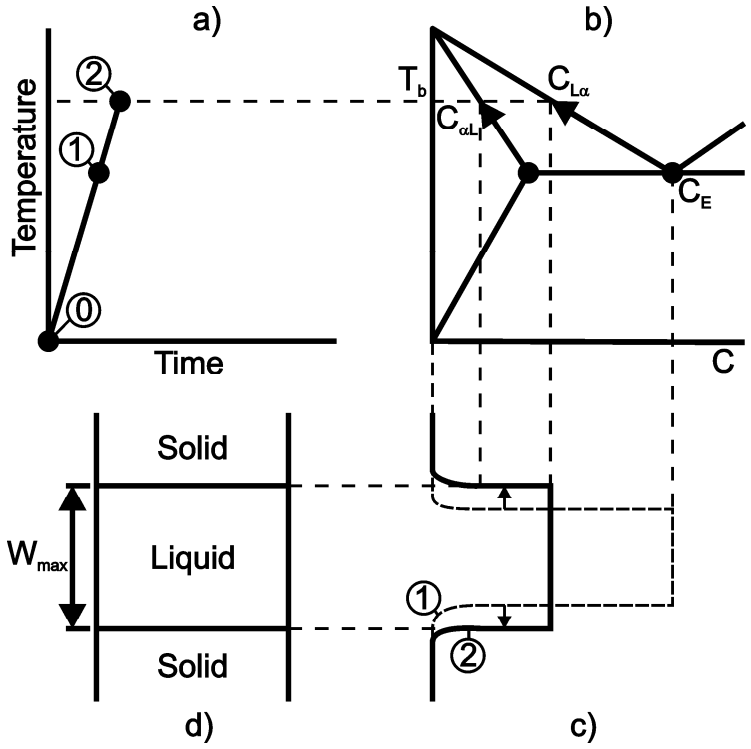

Figure 2-4: TLP bonding process dissolution and widening stage a) temperature profile, b) phase diagram schematic, c) composition profile across the joint, and d) joint schematic.

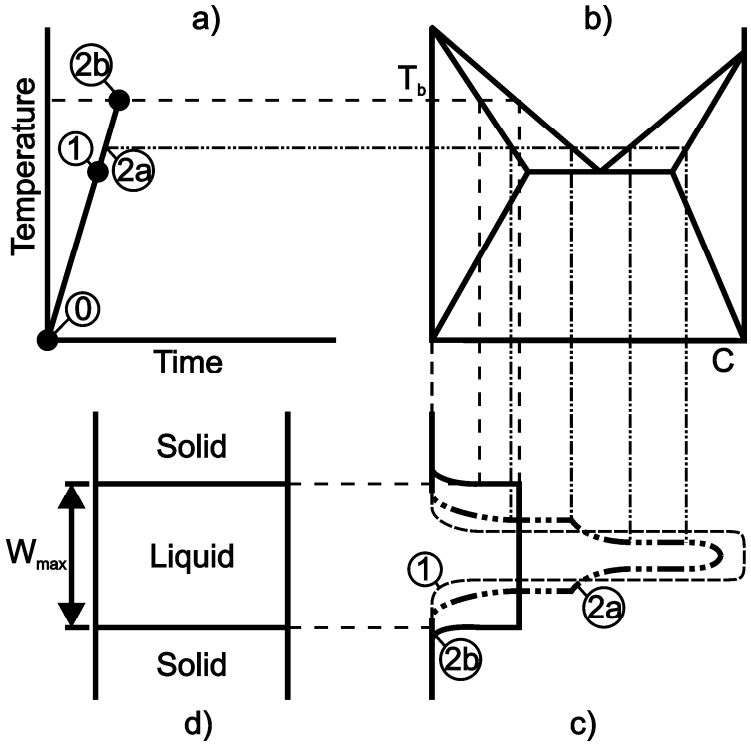

Figure 2-5: Variation of the TLP bonding process for a type-I pure interlayer.

Since the mechanism of dissolution is diffusion, the length of time required will depend not only on the solute diffusivity in the liquid, but also on the initial width (W_o) and composition (C_F) of the interlayer: a thick, type-I interlayer will require the longest time; and conversely the dissolution of a eutectic interlayer will be instantaneous. Additional heating above the eutectic temperature results in widening of the liquid as described in § 2.1.5 above. After the dissolution and widening stage, the isothermal solidification and homogenization of the joint proceeds exactly as described. An off-eutectic type-II (e.g. hypoeutectic) interlayer will follow a combination of the two cases already described. Partial melting of the interlayer will occur upon heating to the eutectic temperature, followed by dissolution of the remaining solid in the interlayer by long range diffusion of the solute and base metal dissolution. As before, isothermal solidification proceeds in exactly the same way as the eutectic case.

Tuah-Poku et al. [39] attempted to observe the process of initial dissolution (i.e. stage 2-I) of the interlayer; however, the process was estimated to be completed on the order of a fraction of a second, far too rapid for successful measurement. Using a 80 μm thick pure Cu foil for TLP bonding of pure Ag, they found that the widening of the liquid zone (i.e. stage 2-II) required times on the order of minutes. For joints heated to 1093 K, the measured liquid width increased from 79 μm to 420 μm after 20 minutes before starting to shrink (due to isothermal solidification). Clearly, under some circumstances the widening stage can be significant in terms of process time.

2.1.7. Isothermal Solidification Stage

After the dissolution and widening stage, an isothermal hold period ensues during which diffusion of the MPD solute across the sold/liquid interface into the base material occurs. This diffusion process is akin to the bi-phase diffusion couple. To maintain equilibrium on the phase diagram at a fixed temperature, the liquid composition at the interface is constant at $C_{L\alpha}$ [2]. Likewise, the composition of the solid at the interface is fixed at $C_{\alpha L}$. Furthermore, it is suggested in the literature that the composition of the liquid can be assumed uniform across the entire liquid width [44]. Since diffusion in the liquid phase is orders of magnitude faster than diffusion in the solid phase and the endpoints of the liquid phase are fixed and equal, this is considered an accurate assumption. The direction and rate of interfacial motion must satisfy a mass balance at each solid/liquid interface such that each of the two solid/liquid interfaces move toward the joint centreline. This interfacial motion is shown schematically is Figure 2-6 c). The mechanism of advancing interface motion is epitaxial growth of the solid phase into the liquid. This process has been coined “isothermal solidification”. The isothermal solidification stage is complete when the two interfaces meet at the centreline of the joint and there is no liquid remaining. The rate of interfacial motion will depend on the diffusivity of the solute in the base material, the miscibility gap between $C_{\alpha L}$ and $C_{L\alpha}$, and the concentration

gradient of the solute in the base material. The length of time required for completion of the isothermal solidification stage will also be greatly dependent upon the initial width of the liquid zone.

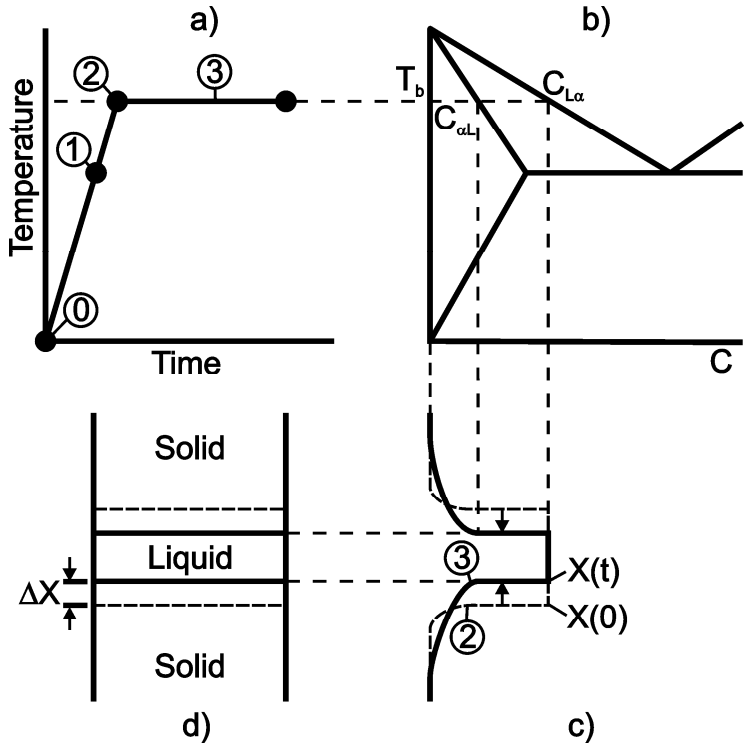

Figure 2-6: TLP bonding process isothermal solidification stage a) temperature profile, b) phase diagram schematic, c) composition profile across the joint, and d) joint schematic.

2.1.8. Homogenization Stage

When the isothermal solidification stage is complete, there will be a peak of solute at the solidus composition ($C_{\alpha L}$) remaining at the joint centreline, shown by the profile in Figure 2-7 c). The assembly is held at an elevated temperature so the magnitude of the solute peak is gradually decreased over time through diffusion. This homogenization of the joint continues until an acceptable level of solute remains. What level is acceptable depends on the material and the application; however, it should be below the concentration at which harmful phases will precipitate in the solid state during cooling. Precipitates may degrade the mechanical properties of the joint [23].

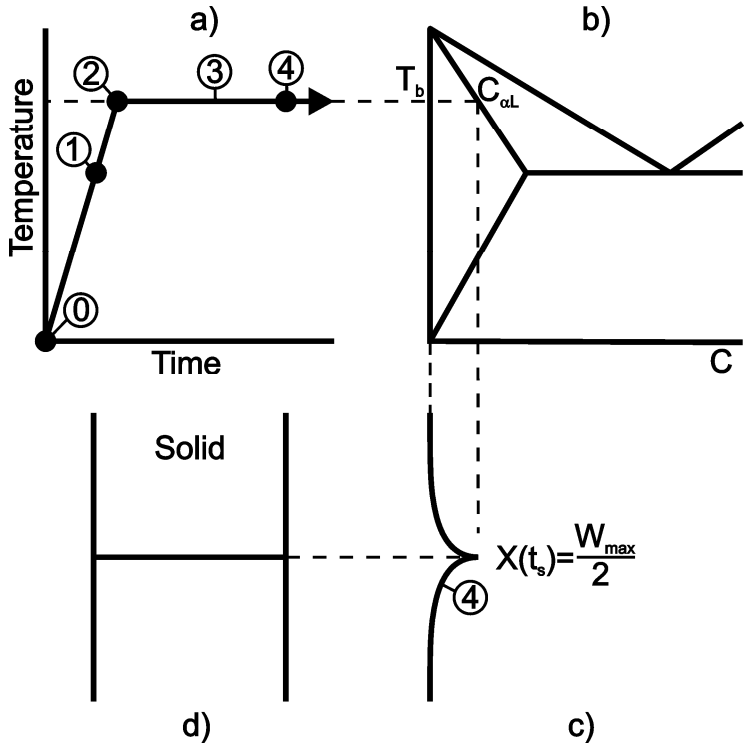

Figure 2-7: TLP bonding process isothermal solidification stage a) temperature profile, b) phase diagram schematic, c) composition profile across the joint, and d) joint schematic.

2.1.9. Critical Stages in TLP Bonding

The two most important stages in terms of joint quality are the isothermal solidification and the homogenization stages [2,23]; coincidently it is also these stages that require the longest time for completion. In systems with a low solubility limit the isothermal solidification stage becomes longer and is more important. It is essential that the stage is not terminated by cooling before all of the liquid has solidified or a cast microstructure and solute rejection will result in segregated phases, which can degrade mechanical properties. Conversely, in some systems with a high solubility limit, the homogenization stage requires longer time for completion and is considered more important. Premature termination of the homogenization stage can result in an inhomogeneous microstructure due to precipitation of additional phases that will adversely affect mechanical properties. Since the isothermal solidification and homogenization stages depend on diffusion of the solute in the solid base metal, they are orders of magnitude longer than the heating or dissolution stages. Thus, it is appropriate that most of the attention given to TLP bonding parameters focuses on the time required for completion of these stages.

2.1.10. Wide Gap TLP Bonding Variation

In some situations, the largest joint gap that can be tolerated is so great that the time required for isothermal solidification exceeds that which is feasible. To shorten the process time, a composite interlayer can be used [41]. The interlayer, usually in the form of a powder compact, contains the melting point depressant plus an additive that is designed not to melt at the bonding temperature. The higher melting point constituent does not melt entirely; however, it does participate in dissolution and is often similar in composition to the base material [23]. The function of the additive is first, to reduce the amount of liquid that is necessary to fill the joint gap; and second, to increase the interfacial area between the liquid and solid phases and effectively increase the diffusion rate [23]. This is shown schematically in Figure 2-8. Gale and Butts have shown that a proper composite ratio is essential; if excessive liquid is formed, the high melting point additive will be completely dissolved [23]. Conversely, if there is insufficient liquid to fill the gap, the joint will be excessively porous [23]. There is a plethora of work published on the metallurgical aspects of wide gap TLP bonding [23]; however, studies on the process kinetics have been somewhat limited to TLP sintering, which is a closely related process.

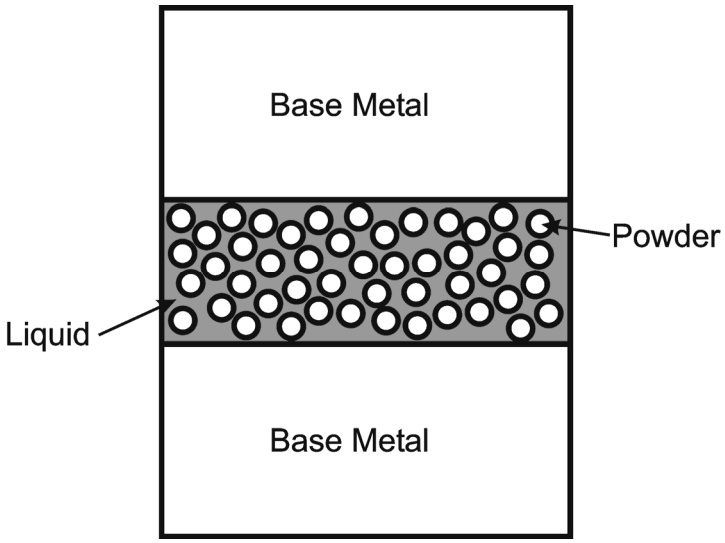

Figure 2-8: Wide gap TLP bonding schematic.

The case of a hypoeutectic type-II interlayer which is heated above the eutectic temperature but not to the liquidus temperature is expected to be similar to the wide gap TLP bonding variant. In this case, partial melting of the interlayer occurs; however, there is insufficient solute to dissolve the interlayer. Interfacial diffusion is not expected in increase since the unmelted solid component of the interlayer will be saturated with solute.

2.1.11. Temperature Gradient TLP Bonding Variation

A novel TLP bonding method for joining Al-based materials where a temperature gradient is imposed across the joint to increase the isothermal solidification kinetics was developed by Shirzadi and Wallach [46]. Since the equilibrium composition at the solid/liquid interfaces is temperature dependent, Shirzadi and Wallach propose that by simply imposing a temperature gradient across the liquid zone, a compositional gradient is induced in the liquid [37]. Since diffusion in the liquid is relatively fast, solute transport across the liquid width occurs rapidly. The solute diffuses from the high concentration (low temperature) interface to the low concentration (high temperature) interface. This results in solidification at the low temperature interface since removal of the solute atoms locally increases the equilibrium solidification temperature. Thus, the liquid zone migrates in the direction of increasing temperature leaving behind a solute build up at the solidus concentration [37]. By means of a mass balance, the solute that is removed from the liquid by solidification will result in a shrinking liquid and eventual isothermal solidification when the two interfaces come together. A schematic of the temperature gradient TLP bonding isothermal solidification mechanism is given in Figure 2-9.

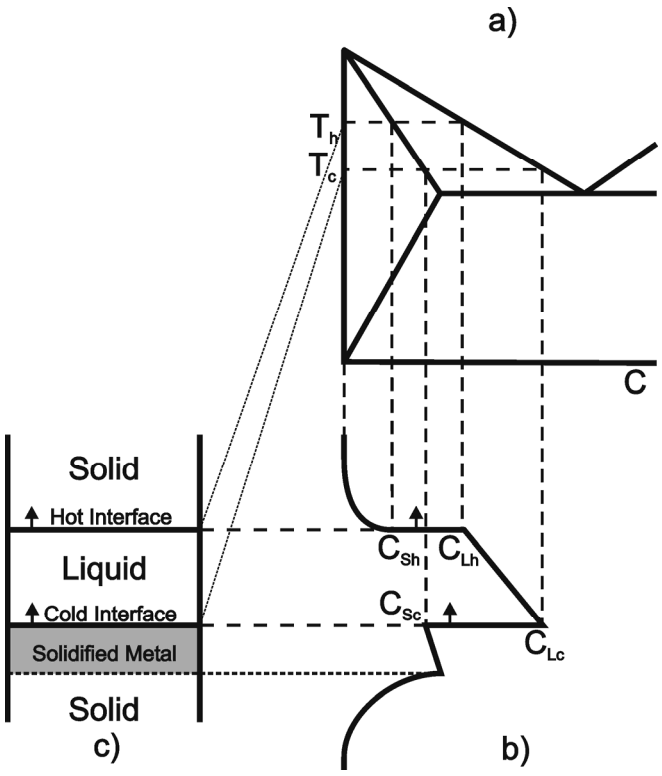

Figure 2-9: Temperature gradient TLP bonding schematic a) phase diagram, b) composition profile, c) bonding schematic.

Shirzadi and Wallach [37] found that bonds in Al-6082 with shear strength as high as that of the parent material are possible with a 1.5 μm sputter coated copper interlayer. The magnitude of the temperature gradient was found to have a profound impact on the joint microstructure [47]. The morphology changes from planar to sinusoidal and then to cellular and dendritic with increasing temperature gradient [37].

Assuming that the temperature gradient is uniform, and neglecting the contribution of solid state diffusion of the solute in the base metal, the mass balance at the cold interface is given by Equation 2-1 [48]:

$$\left(C_l - C_s\right)\cdot\frac{dX}{dt} = -D\cdot\frac{dC}{dX} \qquad \text{Equation 2-1}$$

Given that the temperature gradient $dT/dX = G$, and a linear variation of composition with temperature $dT/dC = m$, the solution of Equation 2-1 gives the position of the cold interface (Equation 2-2). Similarly, the position of the hot interface is given by

$$\left(\frac{G}{2m}\right)X^2 + C_{l0}X + \left(\frac{DG}{(1-k)m}\right)\cdot t = 0 \qquad \text{Equation 2-2}$$

$$\left(\frac{G}{2m}\right)X^2 + \left(C_{l0} - C_0\right) + \left(\frac{DG}{m}\right)\cdot t - \left(C_{l0} - C_0\right)W_o - \frac{G\cdot W_o^2}{2m} = 0 \qquad \text{Equation 2-3}$$

Where k is the partition coefficient (C_s/C_l), and C_{l0} is the initial liquidus composition at the cold interface and m is the slope of the liquidus line on the equilibrium phase diagram (assumed constant). Simultaneous solution of the interface positions gives the position of final solidification, X_b (Equation 2-4) and the time to solidification, t_b (Equation 2-5).

$$X_b = \frac{\left(C_l - C_{l0}k\right)m - \left[\left(-C_0 + C_{l0}k\right)^2 m^2 + W_0 Gk\left(W_0 G + 2C_{l0}m - 2C_0 m\right)^{1/2}\right]}{Gk} \qquad \text{Equation 2-4}$$

$$t_b = \frac{(k-1)}{2DG^2K^2}\cdot\left[\begin{array}{l} W_0^2G^2k + 2C_{l0}W_0Gkm - 2C_0W_0Gkm + 2C_0^2m^2 - 2C_{l0}C_0km^2 - \\ 2C_0m\left(\begin{array}{l} W_0^2G^2k + 2C_{l0}W_0Gkm - 2C_0W_0Gkm + \\ 2C_0^2m^2 - 2C_{l0}C_0km^2 + C_{l0}^2k^2m^2 \end{array}\right)^{1/2} \end{array}\right] \qquad \text{Equation 2-5}$$

Shirzadi and Wallach [48] simplified the above precise solution by solving the problem with a geometric mass balance. Furthermore, by assuming the liquid width is small compared to the base metal and specifying no solute initially in the base metal, the solution for X_b is reduced to Equation 2-6 and the solution for t_b is reduced to Equation 2-7.

$$X_b = \frac{W_0}{k} \qquad \text{Equation 2-6}$$

$$t_b = \frac{W_0(1-k)C_{10}m}{DGk} \qquad \text{Equation 2-7}$$

The significance of this work is how it could affect the process kinetics of traditional TLP bonding when a temperature gradient is induced across the joint unintentionally. The isothermal solidification time required in TG-TLP bonding is drastically lower than what is expected in traditional TLP bonding. An observation of apparent faster than expected experimental results could be due to the influence of temperature gradient, as opposed to other factors which will be discussed. Equally important to this work is the knowledge that temperature gradients have been found to exist in DSC sample cells.

2.2. Analytical Models

Both analytical and numerical models have been developed to simulate each of the four stages of the transient liquid phase bonding process. These models are useful because they develop an understanding of the effects of the various parameters on the process. In this study, modeling of the isothermal solidification stage is emphasized since it is the stage of interest; however, modeling work on the other stages is included to show the potential impact of process parameters on these stages and influence on the isothermal solidification kinetics.

2.2.1. Mathematics of Binary Diffusion

Since the TLP bonding process is diffusion controlled, the mathematics of diffusion can be applied to develop analytical models of the four discrete stages. Fick recognized that the equation of heat conduction developed by Fourier could be applied to quantify mass transfer by diffusion since both processes were based on the mechanism of random molecular motion [49]. Fick's first law gives the mass flux of the diffusing solute:

$$J = -D \cdot \nabla C \qquad \text{Equation 2-8}$$

Where J is the total mass flux; D is the diffusion coefficient, C is the concentration of the diffusing species (solute), and:

$$\nabla C = \frac{\partial C}{\partial x} + \frac{\partial C}{\partial y} + \frac{\partial C}{\partial z} \qquad \text{Equation 2-9}$$

If diffusion is one dimensional, Fick's first law is simplified to give:

$$J = -D \cdot \frac{\partial C}{\partial x} \qquad \text{Equation 2-10}$$

Where x is in the direction of mass transfer. Fick's second law describes the rate of concentration change in any control volume in the diffusion couple through the conservation of mass:

$$\frac{\partial C}{\partial t} = -\nabla \cdot J \qquad \text{Equation 2-11}$$

For a one-dimensional system with relatively small concentration differences, D can be assumed independent of concentration, position, and time [49]. Hence, the average diffusivity may be used resulting in a simplified form of Fick's second law:

$$\frac{\partial C}{\partial t} = D \cdot \frac{\partial^2 C}{\partial x^2} \qquad \text{Equation 2-12}$$

Equation 2-10 and Equation 2-12 form the foundation for the derivation of analytical models that describe the mass transfer in TLP bonding.

In the case of a bi-phase diffusion couple, such as a semi-infinite liquid in contact with a semi-infinite solid, the position of the solid/liquid interface, *X(t)*, will depend on a mass balance.

The mass balance at the solid/liquid interface as shown in Figure 2-10 is given by Equation 2-13, where C_L and C_S are the liquid and solid concentrations, respectively, at the solid/liquid interface; and, D_L and D_S are the solute diffusivities in the liquid and solid, respectively.

$$(C_L - C_S) \cdot \frac{d}{dt} X(t) = D_S \cdot \frac{\partial}{\partial x} C_S - D_L \cdot \frac{\partial}{\partial x} C_L \qquad \text{Equation 2-13}$$

Figure 2-10 shows a schematic of the migrating solid/liquid interface. The interface at a time, t, is shown by the solid line. After an isothermal solidification time, Δt, the new interface has shifted by ΔX as shown by the broken line. It is important to note that in the general case, the direction of interface motion depends on the terms in Equation 2-13.

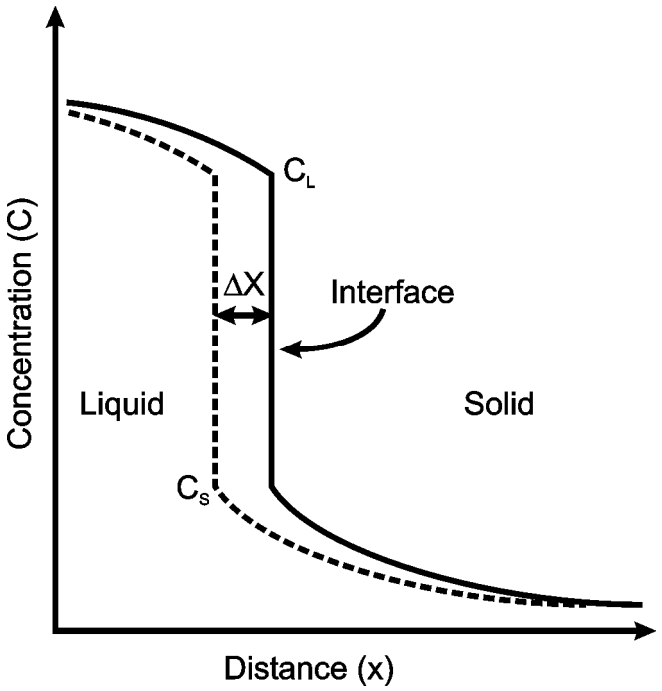

Figure 2-10: Solid/liquid moving interface schematic showing the migration of the interface by a distance ΔX.

2.2.2. Solution for the Heating Stage

An analytical solution for the interlayer width lost during the heating stage was first given by Niemann and Garrett [30]. In their work on TLP bonding of Al-B composites using an electroplated Cu interlayer, they followed Darken and Gurry's analysis [50] to calculate the loss using Equation 2-14.

$$x \cdot \rho_c = 1.1284 \cdot \rho_a (C_{\alpha s} - C_M)(D_s t)^{1/2} \qquad \text{Equation 2-14}$$

The thickness of Cu lost through diffusion is x, the density of the Cu is ρ_c, and the density of the substrate is ρ_a. The diffusivity in Equation 2-14 is assumed to be constant; however, in reality the diffusivity increases with temperature. MacDonald and Eagar [16] used the method of Shewmon [51] to find an effective diffusion coefficient, D_{eff}, to compensate for the temperature changes. This is given by Equation 2-15.

$$D_{eff} = \frac{\int_0^t D(t)dt}{t_o} \qquad \text{Equation 2-15}$$

Where, t_1 is the total time of the heating stage. MacDonald and Eagar claim that the use of Equation 2-15 results in a prediction of interlayer loss that is too high. A proposed reason for

the over prediction is that below 80% of the bonding temperature, the effects of diffusion on solute flux can be neglected. The temperature is given as a function of time starting from $0.8T_b$ as shown in Equation 2-16 where τ is the heating rate [52].

$$T = \tau t + 0.8T_b \qquad \text{Equation 2-16}$$

Substituting this back into Equation 2-15, MacDonald and Eagar used the standard Arrhenius form of the diffusion constant to give Equation 2-17.

$$\frac{D_{eff} T_b}{5\tau} = \frac{1}{\tau} \int_{0.8T_b}^{T_b} D_o \exp\left(\frac{-Q}{RT}\right) dt \qquad \text{Equation 2-17}$$

MacDonald and Eagar show that the analytical solution of Equation 2-17 is a slowly converging series function.

2.2.3. Solution for the Dissolution and Widening Stage

Zhou et al. [2] have shown that there are no suitable analytical solutions for the dynamic temperature portion of dissolution stage, i.e. stage 2-I, heating from melting point to bonding temperature. Since the concentration of the solute at the interfaces (i.e. $C_{\alpha L}$ and $C_{L\alpha}$ or $C_{\beta L}$ and $C_{L\beta}$) varies with temperature, this solution would be very difficult. If it assumed however, that the time to heat to the bonding temperature (T_b) is infinitesimally small, or th,at dissolution occurs only after T_b has been reached, then analytical models can be proposed. Both MacDonald and Eagar [16] and Zhou et al. [2] discuss these models which describe the motion of the solid/liquid interface(s) during stage 2-II, isothermal dissolution at the bonding temperature.

Tuah-Poku et al. [39] used the method proposed by Lesoult [53] to predict the time required for dissolution of a pure Cu interlayer in TLP bonding of pure Ag (i.e. type-I interlayer). This solution assumes initial formation of a liquid layer at the two interfaces between the base metal and interlayer. The liquid then grows into the interlayer through diffusion of the solute in the liquid. The assumption is that the position of the solid/liquid interface ($X(t)$) obeys a general square root law, given by Equation 2-18.

$$X(t) = K\sqrt{4 \cdot D_L t} \qquad \text{Equation 2-18}$$

The constant, K is evaluated at the bonding temperature according to the phase boundaries on the equilibrium phase diagram. Tuah-Poku et al. used values of K that were evaluated by Lesoult for Ag-Cu at 820°C. Tuah-Poku et al. [39] reasoned that when the width of liquid ($2\times X(t)$) was equal to the initial interlayer width (W_o), the interlayer was completely dissolved.

Pursuant to this assumption, the time for the interlayer to dissolve completely is given by Equation 2-19.

$$t_2 = \frac{W_o^2}{16 \cdot K^2 D_L} \qquad \text{Equation 2-19}$$

Tuah-Poku et al. [39] took this approach one step further to predict the time required for the liquid to reach a homogeneous composition through widening of the base metal. Again, it was assumed that the interface motion was diffusion controlled suggesting the adherence to a general square root law; however, in this case it was assumed that the time (t) exponent could have a value other than 0.5. If the diffusivity and constant (K) are constant (combined into a general constant, a), the interface position ($X(t) = 1/2(W-W_o)$) can now be written as Equation 2-20, where n is determined from the experimental results.

$$X(t) = a \cdot t^n \qquad \text{Equation 2-20}$$

An effective diffusion coefficient was determined by Tuah-Poku et al. based on experimental results. They proposed that the effective diffusivity was either a composite of the solid and liquid diffusivities, or a result of surface diffusion control. The results given by the Tuah-Poku et al. model show that initial dissolution of the interlayer is complete in around 3 seconds; however, the homogenization of the interlayer requires times on order of 20 minutes.

MacDonald and Eagar [16] correctly point out that the assumption that the solid/liquid interface moves into the interlayer until it is completely liquid is unfounded. In consideration of a type-I interlayer, the solute concentration must be lowered to $C_{\beta L}$ before the interlayer is completely liquid. Based on the experimental set up of Tuah-Poku et al., the liquid width must increase by more than 2.5 times the initial width (W_o). The liquid zone advances into both the interlayer and the base metal simultaneously to accomplish this.

Nakao et al. [34] suggested that a dissolution parameter (P) based on the Nernst-Brunner theory [54] could be applied to the isothermal dissolution of a type-II interlayer in the TLP bonding of Ni-base superalloy using Ni-15.5% Cr. The dissolution parameter is given by Equation 2-21, where W is the instantaneous liquid width and p is the ratio of liquid to solid density.

$$P = Kt = \frac{W_o}{2} \ln\left[\frac{W_{max}\left(W + \frac{p \cdot W_o}{2}\right)}{\frac{p \cdot W_o}{2}\left(W_{max} - W\right)}\right] \qquad \text{Equation 2-21}$$

From this, the concentration dependence of the interlayer is given by Equation 2-22 where A is the surface area of the solid/liquid interface and V is the volume of the liquid.

$$C_L = C_{\beta L}\left[1 - \exp\left(-\frac{KAt}{V}\right)\right] \qquad \text{Equation 2-22}$$

The dissolution parameter, P gives a linear relation and predicts that dissolution will continue without bound [16]. Nakao et al. [34] show experimental results which support the linear dependence in experimental results. Zhou et al. [2] point out, however, that in the results presented by Tuah-Poku et al. [39] there is a non-linear relation between the dissolution parameter and the hold time. One reason suggested for this was that the liquid layer was constrained by Nakao et al. while free expansion was permitted by Tuah-Poku et al. Nakagawa et al. [44] suggest that the Nernst-Brunner theory is not valid in this case because a required assumption of a thin boundary layer and a large bulk liquid width is not valid in TLP bonding (i.e. the thin boundary layer is the interlayer and hence, there is no bulk liquid).

Liu et al. [55] present an analytical model for the isothermal dissolution of a type-I interlayer using the general error function solution. The numerical solution of two simultaneous solutions gives the time required for complete dissolution of the interlayer, given by Equation 2-23.

$$t_2 = \frac{W_o^2}{4 \cdot G_\beta^2 \cdot D_L} \qquad \text{Equation 2-23}$$

The width of the interlayer at this instant is given by Equation 2-24, where G_α and G_β are dimensionless growth constants for the two interfaces (i.e. base metal (α) and interlayer (β)).

$$W = W_o + 2G_\alpha\sqrt{D_L t_2} \qquad \text{Equation 2-24}$$

The result of Equation 2-23 (Liu et al. [55]) is very similar to that given by Equation 2-19 (Tuah-Poku et al. [39]). Zhou et al. [2] dispute the use of an error function solution to describe the solute distribution in the liquid during dissolution and the assumption that no solute diffuses into the base metal by pointing out that liquid width is very thin in comparison with the solute diffusion rate in the liquid. The error function solution is based on the assumption of infinite or semi-infinite media. This solution is also only valid for a type-I interlayer and until the interlayer has been dissolved. Any additional homogenization and widening through dissolution of the base metal is not included in the time given by Equation 2-23.

Nakagawa et al. [44] present a numerical finite difference model that combines the heating (stage 1), and dissolution and widening (stage 2) stages. Their results show that the time required for dissolution is proportional to the square of the interlayer thickness (W_o), and that the dissolution rate is mostly dependent upon the solute diffusivity in the liquid phase (not the solid phase) as well as the heating rate. The relative influence of heating rate is also dependent upon the interlayer thickness. Zhou and North [56] show that during base metal dissolution, no constant value for a liquid growth parameter can be found. Hence, the analytical models

presented here cannot be applied with confidence to the dissolution stage and numerical models are more representative of the process kinetics. In contrast, Zhou and North [56] conclude that the isothermal solidification stage can be effectively modelled using analytical solutions because the interface motion follows the parabolic law, an assertion that is supported by the results of numerical and experimental results.

2.2.4. Solutions for the Isothermal Solidification Stage

In review of the relevant literature on analytical models for the isothermal solidification stage during TLP bonding, it is found that there are a variety of solutions. In fact, there are three distinct analytical solutions for isothermal solidification that have been used by a number of researchers. These three models are all based on the general solution of Fick's laws for a semi-infinite medium with a constant surface composition, which is now given in detail.

If equilibrium is assumed to be established at the solid/liquid interface, the composition of the solid phase at the solid/liquid interface during the isothermal solidification stage is fixed by the tie-line on the equilibrium phase diagram. In this case diffusion of solute into the base material may be modelled as a semi-infinite medium with a constant surface composition. The initial condition and boundary condition are given by Equation 2-25 and Equation 2-26, respectively, where C_o is the initial composition of solute in the base metal and $C_{\alpha L}$ is the solidus composition at the bonding temperature, T_b. The boundary condition is valid under the assumption that equilibrium is maintained at the solid/liquid interface such that the composition in the solid is fixed by the Gibbs' tie-line.

$$\text{IC} \quad C(x,0) = C_o \qquad \text{Equation 2-25}$$

$$\text{BC} \quad C(0,t) = C_{\alpha L} \qquad \text{Equation 2-26}$$

$$\text{BC} \quad C(\infty,t) = C_o \qquad \text{Equation 2-27}$$

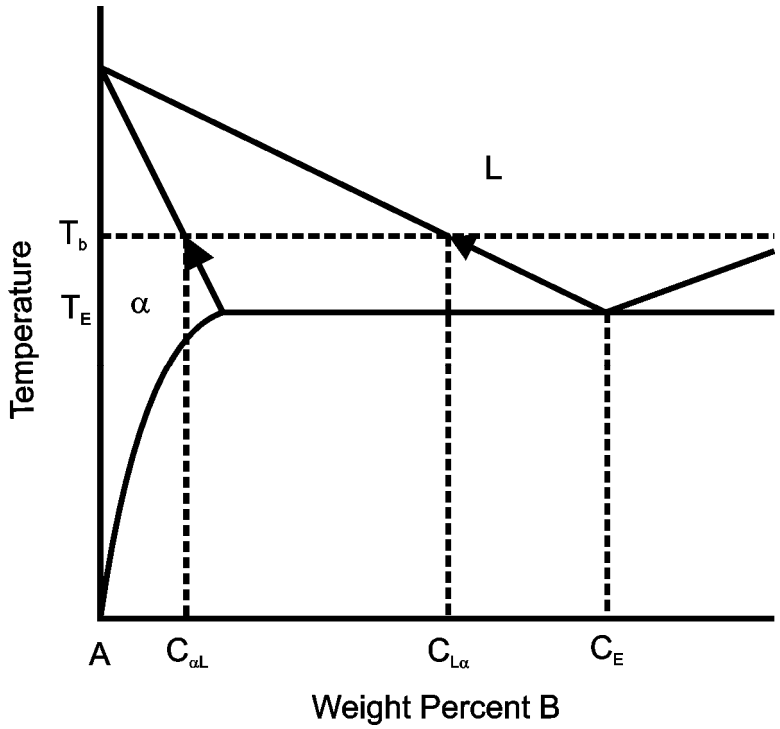

Figure 2-11: Equilibrium phase diagram for a simple binary eutectic system. The solidus (C_S) and liquidus (C_L) concentrations at the interface are given by the phase boundaries ($C_{\alpha L}$ and $C_{L\alpha}$) at the process temperature [57].

The solution for Equation 2-12 (i.e. Fick's second law) can be found for these conditions using the Laplace transform [49]:

$$f(s) = \int_0^\infty e^{-st} \cdot F(t)\,dt \qquad \text{Equation 2-28}$$

Thus, Equation 2-12 becomes:

$$\int_0^\infty e^{-st} \cdot \frac{\partial C(x,t)}{\partial t}\,dt = D\int_0^\infty e^{-st} \cdot \frac{\partial^2 C(x,t)}{\partial x^2}\,dt \qquad \text{Equation 2-29}$$

Assuming the orders of differentiation and integration can be interchanged (Leibniz's rule [58]), and using integration by parts:

$$\left[e^{-st} \cdot C(x,t)\right]_0^\infty - \int_0^\infty C(x,t) \cdot \left(-se^{-st}\right)dt = D \cdot \frac{\partial^2}{\partial x^2}\int_0^\infty e^{-st} \cdot C(x,t)\,dt \qquad \text{Equation 2-30}$$

and

$$\left[e^{-s\infty}\cdot C(x,\infty)-e^{-s\cdot 0}\cdot C(x,0)\right]+s\cdot\int_0^\infty e^{-st}\cdot C(x,t)dt = D\cdot\frac{\partial^2}{\partial x^2}\int_0^\infty e^{-st}\cdot C(x,t)dt \qquad \text{Equation 2-31}$$

Using the initial condition, Equation 2-25, the Laplace transform becomes:

$$-C_o+s\cdot c(x,s)=D\cdot\frac{\partial^2}{\partial x^2}c(x,s) \qquad \text{Equation 2-32}$$

This is in the form of an ordinary differential equation. The solution of Equation 2-32 for which the solution remains finite as *x* approaches infinity is:

$$c(x,s)=A+B\cdot e^{-\sqrt{s/D}\cdot x} \qquad \text{Equation 2-33}$$

where *A* and *B* are constants. Using Equation 2-32 with $x\rightarrow\infty$, the constant *A* can be found:

$$-C_o+s\cdot\left(A+B\cdot e^{-\sqrt{s/D}\cdot\infty}\right)=D\cdot\frac{\partial^2}{\partial x^2}\left(A+B\cdot e^{-\sqrt{s/D}\cdot\infty}\right) \qquad \text{Equation 2-34}$$

$$A=\frac{C_o}{s} \qquad \text{Equation 2-35}$$

Furthermore, using Equation 2-26, the Laplace transform for the boundary condition can be found:

$$\int_0^\infty e^{-st}\cdot C(0,t)\,dt=\int_0^\infty e^{-st}\cdot C_{\alpha L}\,dt \qquad \text{Equation 2-36}$$

$$c(0,s)=\left[e^{-st}\cdot\frac{C_{\alpha L}}{-s}\right]_0^\infty=\frac{C_{\alpha L}}{s} \qquad \text{Equation 2-37}$$

Using Equation 2-33 with Equation 2-35 and Equation 2-37, the constant B can be found:

$$c(0.s)=\frac{C_o}{s}+B\cdot e^{-\sqrt{s/D}\cdot 0}=\frac{C_{\alpha L}}{s} \qquad \text{Equation 2-38}$$

$$B=\frac{C_{\alpha L}-C_o}{s} \qquad \text{Equation 2-39}$$

Thus, the Laplace transform of the solution is:

$$c(x,s)=\frac{C_o}{s}+\frac{C_{\alpha L}+C_o}{s}\cdot e^{-\sqrt{s/D}\cdot x} \qquad \text{Equation 2-40}$$

Which is easily shown to be the transform of the solution of Fick's equations for a semi-infinite medium with a constant surface composition, given by:

$$C(x,t) = C_{\alpha L} + (C_o - C_{\alpha L}) \cdot \mathrm{erf}\left(\frac{x}{2\sqrt{Dt}}\right) \qquad \text{Equation 2-41}$$

A form of Equation 2-41 is used to develop the common solutions for the isothermal solidification stage during TLP bonding.

2.2.5. Stationary Interface Solution for Isothermal Solidification

Tuah-Poku et al. [39] developed a solution for the time required for completion of the isothermal solidification stage based on the earlier modeling work of Lesoult [53]. This solution assumes that the solid/liquid interface is fixed with respect to the base material frame of reference.

The differential of Equation 2-41 with respect to *x* is:

$$\frac{\partial C}{\partial x} = (C_o - C_{\alpha L}) \cdot \frac{\partial}{\partial x}\mathrm{erf}\left(\frac{x}{2\sqrt{Dt}}\right) \qquad \text{Equation 2-42}$$

which is solved by:

$$\frac{\partial C}{\partial x} = \frac{(C_o - C_{\alpha L})}{\sqrt{\pi Dt}} \cdot \exp\left(\frac{-x^2}{4Dt}\right) \qquad \text{Equation 2-43}$$

Substitution of Equation 2-43 into Fick's first law, Equation 2-10, with x = 0 gives the solute mass flux at the solid/liquid interface.

$$J = (C_{\alpha L} - C_o) \cdot \sqrt{\frac{D}{\pi t}} \qquad \text{Equation 2-44}$$

Tuah-Poku et al. [39] suggested that the isothermal solidification stage is complete when all of the solute in the initial liquid has diffused across the solid/liquid interface. The total mass transferred in this time across each interface is given by integrating the flux over time.

$$M = \int (C_{\alpha L} - C_o) \cdot \sqrt{\frac{D}{\pi t}}\, dt \qquad \text{Equation 2-45}$$

$$M = 2 \cdot (C_{\alpha L} - C_o) \cdot \sqrt{\frac{Dt}{\pi}} \qquad \text{Equation 2-46}$$

So a balance of the initial solute mass and the total mass transferred across the interface gives:

$$C_F \cdot W_o = 2 \cdot M \qquad \text{Equation 2-47}$$

Therefore, Equation 2-46 can be substituted into Equation 2-45 and rearranged to give:

$$t_s = \frac{\pi}{16 \cdot D} \cdot \left(\frac{C_F \cdot W_o}{C_{\alpha L} - C_o} \right)^2 \qquad \text{Equation 2-48}$$

As Zhou [59] points out, there can be a significant error associated with this type of "single phase" solution due to the fact that the migrating solid/liquid interface is neglected. The stationary interface solution has been shown to systematically overestimate the time required for isothermal solidification due to the fact that the actual interface is moving. Under limited conditions, this solution can be used with some accuracy [59]; however, in the general case, a more rigorous treatment is required.

2.2.6. Shifting Reference Frame Solution for Isothermal Solidification

In § 2.2.5 the solid/liquid interface is assumed to be stationary with respect to the frame of reference, which is the base metal. In reality the interface is moving toward the joint centreline as isothermal solidification progresses. Lynch et al. [24] was the first to point out that the rate of interface movement in isothermal solidification will be proportional to the difference between solute flux into and out of the solid/liquid interface, as given by Equation 2-49, where *K* is an interface rate parameter that is dependent upon the material system.

$$\frac{d}{dt} X(t) = K[J_L - J_S] \qquad \text{Equation 2-49}$$

In the case of solute diffusion across a planar interface, Lynch et al. [24] also pointed out that the flux (Equation 2-10) can be given by Equation 2-50, where *R* is another constant dependent upon the conditions at the solid/liquid interface.

$$J = R\sqrt{\frac{D}{t}} \qquad \text{Equation 2-50}$$

Combining Equation 2-49 and Equation 2-50 gives Equation 2-51 for the solid/liquid interface velocity. Lynch et al. [24] could not offer a full analytical solution to solve for the constants; however, it was pointed out that R was time dependent, leaving the applicability of Equation 2-51 in question.

$$\frac{d}{dt} X(t) = K\left[\frac{R_1\sqrt{D_L} - R_2\sqrt{D_S}}{\sqrt{t}} \right] \qquad \text{Equation 2-51}$$

Following this approach, Ikawa et al. [60] derived a somewhat different solution to that given by Tuah-Poku et al. [39]. In this treatment of the isothermal solidification problem, the frame of reference is fixed to the solid/liquid interface. Equation 2-41 with a shifting reference frame becomes:

$$C(x,t) = C_{\alpha L} + (C_o - C_{\alpha L}) \cdot \mathrm{erf}\left(\frac{x - X(t)}{2\sqrt{Dt}}\right) \qquad \text{Equation 2-52}$$

The concentration gradient in the liquid is assumed to be zero during the isothermal solidification stage as shown in Figure 2-12; thus, Equation 2-13 can be simplified to:

$$(C_{L\alpha} - C_{\alpha L}) \cdot \frac{d}{dt} X(t) = D \cdot \frac{\partial}{\partial x} C(x,t)_{x=X(t)} \qquad \text{Equation 2-53}$$

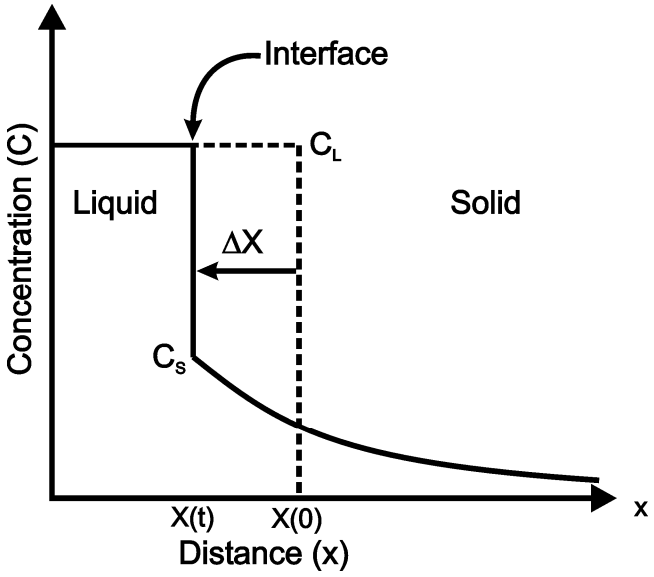

Figure 2-12: A diffusion couple and moving boundary problem in a simple solid/liquid system. After a time step, Δt, the interface has moved ΔX. The solid and liquid concentrations, C_S and C_L respectively, are expected to obey the phase boundaries on the equilibrium phase diagram shown in Figure 2-11 [57].

Figure 2-12 shows the original position of the solid/liquid interface *X(0)* by the broken line. After isothermal solidification has progressed by some amount, the solid/liquid interface and resulting solute distribution in the solid is given by the solid line. Since the concentration gradient terms for the liquid phase in Equation 2-13 is zero, the direction of interface motion is always into the liquid.

Equation 2-53 can be solved with Equation 2-52 to give an equation for the velocity of the solid/liquid interface by Equation 2-54. Note the similarity with Equation 2-51.

$$\frac{d}{dt}X(t)=\frac{C_o-C_{\alpha L}}{C_{L\alpha}-C_{\alpha L}}\cdot\sqrt{\frac{D}{\pi t}} \qquad \text{Equation 2-54}$$

The interface velocity can be integrated with respect to time to give the equation for the solid/liquid interface position:

$$X(t)=\frac{C_o-C_{\alpha L}}{C_{L\alpha}-C_{\alpha L}}\cdot 2\cdot\sqrt{\frac{Dt}{\pi}} \qquad \text{Equation 2-55}$$

The maximum liquid width after the dissolution and widening stage can be found using conservation of mass assuming no diffusion occurs before isothermal solidification begins [39]:

$$W_{max}=\frac{C_F\cdot W_o}{C_{L\alpha}} \qquad \text{Equation 2-56}$$

The isothermal solidification stage will be completed at a time, t_s, when the position of the solid/liquid interface, *X(t)*, in Figure 2-12 reaches the joint centreline. This can be written as Equation 2-57.

$$X(t_s)=\frac{-W_{max}}{2} \qquad \text{Equation 2-57}$$

Substitution into Equation 2-57 gives the time required for the completion of isothermal solidification:

$$t_s=\frac{\pi}{16\cdot D}\cdot\left(\frac{C_F\cdot W_o}{C_{L\alpha}}\cdot\frac{C_{L\alpha}-C_{\alpha L}}{C_o-C_{\alpha L}}\right)^2=\frac{\pi\cdot W_{max}^2}{16\cdot D}\left(\frac{C_{L\alpha}-C_{\alpha L}}{C_{\alpha L}}\right)^2 \qquad \text{Equation 2-58}$$

This solution was also derived by Nakao et al. [34] and used in experimental work on TLP bonding of Ni-based superalloys using Ni-B and Ni-P interlayers [61]. More recently, Equation 2-44 was used to predict the isothermal solidification time of Sn plated Au interlayers in microelectronics joining by Cain et al. [62].

2.2.7. Moving Interface Solution for Isothermal Solidification

Lesoult [53] followed the method derived by Dankwerts [63] for mass and heat transfer. The full derivation of the solution for isothermal solidification in TLP bonding is given here.

The position of the solid/liquid interface can be defined as $x = X(t)$, where $X(0) = 0$ is the initial position of the solid/liquid interface at the start of isothermal solidification [53]. The boundary conditions for this problem now become:

$$\text{BC}\quad C(X(t),t)=C_{\alpha L} \qquad \text{Equation 2-59}$$

$$\text{BC} \quad C(\infty, t) = C_o \qquad \text{Equation 2-60}$$

The solute concentration in the base metal can be assumed to take the general form of Equation 2-41, which is [53]:

$$C(x,t) = A + B \cdot \text{erf}\left(\frac{x}{2\sqrt{Dt}}\right) \qquad \text{Equation 2-61}$$

where *A* and *B* are constants. Combining Equation 2-59 and Equation 2-61:

$$C(X(t),t) = A + B \cdot \text{erf}\left(\frac{X(t)}{2\sqrt{Dt}}\right) = C_{\alpha L} \qquad \text{Equation 2-62}$$

The error function term in Equation 2-62 must be constant; thus, the position of the interface must be proportional to the root of time. For convenience, *X(t)* can be defined as:

$$X(t) = -2K\sqrt{Dt} \qquad \text{Equation 2-63}$$

where *K* is the interface rate parameter. The constants, *A* and *B* can now be solved to give:

$$B = \frac{C_{\alpha L} - C_o}{\text{erf}(K) - 1} \qquad \text{Equation 2-64}$$

$$A = C_o - \frac{C_{\alpha L} - C_o}{\text{erf}(K) - 1} \qquad \text{Equation 2-65}$$

Thus, the solution of Fick's equations for a semi-infinite medium with a constant surface composition and a moving interface is:

$$C(x,t) = C_o - \frac{C_{\alpha L} - C_o}{\text{erf}(K) - 1} + \frac{C_{\alpha L} - C_o}{\text{erf}(K) - 1} \cdot \text{erf}\left(\frac{x}{2\sqrt{Dt}}\right) \qquad \text{Equation 2-66}$$

Once again, the mass balance (Equation 2-53) is given by:

$$(C_{L\alpha} - C_{\alpha L}) \cdot \frac{d}{dt} X(t) = D \cdot \frac{\partial}{\partial x} C(x,t)_{x=X(t)} \qquad \text{Equation 2-67}$$

Equation 2-63 and Equation 2-66 can be substituted into Equation 2-67. This differential equation can be solved to give an equation for the interface rate parameter, *K*, which must be solved numerically. The solution is given as Equation 2-68 by Sakamoto et al. [64].

$$\frac{C_{\alpha L} - C_o}{C_{L\alpha} - C_{\alpha L}} = \sqrt{\pi} \cdot \frac{K \cdot (1 + \text{erf}(K))}{\exp(-K^2)} \qquad \text{Equation 2-68}$$

This derivation was also used by Tuah-Poku et al. [39] and Liu et al. [55]; however, it is interesting to note that in all of the above references a typographical error was carried through in Equation 2-68. The term $exp(-K^2)$ was missing the negative operator.

Using Equation 2-63 and Equation 2-56, LeBlanc and Mevrel [65] gave the time required for the completion of the isothermal solidification stage by Equation 2-69.

$$t_s = \frac{W_{max}^2}{16 \cdot K^2 \cdot D} \qquad \text{Equation 2-69}$$

This solution was also derived by Ramirez and Liu [8], and used in a general form by Sekerka [66] and more recently by Jung and Kang [67]. MacDonald and Eagar [68] suggest a somewhat different derivation using two error functions to describe the solute distribution in the base metal; however, the end result is the same. Changes in density between the solid and liquid phase was taken into account by MacDonald and Eagar [68] and Li et al. [12].

2.2.8. Alternative Solution for a Moving Boundary

To account for the movement of the interface, a solution has been proposed in this work that follows the work of Maugis et al. on biphase diffusion couples [69,70]. A substitution variable, λ, given by Equation 2-70 is substituted into Fick's second law to yield Equation 2-74.

$$\lambda = \frac{x}{\sqrt{t}} \qquad \text{Equation 2-70}$$

$$\frac{\partial \lambda}{\partial x} = \frac{1}{\sqrt{t}} \qquad \text{Equation 2-71}$$

$$\frac{\partial \lambda}{\partial t} = \frac{-x}{2 \cdot t^{3/2}} \qquad \text{Equation 2-72}$$

Fick's second law, given by Equation 2-12, can be rewritten as Equation 2-73. Using Equation 2-71 and Equation 2-72, the form of Fick's second law in λ space is given by Equation 2-74.

$$\frac{\partial C}{\partial \lambda} \cdot \frac{\partial \lambda}{\partial t} = D \cdot \frac{\partial^2 C}{\partial \lambda^2} \cdot \frac{\partial \lambda}{\partial x} \cdot \frac{\partial \lambda}{\partial x} \qquad \text{Equation 2-73}$$

$$-\frac{\lambda}{2} \cdot \frac{dC}{d\lambda} = D \cdot \frac{d^2 C}{d\lambda^2} \qquad \text{Equation 2-74}$$

The solution to Equation 2-74 can be easily found using substitution and separation of variables. If G (Equation 2-75) is the substitution parameter, the resulting form of Fick's

second law is Equation 2-76. This can be rearranged (Equation 2-77) and integrated to give Equation 2-78.

$$G = \frac{dC}{d\lambda} \qquad \text{Equation 2-75}$$

$$-\frac{\lambda}{2} \cdot G = D \cdot \frac{dG}{d\lambda} \qquad \text{Equation 2-76}$$

$$-\frac{1}{2 \cdot D} \cdot \lambda \, d\lambda = \frac{dG}{G} \qquad \text{Equation 2-77}$$

$$\frac{dC}{d\lambda} = A \cdot \exp\left(\frac{-\lambda^2}{4 \cdot D}\right) \qquad \text{Equation 2-78}$$

Integrating Equation 2-78 gives the general form of the solution, Equation 2-79, where *A* and *B* are constants of integration.

$$C = A \cdot \sqrt{\pi D} \cdot \operatorname{erf}\left(\frac{\lambda}{2\sqrt{D}}\right) + B \qquad \text{Equation 2-79}$$

The initial conditions of the problem are given by Equation 2-80. At t_o ($\lambda = \infty$) all concentrations are zero.

$$t = 0 \quad \lambda = \infty \quad C(\infty) = 0 \qquad \text{Equation 2-80}$$

The interface position, *X(t)*, is given by ξ.

$$\lambda_i = \xi \qquad \text{Equation 2-81}$$

The solution assumes a moving interface given by *X(t)*. By definition, *X(t)* must be proportional to the root of time; thus, *X(t)* has the form of Equation 2-82. Where ξ is the interface rate constant.

$$X(t) = \xi \cdot \sqrt{t} \qquad \text{Equation 2-82}$$

The boundary conditions of the problem can then be defined by Equation 2-83. Specifically, the composition of the solid at the solid/liquid interface (ξ) is fixed at the solidus composition ($C_{\alpha L}$).

$$x = X(t) \quad \lambda = \xi \quad C(\xi) = C_{\alpha L} \qquad \text{Equation 2-83}$$

Using the initial conditions given by Equation 2-80 in Equation 2-79 gives the constant *B*.

$$B = -A\sqrt{\pi D} \qquad \text{Equation 2-84}$$

Thus, the solution becomes:

$$C = A\sqrt{\pi D}\left[\operatorname{erf}\left(\frac{\lambda}{2\sqrt{D}}\right) - 1\right] \qquad \text{Equation 2-85}$$

Substitution of the boundary conditions (Equation 2-83) into Equation 2-85 gives:

$$A = \frac{C_{\alpha L}}{\sqrt{\pi D}\left(\operatorname{erf}\left(\frac{\xi}{2\sqrt{D}}\right) - 1\right)} \qquad \text{Equation 2-86}$$

Thus, the solution of the ordinary differential equation given by Equation 2-74 is the concentration profile of the solute in the base metal, given by Equation 2-87.

$$C(\lambda) = C_{\alpha L} \cdot \frac{\operatorname{erfc}\left(\frac{\lambda}{2 \cdot \sqrt{D}}\right)}{\operatorname{erfc}\left(\frac{\xi}{2 \cdot \sqrt{D}}\right)} \qquad \text{Equation 2-87}$$

The mass balance given by Equation 2-67 can be used to find the interface rate constant, ξ, and the time required for completion of the isothermal solidification stage. The interface velocity in terms of ξ is found by differentiating Equation 2-82.

$$\frac{d}{dt}X(t) = \frac{1}{2\sqrt{t}}\xi \qquad \text{Equation 2-88}$$

The partition coefficient, k, is given by Equation 2-89.

$$k = \frac{C_{L\alpha}}{C_{\alpha L}} \qquad \text{Equation 2-89}$$

Substituting Equation 2-71, Equation 2-88, and Equation 2-89 into the mass balance gives:

$$C_{\alpha L} \cdot (k-1) \cdot \frac{\xi}{2\sqrt{t}} = D \cdot \frac{dC}{d\lambda}_{\lambda=\xi} \cdot \frac{1}{\sqrt{t}} \qquad \text{Equation 2-90}$$

$$C_{\alpha L} \cdot (k-1) \cdot \frac{\xi}{2} = D \cdot \frac{dC}{d\lambda}_{\lambda=\xi} \qquad \text{Equation 2-91}$$

The concentration gradient in λ can be solved by substituting Equation 2-86 into Equation 2-85, or by differentiating Equation 2-87, both with the same result.

$$\frac{dC}{d\lambda} = \frac{-C_{\alpha L} \cdot \exp\left(\frac{-\lambda^2}{4 \cdot D}\right)}{\sqrt{\pi D} \cdot \operatorname{erfc}\left(\frac{\xi}{2\sqrt{D}}\right)} \qquad \text{Equation 2-92}$$

Finally, the solution for ξ can be found by substituting Equation 2-92 into Equation 2-91. The resulting solution for the interface rate constant (Equation 2-93) must be solved using iterative methods.

$$\xi = -2 \cdot (k-1)^{-1} \cdot \sqrt{\frac{D}{\pi}} \cdot \frac{\exp\left(\frac{-\xi^2}{4 \cdot D}\right)}{\operatorname{erfc}\left(\frac{\xi}{2\sqrt{D}}\right)} \qquad \text{Equation 2-93}$$

The significance of the constant, ξ, is that it is an indication of the solidification rate of the system. Increasing ξ results in faster solid/liquid interface motion, and shorter duration of the isothermal solidification stage. Furthermore, ξ is independent of the initial liquid width, thus it is useful to discuss process kinetics in terms of ξ rather than the time required for isothermal solidification when the temperature and initial liquid width are varied.

The isothermal solidification stage is complete when the solid/liquid interface reaches the joint centerline. Assuming no solute is lost before the isothermal solidification stage begins; the time required for completion of the isothermal solidification stage is given by Equation 2-94.

$$t_s = \left(\frac{-W_{max}}{2 \cdot \xi}\right)^2 \qquad \text{Equation 2-94}$$

The solution given by Equation 2-94 is similar to Equation 2-69; and, in fact gives the exact same solution. The method derived in § 2.2.8 was first applied to the TLP bonding process by Sinclair et al. [71]. The results are similar to the method derived in § 2.2.7, thus confirming the validity of both models. In this study, the process kinetics will be discussed in terms of the interface rate constant, ξ. As noted, the interface rate constant gives a solution that is independent of the initial liquid width and is useful in discussions comparing initial conditions.

2.2.9. Summary

In summary, there are three methods for predicting the process kinetics that have been presented here from the literature. The simplest of the solutions assumes a stationary interface and predicts the completion of isothermal solidification when the total amount of solute in the interlayer has diffused across the interfaces. The other two methods assume an interface that

moves towards the joint centreline over time. The shifting reference frame solution assumes the solute composition profile from the interface into the base material is the same as the stationary solution. The moving interface solution assumes a solute composition profile that accounts for the sweeping action of the interface as it moves with respect to the base material.

2.2.10. Assumptions in Model Derivation

The assumptions used in derivation of the analytical models above are summarized by Ramirez and Liu [8]:

1. One-dimensional diffusion: solute diffusion in the base metal is assumed to be in one direction only, i.e. in a direction perpendicular to the base metal. Solute flux is a function of concentration gradient.
2. Quiescent liquid: there is no mixing in the liquid. Solute redistribution is a function of diffusional motion only. This assumption is generally considered valid unless induction heating is used for a heat source.
3. Constant diffusivities: the coefficient of diffusion is constant over the isothermal hold time and independent of solute concentration. In fact, diffusivity is related to the local chemical composition; however, the assumption is required to simplify the solution.
4. Semi-infinite base metal: the base metal can be considered semi-infinite so long as the diffusion distance of the solute ($\sqrt{Dt}$) is much less than the thickness.
5. Equilibrium at the solid/liquid interface: the conditions at the interface are assumed to obey local equilibrium and follow the phase boundaries on the equilibrium phase diagram [72].
6. Constant solid/liquid interface area: the interface is assumed to maintain a planar profile. It will be shown that grain boundary grooving has been shown to occur during widening and isothermal solidification and the effect on process kinetics will be discussed.

2.3. Previous Experimental Results

2.3.1. Interface Kinetics in Binary TLP Bonding

A number of experimental studies have been carried out in order to characterize the nature of interface kinetics during isothermal solidification and compare to the results of analytical model predictions. The first observation of isothermal solidification in a TLP bonding application was by Ikawa et al. [60]. In TLP bonding of Ni using a Ni-B interlayer, it was

determined that the solid/liquid interface position (*X(t)*) obeyed a square root relation with respect to the isothermal hold time. From this, it was determined that the mechanism of interface motion was controlled by solute diffusion into the base metal.

In the experimental studies on interface kinetics during isothermal solidification, the position of the solid liquid interface, or the width of solidified liquid is measured after an isothermal hold period. The isothermal solidification stage is interrupted prematurely by cooling of the assembly. In most cases, the width of a solidified liquid phase is identified by a eutectic microstructure and measured from a cross section of the joint using conventional metrology practice. Ikawa et al. [60] found that the width of the solidified layer was not uniform across the length of the joint due to irregularity and a non-planar solid/liquid interface. This made measurement of the liquid width considerably more difficult. They measured the planimetric area of solidified eutectic phase and divided by the length to determine the average width. This technique was also used by Tuah-Poku et al. [39], Nakao et al. [34], and MacDonald and Eagar [68], who used weight fractions of photographs to find the eutectic width. In other studies, an average value of manual measurements was found [8]. Saida et al. [75] found an average eutectic width by taking the average of a number of measurements taken over a 5 mm length near the center of the TLP bond.

Ikawa et al. [60] assumed that the measured eutectic width is representative of the liquid width at the time that the isothermal hold was interrupted by cooling. This approach was followed by a number of researchers [34,39,45,64,65,67]. Nakao et al. [61] converted the measured eutectic thickness to the liquid width by a factor that is found using the lever rule (Equation 2-95). This multiplication is required because some of the liquid solidifies during cooling from the bonding temperature to the eutectic temperature. The eutectic width is then proportional to the actual liquid width at the bonding temperature. Nakao et al. [61] assumed that equilibrium solidification applied in this case. MacDonald and Eagar [68] also applied the lever rule to calculate the liquid width, *W(t)*, from the measured eutectic width, W_E.

$$W(t) = W_E \cdot \frac{C_E - C_{max}}{C_{L\alpha} - C_{max}} \qquad \text{Equation 2-95}$$

The actual extent of solidification that occurs on cooling from the bonding temperature to the eutectic temperature has not been determined. Sakamoto et al. [64] suggested that epitaxial growth was observed after an isothermal hold period; however, it was impossible to ascertain if the nature of solidification was isothermal or athermal. In their experimental work on TLP bonding Ni with Ni alloy interlayers containing Si or B melting point depressants, Sakamoto et al. [64] also determined that the experimental results for the solid/liquid interface position as a function of time did not intercept at the origin. This was not explained; however, it is possible that this was a result of primary solidification of a Ni-rich phase during cooling. The observed

deviation increased with increasing temperature, a result that would be expected since more primary solidification is expected during cooling from higher temperatures by the lever rule.

Shinmura et al. [73] assumed that during cooling from the bonding temperature to the eutectic, a fraction of the liquid will solidify. After an isothermal hold period in TLP bonding of Ni with a Ni-P interlayer, a residual of 100 μm liquid width resulted in a eutectic width of 37.8 μm remained after solidification (furnace cooled); The details, however, of liquid measurement are unclear and it is likely that model results were used to determine the liquid width before cooling.

Saida et al. [74] experimented with different cooling rates in TLP bonding of Ni using a Ni-P interlayer. The cooling rates from slowest to fastest were obtained by air cooling, oil quenching, and water quenching. The air cooled and oil quenched samples show less measured eutectic width and a cellular eutectic interface. The water quenched sample shows a dendritic morphology and a eutectic width that is considered to approach the width of the liquid. The presence of dendrites shows that primary solidification did occur. Substantial evidence is available to show that primary solidification occurs during cooling from the bonding temperature to final eutectic solidification; and the fraction of liquid that solidifies athermally is a function of temperature and cooling rate; however, no direct measurement of the eutectic fraction has been made. Some researchers [61,68] have applied the lever rule under the assumption that solidification occurs under equilibrium conditions but this is not likely the case. Solidification theory will be developed in § 2.7.

Tuah-Poku et al. [39] studied the process kinetics of the TLP bonding process using Ag base metal with a pure Cu interlayer. The time required for complete dissolution of the interlayer could not be found because the process kinetics were so rapid. It was estimated that dissolution was complete on the order of seconds. Widening of the liquid was measured to be complete after 18-20 minutes at 1093 K. From this, an effective diffusivity for the widening stage was proposed to be of the form of Equation 2-96.

$$D_{eff} = D_S^{1/2} \cdot D_L^{1/2} \qquad \text{Equation 2-96}$$

The solid/liquid interface kinetics measured by Tuah-Poku et al. [39] were considerably faster than predicted. The experimental rate constant for isothermal solidification was found to be K = 0.75. The rate constant predicted by Lesoult [53] for this system was K = 0.28. Tuah-Poku et al. [39] attributed this discrepancy to two factors. The first was a ledge-type migration mechanism that increased solidification rates. The second reason was attributed to enhanced grain boundary diffusion. MacDonald and Eagar [68] point out that the experimental setup likely contributed to some of the error as liquid could have been extruded from the joint. Tuah-Poku et al. [39] used a 100 μm thick Ta washer at the interface and held the joint together with a miniature clamp. It is likely that some liquid was squeezed out as the

maximum liquid width was 420 μm before isothermal solidification began. This would upset the mass balance and result in an apparent reduction in the time required for isothermal solidification to be completed. Another source of error is the use of the stationary interface solution (Equation 2-48) to estimate the completion time. Use of a moving interface solution (Equation 2-94) would give a shorter t_s.

A number of other authors have also reported that the experimental solid/liquid interface kinetics are found to be much faster than predicted using the variety of analytical solutions available [8,45,64,65,68]. In many cases, the discrepancy has been attributed to experimental setup. Ramirez and Liu [8], like Tuah-Poku et al. [39], used a hand-clamp to fix the Ni base metal substrates together and apply pressure to the joint. A fast regime of interface motion was observed at the beginning of the isothermal hold period, followed by a slow regime. The fast regime is likely to be a result of some amount of liquid being extruded from the joint, which is certain to occur under these circumstances. It is also possible that the base metal became saturated with the melting point depressant solute since a Ni-B interlayer was used (B has limited solubility in Ni, the base metal thickness was not reported). The base metal must be sufficiently thick to approximate a semi-infinite plate.

Alternatively, Nakao et al. [34] spot welded the two base metal substrates together using bars in their study of TLP bonding on Ni using Ni-P and Ni-B interlayers. A stop-off was applied at the periphery of the joint to prevent liquid leakage; however, as MacDonald and Eagar [68] pointed out, the nature of the stop-off was not given in the article, and it is still expected that the liquid will be lost because it wets the solid. Furthermore, spot welding the substrates together does not allow for volumetric changes to be accommodated, which could lead to porosity or extrusion. This technique was also used by Saida et al. [75], who employed an alumina-based stop-off to prevent the liquid from wetting the sides of the base metal.

MacDonald and Eagar [7] developed an experimental apparatus for TLP bonding Cu using a Ag-Cu interlayer that was designed to minimize the pressure at the solid/liquid interface while allowing for free expansion or contraction of the bonding assembly; thereby reducing the possibility of liquid leakage from the joint. A Cr coating was applied to all sides of the base metal except the faying surface to prevent wicking of the liquid from the joint by wetting. This was deemed an effective method by SEM-EDS analysis since there was no evidence of Ag away from the interface. In their results, however, the rate of isothermal solidification was still significantly faster than expected. Isothermal solidification was complete after only 300 hours, compared to the predicted t_s of 1393 hours. MacDonald and Eagar [68] conceded that the accuracy of the experimental results was suspect because it was difficult to find the true value of the liquid width (they used area analysis and applied a factor by the lever rule). Furthermore, they pointed out that vaporization of Ag in the vacuum environment had contributed to the liquid loss. Evidence of this was found by Ag deposits on the fixturing apparatus.

It is generally accepted in the literature that the isothermal solidification kinetics of the solid/liquid interface are much faster than expected. Most results [4,60,64], with the exception of Ramirez and Liu [8], agree with the linear dependence of the solid/liquid interface position on the square root of time at the isothermal hold temperature. However, the time required for the completion of isothermal solidification is typically less than what is predicted using any of the analytical models available. LeBlanc and Mevrel [65] observed a discrepancy between calculated and experimental results in TLP bonding Ni-based superalloys using B and Si containing interlayers. This discrepancy was attributed to uncertainty in physical parameters input to the model. Furthermore, the effect of boride precipitation is neglected by the model. In TLP bonding Ni using Ni-P interlayers, North et al. [45] found that the calculated rate of isothermal solidification was slower than that measured and attributed the difference to incorrect values for diffusivity and grain boundary enhanced diffusion of the solute. The effect of grain boundaries on isothermal solidification kinetics has been studied in depth in order to explain the observed discrepancies.

Nishimoto et al. [4] and Ramirez and Liu [8] fit the linear results to find the activation energy for isothermal solidification. This activation energy was then related to find the diffusivity of the solute in the base metal.

2.3.2. Effect of Grain Boundaries

Grain boundary grooving and enhanced grain boundary diffusion has been cited by a number of researchers in order to explain faster than expected isothermal solidification rates [8,39,45,76]. Liquid penetration, or grain boundary grooving has been observed in essentially all studies of TLP bonding with polycrystalline materials [8,39,45,68,74,75,76,77]. Tuah-Poku et al. [39] pointed out that liquid penetration at the grain boundaries and the accompanying departure from a planar solid/liquid interface made measurement of the liquid width very difficult, in some areas isothermal solidification was complete but there was still liquid remaining at pockets where grain boundary grooving had occurred. A direct observation of grain boundary grooving was made by MacDonald and Eagar [68] who used a TLP "half-sample" to show protrusions on the free surface of an extremely fine grained metal after isothermal solidification was complete.

Ramirez and Liu [8] suggested that liquid penetration at grain boundaries increases the isothermal solidification rate as a result of increased surface area of the solid/liquid interface that would increase solute diffusion. It would be reasonable to assume that there would be some significance to increased surface area effects if the diffusion distance ($\sqrt{Dt}$) was on the same order of magnitude as liquid penetration and grain diameter.

A study on the influence of grain boundary character on the rate of isothermal solidification was completed by Kokawa et al. [78]. They found significant liquid penetration where grain

boundaries intersected with the solid/liquid interface. In fine grained base metals, the resulting solid/liquid interface was non-planar because magnitude of grain boundary grooving was on the scale of the grain diameter, i.e. the greater the number of grain boundary intersections per unit length, the greater the departure from a planar interface.

Kokawa et al. [78] observed that grain boundary energy has an effect on the deviation of the solid/liquid interlayer from planar. Liquid penetration is a function of grain misorientation; high angle grain boundaries show deeper penetration because the grain boundary energy is higher and the diffusion rates along the grain boundary are faster. Low angle grain boundaries show less penetration and the effects of twin boundaries was found to be negligible.

MacDonald and Eagar [68] observed isothermal solidification in TLP bonding of very fine grained (20 μm) base metal substrates. It was found that grain boundary grooving evolves into spherical protrusions as the growth process favours the elimination of regions of high curvature next to grain boundary cusps. Furthermore, the kinetics of isothermal solidification and grain boundary grooving were suggested to be on the same order of magnitude.

In large grained samples (250 μm), the tendency to form protrusions is less. MacDonald and Eagar [68], however, noted a breakdown of the planar interface to form cells away from grain boundaries. This was attributed to high diffusion paths, subgrain and twin boundaries, as well as diffusion induced grain boundary motion (DIGM). The possibility that the cells formed during cooling from T_b was not discussed.

The rate of isothermal solidification was qualitatively shown to be higher in fine grained samples versus coarse grained samples [78]. Saida et al. [75] studied isothermal solidification rates as influenced by base metal grain size. Results show faster interface kinetics in fine grained samples when compared to coarse grained samples; however, the difference in isothermal solidification rate between coarse grained samples and single crystal base metal were indiscernible. Grain growth was also observed to occur in the fine grained samples. The authors reasoned that increased surface area for diffusion and a greater number of enhanced diffusion paths resulted in a nearly linear decrease in t_s with the number of grain boundaries. Interestingly, the rate of base metal dissolution also increased with finer grain size during the dissolution and widening stage [79].

MacDonald and Eagar [68] found that the isothermal solidification rate of a fine grained sample was twice that of a coarse grained sample. To explain the increased kinetics, Hart's relation, given by Equation 2-97, has been considered [68,76,80]. In this treatment, an effective diffusivity (D_{eff}) is found to be a combination of the lattice diffusivity (D_s) with a grain boundary diffusivity (D_{gb}) that is scaled by fraction that accounts for the number of diffusion paths available.

$$D_{eff} = D_s + \frac{\delta}{l} \cdot D_{gb} \qquad \text{Equation 2-97}$$

The use of an effective diffusivity given by Equation 2-97 only accounted for a 6% increase in diffusion rates in the system used by MacDonald and Eagar [68]. In order to achieve the diffusion rates needed to explain the observed results with analytical models, an effective diffusivity approaching that of the grain boundary diffusivity (i.e. $D_{eff} \approx D_{gb}$) was required. To justify the increased diffusivity value, it was suggested that irrigation of the base metal by composition dependent diffusion enhancement was occurring along the grain boundaries (i.e. increasing solute content in the base metal increases the solute diffusivity).

Ikeuchi et al. [81] used numerical modeling to evaluate the effect of grain boundary regions on isothermal solidification. A two-dimensional numerical solution that considered grain boundary energy and enhanced grain boundary diffusion showed that high grain boundary diffusion alone does not fully explain liquid penetration that was observed. The model was able to show that isothermal solidification is slightly accelerated when high grain boundary diffusion rates are assumed; however, the large variation between observed interface kinetics in fine grained and coarse grained samples could only be explained if extremely high values of grain boundary diffusivity were assumed.

The numerical modeling approach was further developed by Zhou and North [76], who proposed that Equation 2-97 is not sufficient alone to describe the diffusion conditions occurring during the isothermal solidification stage. During isothermal solidification, there will be a transition from type C to type B to type A conditions. Type A conditions are those assumed by Equation 2-97, where the diffusion distance ($\sqrt{Dt}$) is greater than the grain size. In type B kinetics, the diffusion distance is less than the grain size such that the grain boundaries can be assumed to be isolated. In this case, there is no single effective diffusion coefficient. The amount diffused is proportional to $t^{3/4}$. Type C behaviour can be characterized by grain boundary diffusion only as the lattice diffusion is neglected.

In this important study, Zhou and North [76] found that when the isothermal hold temperature approaches the melting point of the base metal (i.e. $T \geq 0.75T_m$), the contribution of grain boundary diffusion on the total amount diffused becomes less significant, even more so with increasing grain size. Furthermore, the effect of grain boundary migration is greater at shorter hold times and faster grain boundary velocities, but becomes negligible at longer isothermal hold times. Additionally, it was shown that at longer isothermal hold times, type A conditions prevail and Equation 2-97 can be used to predict the effective diffusivity.

Takahashi et al. [82] developed a numerical model that emulated a saw tooth profile to account for a non-planar solid/liquid interface. They observed dissolution and isothermal solidification processes using the model; however, they did not focus on interface kinetics of the process and did not provide insight on the effects of grain size or migration on t_s.

In summary, it has been shown through both experimental and numerical work that the effects of grain boundaries on the nature of solid/liquid motion are varied. Fine grained base metal samples show grain boundary grooving and spherical protrusions causing a significant

deviation from the planar solid/liquid interface. Coarse grained substrates show less deviation from the planar morphology [68,78]. The time required for isothermal solidification to be complete is reduced significantly with fine grained base metal; however, the difference in isothermal solidification rates between coarse grained and single crystal base metal is negligible [68,75,78]. The increase in interface kinetics with finer grain size has been attributed to enhanced grain boundary diffusion and grain boundary grooving but support for this theory by numerical modeling has only been qualitative to date. On the other hand, for coarse grained substrates bonded at higher temperatures and longer isothermal hold times, it has been shown that the effect of grain boundaries on solid/liquid interface motion is much less significant, and can be considered with an effective diffusivity (Equation 2-97) if required [68,76,81].

2.4. Numerical Modeling in TLP Bonding

The finite difference method has been applied to model the kinetics of diffusion controlled, two phase moving interface problems [83,84,85,86,87]. This numerical method was first applied to TLP bonding by Nakagawa et al. [44] who applied the technique to model base metal dissolution behaviour. Zhou and North [88] developed a fully implicit finite difference solution for the dissolution, isothermal solidification, and homogenization stages as one continuous process. The fully implicit model reduces calculation time over an explicit scheme, as used in previous works. The assumptions made in the derivation of the solution are: a planar solid/liquid interface; constant diffusivities in solid and liquid; constant and equal molar volumes in solid and liquid; local equilibrium at the solid/liquid interface; and a quiescent liquid [88]. Shinmura et al. [73] used an explicit finite difference solution to simulate TLP bonding of Ni with Ni-11%P filler metal. Jen and Jiao [89] attempted to develop a numerical solution for TLP bonding with an Al-Cu binary system; however, in the theoretical treatment of the problem, a mushy zone was assumed to exist between the solid and liquid phases. The mushy zone was found to increase indefinitely with time. This is counterintuitive to the assumption of equilibrium at the solid/liquid interface and the solution is erroneous.

The one-dimensional model has evolved with additional development for more complex systems. Ikeuchi et al. [81] and Zhou and North [76] extended the model into two dimensions in order to account for grain boundary effects. Takahashi et al. [82] modelled the system with a saw-tooth profile solid/liquid interface in order to characterize the effects on a non-planar interface on process kinetics. With these more complex models, the nature of assumptions becomes more complex as well, i.e. the size, spacing and orientation of grain boundaries and morphology of the interface must be assumed to be uniform while in reality these parameters are often random.

Modeling results of the dissolution stage show that the time required for dissolution and widening of the liquid to be complete are dependent upon a number of factors, including initial interlayer width (W_o), interlayer composition (C_F) and heating rate from the onset of melting to the bonding temperature (T_b). Thinner interlayers (less than 200 μm) show less dissolution and more tendency to follow the liquidus composition at lower heating rates [44].

Zhou and North [56] compared the one dimensional, fully implicit numerical model output with results of the moving interface analytical analysis given in § 2.2.7. The results show that the interface rate constant during isothermal solidification is equal for both the numerical and analytical solutions. The major difference in the results is in the dissolution and widening stage for which no complete analytical solution exists due to the complexity of variable temperature. In this sense, if the prevailing conditions are such that the dissolution time and width are minimal, i.e. low interlayer solute content and small interlayer width, then the time required for the dissolution stage as a fraction of the total process time approaches zero and can be considered negligible.

In a modeling review of TLP bonding, Zhou et al. [2] point out that the interface kinetics during the isothermal solidification stage can be estimated using an analytical solution so long as the effects of grain boundaries can be neglected. From experimental and modeling results in § 2.3.2, when the grain size is large, the bonding temperature approaches the base metal melting point, and the isothermal hold time is long, the effect of grain boundaries on the process kinetics is minimized. During dissolution, however, no single interface rate constant can be found with an analytical solution and numerical methods are required to characterize solid/liquid interface motion. The dissolution stage is negligible; though, if the time required is sufficiently short.

2.5. TLP Bonding in Ternary Systems

The addition of a second solute to the interlayer complicates the TLP bonding process significantly. The problem can be formulated by considering a pure semi-infinite base metal substrate (A) with a binary eutectic interlayer (B & C). Upon heating, the interlayer will melt and dissolution will occur. It is assumed that the dissolution will occur on a straight line from the initial interlayer composition to the pure base metal composition as shown in Figure 2-13. Thus, the initial liquidus composition will lie at the intersection of this line and the liquid phase boundary on the Gibbs' isotherm for the bonding temperature [70].

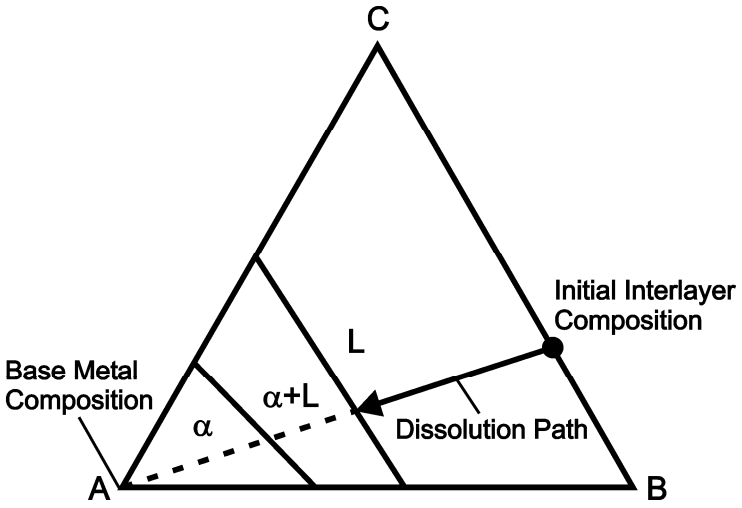

Figure 2-13: Dissolution path of the interlayer. Dissolution is assumed to follow a straight line from the initial composition to the base metal composition [70].

As in the isothermal solidification of binary systems, the mechanism of the process in ternary systems is the diffusion of both solutes across the solid/liquid interface and into the base material. A mass balance can be written for each of the solutes in the system. From Equation 2-13, the mass balance for each solute can be written:

$$\left(C_{L\alpha,B} - C_{\alpha L,B}\right)\cdot\frac{d}{dt}X(t) = D_B \cdot \frac{\partial}{\partial x}C_B(x,t)_{x=X(t)} \qquad \text{Equation 2-98}$$

$$\left(C_{L\alpha,C} - C_{\alpha L,C}\right)\cdot\frac{d}{dt}X(t) = D_C \cdot \frac{\partial}{\partial x}C_C(x,t)_{x=X(t)} \qquad \text{Equation 2-99}$$

Where the concentration gradient in the liquid is assumed negligible, and B and C are the respective solutes.

It is immediately clear that the interface velocities supported by each solute will be the same for only a limited number of cases. Since there can only be one single solid/liquid interface velocity, there must be some mechanism controlling the isothermal solidification behaviour. The Gibbs' phase rule for an isobaric, isothermal system is given by:

$$f = n - p \qquad \text{Equation 2-100}$$

Where *n* is the number of components, *p* is the number of phases, and *f* is the degrees of freedom of the system.

In the binary case there are zero degrees of freedom; however, in the ternary case the additional component affords the system one degree of freedom. This allows isothermal solidification to proceed by way of a shifting liquid composition.

Sinclair et al. [71] have suggested that the interface velocity will be initially controlled by the solute that supports the faster velocity. That is to say that the combination of flux and miscibility gap in Equation 2-98 and Equation 2-99 that results in the fastest interface velocity will govern the kinetics. To maintain the mass balance, the second solute must be partitioned back into the liquid. The composition of the liquid tracks along the liquidus line on the Gibbs' isotherm of the ternary equilibrium phase diagram. Figure 2-14 shows the dissolution path of the interlayer, and subsequent shifting of the tie-line during the isothermal solidification stage in a system with linear phase boundaries. From this theory of isothermal solidification mechanics, there are a number of different situations that can occur, as follows.

1. The composition of the liquid will continually shift until isothermal solidification is complete [71].
2. If a special set of conditions exists in the system, there is a possibility of a "stationary case" where the composition of the liquid will remain constant throughout the isothermal solidification stage [71].
3. In a combination of the previous two cases, the liquid composition may shift until a stationary condition exists [71]. These conditions are history dependent and will not be the same initial conditions that support the stationary case.

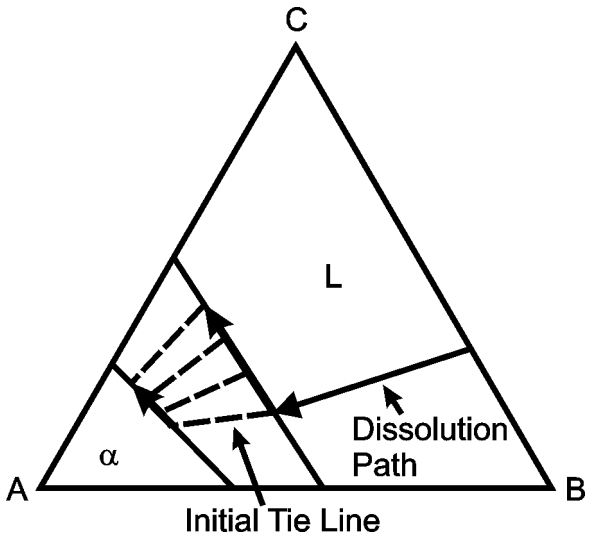

Figure 2-14: Isothermal solidification is expected to proceed via a shifting tie line.

2.5.1. Diffusion in Ternary Alloys

The development of models for TLP bonding in ternary systems requires a review of the theory of multicomponent diffusion in solids. Before solutions to Fick's equations can be explored, the relationship between fluxes and forces must be developed. Experimental data

has shown that relations for heat and electricity are linear, and mass transport follows suit. Thus, it is clear that in this case, the flux of each and every component is related to the chemical potential gradients of all the components. This can be expressed by Equation 2-101 [90]:

$$-J_i = \sum_{j}^{n-1} D_{ij} \nabla C_j \qquad \text{Equation 2-101}$$

where n = 3 for a ternary system, and i = 1,2 for the respective solutes.

Thus, the diffusivities are given in matrix form. The off-diagonal coefficients (D_{12}, D_{21}) are the cross diffusion terms, and are the result of interaction between the individual solutes. In some cases where the cross diffusional effects are negligible, the off-diagonal coefficients can be assumed to be zero and thus, only the on-diagonal terms (D_{11}, D_{22}) define the diffusivity matrix. The consequence of this assumption is that the flux of each solute depends solely on the concentration gradient of that solute.

In ternary diffusion, the *D* coefficients are not unique as they are in a binary system. The values of the coefficients will vary depending on the choice of solvent for the system. Attaching a superscript to the coefficient can identify the solvent. It is possible to derive a relation that allows transformations between solvents [91]:

$$D_{ik}^{m} = D_{mm}^{k} - D_{kk}^{m} = D_{ii}^{m} - D_{ii}^{k} = -D_{im}^{k} \qquad \text{Equation 2-102}$$

These relations have been rearranged into simple transformations by Ziebold and Ogilvie for a ternary system [92]:

$$\begin{aligned}
D_{11}^{2} &= D_{11}^{3} - D_{12}^{3} \\
D_{13}^{2} &= -D_{12}^{3} \\
D_{31}^{2} &= D_{22}^{3} + D_{12}^{3} - D_{11}^{3} - D_{21}^{3} \\
D_{33}^{2} &= D_{22}^{3} + D_{12}^{3} \\
&\text{and} \qquad \text{Equation 2-103} \\
D_{22}^{1} &= D_{22}^{3} - D_{21}^{3} \\
D_{23}^{1} &= -D_{21}^{3} \\
D_{32}^{1} &= D_{11}^{3} + D_{21}^{3} - D_{22}^{3} - D_{12}^{3} \\
D_{33}^{1} &= D_{11}^{3} + D_{21}^{3}
\end{aligned}$$

It should be noted that the selection of the element which will be the solvent in multicomponent systems can be important. Usually the compositionally rich element is chosen as the solvent; however, the solvent should also be neutral. Proper interpretation of the *D* matrix is based on the correct solvent selection; conversely, illogical solvent selection can lead to *D* matrix coefficients that may seem irrational.

Now that the diffusivity matrix, D has been established, Fick's equations for ternary systems can be developed and solved. From Fick's second law for a source free system n-1 independent equations can be developed for an n component system [93]:

$$\frac{\partial C_i}{\partial t} = \sum_{k=1}^{n-1} \nabla D_{ik} \nabla C_k \qquad \text{Equation 2-104}$$

In the special case where concentration gradients are small and D coefficients do not change too much, the average value of D coefficients can be used in the D matrix, giving [90]:

$$\frac{\partial C_i}{\partial t} = \sum_{k=1}^{n-1} D_{ik} \nabla^2 C_k \qquad \text{Equation 2-105}$$

2.5.2. Modeling Isothermal Solidification in Ternary Systems

For a ternary system, there is one degree of freedom; hence, there must be some other rules controlling the system that can be used to predict isothermal solidification behaviour [70]. The constant, ξ (Equation 2-82), is the rate constant that describes the interface movement. If the cross-diffusional effects are assumed negligible, then the rate constant can be found for each solute in the liquid through a mass balance (Equation 2-91).

$$C_{\alpha L} \cdot (k_i - 1) \cdot \frac{\xi_i}{2} = D_i^{\alpha} \cdot \frac{dC_i}{d\lambda}_{\lambda=\xi_i} \qquad \text{Equation 2-106}$$

Where k_i is the ratio of liquidus to solidus equilibrium concentrations for the i^{th} component, and D^{α}_i is the diffusion coefficient in the solid for the i^{th} solute. The solution for the rate constant is given in Equation 2-107, which must be solved numerically [70].

$$\xi_i = -2(k_i - 1)^{-1} \cdot \sqrt{\frac{D_i^{\alpha}}{\pi}} \cdot \frac{\exp\left(\frac{-\xi_i^{\,2}}{4 \cdot D_i^{\alpha}}\right)}{\operatorname{erfc}\left(\frac{\xi_i}{2\sqrt{D_i^{\alpha}}}\right)} \qquad \text{Equation 2-107}$$

If the phase boundaries are assumed linear, then Equation 2-108 can approximate the tie lines on the Gibbs' isotherm [70].

$$\frac{\Delta C_1}{\Delta C_{10}} + \frac{\Delta C_2}{\Delta C_{20}} = 1 \qquad \text{Equation 2-108}$$

The terms in Equation 2-108 are defined in Figure 2-15. The significance of Equation 2-108 is that each and every tie-line on Gibbs' isotherm is defined by this relationship, and k_i is constant. In real systems, the tie-lines are determined by thermodynamic relationships between

the phases at the interface. However, for developing a general understanding of isothermal solidification this simplification is useful.

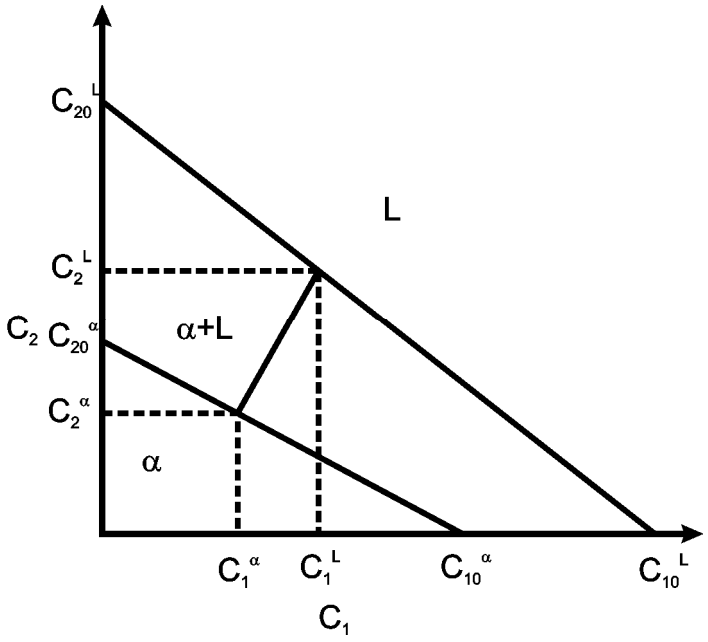

Figure 2-15: Definition of the tie lines as given by Equation 2-107 [71].

By examination, all of the terms in Equation 2-107 are constant for a given temperature. This means that unless all of the solutes have a certain combination of D^{α}_{i} and k_i, ξ_1 and ξ_2 will be different. There is no way that the interface can sustain a different rate of solidification for each solute. The only way to maintain a single velocity of the solid/liquid interface is for the solid and liquid compositions to track along the phase boundary lines [70]. Sinclair suggests that the solidification rate will be initially controlled by the solute with the faster solidification rate [70]. The other solute must partition back into the liquid to satisfy conservation of mass. That is to say that the flux of this solute across the interface is too slow and the concentration in the liquid will increase. As a result, the system will follow one of two possible solidification paths.

The first solidification path is considered for a system with one fast diffusing and one slow diffusing solute. The ratio of the predicted interface velocities for each solute, v_1/v_2, can be used to calculate which direction the interfacial concentrations will follow [70]. If the ratio is greater than one, the liquid will be enriched with solute 2; and if it is less than one, the concentration of solute 1 in the liquid will increase. This is shown in Figure 2-16, where the system starts at one of the arrows and tracks in the direction indicated.

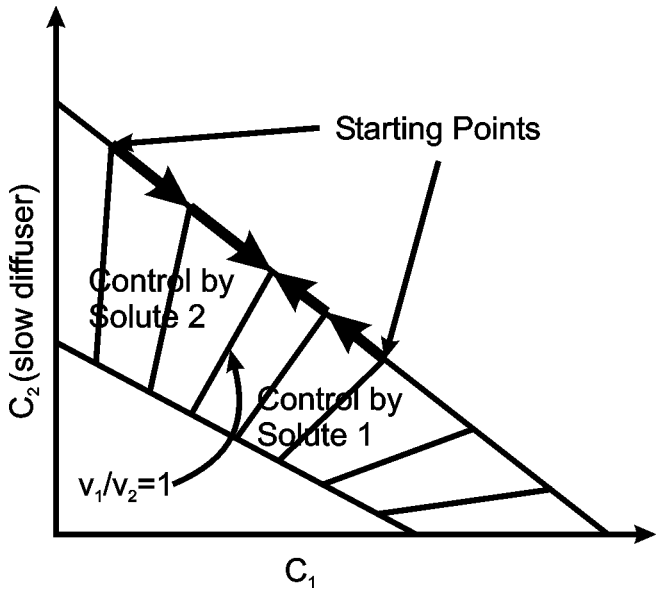

Figure 2-16: Solute control of tie line shift [70].

The second solidification path occurs when a tie line is reached on the Gibb's isotherm that predicts an equal rate of solidification for each solute. At this point, solidification occurs as it would in the binary system with a constant liquid composition [70]. It was shown that Equation 2-107 as given by Sinclair is independent of time and concentration. In this case, the ratio of interface rate constants will be constant across the isotherm and the second solidification path will never occur. In real systems, however, the phase boundaries are not linear and tie-lines cannot be defined by Equation 2-108, so a tie-line may be reached that satisfies equal rate constants for both solutes.

Sinclair proposes a simple iterative model to predict the interface kinetics during isothermal solidification. A Zener diffusion profile [94] in the solid is assumed so a simple mass balance is developed to simulate liquid width shrinkage over a given time for a small increment in the concentration of each solute [70].

$$\left[C_i^{\alpha}\right]_{j+1}\sqrt{D_i^{\alpha} t_{j+1}} - \left[C_i^{\alpha}\right]_j\sqrt{D_i^{\alpha} t_j} = \left[C_i^{L}\right]_j w_j - \left[C_i^{L}\right]_{j+1} w_{j+1} \qquad \text{Equation 2-109}$$

The subscript i=1,2 represents the two solutes, and the subscript j=0…N represents the position of the tie line on Gibb's isotherm. The mass balance for each solute must be satisfied simultaneously. Figure 2-17 shows the mass balanced used in the derivation of Equation 2-109.

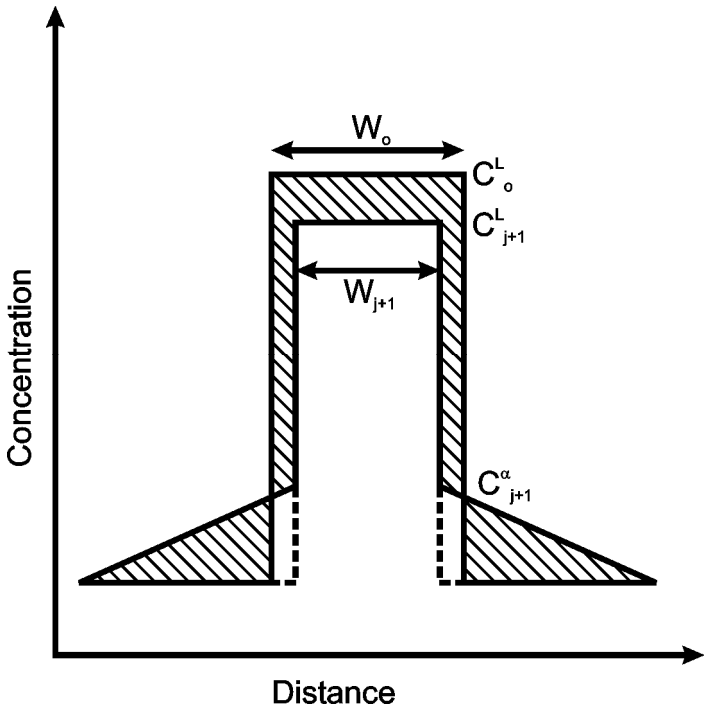

Figure 2-17: Zener approximation mass balance [71].

One weakness of the above numerical model is that it assumes a linear diffusion profile by Zener's approximation [71]. To increase the accuracy of the model, Sinclair et al. use the finite difference approximation for the flux of each solute at the interface (Equation 2-110) in a mass balance to solve for the interfacial concentrations and change in liquid width [71].

$$J_i = \frac{\Delta w}{\Delta t}\left[C_i^L - C_i^\alpha\right]_{t=t} + \frac{w+\Delta w}{\Delta t}\left[C_i^L\right]_{t=t} - \frac{w+\Delta w}{\Delta t}\left[C_i^L\right]_{t=t+\Delta t} \qquad \text{Equation 2-110}$$

Where J_i is the flux of each solute across the interface as defined by Fick's first law, or Equation 2-101. Thus, Equation 2-110 is capable of simulating systems where the effects of cross-diffusion are not negligible. The results of simulations conducted by Sinclair et al. show the importance of the effect of a second solute on the solidification kinetics of the process. The simulation predicts two kinetic regimes during solidification [71]. Figure 2-18 shows the two different solidification regimes modeled for a hypothetical system with $D_1 >> D_2$. The first is a fast regime controlled by the solute that supports the faster interface velocity. The build up of the other solute causes a slowing of the isothermal solidification kinetics and a second regime of motion. This second regime can prolong the solidification stage and even prevent complete isothermal solidification. Good experimental data to confirm the validity of this model is not yet available [71].

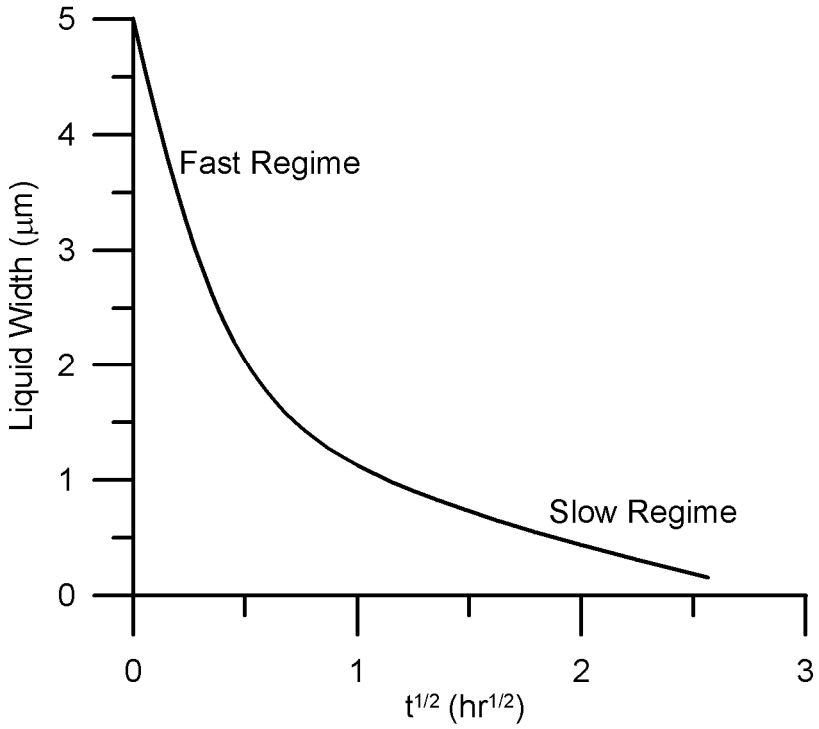

Figure 2-18: Two regimes of interface motion as predicted by the stepwise model [71].

These results can also be used to predict the effect of impurities on the behaviour of binary systems. If even a small amount of impurity is present in the interlayer, complete solidification may not be possible within a reasonable time period.

Purdy et al. [95] modelled the homogenization of multicomponent alloy castings via partial melting using a similar approach. The mass balance used by Purdy et al. [95] (Equation 2-111) is slightly different than that given in Equation 2-110. Inspection of the mass balance equations immediately reveals that the difference between the fluxes is $\Delta w \times ([C^{\alpha}]_{t+\Delta t} - [C^{\alpha}]_{t})$. Neither Equation 2-110 nor Equation 2-111 is incorrect; however, the difference between them is small and can be neglected.

$$J_i = \frac{w}{\Delta t}\left[C_i^L\right]_{t=t} - \frac{w+\Delta w}{\Delta t}\left[C_i^L\right]_{t=t+\Delta t} - \frac{\Delta w}{\Delta t}\left[C_i^{\alpha}\right]_{t=t+\Delta t} \qquad \text{Equation 2-111}$$

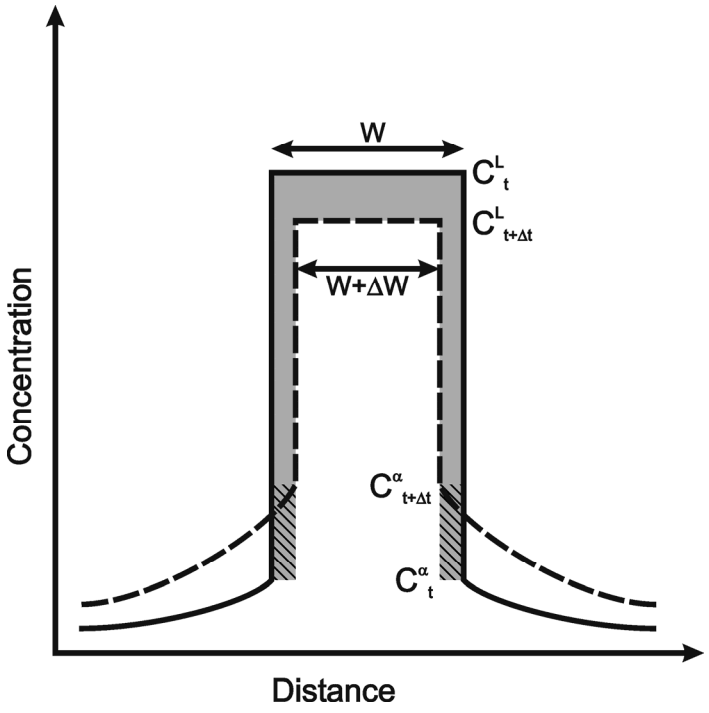

Figure 2-19: Mass balance schematic for isothermal solidification in ternary TLP bonding. The solid area is the amount of solute removed according to Equation 2-110 and the solid plus hatched area is the amount of solute removed according to Equation 2-111.

Ohsasa et al. [96] wrote explicit finite difference equations for each solute diffusant and then solved for the interface position using an iterative procedure and a commercial software package to find the phase boundaries in the Ni-Cr-B ternary system. Constant diffusivities and negligible cross-diffusion effects were assumed. Campbell et al. [97] modelled the Ni-Al-B system using a commercial finite difference software package that accounts for diffusion in multicomponent systems; however, very few details about the simulation are given.

2.5.3. Isothermal Solidification in Ternary Alloy Systems

Very little experimental work has been presented on isothermal solidification kinetics in ternary alloy systems. Bernstein and Bartholomew [10] were the first to consider TLP bonding with ternary interlayers and pure base metals. They conducted brazing trials on a number of TLP bonding systems including Ag/In on Cu, Cu/In on Au, Cu/Sn/In on Cu, Ag/In on Au plated Kovar, and Ag/In on Au or Ni plated Si. In this study, only qualitative observations were made. All bonding was conducted at 300°C for 60 minutes, so the isothermal solidification kinetics of each system could not be compared. It was found that the diffusion rate of Au, Ag and Cu in In decreased in that order.

Wide-gap TLP bonding of 304 stainless steel was investigated by Zhuang and Eagar [40]. In this study, 304L and Ni-20%Cr powders were coated with Ni-10%P and used as interlayers. The resulting ternary system was Fe-Ni-P, although some Cr would also be present in a composition that matched the base metal. Again, the kinetics of isothermal solidification were not studied. Nishimoto and Saida [98] used a multi-objective programming method to optimize the chemical composition of the interlayer to best match the base metal properties in TLP bonding of γ/γ′ type high Al - Ni superalloy. The resulting interlayer was composed of Ni-Cr-B-Ti; however, no attempt was made to optimize the system for isothermal solidification time.

Ohsasa et al. [96] used a simple explicit finite difference scheme to model isothermal solidification in TLP bonding of Ni using a Ni-B-Cr ternary interlayer. A Scheil simulation was used to account for the effects of primary solidification during cooling from T_b. Only one experimental data point was presented for each of the two bonding conditions (1373 K and 1473 K). The experimental result compared with the modeling results but with only one data point, the overall process kinetics cannot be evaluated.

Campbell and Boettinger [97] examined TLP bonding in the Ni-Al-B system using numerical and experimental techniques. In their work, a Ni-10.3%Al base metal was joined using a Ni-10%B foil interlayer at 1315°C. The heating rate was 48°C/min and the typical cooling rate was 300°C/min. Some samples were also quenched in water. The isothermal hold times were 0.25, 0.5, and 1 hour. The process kinetics were determined by visual inspection of a cross-sectioned interface with the average apparent liquid width measured at five locations approximately 100 μm apart. The apparent liquid width was defined as the width of the eutectic phase in the cross section, and was assumed to equal the actual liquid width before cooling in the water quenched samples. In the slowly cooled samples, the apparent liquid width was about 25% less due to primary solidification during cooling.

The modeled results compare reasonably well to the experimental for both the quenched and slow cooled tests; however, it is important to note that the thermodynamic and diffusion data used in the numerical analysis was modified in order to best fit the data. This was done to improve the model accuracy to account for limited and inaccurate data. The limited number of experimental test points (i.e. three different isothermal hold times) is not sufficient to completely characterize the isothermal solidification kinetics when non-linearity is expected. The authors point out that the accuracy of the model is limited by the assumed diffusion mobility and thermodynamic description of the system. Furthermore, the material system selection complicates matters since both the base metal and interlayer are binary alloys with the common element being Ni. Upon dissolution of the interlayer, enrichment of the liquid in Al is expected to occur while B is diffusing into the base metal. When the homogeneous liquid solution is saturated in Al, the system would be expected to act similar to the binary Ni-B case.

This is reflected in the results, where the liquid width tends to be linearly proportional to the square root of the isothermal hold time.

There has been no comprehensive study of the isothermal solidification kinetics in ternary alloy system.

2.6. Differential Scanning Calorimetry (DSC)

Differential scanning calorimetry (DSC) is a thermal analysis tool designed to compare thermal events of a sample to a reference. Thermal analysis is an analytical method based on three elements, the sample, heat, and the signal. The definition of thermal analysis also includes measurement of the property with time under isothermal conditions [99]. The measurements are given as thermal analysis curves whose features can be related to thermal events.

DSC is a variation of differential thermal analysis (DTA). In DTA, the temperature difference, ΔT, is measured between a sample cell and a reference cell. Both the sample and the reference cells are subjected to the same temperature program. A thermal event in the sample cell will induce a temperature difference given by Equation 2-112 [99], where T_s is the temperature of the sample and T_r is the temperature of the reference.

$$\Delta T = T_s - T_r \qquad \text{Equation 2-112}$$

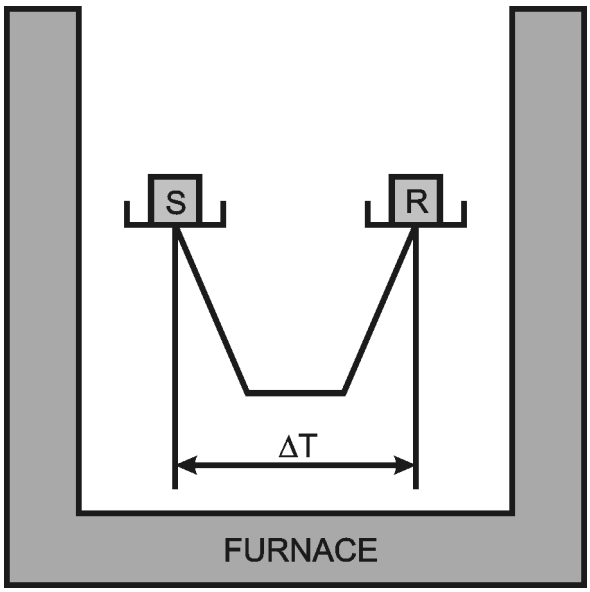

Figure 2-20: DSC operational schematic.

If the event is endothermic, such as melting, the temperature of the sample will lag behind that of the reference, and ΔT will be negative. If the event is exothermic, such as freezing, the

opposite will be true and ΔT will be positive. The measurements can be plotted as a function of T_r with the sense of ΔT clearly marked. A peak in the endothermic direction is called an endotherm, and conversely an exothermic peak is an exotherm. The endotherms (or exotherms) are characterized by the onset temperature and the area under the peak. The area is related to the enthalpy change (ΔH) for the event.

The material in the reference cell should have the same thermal conductivity and heat capacity characteristics as the sample cell; however, it should not undergo any thermal events over the temperature program or react with the sample holder [99].

The signal that is measured is generated by thermocouples. In classical DTA the thermocouples are placed within the sample holder, next to the sample or reference material. In "heat-flux" DSC, the samples are placed on top of a conductive base with the thermocouples attached. The advantage of this set-up is that the measurement is not as dependent on the thermal properties of the sample; however, the response will be slower [99].

The principle of operation of the heat-flux DSC can be explained using the following equations. Equation 2-113 gives the heat flow into the sample holder as governed by Newton's law where R is the thermal resistance, T_h is the heat source temperature, and T_{sm} is the measured sample temperature [99].

$$\frac{dq_s}{dt} = \frac{1}{R} \cdot \left(T_h - T_{sm}\right) \qquad \text{Equation 2-113}$$

Similarly, for the reference side:

$$\frac{dq_r}{dt} = \frac{1}{R} \cdot \left(T_h - T_{rm}\right) \qquad \text{Equation 2-114}$$

In the absence of thermal events, the heat flow into the sample side will heat both the sample monitoring station and the sample (including holder). This is given by Equation 2-115 where C_{sm} is the heat capacity of the monitoring station, and C_s is the heat capacity of the sample and holder [99].

$$\frac{dq_s}{dt} = C_{sm} \cdot \frac{dT}{dt} + C_s \cdot \frac{dT}{dt} \qquad \text{Equation 2-115}$$

And accordingly for the reference side:

$$\frac{dq_r}{dt} = C_{rm} \cdot \frac{dT}{dt} + C_r \cdot \frac{dT}{dt} \qquad \text{Equation 2-116}$$

Using Equation 2-112 through Equation 2-116, the measured signal in the absence of thermal events is given by:

$$\Delta T = T_{rm} - T_{sm} = R \cdot \frac{dT}{dt} \cdot (C_s - C_r) \qquad \text{Equation 2-117}$$

Thus, in the occurrence of a thermal event, Equation 2-117 will be modified such that the total area of the endotherm or exotherm is related to the enthalpy change, ΔH, by:

$$\Delta H = A \times K \qquad \text{Equation 2-118}$$

Where A is the area of the endotherm or exotherm, and K is a calibration constant generated by measurement of a known enthalpy change. The thermal resistance, R, is temperature dependent and is compensated for by the DSC controller, which gives the measurement output in units of power. The calibration of the DSC is completed manually through the use of calibration standards.

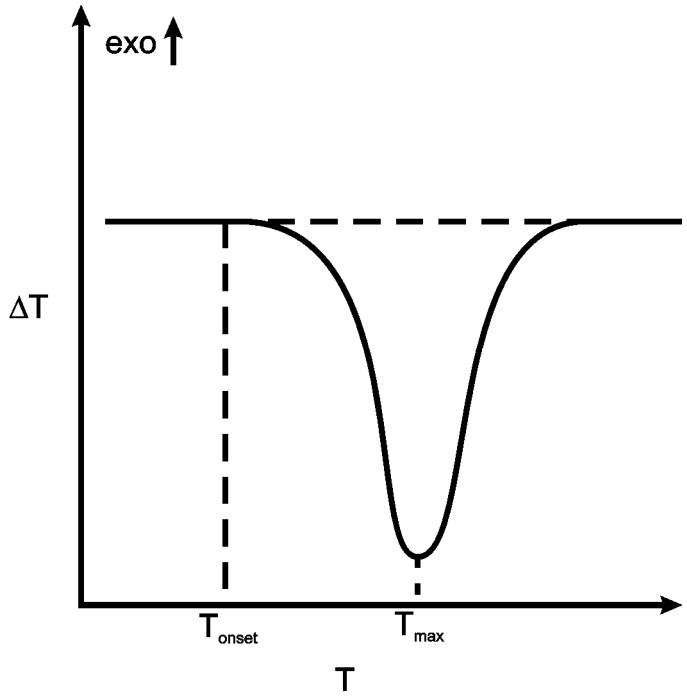

Figure 2-21: Temperature difference between sample and reference cell showing an endothermic event.

Measurement of the area under an endotherm or exotherm requires a straight, horizontal baseline. The DSC trace will not return to the original baseline after a thermal event if the total heat capacity of the sample has changed during the event. In this case, the area must be measured by establishing an approximate baseline.

A correction file can be used to reduce baseline drift (sloping baseline) that is inherent in the system. The correction file is created by running a DSC trial with the desired temperature program; however, without the sample. When the DSC sample is run, the controller subtracts the correction file from the data. The result is a horizontal baseline instead of one that drifts.

It has been shown that the DSC is capable of quantifying enthalpy change during changes of state. When the latent heat of fusion for a material is known, DSC results can be used to determine the mass of material involved in the melting or solidification. It is immediately clear that this measurement tool has potential in characterizing the process kinetics of isothermal solidification during TLP bonding. Corbin and Lucier [15] have successfully developed a technique for measuring the extent of isothermal solidification in the transient liquid phase sintering process. From this seminal work, an experimental method applying DSC to TLP bonding has been developed.

2.6.1. Using DSC to Measure Interface Kinetics

The measurement of isothermal solidification kinetics using DSC was first reported by Venkatraman et al. [77] in a study of TLP bonding Au-Sn layers electroplated on Cu foils. TLP "half-samples" were electroplated on a Cu substrate. A 6 μm Au layer formed the base metal with a 2 μm Sn layer added for the interlayer. A 1 μm Au top coat was added to prevent Sn oxidation, bringing the total Au thickness to 7 μm. Venkatraman et al. [77] found that the liquid was formed in-situ through a reaction between intermetallic layers that formed during heating. The bonding temperature (T_b) was 295°C, well above the eutectic temperature of 280°C. A 10°C/min heating rate and 20°C/min cooling rate was used.

The isothermal solidification rate was determined by measuring the amount of liquid remaining after an isothermal hold period of varying lengths. The fraction of liquid was determined by comparing the melting endotherm and solidification exotherm of an isothermal hold sample. There are, however, some serious problems with this study. The amount of liquid formed was found to be equal to the eutectic melted, even though the bonding temperature was 15°C above the eutectic and additional base metal dissolution is expected to occur. Likewise, the amount of liquid after isothermal hold time was taken to be equal to the eutectic liquid solidified even though a cellular interface morphology indicative of primary solidification was observed.

The results are presented as the fraction of liquid remaining as a function of the square root of time above the eutectic temperature. A linear fit of the results does not extrapolate to unity on the ordinate axis. This irregularity was attributed to a lack of experimental data at short isothermal hold times. Additional data was acquired at lower temperatures with faster heating and cooling rates that extrapolates closer to unity but this data is not comparable because of the different parameters. The gold layer was also too thin to be considered infinitely thick and this was thought to reduce the process kinetics as Sn accumulated in the base metal; however, this effect seems to be overemphasized since the Sn would still diffuse into the Cu base metal and the net effect would depend on relative Sn diffusion rates in each substrate. Despite the problems with the results, Venkatraman et al. [77] were still able to extract an effective

diffusivity from the results that was said to account for bulk diffusion as well as grain boundary effects. This effective diffusivity was then compared to the results of analytical modeling [62]. It is clear that there is little value in such a comparison since there are serious unresolved problems with the results.

Corbin and Lucier used DSC to measure the isothermal solidification kinetics during TLP sintering [15] of Pb powder using a Pb-Sn eutectic powder. TLP sintering is similar to wide-gap TLP bonding in that a powder substrate is surrounded by a liquid rich in a melting point depressant solute. The isothermal hold temperature was just above the eutectic; however, some base metal dissolution was observed in the DSC results. It was assumed that all liquid formed a eutectic phase upon cooling; thus, no primary solidification took place. The results do not follow the linear square root relation observed in TLP bonding in binary systems because the solid/liquid interface is not planar.

2.7. Solidification Theory

2.7.1. Mechanism of Isothermal Solidification

It has been reported that the solidification process during isothermal solidification is epitaxial in nature [64,100]. Epitaxial solidification is the growth of solid on an existing solid substrate in which the solidifying material is clearly derived from the grains of the base metal [101]. The crystallographic orientation of the new solid is the same as the substrate. The heterogeneous growth of a solid is governed by a balance of the surface energies between the base metal and liquid (γ_{ML}), the solidifying metal and liquid (γ_{SL}), and the base metal and solidifying metal (γ_{SM}). In TLP bonding, the liquid is very similar in composition to the base metal, so a balance of the surface energies (Equation 2-119) can be simplified by the assumption of $\gamma_{SM} = 0$, and $\gamma_{ML} = \gamma_{SL}$ [101]. From this, the wetting angle, $\psi = 0$ and there is a negligible barrier to solidification at the solid/liquid interface.

$$\gamma_{ML} = \gamma_{SM} + \gamma_{SL} \cdot \cos\psi \qquad \text{Equation 2-119}$$

There is very little in the literature about the mechanism of isothermal solidification; however, Tuah-Poku et al. [39] suggest that the growth is likely to involve ledge-type migration. The growth of an atomically smooth surface is unstable if a single atom arrives at the surface but if the interface contains ledges with jogs, solidification can proceed without any increase in interfacial energy [102]. Screw dislocations can serve as sources for ledges and result in spiral growth. Likewise, twin boundaries are a permanent source of steps providing easy growth.

2.7.2. Epitaxial Solidification During Cooling

Upon cooling after the isothermal hold period, the residual liquid solidifies athermally. The composition of the liquid at the start of cooling will be $C_{L\alpha}$. Solidification is expected to follow that of an off-eutectic alloy. It can be shown that the activation energy barrier against heterogeneous solidification is lower than that of homogeneous nucleation [102]. Thus, initial solidification of the primary phase is expected to be epitaxial in nature.

The mode of primary solidification in an alloy depends on a number of factors including the cooling rate and solute diffusivity. Under equilibrium conditions, or infinitely slow solidification, the relative amount of liquid at any temperature is given by the lever rule. Complete solute redistribution in the solid and liquid occurs by diffusion. If the bulk liquid composition before cooling is greater than the maximum solute solubility, then the amount of eutectic formed will be given by the lever rule. This solidification mode was assumed by Nakao et al. [61] and MacDonald and Eagar [68] when converting the eutectic width to the actual liquid width at the cooling onset.

In reality, the cooling rate is too high to allow a homogeneous solid composition by diffusion. In this case, diffusion in the solid can be considered negligible and the liquid is assumed either homogeneous (perfect mixing) or diffusional mixing only. In the first case, the liquid fraction that solidifies as eutectic can be found using the Scheil equation [102]. This assumption was used by Ohsasa et al. and Campbell and Boettinger [97,96] to model the primary solidification during cooling from T_b.

In the second case, a bow wave of solute is built up ahead of the solidifying interface as the rejected solute is redistributed by diffusion into the liquid and the solidifying solid has the composition $C_{L\alpha}$.

The actual solidification mode will be a combination of the three cases with some solute diffusion in the solid and a combination of mixing and diffusion in the liquid. Since the liquid is close to quiescent, mixing will be very limited. Solute diffusivity in the liquid and the solidification rate will be important in determining the growth of the primary phase and, by extension, the amount of eutectic formed.

It has been shown that if the growth rate of the solid is fast enough, the alloy can solidify with a microstructure that appears as 100%; however, the actual composition is closer to $C_{L\alpha}$ [102]. This was observed by Saida et al. [74] when studying the effect of cooling rate on the apparent liquid width.

Zhou et al. [100] have shown that because the mechanisms of isothermal and athermal solidification are both epitaxial, it is impossible to differentiate between the solidified material in order to find actual liquid width after an isothermal hold. Clearly, the conditions for which solidification occurs during cooling from the bonding temperature to the final eutectic

solidification are important in understanding the significance of the apparent (eutectic) liquid width.

2.7.3. Interface Morphology

It has been shown that the non-planar nature of the eutectic interface creates difficulty in measurement of an average width [39,68]. The effects of grain boundary grooving have already been discussed (§ 2.3.2); however, the formation of cells resulting in a scalloped interface with cusps away from the grain boundaries has been noted [68,100]. The formation of the cells is a result of a breakdown in the solid/liquid interface during cooling. It has been shown that there is some undercooling during eutectic solidification in TLP bonding [100]. This undercooling can result in an inherent instability of the solid/liquid interface and result in the formation of protrusions that can develop into cells as a result of improved removal of the latent heat of fusion and constitutional supercooling [102].

3. Experimental Methods

3.1. Material Systems

3.1.1. Ag-Cu Binary System

A primary objective in this study was to develop and validate the experimental method for using DSC to quantify metallurgical interactions in a solid/liquid diffusion couple. With the study criteria outlined in § 1.4 in mind, the materials employed for this objective were selected based on the following criteria.

1. The elements must form a simple binary eutectic with a eutectic temperature within the operating range of the DSC (1500°C).
2. There should be no stable intermediate phases between the eutectic composition and the solubility limit of the solvent (base material).
3. The diffusivity of the solute in the solvent must not be too low.
4. The solubility of the solute must not be too low so as when considered together with the diffusivity, the time required to isothermally solidify any liquid becomes unreasonably long (on the order of days).
5. The components must not be too reactive in air so that no tenacious oxide layers form on the faying surfaces requiring significant pre-bond cleaning.
6. The selected MPD interlayer must be widely available in thin foils, around 25 μm, and at a reasonable cost.
7. Accurate diffusivity and phase diagram data must be available.
8. Previous work on TLP bonding process kinetics in the same material system would be advantageous.

Based on the selection criteria, the best system for experimental DSC work was found to be the silver (Ag) – copper (Cu) binary system. From the binary equilibrium phase diagram for Ag-Cu (Figure 3-1), these elements form a simple binary eutectic at 780°C and 28.1 wt. % Cu. Based on the partition coefficients and diffusivity data, Ag was initially selected for the base material, and Cu was selected for the MPD solute since this is expected to minimize the time required for isothermal solidification to be completed.

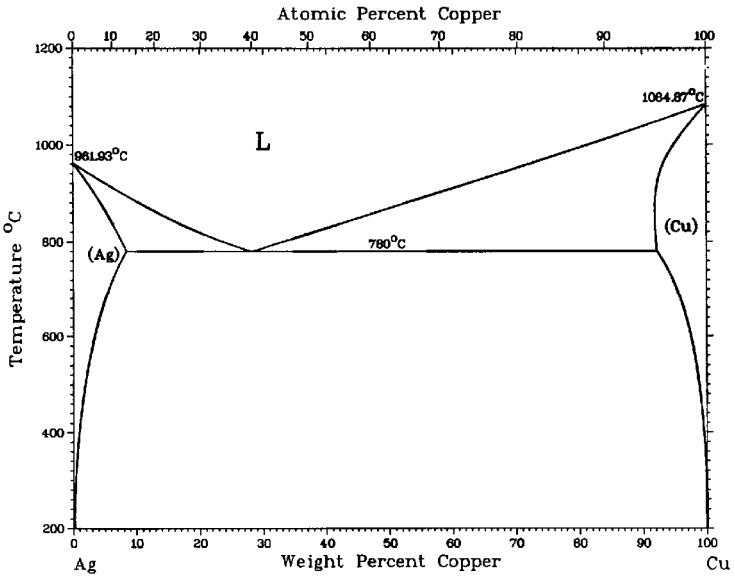

Figure 3-1: Ag-Cu binary equilibrium phase diagram [103].

The precious metal, Ag, can be considered noble under the conditions in this study. There will be no stable oxides that form in the temperature range of interest, although Ag will oxidize in air, the oxidation reaction is reversed at temperatures above 468 K following the reaction: $2Ag_2O_{(s)} \rightarrow 4Ag_{(s)} + O_{2(g)}$. Ag will tarnish in time due to the formation of the sulphide Ag_2S. To prevent the Ag from tarnishing, the materials were stored in a N_2 environment away from possible sources of S such as rubber products.

Previous work on TLP bonding in the Ag-Cu binary system has been completed by Tuah-Poku et al. [39] and MacDonald and Eagar [7]. This work, which includes modeling as well as experimental (non-DSC) techniques, will assist in the development and validation of an experimental method and will be useful in the discussion of the results.

Two interlayer foils were used in the development of an experimental method. A 10 μm thick Cu foil with a purity of 99.8 % was obtained from Alfa Aesar, and an Ag-Cu eutectic (Ag-28 wt. % Cu) foil that had a purity of 99.99 % and a thickness of 25 μm was obtained from Lucas Millhaupt. The pure Ag base material was purchased from Alfa Aesar in the form of a 5 mm diameter rod with a purity of 99.95 %. The commercial availability of interlayer and base metal materials made preparation of the samples significantly easier.

3.1.2. Ag-Au-Cu Ternary System

Ag-Au-Cu system, an extension of the Ag-Cu binary system formed with the addition of an additional solute. This alloy system was used for ternary TLP bonding DSC experiments. The liquidus projection is shown in Figure 3-2 and the Gibbs' isotherm at 800°C is shown in Figure

3-3. There is a eutectic trough that runs from the Ag-Cu eutectic down to the ternary Ag-Au-Cu ternary eutectic point. This results in a liquid solubility loop formed by the phase boundaries of the Gibbs' isotherm at 800°C that runs from the Ag-Cu base line out past the ternary eutectic point. Inspection of the Ag-rich corner of the isotherm shows that the solidus phase boundary decreases in Au with a decrease in Cu. This system does not fit the paradigm constructed for isothermal solidification in ternary systems where a decrease in one solute results in an increase in the other via tie line shifting. Thus, the results of a study into the isothermal solidification kinetics are potentially interesting. This system was chosen, however, because of the absence of intermetallic compounds at the temperature of interest. The resulting analysis of interface kinetics is simplified.

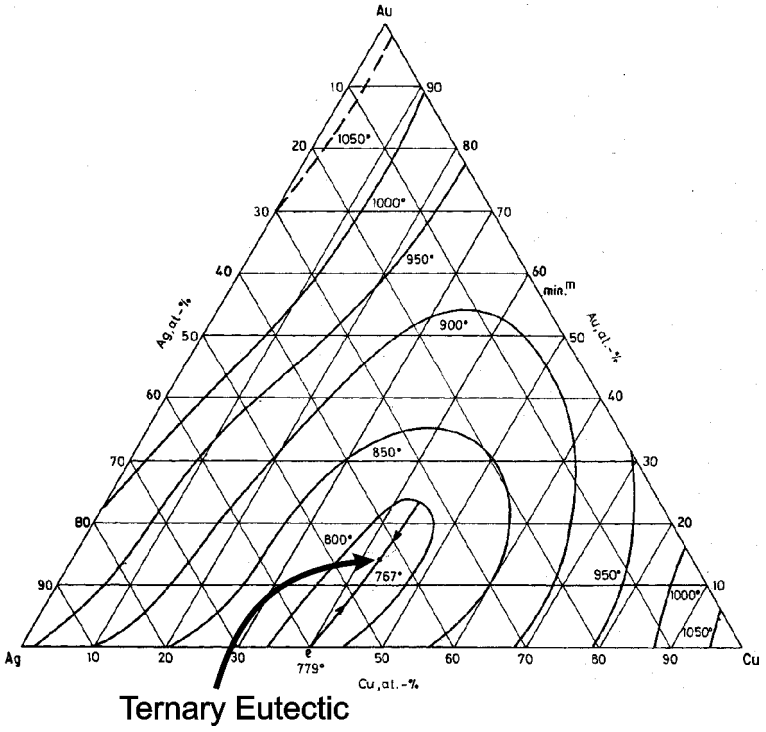

Figure 3-2: Ag-Au-Cu ternary liquidus projection [104].

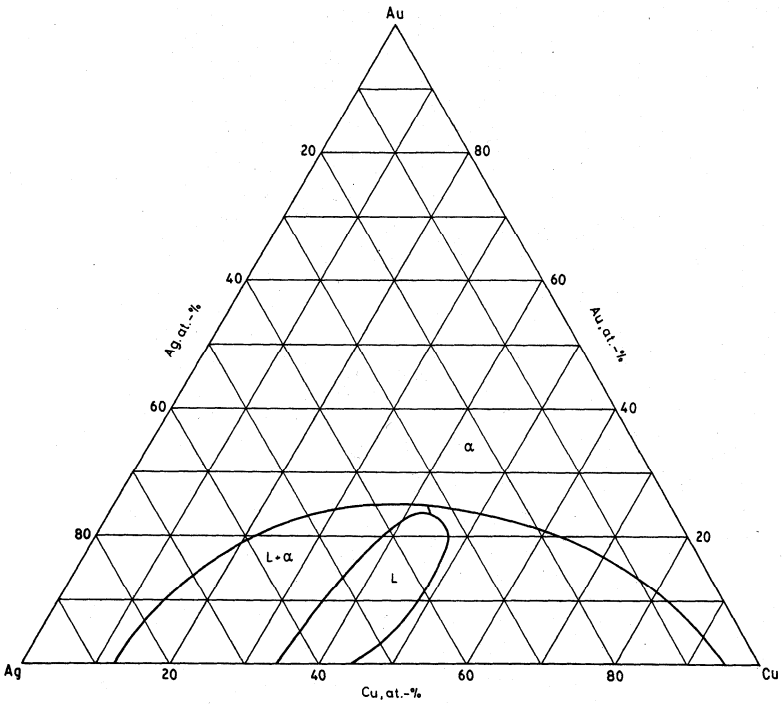

Figure 3-3: Gibbs' isotherm at 800°C for Ag-Au-Cu ternary phase diagram [104].

3.2. Sample Preparation

3.2.1. Ag and Cu Base Metal Fabrication

The Ag base metal was obtained from Alfa Aesar. The Ag was supplied in 5 mm diameter rods. The purity of the Ag is 99.99%. The Cu base metal with a purity of 99.999% was also supplied by Alfa Aesar. Right cylinders with a nominal height of 3 mm were cut from the Ag rods using a Struers Accutom metallurgical cut-off saw and the Accutom aluminum oxide wheels (0.5 mm thick).

The faying surface of each base metal cylinder was ground flat. Approximately eight samples at a time were mounted in black bakelite for the grinding operation. The samples were ground from 150 grit to 1200 grit silicon carbide sandpaper in increasingly fine steps. This operation is required to ensure a uniform, flat surface with consistent roughness from sample to sample. Another function of the grinding is to remove the burr that forms from the abrasive cutting operation used to prepare the cylinders. When the grinding operation is complete, the samples were broken from the bakelite using a bench vice. Each base metal sample was cleaned ultrasonically in acetone for 10 minutes following the grinding operation to remove any impurities or debris (e.g. SiC particles) remaining to ensure a clean faying surface.

3.2.2. Interlayer Foil Preparation

The interlayer foils were prepared using a variety of methods depending upon the commercial availability of finished product or raw materials. Pure Cu and the Ag-Cu eutectic foils are widely available and easily processed. Discs with a diameter of 5 mm were prepared by punching the foil with a custom made punch. The foil discs were then weighed using an analytical balance.

When the desired foil composition was not commercially available, the foils were fabricated using a miniature rolling mill. An ingot was first cast from pure powders mixed in the desired proportions. The powder mixture was melted in an alumina crucible with the DSC and resolidified into a homogeneous mixture. The resulting ingot was then formed into a flat disc using a hydraulic press. The flat disc was then rolled into a thin foil in a series of steps. Typically, a 50% reduction was attained at each rolling step. Each step was followed by a recovery anneal at a temperature near $0.5T_m$ (half the melting point of the foil). When the desired foil thickness was achieved, foil discs were punched from the foil and weighed.

3.2.3. Base Metal Coating

All sides of the base metal substrate except the faying surface were coated with a ceramic stop-off. This is designed to prevent the molten interlayer from wetting any surface of the sample other than the interface in order to maintain an assumption of planar geometry. The coating was applied by an alumina (Al_2O_3) spray. The spray was supplied by Alfa Aesar.

3.3. DSC Experimental Setup

3.3.1. Equipment

The equipment used for all solid/liquid diffusion couple experiments was a NETZSCH 404C Pegasus DSC. The system is comprised of a DSC measurement cell, controller, computer, vacuum system, power supply, and shielding gas supply and delivery system. These systems are integrated to enable processing, data collection, and data analysis. A photograph of the system is shown in Figure 3-4.

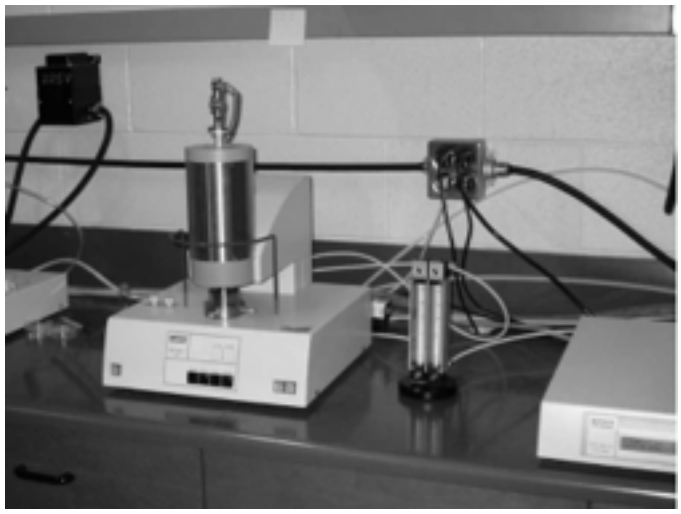

Figure 3-4: Differential scanning calorimeter.

The measurement unit is a tube furnace with a thermal analysis measurement head located in the hot zone. The maximum temperature of this model is 1500°C. The heating rate range below 1200°C is 0.1 to 50°C/min. The measuring head used is a DSC-Cp model with a type-S thermocouple (Pt – 10% Rh vs. Pt). The maximum temperature of the measuring head is 1650°C. Specific heat can be measured accurate to ±2.5%, and the enthalpy determination is ±3.0%. The reproducibility of the system is < 1.5% for enthalpy changes and < 0.3 K for temperatures below 1000°C. The baseline reproducibility is < ±2.5 mW. The sample carrier system consists of a measurement head supported by an alumina capillary on which radiation shields are mounted. The capillary is covered by a protective tube and anchored to the DSC by the plug.

Temperature control and signal acquisition is achieved by the TASC 414/3A TA system controller. The functions of the controller are temperature control, temperature linearization, data acquisition, and measurement range switching. The system controller can program up to 64 temperature segments with a time range of 1 minute to 100 hours. The TASC 414/3A is equipped with a sample temperature controller (STC), with this feature the sample temperature is included in the furnace control which minimizes the difference between the nominal and sample temperatures. Adjustment is based on PID control. The data acquisition resolution is ±20 000 digits with a data acquisition rate of 20/s. The sample temperature resolution is 0.1°C with an accuracy of better than 0.5°C.

Experimental setup is accomplished through the personal computer (PC). The system is based on a Pentium 133 MHz processor with 64 MB of RAM. An IEEE 488 interface is used for communication between the computer and system controller. The operating system is Microsoft Windows 98 SE. Experimental setup is programmed using the NETZSCH DSC

specific software and data analysis is accomplished with the NETZSCH Thermal Analysis Version 3.6 software.

Shielding gas flow is controlled through an internal solenoid in the DSC measurement cell, and a manual flow control. The flow is measured using an external flow meter which is inline with the gas flow. The nominal gas flow rate was 150 ml/min. Gas pressure is restricted with a two-stage regulator mounted on the gas supply bottle. High purity N_2 (99.998% pure) was used for shielding in all cases, the gas was supplied by Praxair.

The sample and reference materials are contained in crucibles. Alumina (Al_2O_3, or corundum) crucibles were used for the DSC experiments. While not ideal for thermal analysis because of the conductive properties, the alumina crucibles are not dissolved by the melt and are thus safe to use in this application. Metal crucibles, although superior for thermal analysis, are not suitable because they may be dissolved, for example, if Al was used for a crucible material, it would be dissolved by Ag and the crucible would melt resulting in extensive damage to the instrument. Alumina lids were also used.

The alumina crucibles are reusable and were cleaned after every sample run. The crucibles were soaked in a warm aqua regia solution for at least 30 minutes before being rinsed with distilled water. The crucibles were then cleaned ultrasonically in acetone for 30 minutes and rinsed again with distilled water. This was followed by a baking operation during which the crucibles were heated to 1500°C and cooled.

The bottom of the inside of the crucibles was coated with a thin layer of alumina lubricant supplied by Alfa Aesar. The function of the lubricant was to prevent sticking of the diffusion couple to the bottom of the crucible. The lubricant was applied manually through a spray operation. With the nozzle of the aerosol container about 18 inches above the crucible, a short (~0.5 seconds) spray was directed into the crucible. The lubricant coating was examined visually for uniform application.

3.3.2. TLP Half-Sample Setup

The typical joint geometry of a TLP bond is not suitable for DSC work. The base metal that would be placed at the bottom of a crucible has a dampening effect on the signal generated at the joint interface. The sensors (i.e. thermocouples) are located in the measuring head, below the crucible. Thermal events, such as melting and solidification occur at the joint interface, well away from the measuring head. The enthalpy of reaction must be conducted across the width of the base metal which also acts as a heat sink. The result is that the magnitude of the endotherm or exotherm is reduced to such an extent that it cannot be measured.

To keep the area of interest close to the measuring head, a TLP half-sample can be used. A TLP half-sample is one half of a TLP bond divided by the joint centerline. Since one half of

the joint is a mirror of the other, the use of a TLP half-sample is not expected to have an effect on the process kinetics of isothermal solidification.

The TLP half-sample is similar to a solid/liquid diffusion couple with a thin liquid film on an infinite solid substrate. The diffusion couple is arranged in the sample crucible with the foil interlayer at the bottom and the base metal on top. The faying surface of the base metal is in intimate contact with the foil interlayer. The sample crucible is loaded into the sample carrier in the DSC measurement cell. At this point the sample is ready for heating. The experimental setup of the sample cell is shown schematically in Figure 3-5.

A slug of base metal is added to the reference crucible. The reference mass is comparable to that of the base metal in the sample cell. The thermal characteristics of the reference cell are very similar to that of the sample cell, with the exception of the interlayer presence.

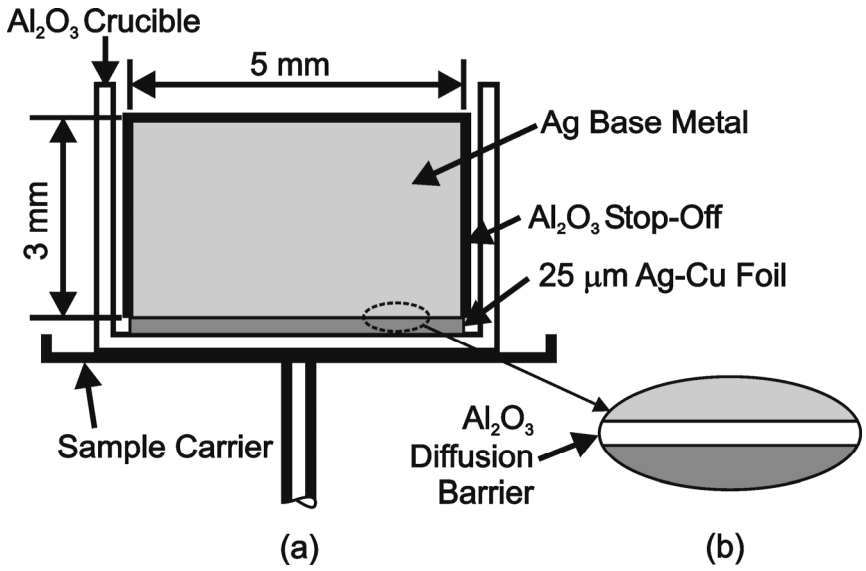

Figure 3-5: (a) Setup of diffusion couples in the sample crucible in DSC, and (b) type-1 variation showing diffusion barrier placed at the faying surface [57].

3.3.3. DSC Operation

The sample and reference crucibles are loaded into their respective spaces on the measurement head. The DSC furnace is then lowered into position. The chamber is purged of air using the mechanical vacuum pump with the gas exhaust valve in the closed position. The DSC is backfilled with N_2 gas, and the purge cycle is repeated again to ensure the atmosphere is as inert as possible.

The DSC system controller is programmed using the DSC specific software on the PC. Before the solid/liquid diffusion couple can be run, a correction file has to be created. The function of the correction file is to remove the background effects from the DSC results.

Positioning of the measurement head in the furnace and differences in thermal properties between the reference and sample cells can induce baseline drift in the DSC trace. If the measurement head is positioned slightly off-center, one of the cells will be closer to the furnace element and tend to run hotter, this will result in a deviation of the baseline from the horizontal norm (i.e. drift). Reference to Equation 2-117 shows how thermal properties affect the baseline under changes in the heating rate. Differences in heat capacity (C_s and C_r) as well as the thermal resistance of the cells can induce a hysteresis in the DSC trace. The correction file is generated using the same temperature program as will be used for the solid/liquid diffusion couple. For the correction file, the base metal is included in both the sample and reference crucibles. In conventional DSC experiments, the sample and reference cells are empty for the correction run; however, the addition of the large mass of base metal will significantly influence the thermal properties of the cell. Hence, the base metal is included in the correction run. The setup and execution of a DSC trial is similar for correction and sample files.

The foil interlayer mass is measured with a Scientech SA 210 analytical balance with a resolution of 0.1 mg. The measured foil mass is entered in the sample mass field on the setup screen. For a correction file, this field is blacked out. The reference mass field is left zero because the base metal in the reference crucible has already been included in the correction file.

The temperature profile is programmed next. The initial conditions are a temperature of 20°C with the shielding gas turned on. The heating and cooling segments are programmed using the dynamic option by specifying heating rate and final temperature. Isothermal segments are programmed with the isothermal option by specifying the hold time. The data acquisition rate has to be specified for each segment. For dynamic segments the acquisition rate of 40 points/min was used. Since the isothermal segments are not used in the analysis, a reduced rate of 10 points/min was usually used. In some cases where the isothermal period was very long, a data acquisition rate of 10 points/min would result in a data file that was too large and a reduced rate had to be used. This was a function of the control software.

The DSC trial is started automatically using the control software. When positive pressure inside the DSC furnace has been established (i.e. shielding gas has begun to flow), the gas exhaust valve is manually turned to the open position. This enables the dynamic flow of N_2 shielding gas and prevents the backfill of air into the chamber where some residual vacuum still remains after the purge operation. When the DSC trial is completed, the sample is removed from the sample cell and visually inspected using the optical stereo microscope to check for uniform wetting of the liquid on the solid only at the faying surface, and inspect for any other defects or inconsistencies.

3.3.4. DSC Temperature Programs

Table 3-1 summarizes three types of experiments that were developed for this project. In the first type, an Al_2O_3 diffusion barrier (shown schematically in Figure 3-5(b)) is applied to the faying surface to prevent metallurgical interaction between the base metal and the liquid. In this case, the melting and solidification characteristics of the foil can be observed in the presence of the base metal but without association. Since there is no interaction with the base metal, isothermal solidification will not occur and there is no reason for an isothermal hold period between the heating and cooling segments. The second type of experiment is the basic diffusion couple with a standard heating and cooling segment separated by an isothermal hold period. The temperature program is modified in the third type of experiment to include a heating/cooling cycle before and after the basic temperature program. The temperature programs used in this study are shown graphically in Figure 3-6.

Table 3-1: Setup and corresponding temperature program for the 3 types of DSC experiments.

Type	Description	Setup	Temp. Program
1	w/ diffusion barrier	Figure 3-5 (b)	Figure 3-6 (a)
2	basic w/o diffusion barrier	Figure 3-5 (a)	Figure 3-6 (b)
3	modified temp. program	Figure 3-5 (a)	Figure 3-6 (c)

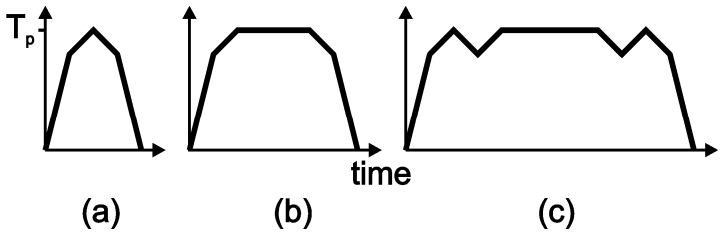

Figure 3-6: Temperature programs: (a) no isothermal hold time; (b) isothermal hold of varying lengths of time; (c) additional thermal cycle before and after isothermal hold.

3.4. Analysis of DSC Results

Analysis of the DSC results was conducted using the NETZSCH Thermal Analysis software Version 3.6. The DSC trace is given as a function of heat flow with respect to time. A typical DSC trace of a solid/liquid diffusion couple with a one hour isothermal hold time is given in Figure 3-7. The solid line shows the heat flow results with the temperature represented by the broken line in the background. Following the conventions used in DSC thermal analysis, the exothermic direction is down. The temperature segments in Figure 3-7 have been labeled *A* through *E*. Segments *A* and *B* are heating segments, *C* is the isothermal hold, and segments *D* and *E* are the cooling segments.

The DSC trace corresponds to the respective temperature segment. The initial segment (*A*) on the DSC trace shows a significant amount of noise and baseline drift during the early stages of heating as a result of the high heating rate employed. Similarly, segment E shows a drastic baseline drift resulting from fast cooling. The heating and cooling rate is decreased in segments B and D and the corresponding baseline is much more stable. Segment C is the isothermal hold period and the DSC trace does not show any interesting features.

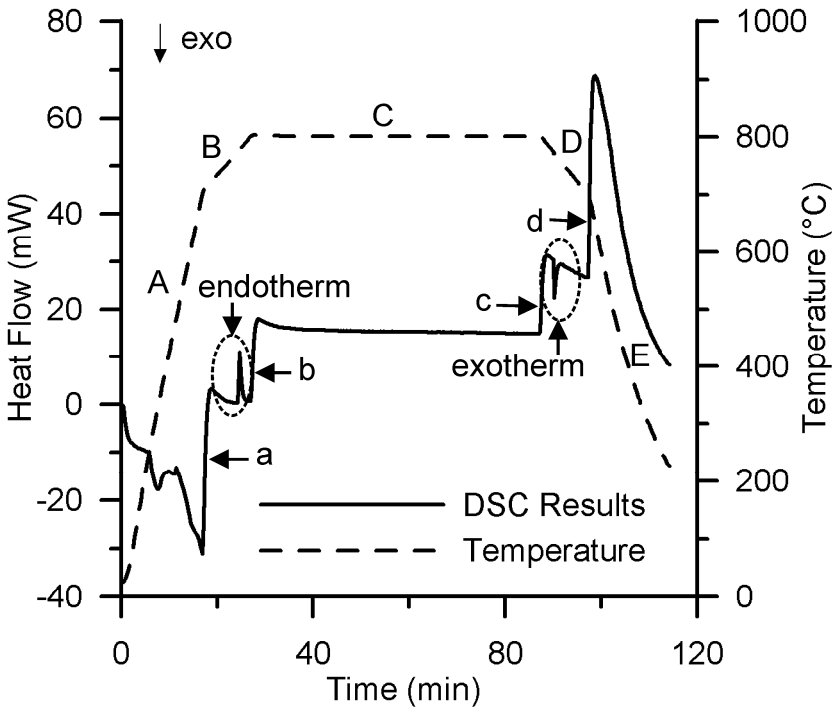

Figure 3-7: The temperature program for a typical DSC trial and the corresponding DSC trace. The isothermal hold time (segment C) is varied [57].

The DSC trace has been labeled *a* through *d*. These labels point out significant shifts in the baseline. These shifts coincide with changes in the heating rate (*dT/dt*) and are attributed to hysteresis of the baseline. The hysteresis should not be confused with exothermic or endothermic peaks which are shown in segments B and D, respectively. These segments are the areas of interest.

The DSC trace is loaded using the Thermal Analysis software and can then be manipulated. The individual segments can be isolated and compared. The heat flow for dynamic segments can be plotted as a function of temperature instead of time. The first and second derivatives of the DSC trace can be calculated and plotted. From this, the onset and end temperatures of peaks can be found along with inflection points and peak temperatures.

In some cases, baseline shift can be observed across a change of phase. This can be attributed to a change in the specific heat (C_p) of the sample upon the phase change. The

specific heat of the sample can be measured as the distance between the DSC trace and the natural baseline (assuming the reference cell is empty). Figure 3-8 shows the difference between a DSC trace without baseline shift (i.e. $C_{p(S)} = C_{p(L)}$) and with a shift due to a change in the specific heat (i.e. $\Delta C_p = C_{p(L)} - C_{p(S)}$). In both cases, it is assumed that there is no temperature dependence of the specific heat. Case 2 in Figure 3-8 shows a linear interpolation of the DSC trace baseline across the peak; however, this interpolation may not be correct. In fact, there are a number of methods commonly used to measure the enthalpy of a phase change.

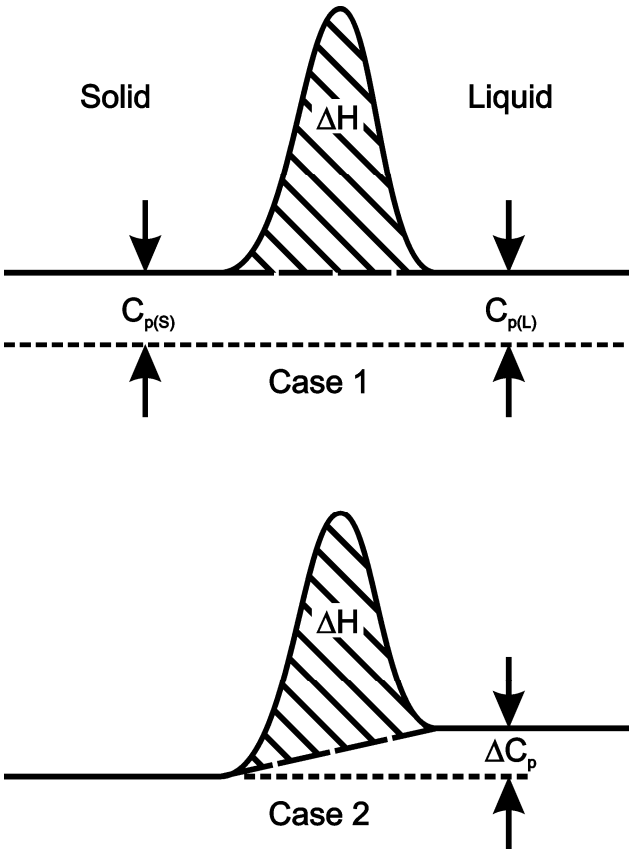

Figure 3-8: Conceptual analysis of baseline shift occurring during a phase change. In case 1, there is no change: $C_{p(S)} = C_{p(L)}$, the broken line is the natural baseline with no sample. In case 2, a baseline shift is observed due to a change in specific heat: $C_{p(L)} - C_{p(S)} = \Delta C_p$. In both cases, the specific heat is independent of temperature: $C_p(T)$ = constant.

The area of a peak can be found by integration. There are a variety of methods available in the software to integrate the peaks in the presence of a baseline shift as shown in Figure 3-9, including: linear (b), tangential sigmoidal (c), horizontal sigmoidal (d), and horizontal: left or right starting (e). In the linear case, the peak is integrated between the DSC trace and a line with endpoints on the DSC trace at the integration limits. The equation for the baseline is

given by Equation 3-1, where *B(t)* is the baseline, *D(t)* is the differential signal, t_s and t_f are the start and end time of the peak (i.e. integration limits), respectively.

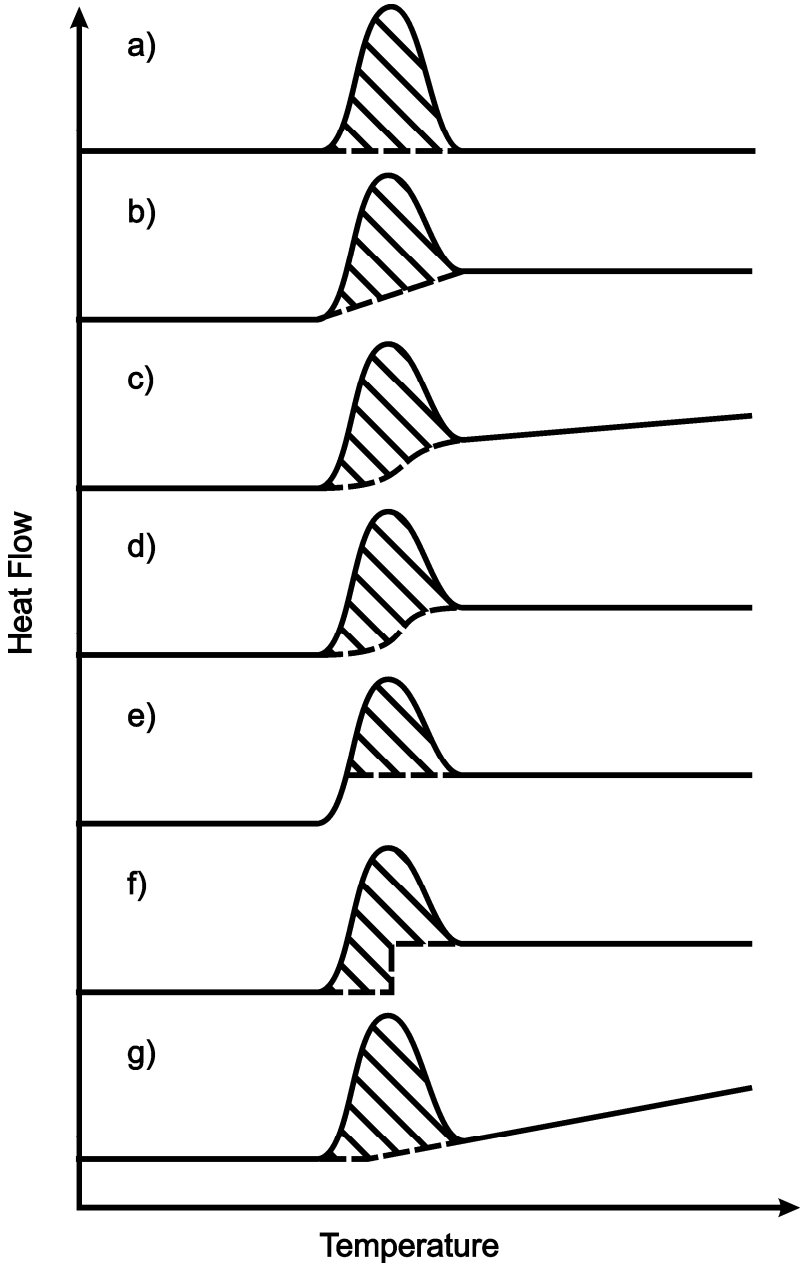

Figure 3-9: Baseline correction methods.

$$B(t) = D(t_s) + (D(t_f) - D(t_s)) \times \frac{t}{t - t_s} \qquad \text{Equation 3-1}$$

In the linear case, it is assumed that there is a linear change in the specific heat; or in other words, the correction accounts for all influences that are related to a linear change in the specific heat, while the specific heat change due to the reaction itself is not included.

The horizontal sigmoidal baseline correction accounts for a change in the specific heat during a reaction where the specific heat is not temperature dependent under the assumption that the change in specific heat is proportional to the reaction progress. The baseline correction is given by Equation 3-2 where $0 \le \alpha(t) \le 1$ is given by Equation 3-3.

$$B_k(t) = D(t_s) + (D(t_f) - D(t_s)) \times \alpha(t) \qquad \text{Equation 3-2}$$

$$\alpha(t) = \frac{\int_{t_s}^{t} (D(t) - B_{k-1}(t))dt}{\int_{t_s}^{t_f} (D(t) - B_{k-1}(t))dt} \qquad \text{Equation 3-3}$$

The tangential sigmoidal baseline correction is the most powerful correction method available in the Thermal Analysis software package since it leads the baseline at $\alpha(t) \rightarrow 0$ and $\alpha(t) \rightarrow 1$ into the tangent at the respective start and end of the peak. This allows for correction of the baseline under conditions of specific heat change due to reaction as well as temperature dependence. The baseline correction is given by Equation 3-4, where $\alpha(t)$ is given by Equation 3-3.

$$B_k(t) = (1 - \alpha(t)) \times (a_o + a_1 \cdot t) + \alpha(t) \times (b_o + b_1 \cdot (t_f - t)) \qquad \text{Equation 3-4}$$

The horizontal (left or right starting) integration methods assume a horizontal baseline correction in which all points within the integration limits that fall below the baseline are not included in the area.

In this study, the linear baseline correction method is used exclusively, as shown in Figure 3-10. Baseline shifts occurring in the DSC results of solid/liquid diffusion couple experiments cannot be attributed to a change during reaction or temperature dependence of the interlayer specific heat alone. Acknowledging this, the nature of the needed baseline correction is unknown; thus, a linear interpolation scheme is used.

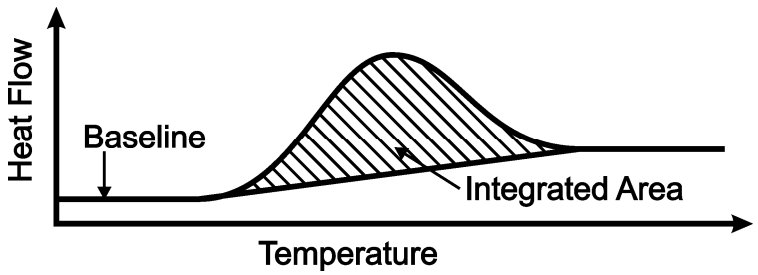

Figure 3-10: Baseline correction method for current study.

Integration of an endotherm or exotherm peak requires manual selection of the range to integrate over. The integration limits are determined by examination of the first and second derivatives of the DSC trace. The start of a peak can be considered the temperature where the DSC as well as first and second derivative curves start to increase in Figure 3-11. Recognizing the end of the peak is made difficult when a baseline shift occurs across the peak; however, selection of the limits has a significant effect on the measured enthalpy. The end of the peak is determined by the temperature where the second derivative of the DSC trace returns to zero. At this point, the slope of the trace is no longer changing and the baseline can be said to be re-established after the thermal event. There is expected to be some measurement error with determining the limits of integration manually. Using this procedure gives the most consistent results.

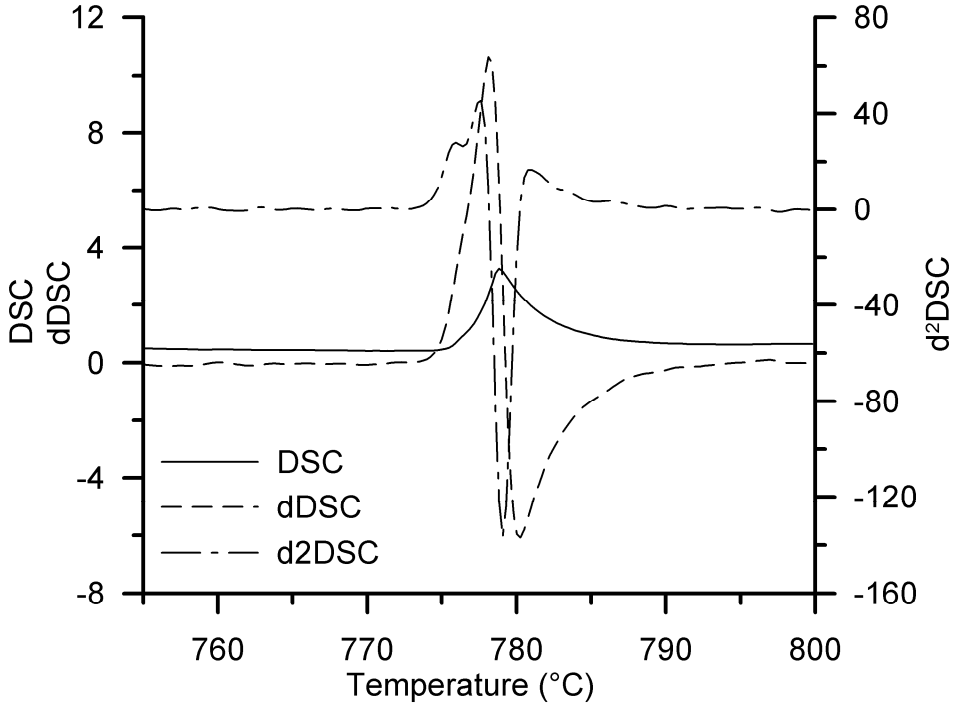

Figure 3-11: Melting endotherm of a DSC trace for a solid/liquid diffusion couple showing the first and second derivatives of the DSC curve with respect to time. The limits of integration of the DSC trace are determined by examination of the derivative curves.

The magnitude of the baseline shift can also be measured using the Thermal Analysis software. The baseline shift is calculated using Equation 3-5 where *D(T)* is the differential signal.

$$BS = \frac{D(T_2) - D(T_1)}{dT/dt} \qquad \text{Equation 3-5}$$

3.4.1. Correction Files

Correction files are necessary to remove crucible and furnace effects from the results. The result is obtained by subtracting the correction signal directly from the sample signal. A typical correction file is shown in Figure 3-12. Also shown is the raw DSC signal for a solid/liquid diffusion couple sample. Figure 3-13 shows the corrected DSC trace. The correction file is a DSC run with an identical temperature program. A slug of Ag base metal was inserted in both the sample and reference crucible for determination of the correction files. A new correction file was run before each DSC diffusion couple run.

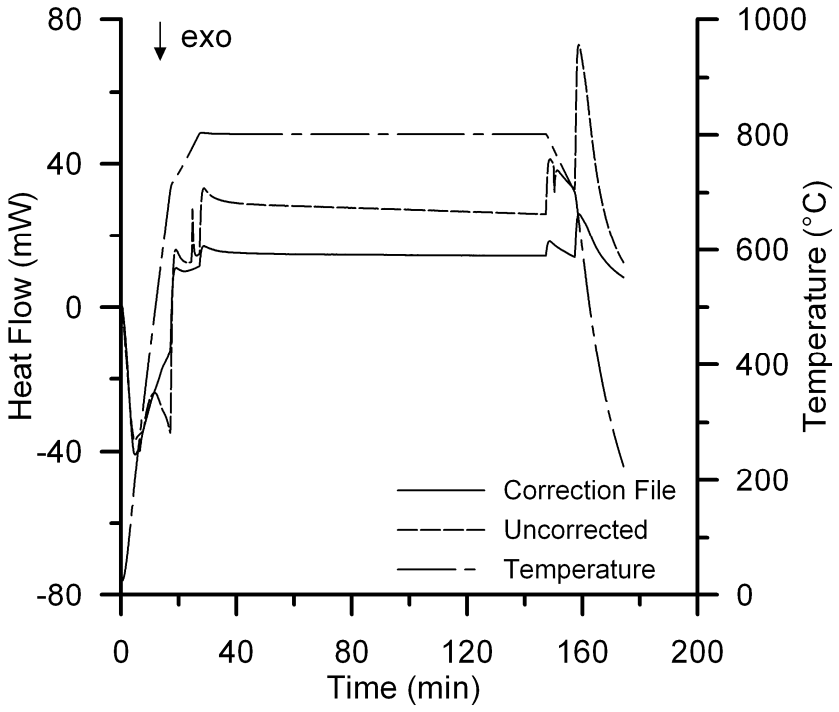

Figure 3-12: Typical correction file with overlay of a solid/liquid diffusion couple DSC signal trace (uncorrected).

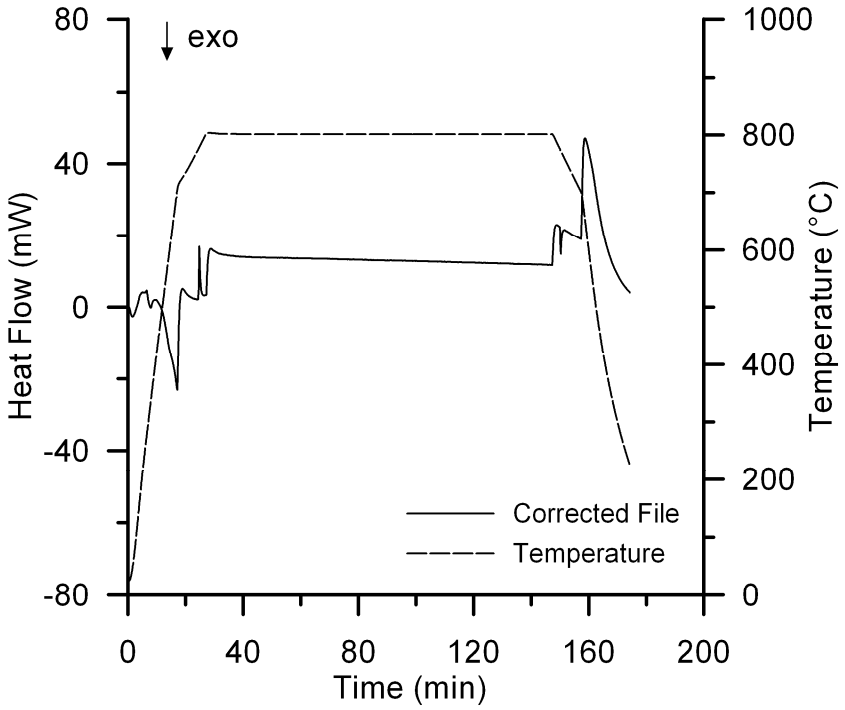

Figure 3-13: Typical corrected DSC trace for a solid/liquid diffusion couple.

3.5. Metallurgical Analysis

3.5.1. Sample Preparation

Following the DSC trial, the diffusion couple specimen was sectioned, polished, and etched if necessary. A cross section of the TLP half-sample was obtained through bisecting the sample along the diameter. The specimen was sectioned using a Struers Accutom cut-off saw and the section was mounted in either bakelite or epoxy resin.

The mounted sample was then manually ground using progressively finer SiC paper. Each specimen was ground to 1000 grit then cleaned ultrasonically in water before polishing. The sections were polished with 6 μm, and then 1 μm diamond slurry.

If the samples were to be etched, a solution was prepared. The section is etched by immersing the sample in the etchant for 3 to 5 seconds.

3.5.2. Optical Microscopy

Cross sections of the solid/liquid diffusion couples were examined using optical microscopy. Images were captured with a digital camera. The Image Pro image analysis software package was used for analyzing the images where appropriate.

3.5.3. Scanning Electron Microscopy

A scanning electron microscope (SEM) was used for high magnification examination and backscatter electron (BSE) imaging. The SEM is fitted with an Oxford energy dispersive x-ray spectrometry (EDS) analysis system. EDS was used to analyze the chemical composition of the sample at spots along the cross section.

4. Using DSC to Measure Interface Kinetics

An objective of this study is to develop an experimental approach for quantifying the isothermal solidification kinetics during TLP bonding using DSC. Venkatraman et al. [77] used DSC to measure interface kinetics in the Au-Sn binary system. There were, however, many problems in the results of that study, most notably, the fraction of liquid as a function of isothermal hold time did not extrapolate back to unity at the start. In theory, this method is capable of quantifying the liquid width more accurately than the typical method of visual inspection; hence, the reason for the error must be fully understood. In Corbin and Lucier's [15] study of isothermal solidification kinetics using DSC, the base metal powder was completely surrounded by liquid. The differences between TLP sintering and the TLP half sample geometry are expected to significantly affect the DSC response. In this chapter, the effects of TLP bonding process parameters and the half sample geometry on the DSC measurements are characterized. A method for accurately quantifying the interface kinetics is then developed.

4.1. Experimental Development and Selection of Process Parameters

4.1.1. Effect of Interlayer Composition

Interlayer composition has been shown to be an important process parameter in terms of process kinetics of both liquid formation and isothermal solidification. The dissolution of a Type-I (pure) interlayer requires a longer time than a Type-II (e.g. eutectic) interlayer. During Type-I dissolution a thin band of material initially melts at the interlayer/base metal interface [7], whereas a eutectic interlayer melts almost instantaneously upon reaching T_E. If the temperature was held constant at the eutectic, the Type-I interlayer will dissolve according to the square root law [55] requiring a time according to Equation 2-23. Of course, during heating the temperature is not static and the time for dissolution can only be found with numerical methods.

The heating segment of a DSC trace for solid/liquid diffusion couples for both a pure Cu (Type-I) interlayer and a Ag-Cu eutectic (Type-II) interlayer (i.e. C_F = 1.0 and 0.28, respectively) are shown in Figure 4-1. The endotherm resulting from melting for the pure interlayer is delayed to a higher temperature, whereas the onset of melting in the eutectic interlayer case is coincident with the eutectic temperature. The DSC results confirm that dissolution of the eutectic interlayer is instantaneous upon reaching the eutectic temperature.

Comparison of the two endotherms suggests that the kinetics of interlayer dissolution may be significantly slower for the pure interlayer. The onset of melting is 5 to 10° higher than the eutectic interlayer.

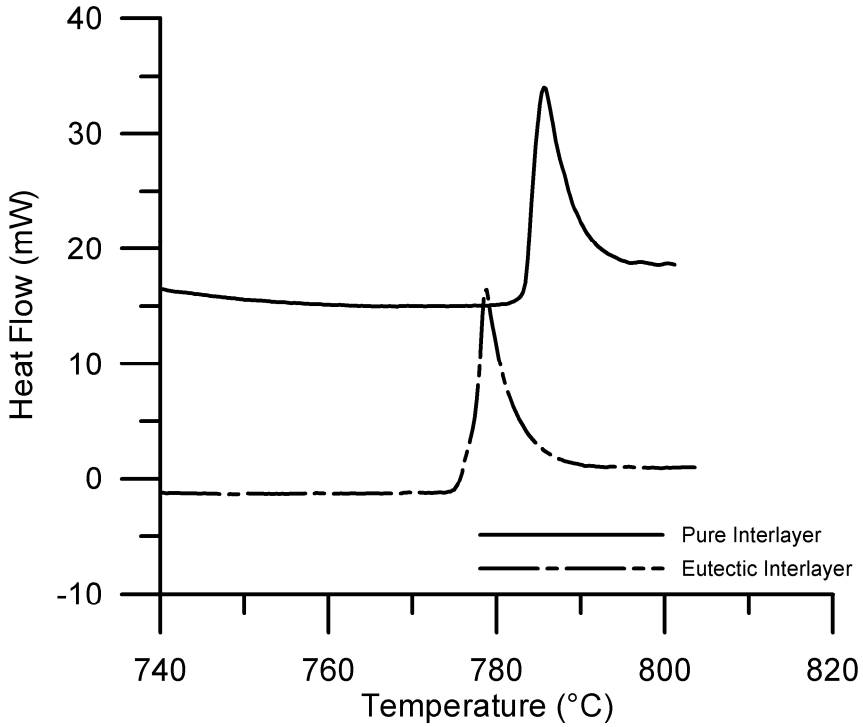

Figure 4-1: Effect of initial interlayer composition on the melting endotherm during the heating segment.

The results in Figure 4-1 suggest that dissolution of the pure interlayer requires times on the order of 1 to 2 minutes. This result does not agree well with that observed by Tuah-Poku et al. [39]; however, they used a significantly thicker foil (80 μm compared to 10 μm). They were unable to measure the process kinetics of interlayer dissolution because the process was very rapid. They concluded that dissolution was complete after as short a time as a fraction of a second. The heating rate in their study was unknown because the diffusion couples were inserted into a preheated furnace; although, it is expected to be higher than that used in this study and this may help explain the discrepancy in the results.

The kinetics of dissolution cannot be precisely characterized using this method because the actual start and end of interlayer melting is not clear. It is clear, however, that dissolution of the pure Cu interlayer is completed during heating from the eutectic temperature to the isothermal hold temperature, and that this process requires between 1 and 2 minutes. Widening of the liquid (i.e. dissolution of the base metal) occurs concurrently with dissolution of the interlayer up to the point that the interlayer is completely molten. Widening continues during additional heating, and further widening occurs for a short time after the bonding

temperature is reached (i.e. Stage 2-II). There is no indication of the time required for widening to be complete in the DSC trace; so the kinetics cannot be characterized using this process. The time required is expected to be less than that observed by Tuah-Poku et al. [39] because it has been shown that increasing the interlayer thickness increases the liquid widening.

Examination of Figure 4-1 shows that the melting endotherm for the pure Cu interlayer is shifted to a higher temperature and, as a result, the temperature at which the DSC trace returns to the baseline is higher than that for the eutectic interlayer. It is desirable to minimize the "superheating" above the eutectic temperature that the assembly must be heated. This is in order to reduce the time that is required for stage 2-I. Furthermore, reducing the superheat will minimize the liquid width and shorten the process time. In the assumption that the isothermal solidification stage is independent of the other stages, it is implied that the solute diffusion occurring during the heating and dissolution and widening stages is negligible. In order that the DSC solid/liquid diffusion couple experiments match the assumptions as closely as possible, the lowest feasible isothermal hold temperature should be used as this will minimize the time required to the peak temperature. Thus, the eutectic interlayer is used to measure the process kinetics.

4.1.2. Effect of Heating Rate

The heating rate during the heating and dissolution stages is expected to have a profound impact on the amount of solute transported during this time. Additionally, the heating rate will affect the kinetics of interlayer and base metal dissolution. Niemann and Garrett [30] have shown that during the heating stage, excessive solute can be diffused from the interlayer to the base metal if the heating rate is too slow. In order to minimize diffusion the heating rate during stage 1 should be as high as possible. The maximum heating rate of the DSC is 40°C/min.

A high heating rate during stage 2 is also desirable to reduce solute diffusion from the liquid into the base metal before the isothermal solidification stage begins; however, the heating rate from the eutectic temperature to the bonding temperature can also affect the DSC trace. Figure 4-2 shows the effect of reducing the heating rate from 40°C/min to 10°C/min for a solid/liquid diffusion couple using the eutectic interlayer. The onset temperature of melting is similar although the shape of the melting endotherm is significantly different. The endothermic peak is narrower with the lower heating rate while the higher heating rate shows a broadened peak.

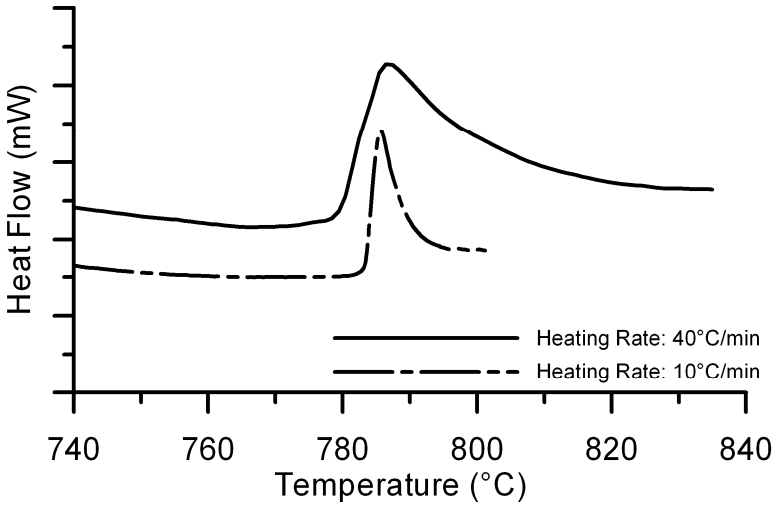

Figure 4-2: Effect of heating rate on the shape of melting endotherms during the heating segment (28%Cu interlayer, 25 μm thick).

The broadening of the melting endotherm in Figure 4-2 for the 40°C/min heating rate is due to a number of factors. Dissolution of the interlayer requires time, and the time elapsed during the melting endotherm in both the 10 and 40°C/min DSC traces is similar (i.e. ~2 minutes). There is also some thermal lag in the measurement, and the thermal lag is expected to be greater with the higher heating rate. Finally, the kinetics of base metal dissolution will change with heating rate. The 10°C/min heating rate is closer to equilibrium and thus, dissolution of the base metal proceeds following the phase boundaries on the phase diagram. Dissolution is a diffusion dependent process; hence, increasing the heating rate results in a greater departure from equilibrium. As a result, widening of the liquid continues after the isothermal hold temperature has been reached. Furthermore, the higher temperature reached in the 40°C/min DSC trace in Figure 4-2 results in a greater maximum liquid width, W_{max}. Hence, the broadened melting endotherm for the higher heating rate is also a result of the increased base metal dissolution occurring at higher temperatures.

A consequence of the higher heating rate is that the amount of superheating above the eutectic temperature that is needed to completely resolve the endotherm is increased. This superheat is required so that the endotherm can be integrated according to the experimental method and is absolutely necessary for accurate enthalpy measurements.

The maximum width of the liquid (W_{max}) is related to the peak temperature (Equation 2-56); the liquid width increases with increasing peak temperature. This has the potential to increase the time required for isothermal solidification to complete (Equation 2-69). For these reasons, the lower heating rate of 10°C/min is used for the areas of interest during heating (i.e. heating between T_E and T_B). Since solid-state diffusion during the heating stage will affect the process kinetics of isothermal solidification, minimizing the duration of the heating stage is important.

Use of a slower heating rate at lower temperatures will increase the diffusional exchange between the interlayer and base metal during the heating stage. At lower heating rates, it is no longer valid to assume that this loss of solute is negligible. Thus, the heating rate is initially 40°C/min and is decreased to 10°C/min at a temperature low enough to establish a base line before melting begins (i.e. 700°C). The corollary for the cooling stage is that the inverse temperature program is used. The initial cooling rate is 10°C/min, increasing to 40°C/min after a base line has been established following the freezing exotherm.

4.1.3. Effect of Reference Crucible on DSC Trace

In order to fully characterize the effects of the solid/liquid diffusion couple geometry on the DSC results, the influence of all parameters was determined. It is recommended that the reference crucible contain a sample material with thermal diffusivity and conductivity, and heat capacity similar to the contents of the sample cell; however, the reference material must not participate in the thermal events to be measured in the sample cell [99]. The effect of the reference crucible contents on the DSC trace was investigated. Using the Ag-Cu eutectic foil, the DSC trace of a solid/liquid diffusion couple was collected with an empty reference crucible at a heating rate of 40°C/min. A similar DSC trace for a diffusion couple with a slug of Ag base metal in the reference crucible. The mass of the reference slug was similar to that of the Ag in the sample crucible.

The difference between the two results is shown in Figure 4-3. The heating segment of the DSC trace for the empty reference crucible case is given by the solid line, while the case for the reference crucible containing a Ag slug is given by the broken line. Inspection of Figure 4-3 shows that the noise in the DSC trace at lower temperatures when the reference crucible is empty tends to be smoothed out by the addition of the Ag slug to the reference cell. This trend is consistent trace-to-trace. In theory, there should be no effect of the Ag slug in the reference crucible on the measured enthalpy. Examination of the endotherms in Figure 4-3 shows a baseline shift across both peaks during melting. With the empty reference crucible the shift is more severe, which will have an impact on the measured enthalpy. To minimize noise, trace hysteresis, and baseline shift, a mass of base metal should be placed in the reference crucible for all solid/liquid diffusion couple experiments.

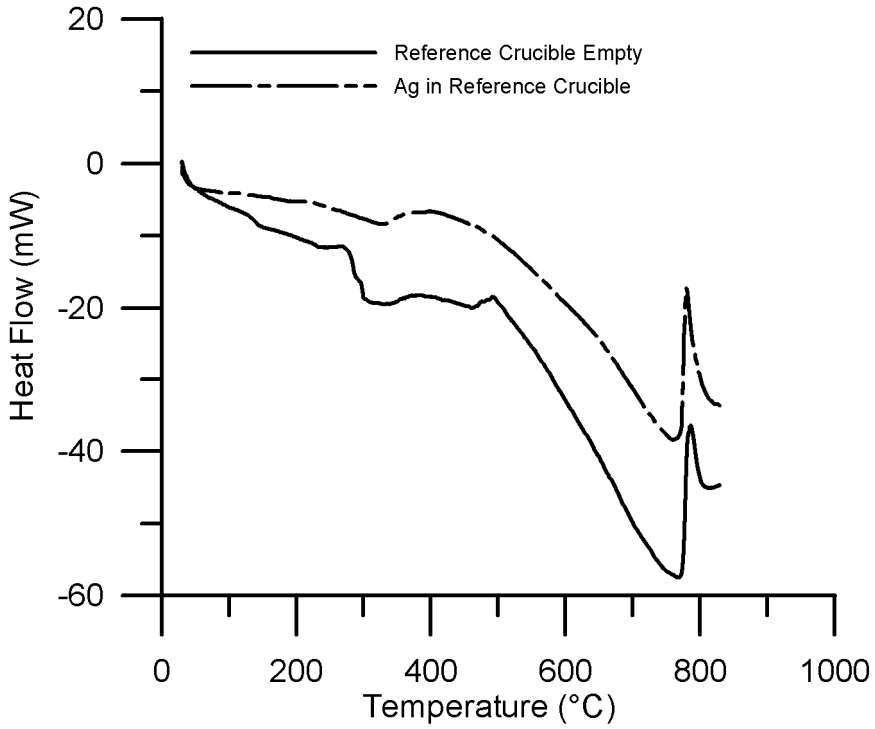

Figure 4-3: Effect of base metal in reference crucible on heating segment of DSC trace (28%Cu interlayer, 25 μm thick).

4.1.4. Effect of Alumina Coating

The base metal substrate was coated with an alumina coating on all sides except the faying surface in order to prevent the liquid from spreading up the sides of the cylinder. As shown in § 2.3.1, many authors have reported that liquid at the interface can be squeezed out of the joint, or can wet the side of the base metal and wick away from the joint. One solution is to use apply a washer that is designed to seal the liquid at the interface by welding the substrates together [34,39]. Alternatively, coatings such as Cr [7] and alumina [75] have been used to prevent the loss of liquid from the interface. The liquid does not wet the coating material and is held in place by surface tension. For this study, it is important that the liquid interacts with the faying surface only since spreading increases the surface area for diffusion. Furthermore, liquid that is wicked away from the interface is removed from the area of interest that is measurable with the DSC thermocouple.

A DSC trace that shows the effect of the alumina coating is given in Figure 4-4. The thermal cycles of diffusion couples with and without the alumina coating are given. The melting endotherm was unaffected by the absence of a coating; however, examination of the solidification exotherm shows a difference. The exotherm for the sample without the coating is smaller in magnitude. This is a result of a decrease in liquid at the interface. Visual

examination of the sample after the thermal cycle shows evidence of liquid up the sides of the base metal cylinder. In comparison, the sample with the alumina coating shows no signs of liquid away from the faying surface under visual inspection using a stereomicroscope. A sectioned sample was also examined using SEM and showed that liquid was contained by the coating. The enthalpy measurements given in Table 4-1 suggest that up to 15% of the liquid is squeezed out of the sample that was not coated after 2 hours of isothermal hold time (n.b. the methodology used to find this value is derived in sections below).

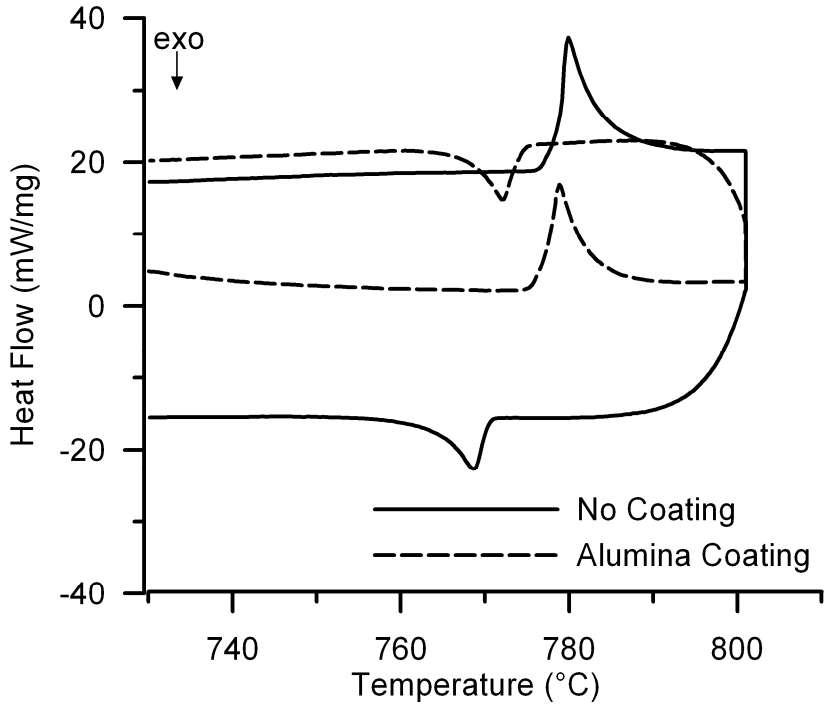

Figure 4-4: Effect of alumina coating on DSC trace (28%Cu interlayer, 25 μm thick).

Table 4-1: Enthalpy measurements from Figure 4-4.

Sample	Coating	Initial Enthalpy (mJ), ΔH_m	Final Enthalpy (mJ), ΔH_s	% Liquid Remaining (%)	Corrected% Liquid Remaining (%)
Ag-Cu-13	No	566	206	36.4	49.5
Ag-Cu-24	Yes	419	200	47.6	64.8

4.2. Preliminary Results

4.2.1. Baseline Enthalpy Measurement for Ag-Cu Eutectic

A baseline value for the enthalpy of formation (Δh_f) as measured for the Ag-Cu eutectic foil alone was 116 mJ/g and 114 mJ/g for melting and solidification respectively (for a foil with a mass of 5.3 mg). The small difference between these measurements is attributed to variation in the measurement system and is expected. ΔH_s is the enthalpy measured from the solidification exotherm in a DSC diffusion couple experiment. Since the mass of liquid involved in solidification is given by $\Delta H_s/\Delta h_f$; where Δh_f is constant, the enthalpy of formation can be used as a reference to determine the amount of liquid remaining (and thus interface position) in a solid/liquid diffusion couple after an isothermal hold period. Equation 4-1 gives this relationship, where *m* is the mass of the original eutectic foil.

$$\%\ \text{liquid remaining} = 100 \times \frac{\Delta H_s}{\Delta h_f \cdot m} \qquad \text{Equation 4-1}$$

4.2.2. Process Kinetics for Ag-Cu Eutectic Interlayer

The enthalpy measurements of the solid/liquid diffusion couple DSC experiments are given in Table 4-2 [100]. The fraction of liquid remaining after the respective isothermal hold period is calculated using Equation 4-1. As expected, the amount of liquid remaining decreases with increased isothermal hold time as the solid/liquid interface advances into the liquid phase through epitaxial growth.

According to Equation 2-57 and Equation 2-69, the position of the solid/liquid interface (i.e. width of the liquid phase) is expected to be proportional to the square root of the isothermal hold time. If the fraction of liquid remaining from Table 4-2 is plotted as a function of the square root of the isothermal hold time, it is shown that the experimental results support the kinetics as predicted by the analytical models; specifically: the fraction of liquid remaining is inversely proportional to the square root of the hold time.

Table 4-2: Enthalpy measurements taken from the exotherms of solid/liquid diffusion couple DSC experiments using Ag base metal with Ag-Cu eutectic interlayer.

Hold Time (hrs)	Final Enthalpy (ΔH_s)	Liquid Remaining ($\Delta H_s/\Delta h_f \cdot m$)
0.00	66.2	57.6
0.02	64.8	56.3
0.17	56.4	49.0
0.25	52.8	45.9
0.33	58.2	50.6
0.33	56.9	49.5
0.50	47.5	41.3
1.00	39.2	34.1
2.00	37.6	32.7
3.00	36.9	32.0
4.00	35.5	30.9
5.00	28.8	25.1
6.00	24.0	20.8
8.00	16.0	13.9
10.00	12.9	11.2
12.00	3.90	3.40
14.00	3.00	2.60

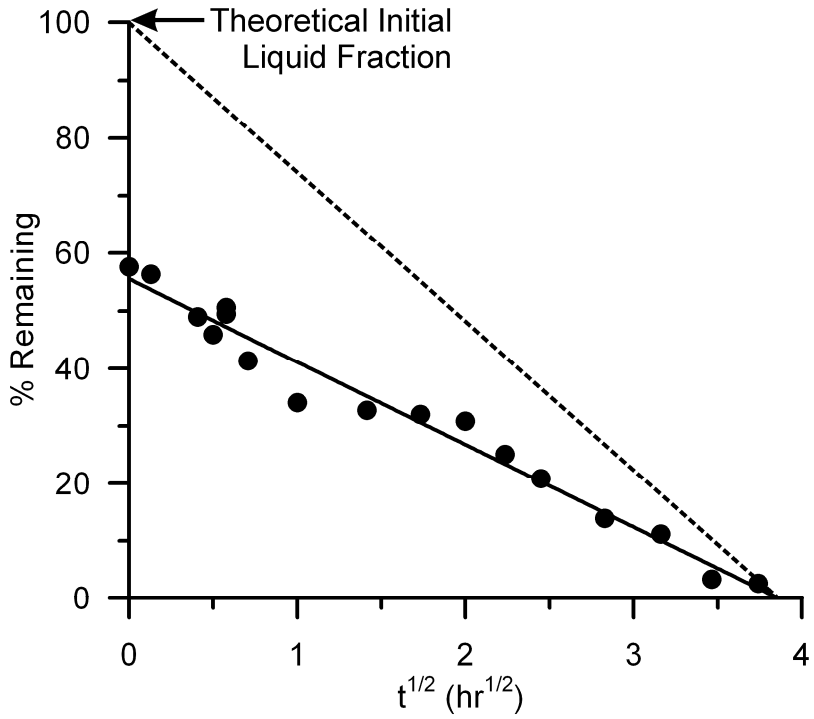

Figure 4-5: Isothermal solidification kinetic results showing theoretical liquid remaining line (28%Cu interlayer, 25 μm thick, T_b = 800°C).

A linear trend line can be fit to the experimental data by applying the least squares regression using the Grapher version 5.02 software. This analysis fits the data to a straight line with the form of Equation 4-2 where the best fit equation has the least square error (i.e. Equation 4-3)

$$y = bx + a \qquad \text{Equation 4-2}$$

$$\Pi = \sum_{i=1}^{n} \left[y_i - (a + b \cdot x_i) \right]^2 = \min. \qquad \text{Equation 4-3}$$

The fit line in Figure 4-5 has the coefficients: b = -14.4, and a = 55.5. The residual sum of squares (*SSe*) is 136 and the regression sum of squares (*SSr*) is 4943. From this, the coefficient of determination (R^2) is found to be 0.973 using Equation 4-4. R^2 is a figure of merit that shows how well the data are explained by the best fit line, the closer to one, the better the fit.

$$R^2 = 1 - \frac{SSe}{SSe + SSr} \qquad \text{Equation 4-4}$$

From the value of R^2 it is revealed that the fitted line agrees well with the DSC results and, through analysis, information regarding the interface kinetics can be obtained. By extrapolating the trend line forward to zero percent liquid remaining, the time required for the completion of isothermal solidification (t_s) can be found (i.e. 15.5 hours). Conversely, the

trend line can be extrapolated back to the start of the isothermal hold period. Examination of Figure 4-5 reveals that the trend line does not intersect the fraction of liquid remaining axis at unity, but instead at 55.5%. This result is counter-intuitive; furthermore, it makes a comparative measure of the interface kinetics impossible.

The result at the start of the isothermal hold period (t_o) suggests that a large fraction (i.e. ~45%) of the liquid disappears during stage 2-I. Heating from the eutectic temperature to the hold temperature requires approximately 2 minutes (nominal) during which the liquid width is expected to increase due to widening. An explanation of this observation in the literature was not found; however, Zhou et al. [2] showed through numerical modeling that in some cases the liquid width is still increasing during the early stages of isothermal holding due to diffusion dependent dissolution of the base metal.

From Figure 4-5, t_s is easily found when the line crosses the abscissa but a true measure of the interface kinetics is the slope of the line (i.e. the coefficient b in Equation 4-2) as given by Equation 4-5.

$$\xi = -b \cdot \frac{W_{max}}{2} \qquad \text{Equation 4-5}$$

The glaring discrepancy between the expected process kinetics shown by the broken line in Figure 4-5 and the actual measured process kinetics given by the fit trend line shows that the DSC results cannot be used to accurately quantify interface motion in the solid/liquid diffusion couples until the discrepancy can be explained.

The apparent loss at t_o of a large fraction of the initial liquid formed may be due to transient effects at the beginning of isothermal solidification. Due to the nature of the DSC experiments (i.e. required heating and cooling rates), the actual time above the eutectic temperature is over 3 minutes when the nominal isothermal hold time is zero. If the interface kinetics at the early stages of the isothermal hold period are extremely fast before reaching a “steady state” it is possible that the trend was missed because measurement data to verify the non-linearity of the results could not be collected. It can be recalled that in the results of Venkatraman et al. [77] a similar result of liquid loss was observed and the explanation given was a lack of data at short hold times. A review of relevant literature did not provide any examples, nor a physical explanation for this; therefore, the apparent loss of liquid is more likely an artefact of the experiment.

The geometry of the solid/liquid diffusion couple DSC setup induces the discrepancy in the DSC results that is observed in Figure 4-5. It was found that the compounded effects of a large base metal-to-interlayer mass ratio, primary solidification during cooling, and solid/liquid interface development result in the gross underestimation of the fraction of liquid remaining as measured by the DSC. One of the objectives of this project is to investigate the root causes of these effects and quantify the respective impact on the DSC results so that an appropriate

correction can be applied. To this end, the DSC data generated by the diffusion couple experiments can be exploited to provide a physical understanding of the aberration in the results.

4.3. Discussion of Preliminary Results

4.3.1. Effect of Base Metal Mass on DSC Results

A reference value for the enthalpy of formation (Δh_f) as measured for the Ag-Cu eutectic (Ag – 28% Cu) was 115 J/g (averaged, for a foil with a mass of 5.3 mg). In the diffusion couple experiments, however, the mass ratio of foil to base metal is less than one percent. Since the large solid mass is not involved in the phase change, the influence on enthalpy measured will be significant and must be considered.

The effect of the large base metal mass on the DSC results can be evaluated by observing the melting characteristics of the interlayer in the absence of metallurgical interaction. To achieve this, an Al_2O_3 diffusion barrier was applied to prevent interaction between the solid and liquid phases, as described by the type-1 experiment in Table 3-1. The objective of this experiment is to determine what effect, if any, the base metal has on the measured enthalpy during a solid/liquid diffusion couple trial by measuring Δh_f of a Ag-Cu eutectic foil when a typical mass of base metal is present in the DSC crucible. The diffusion barrier is necessary to prevent the liquid from wetting the base metal since the effects of this interaction could be to further influence the results.

The measured Δh_f for the eutectic foil in the type-1 experiment is 85 J/g. Compared to the Δh_f measured for the eutectic interlayer without the base metal (115 J/g), it is clear that the enthalpy measured with the base metal in the crucible is lower than that without. The mass ratio of the inert base metal to the eutectic interlayer is so high that the base metal is observed to alter the DSC heat flow measurements. The base metal acts as a heat sink in the sample cell; and, by conduction, reduces the measured total heat of formation by 26%. The reduction is expected to be even more significant without the ceramic diffusion barrier, which will inhibit heat flow.

Table 4-3 shows a comparison of thermal measurements taken from solid/liquid diffusion couples with different base metal thicknesses. The results show that the thickness of the substrate has no effect on enthalpy measurements, down to thicknesses at least 20 times the interlayer width. Even the 0.5 mm substrate is many times thicker than the liquid width and is still expected to have an effect on heat flow within the crucible.

Table 4-3: Effect of base metal mass on DSC measurements in Type-I solid/liquid diffusion couple experiments.

Sample	Base metal mass (mg)	Base metal thickness (mm)	Melting, ΔH_f (J/g)	Solidification, ΔH_s (J/g)
Ag-Cu-93	42.8	0.5	108	110
Ag-Cu-95	93.4	1.0	105	109
Ag-Cu-96	219.9	2.0	107	106

Dumas et al. [105,106] studied the heat transfer within emulsions during melting and solidification of droplets and the effect on the DSC trace using a numerical model. The results of their study show that the assumption of uniform temperature within the sample cell is not valid. Temperature gradients within the cell explain the variation in shape and magnitude of the melting endotherms and solidification exotherms. These temperature gradients were found to exist in dispersed solutions of pure droplets and eutectic saline solutions [107,108] in oil. In these cases the fraction of mass involved in the thermal event was small, similar to the case of the solid/liquid diffusion couple used in this study. The effect of the temperature gradients was dependent on the heating or cooling rates. Jamil et al. [109] found that during melting of a binary saline solution where three phases co-exist at the same time, temperature gradients affecting heat transfer existed with a resulting impact on the shape of the DSC trace. Following these results, it is clear that during phase changes in the solid/liquid diffusion couple, significant temperature gradients exist within the base metal in the sample crucible, and these temperature gradients which are heating rate dependent will affect heat transfer within the cell. Simply, heat will be transferred away from the measuring head.

It was shown how a temperature gradient across the liquid width of a TLP bond can affect the process kinetics of isothermal solidification in § 2.1.11. In the DSC experiments, however, a TLP half-sample is used to simulate isothermal solidification. Since there is only a single interface in the half-sample set up, there cannot be a temperature differential between a hot and cold interface as is required during temperature gradient TLP bonding. As a result, any temperature gradient within the sample cell is expected to have minimal impact on the process kinetics.

To remedy the effect of base metal on DSC results, both the solidification exotherm (ΔH_s) and the melting endotherm (ΔH_m) can be considered. For instance, if the segments of interest in the sample DSC trace in Figure 3-7 are plotted as a function of temperature as shown in Figure 4-6, the endotherm and exotherm can be compared to each other. The fraction of liquid remaining can be found by taking a ratio of ΔH_s to ΔH_m (Equation 4-6). It is suggested that in this manner, the heat flow influence from the base metal is constant during both the melting and solidification events.

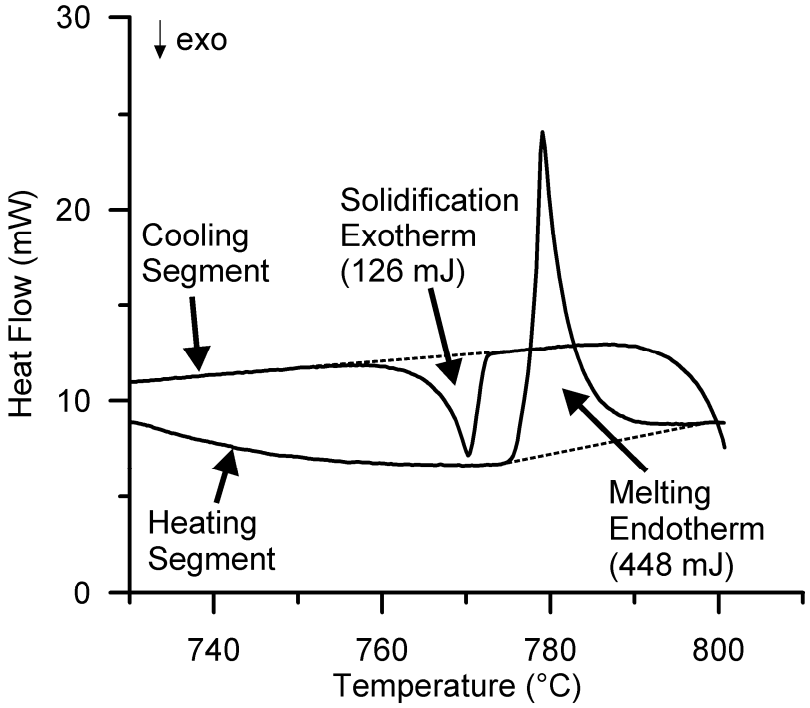

Figure 4-6: The DSC results plotted as a function of temperature. The integral of the exotherm (cooling segment) and endotherm (heating segment) is shown (28%Cu interlayer, 25 μm thick, T_b = 800°C) [57].

$$\%\ \text{liquid remaining} = 100 \times \frac{\Delta H_s}{\Delta H_m} \qquad \text{Equation 4-6}$$

The DSC results from Figure 4-5 can be recalculated using Equation 4-6 to account for the effect of the base metal on the DSC measurements. The fraction of liquid remaining as a function of isothermal hold time is given in Figure 4-7. The effect of the calculation method on the fraction of liquid remain can be clearly observed. There is marginal improvement in the apparent loss of liquid at t_o; however the problem persists as the measured fraction of liquid remaining at this time is approximately 75%. There are still other factors which need to be considered in the DSC analysis but, henceforth, to account for the base metal heat sink effects Equation 4-6 is used to describe the fraction of liquid remaining.

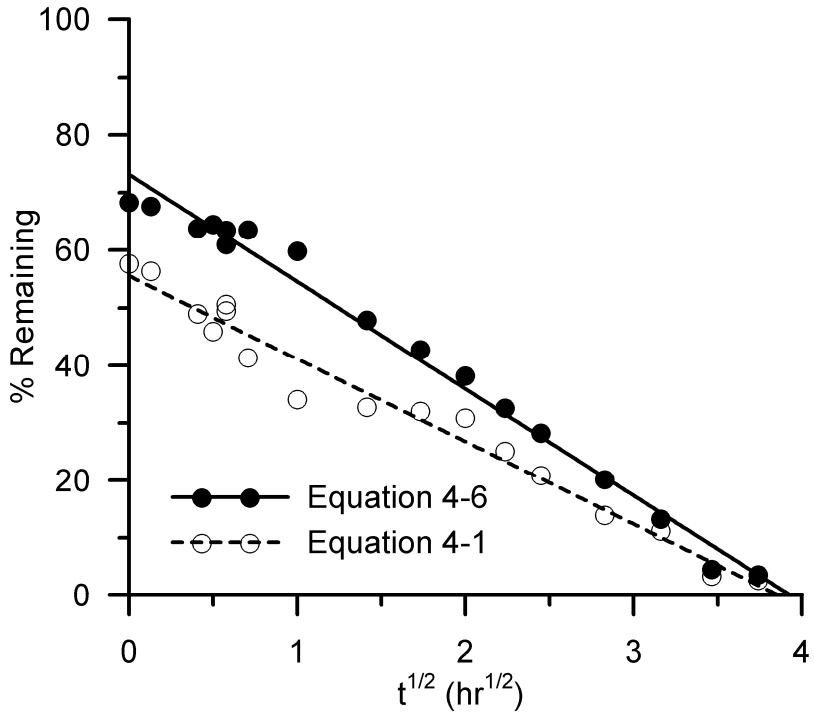

Figure 4-7: Effect of calculation method on results and corresponding effect of base metal on measurements (28%Cu interlayer, 25 μm thick, T_b = 800°C).

A summary of the enthalpy measurements of the solid/liquid diffusion couple experiments are given in Table 4-4 with the percent liquid remaining calculated using Equation 4-6.

Table 4-4: Results of DSC experiments with a eutectic Ag-Cu foil.

Isothermal Hold Time (hrs)	Square Root Time ($hrs^{1/2}$)	Foil Mass (mg)	Melting Onset (°C)	Initial Enthalpy (mJ), ΔH_m	Final Enthalpy (mJ), ΔH_s	% Liquid Remaining (%)
0	0.00	5.30	777	514	351	68.2
0.02	0.13	5.20	777	499	337	67.6
0.17	0.41	5.20	777	460	293	63.7
0.25	0.50	5.10	777	418	269	64.4
0.33	0.58	5.10	777	468	297	63.4
0.33	0.58	5.30	778	495	302	60.9
0.50	0.71	5.14	777	385	244	63.5
1.00	1.00	5.20	776	341	204	59.8
2.00	1.41	5.19	777	408	195	47.9
3.00	1.73	5.20	777	449	192	42.7
4.00	2.00	5.19	777	482	184	38.2
5.00	2.24	5.21	777	460	150	32.6
6.00	2.45	5.27	777	448	126	28.2
8.00	2.83	5.11	777	407	82	20.1
10.0	3.16	5.25	778	510	68	13.3
12.0	3.46	5.17	777	445	20	4.51
14.0	3.74	5.18	776	440	16	3.56

The time required for isothermal solidification (t_s) in Figure 4-7 is not affected by the calculation method. The linear trend line applied to the new data has the form of Equation 4-7. The residual sum of squares (*SSe*) is 110 and the regression sum of squares (*SSr*) is 8269. From this, the coefficient of determination (R^2) is found to be 0.987. This implies that the results of the new calculation method (Equation 4-6) are better represented by a line.

$$\%LR = -18.6 \cdot \sqrt{t} + 73.1 \qquad \text{Equation 4-7}$$

4.3.2. Influence of Interlayer Thickness

The DSC diffusion couple experiments were repeated with increased liquid widths and no isothermal hold time. The results given in Table 4-5 show that roughly the same fraction of liquid remains regardless of the initial liquid width. The increase in the fraction of liquid remaining from 5.30 mg (initial eutectic foil mass) to 10.3 mg is likely due to time dependent dissolution of the base metal. With the thicker liquid (produced by stacking nominal thickness

foils), there is more dissolution during heating. Hence, with thicker interlayers, the dissolution may not be instantaneous as it is assumed with the thin foil, resulting in less liquid measured upon melting. Also, any interface movement that occurs during the 3 minutes above the eutectic represents a larger fraction of the thinnest foil, which agrees with the measurements. If there was a transient effect at the beginning of the isothermal solidification process, the absolute width of liquid consumed would be independent of the initial liquid width. This elucidates the argument that the apparent liquid loss is due to the measurement system and not physical interaction between the phases.

Table 4-5: Results of multi-thickness interlayer study.

Foil Mass (mg)	Onset (°C)	ΔH_f (mJ)	ΔH_s (mJ)	% Liquid Remaining
5.3	776.9	514.3	350.9	68.2
10.3	777.8	884.3	702.4	79.4
14.8	778.9	1411	1085	76.9
20.7	777.5	1806	1423	78.8
25.9	778.9	2317	1844	79.6

4.3.3. Influence of Primary Solidification

During the initial cooling period between the peak temperature and the eutectic, primary solidification of the melt is expected to occur [74]. During the TLP bonding of Ni using a Ni-P interlayer, Saida et al. found that the fraction of the liquid solidified as primary Ni was affected by the cooling rate [74]. Campbell and Boettinger later confirmed this in the Ni-Al-B system [97]. In the DSC experiments, the cooling rate is 10°C/min during cooling from the process temperature (800°C) to the eutectic temperature (780°C). Thus it is expected that some primary α-phase solidification will occur.

Metallurgical examination of the interface of a DSC diffusion couple after cooling from an isothermal hold period shows a fine lamellar eutectic structure. The base metal adjacent to the interface shown in Figure 4-8 has undergone a solid-state transformation upon cooling below the solvus temperature following solidification. This cellular precipitation in the Cu-saturated base metal has obscured the underlying solidification structure [102,110]. The scalloped interface, however, provides some evidence that epitaxial solidification has occurred in a cellular mode. Thus, it is likely that athermal primary solidification has occurred at the solid/liquid interface.

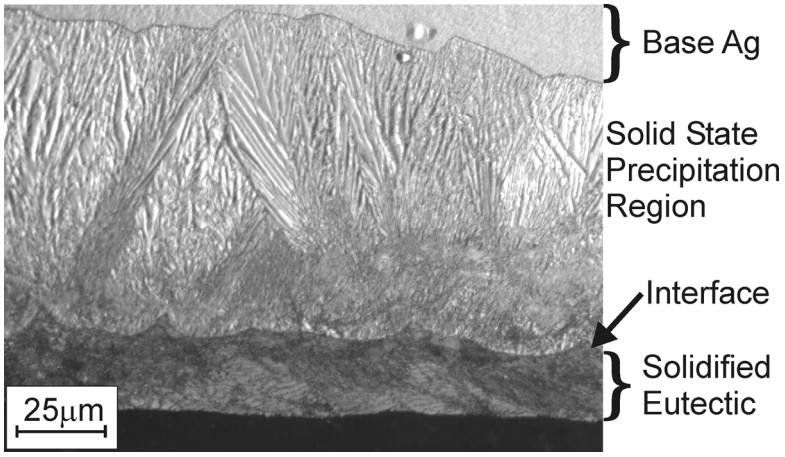

Figure 4-8: Optical micrograph of the interface showing the solidified eutectic and the cellular precipitation adjacent to the interface [57].

Observation of DSC trace cooling segments for diffusion couples (type-2) shows that only the solidification of eutectic is represented in the solidification exotherm. Upon cooling from the isothermal hold temperature, heterogeneous nucleation of α-phase occurs almost immediately at the solid/liquid interface. The primary phase then grows into the liquid, rejecting solute as the temperature decreases. This would lead to an expected exothermic peak on the DSC trace; however, it is conspicuously absent in all results. Conversely, after the required undercooling below T_E, eutectic solidification is initiated. This releases a sharp burst of energy, resulting in a very well defined exothermic peak with a clear onset temperature that is separated from the primary solidification event. Therefore, it appears the measured exothermic energy ('final enthalpy', ΔH_s) includes only the eutectic fraction of the solidified liquid.

Conversely, it is proposed that the heating segment includes melting of the eutectic foil plus some amount of base metal dissolution. During heating the endothermic peak on the DSC trace begins at the onset of eutectic foil melting. In the absence of any thermal lag, the melting endotherm of a eutectic phase should appear as a single, narrow and sharp peak. However, the presence of the Ag base metal will tend to increase thermal lag and the endotherm appears as a broadened peak. During this elapsed time the eutectic liquid wets with the faying surface of the base metal and, as the sample is heated from T_E to T_b, dissolution of the base metal Ag will increase the liquid formed. As a result it is argued that at least part of the energy of dissolution is included in the measured endothermic energy ('initial enthalpy', ΔH_m).

A schematic of the physical melting event as it corresponds to the heating segment of the DSC trace is shown in Figure 4-9 a). The temperature increases from left to right in the diagram and shows the heating and dissolution and widening stages. Similarly, Figure 4-9 b) summarizes the hypothesis that the measured exothermic energy includes only the eutectic

fraction of the solidified liquid. The sequence of solidification proceeds from right to left in this figure, following the sense of decreasing temperature in the DSC trace. At some temperature below the peak (T_b), initiation of primary solidification occurs. This is shown by the primary phase cells nucleating at the solid/liquid interface, protruding into the liquid phase. These cells will grow epitaxially with increased cooling below T_b until the rest of the liquid solidifies following the eutectic solidification mechanism.

The calculation of 'percent liquid remaining' (Equation 4-6) requires calculation of $\Delta H_s/\Delta H_m$, and if the exothermic energy includes only the eutectic fraction of solidified liquid, Equation 4-6 will report lower than actual values. This supports the observation made in Figure 4-5 and Figure 4-7 that the fraction of liquid remaining is under represented. Elucidation that primary solidification is not measurable in the diffusion couple DSC traces can be obtained through a comparison of DSC traces from type-1 experiments (i.e. liquid in the presence of base metal but without interaction) with DSC traces from type-2 diffusion couples.

To confirm the effect of primary solidification on the DSC results, a hypoeutectic foil with a composition of 24%-Cu was prepared and subjected to the same DSC heating cycle. Following the Ag-Cu phase diagram in Figure 3-1, the liquid composition in the diffusion couples will shift to 24%-Cu (which is the liquidus composition, $C_{L\alpha}$ at $T_b = 800°C$) due to base metal dissolution during heating. Appositely, inspection of the cooling segment of a DSC trace for a type-1 experiment using 24%-Cu highlights the exclusion of primary solidification in the diffusion couple results. Similar to the experiments of § 4.3.1, an Al_2O_3 barrier was added between the foil and Ag base metal to prevent metallurgical interaction. The resulting DSC trace of this experiment is shown in Figure 4-10. For the sake of comparison, the DSC trace resulting from a type-1 experiment for the eutectic foil (28%-Cu) is shown in Figure 4-11.

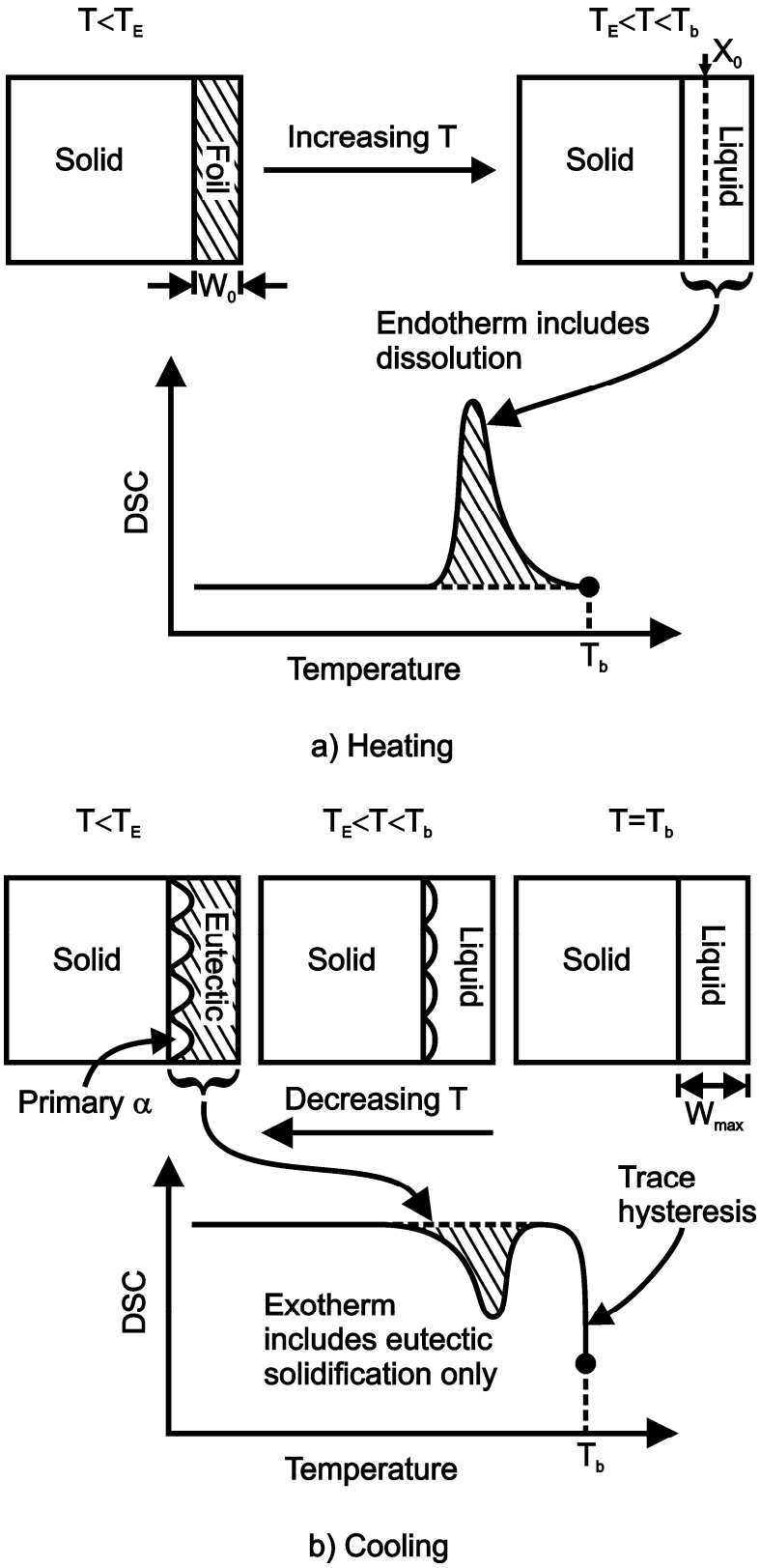

Figure 4-9: Schematic of phase change and corresponding DSC trace segment, a) heating above T_E, and b) cooling from T_b through T_E [57].

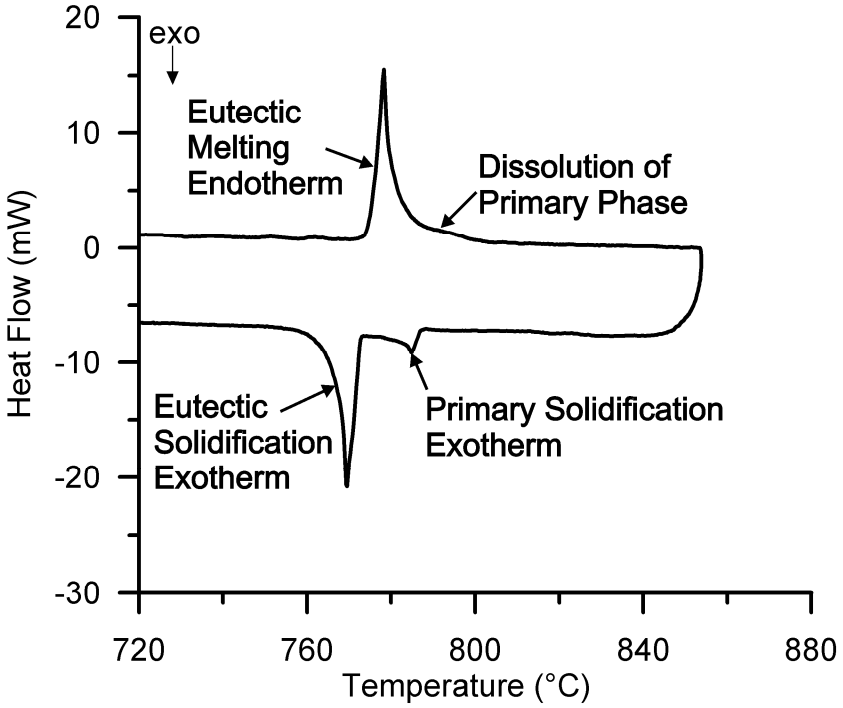

Figure 4-10: DSC trace of Ag - 24% Cu foil with a diffusion barrier between liquid and base metal to prevent metallurgical interaction. Two heating and cooling cycles are shown [57].

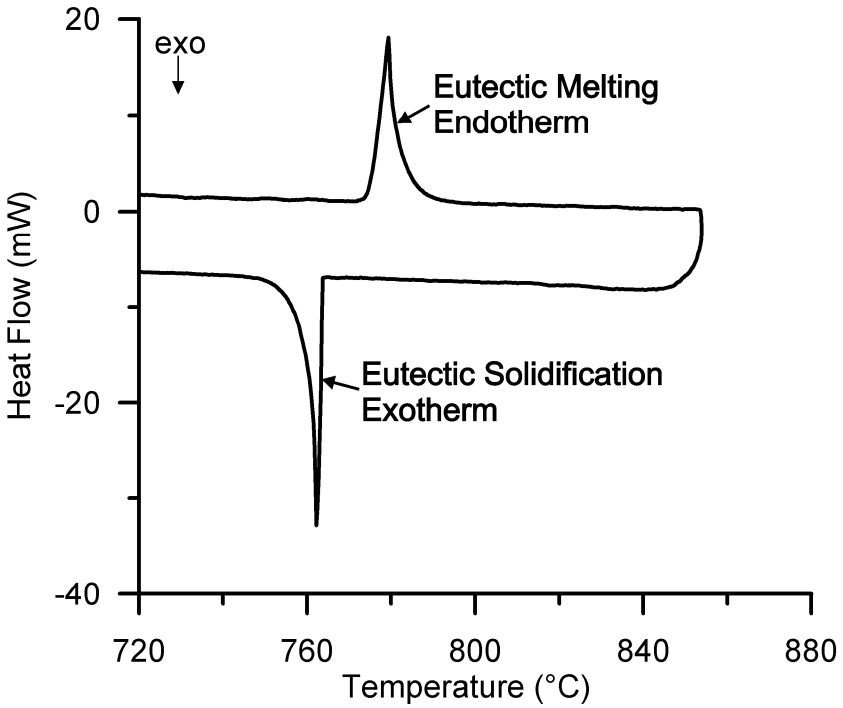

Figure 4-11: DSC trace of eutectic foil with a diffusion barrier between liquid and base metal to prevent metallurgical interaction. Two heating and cooling cycles are shown [57].

The first observation from Figure 4-10 is that the cooling segment shows two exothermic peaks. The first peak is due to the primary α-phase solidification, while the second (larger) peak represents the enthalpy of the eutectic solidification. The solidified microstructure, shown in Figure 4-12, differs from the solidification structure of the diffusion couple (Figure 4-8), both starting with the same liquid composition. The primary α-phase (white) is clearly shown in the eutectic matrix; the solidification structure is distinguished by the dendritic nature and is indicative of a solidification process requiring nucleation. This is consistent with the fact that the measured onset temperature of the primary phase solidification exotherm in Figure 4-10 was 786°C (i.e. 14°C undercooling). This provides further evidence that primary solidification is occurring in the diffusion couple of Figure 4-6 but in an epitaxial manner such that the exothermic energy associated with it is not visible on the DSC trace. It is also worth noting that the second solidification peak in Figure 4-10 has a very similar shape (i.e. a sharp onset) and onset temperature as the eutectic foil of Figure 4-11. Both these peaks are also very similar in shape and onset temperature as the solidification peak from the diffusion couple of Figure 4-6. This confirms that the solidification peaks that are observed in the diffusion couple experiments of Figure 4-7 and measured in Table 4-4 (i.e. final enthalpy) are due only to the solidification of the eutectic.

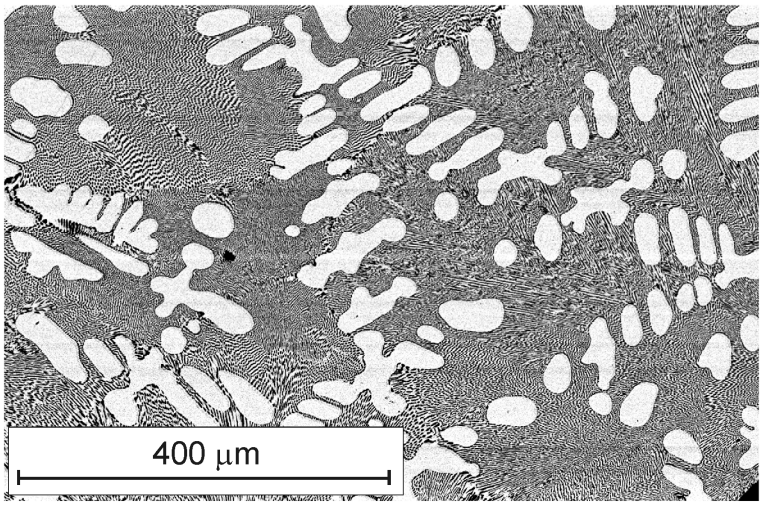

Figure 4-12: Solidified microstructure of Ag - 24% Cu cooled at 10°C/min [57].

The second observation is that the shape of the melting endotherm for the off-eutectic foil does not indicate separate melting peaks for the eutectic and primary phase that it contains. (i.e. these melting events overlap). This shows that in the case of the eutectic/Ag diffusion couple, if melting due to dissolution of the base metal was taking place during heating it would not show as a separate peak in a trace such as Figure 4-7. Therefore it can be concluded that the

endothermic energy measured from the initial melting peak may include dissolution of the base metal.

The above arguments indicate that the measured solidification exothermic energy, ΔH_s, includes only the solidification of the eutectic fraction remaining in the sample and not the entire liquid. Conversely the melting endothermic energy, ΔH_m, may contain not only the initial eutectic but also some dissolution. Therefore calculating the percent liquid remaining by Equation 4-6 yields a systematic underestimation of the liquid fraction present after an isothermal hold time.

From the DSC trace of Figure 4-10 the exothermic energy from the solidification of eutectic phase can be determined (i.e. 73 J/g), and compared to the value obtained from the parallel trace for eutectic foils only from Figure 4-11 (i.e. 101 J/g). This reveals that, for the hypoeutectic liquid, the endothermic energy of the eutectic portion is approximately 72% of the total endothermic energy due to solidification of the liquid remaining (note, however, that the primary and eutectic exotherms overlap in Figure 4-10, which will decrease the measured enthalpy, possibly as much as 10%). This agrees with the measurement of area fraction of α-phase Ag in the microstructure of Figure 4-12, measured using image analysis software to be 25%. Therefore it can be suggested that the exothermic energies for the final enthalpy in Table 4-4 represents only 75% of the total liquid remaining in the sample after a specific hold time, and that the apparent loss of 25% of the liquid at zero hold time in Figure 4-7 is the fraction of primary solidification.

A typical DSC trace of a type-2 diffusion couple experiment with the 24%-Cu foil is shown in Figure 4-13. The heating segment of the trace is similar to the eutectic foil case, there is a clearly defined endotherm representing eutectic melting. In this case, there is not expected to be any dissolution of the base metal. Dissolution of the primary phase within the hypoeutectic foil occurs during heating above the eutectic temperature. There does not appear to be a discernable difference between the DSC results in these two dissolution modes. Comparison of the cooling segments of the 24%-Cu and eutectic foils also does not yield any significant difference. This is the expected result since after dissolution is complete, the solid/liquid interface conditions are the same in each case. The clearly defined exotherm represents the eutectic portion of solidification and there is no indication of primary solidification in the DSC trace.

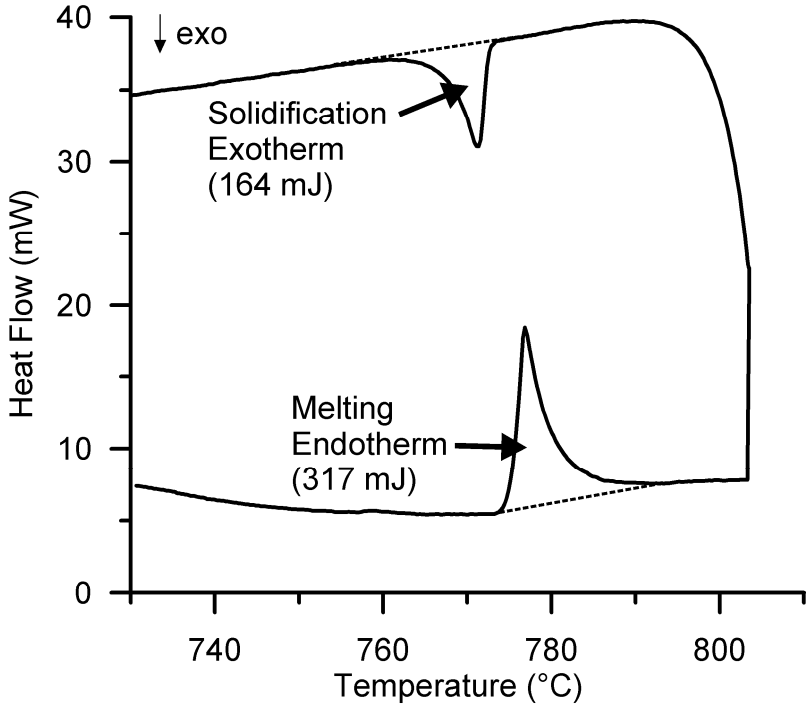

Figure 4-13: Typical 24%-Cu type-2 diffusion couple DSC trace.

A type-1 experiment DSC trace of a 10%-Cu foil heated to the liquidus temperature of 880°C is shown in Figure 4-14. The heating segment shows a distinct peak at the eutectic temperature; and a broad, less distinct peak that follows eutectic melting and extends to the liquidus temperature. Conversely, the cooling segment shows two distinct peaks. The first exotherm represents the primary solidification that is expected to occur upon cooling below the liquidus temperature. The second exotherm represents the eutectic portion of the solidified melt.

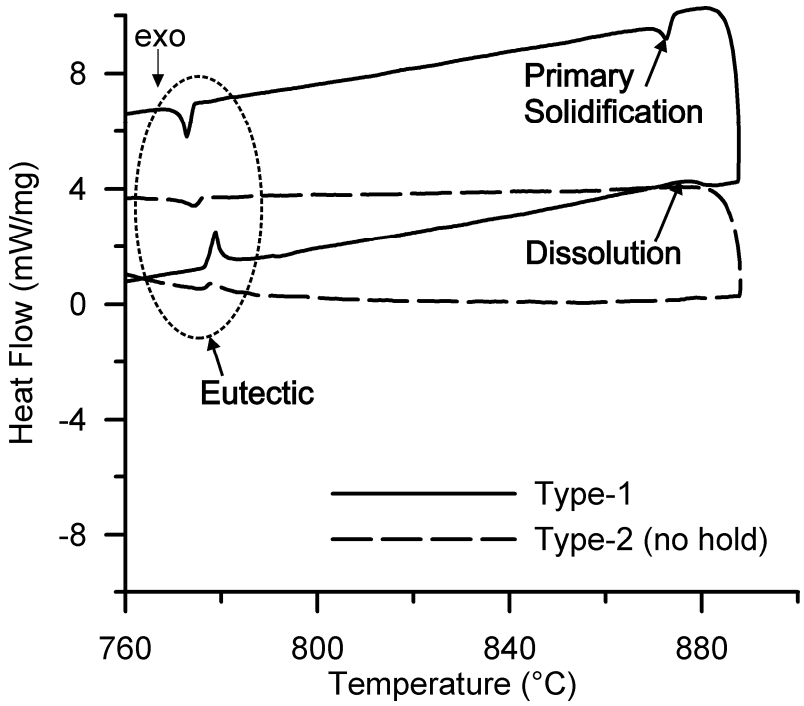

Figure 4-14: DSC traces with and without diffusion barrier of Ag - 10%Cu foil heated to 880°C and cooled.

The corresponding type-2 diffusion couple experiment for a 10%-Cu foil with no isothermal hold is also shown in Figure 4-14. Examination of the DSC trace shows that only one distinct peak can be resolved on both the heating and cooling segments. The heating segment shows a shallow, but distinct peak with an onset at the eutectic temperature. There is no significant indication of primary phase dissolution in the DSC trace. The cooling segment shows an exothermic peak with an onset temperature similar to what is seen with the eutectic and 24%-Cu foils, indicating that the peak represents eutectic solidification. Again, as with the other compositions, primary solidification is not represented in a measurable sense on the DSC trace.

The type-1 DSC experiment was repeated for a 5%-Cu foil without base metal interaction. Since the composition of this foil is below the α-phase solubility limit, no eutectic is expected to form on solidification under equilibrium conditions. As shown by the DSC trace in Figure 4-15, a distinct peak is observed for melting and solidification during the heating and cooling segments, respectively. The onset temperatures for these peaks are well above the eutectic temperature; and no eutectic peak is present on either heating or cooling through the eutectic temperature.

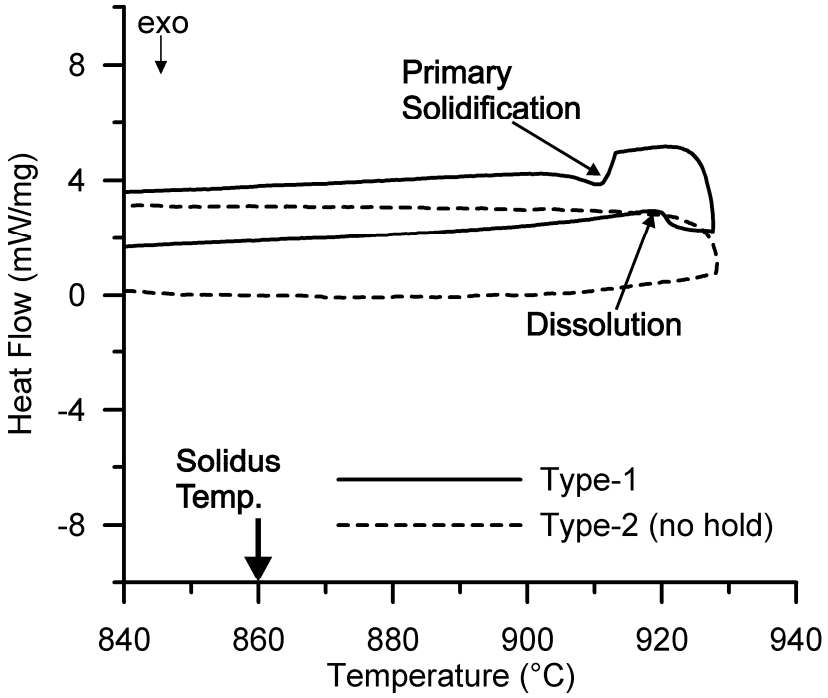

Figure 4-15: DSC traces with and without diffusion barrier of Ag – 5%Cu foil heated to 920°C and cooled.

When base metal interaction is allowed in the type-2 experiment diffusion couple, the DSC trace does not show any discernable peaks at all, as shown in Figure 4-15. In this case, all solidification is in the epitaxial, primary mode, and no eutectic forms from the solidifying melt. A metallurgical examination of the interfacial area of the solidified diffusion couple supports this since a visual eutectic phase is not present. The implication of this result is that since no peaks can be resolved, this DSC method cannot be used to measure the process kinetics of isothermal solidification when no liquid solidifies to eutectic.

The effect of primary solidification on DSC measurements is magnified by the extent of heating above the eutectic temperature. This is illustrated by heating a type-2 diffusion couple with a eutectic foil to 920°C. As a result of base metal dissolution during heating, the liquid composition shifts from the eutectic to 5%-Cu (below the solubility limit). The DSC results shown in Figure 4-16 reveal the expected eutectic melting peak during the heating segment. Upon cooling there is no eutectic solidification peak indicating no eutectic phase has formed. There does appear to be a solidification peak after some undercooling, which is an indication of primary phase solidification. This peak, which is not present in the other experiments, is attributed to equiaxed nucleation of primary α-phase within the liquid. Since the foil has been heated well above the eutectic temperature, a disproportionate amount of base metal dissolution occurred, resulting in a very large liquid width and enabling a change in the solidification mechanism from purely epitaxial to mixed equiaxed and epitaxial as shown by the micrograph in Figure 4-17. Thus, the cooling segment peak seen in Figure 4-16 is a result

of the large liquid width and would not normally be present. This suggests that the liquid film thickness can also be a factor in interpreting the DSC traces of solid/liquid diffusion couples.

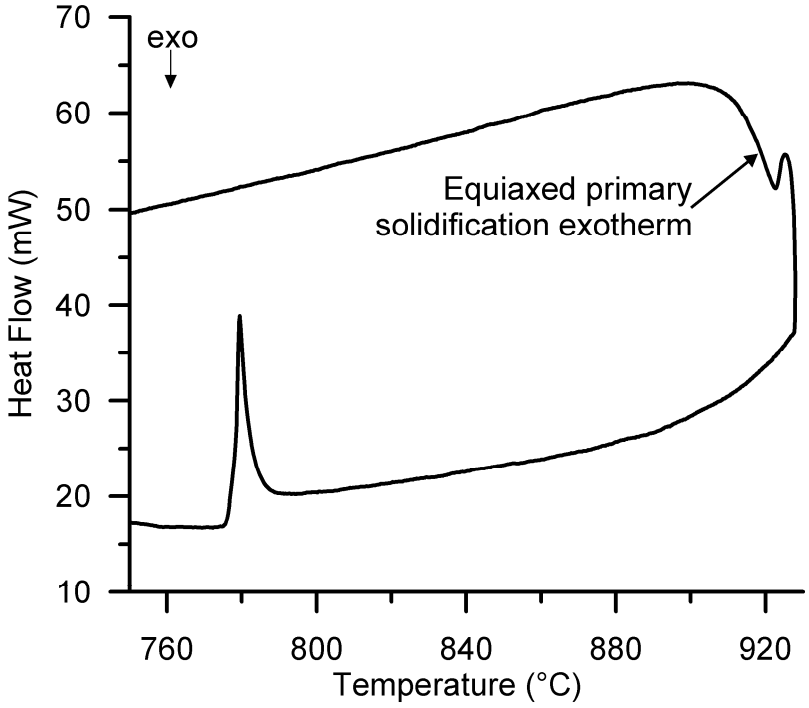

Figure 4-16: DSC trace for type-2 diffusion couple with eutectic foil heated to 920°C with no hold time.

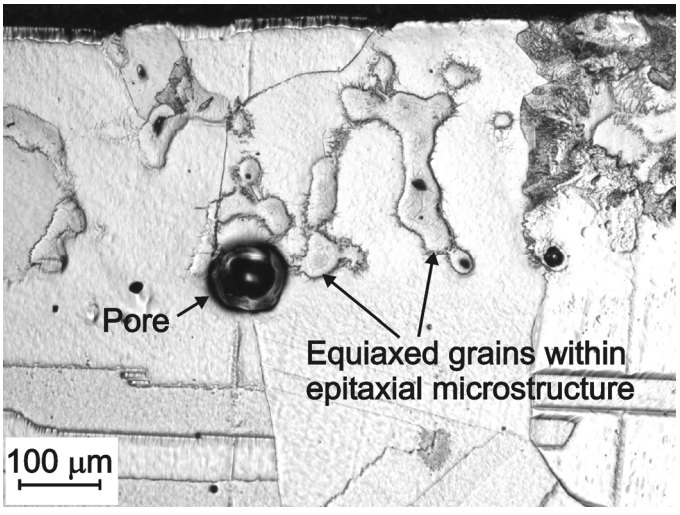

Figure 4-17: Mixed mode solidification observed in the solidified microstructure of the DSC diffusion couple in Figure 4-16. The base metal is at the bottom with the solidified region above the pore. Solid-state cellular precipitation is observed in the top-right corner, for a detailed description of the precipitation see [102].

Interestingly, the problem of liquid loss at short hold times has been found in the literature, but not explored. Venkatraman et al. noticed that the fraction of liquid remaining did not extrapolate to unity in their study of isothermal solidification in electroplated Au-Sn layers on Cu [77]. The investigators offered that the lack of experimental data at short hold times along with a decrease in the isothermal solidification rate due to solute saturation was responsible; however, it is possible that the primary solidification of a fraction of liquid was missed. If the data were adjusted to account for the primary solidification, the experimental results would likely agree more closely with the modeled results [62].

4.3.4. Baseline Shift on First Heating Cycle

Examination of the melting endotherm on the heating segment of the DSC traces in Figure 4-6 and Figure 4-13 reveals a significant baseline shift across the peak. This baseline shift is unusually large in comparison to other DSC results. A shift in the baseline is not observed in the type-1 experiments of Figure 4-10 and Figure 4-11, where no interaction between the liquid and solid phases has been allowed. As outlined in § 3.4, the linear scheme was used to correct the baseline when integrating. Since the nature of the baseline shift is thus far unknown, the accuracy of the linear correction is called into doubt, and any confidence in the resulting enthalpy measurements is weakened. Again, the calculation of 'percent liquid remaining' (Equation 4-6) requires calculation of $\Delta H_s/\Delta H_m$, if the value of ΔH_m is measured higher than actual as a result of baseline correction; the systematic underestimation of the fraction of liquid remaining will be propagated.

The baseline shift occurs only in type-2 diffusion couples and not when metallurgical interaction is prevented in type-1 experiments. Furthermore, the cooling segments in Figure 4-6 and Figure 4-13 do not show a baseline shift across the solidification exotherm. From these observations, it is suspected that the observed baseline shift is due to metallurgical interactions between the foil interlayer and the base metal during melting and subsequent wetting on the faying surface.

In order to confirm the effect of interface development, a multiple heating cycle schedule was used. During the initial cycle, the interlayer melts, wets the faying surface, and solidifies upon cooling. A re-melt cycle appended to the end of the initial cycle allows observation of a melting event without the development of a metallurgical interface between the liquid and solid (i.e. wetting of the faying surface), since this has already occurred.

The resulting DSC trace of the re-melt cycle temperature program is shown in Figure 4-18. A shift in the baseline is clearly evident on the initial heating segment but on the subsequent heating segment, there is no significant observable shift. The DSC trace returns to a path that is collinear with the trace before the melting event. Examination of the cooling segments shows that there is no quantifiable baseline shift across the solidification exotherm. Thus, it

appears that the baseline shift is related to the establishment of a solid/liquid interface in the solid/liquid diffusion couple.

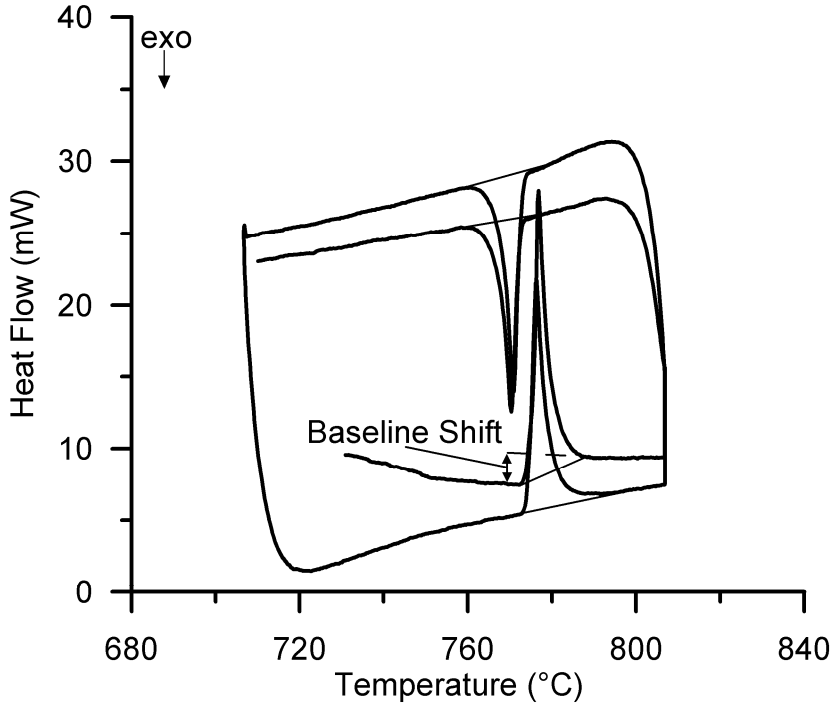

Figure 4-18: DSC trace of Ag-Cu solid/liquid diffusion couple endotherm showing baseline shift on first heating cycle only (28%Cu interlayer, 25 μm thick, T_b = 800°C) [57].

The magnitude of the baseline shift on the first heating segment is greater than expected. With the change of state of the foil interlayer, the specific heat of that material involved in the phase change is expected to change as well. The magnitude of the baseline shift is an indication of the change in specific heat of the sample. If the baseline shift was due only to the change in specific heat, the shift across the melting peak would be equal to the shift across the solidification peak, assuming that no liquid was lost to isothermal solidification in the time required to heat and cool.

It is argued that in this work, the cause of the shift in the DSC trace baseline is due to changes in the thermal coupling of the crucible and the sample before and after melting. This can be described with reference to Figure 4-19. Before melting, there are two interfaces between the Ag base metal and the crucible: the crucible/foil interface and the foil/base metal interface. During initial heating, these interfaces are unbonded, mechanical interfaces with a certain thermal contact resistance. Upon melting, the foil wets and bonds to the base metal and, while there are still two interfaces between the base metal and the crucible, the thermal coupling of the metallurgical solid/liquid interface is much better for heat conduction. The thermal resistances across these interfaces are part of the thermal characteristics of the DSC

cell and as shown by Equation 2-117, a change in the thermal resistance, *R*, will result in a DSC trace baseline shift that is unrelated to the hysteresis discussed in § 3.3.3.

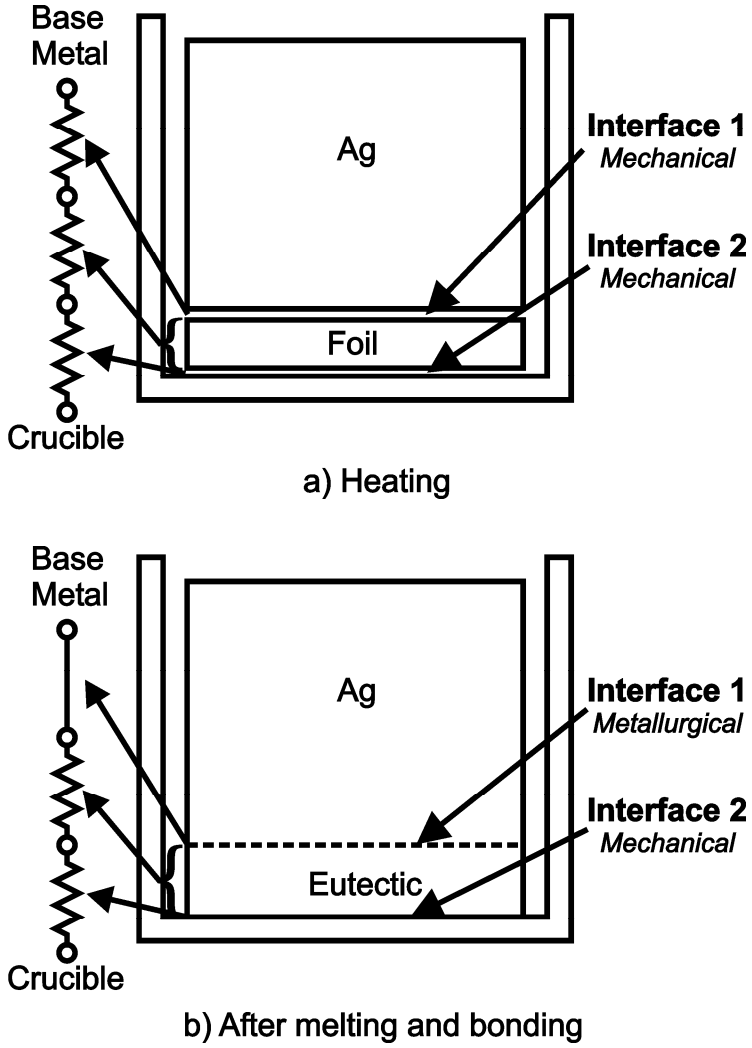

Figure 4-19: Effects of melting on the thermal contact resistance in the DSC sample cell, a) initial heating cycle, and b) subsequent heating cycles [57].

By adding a second heating cycle after solidification, it is clearly seen that the baseline shift only occurs in this magnitude on the first cycle. Since the nature of these interfaces change during the initial heating segment, the observed baseline shift across the melting endotherm is the result. However, once these interfaces develop a stable coupling as in Figure 4-19 (b), the influence of contact resistance is constant. On subsequent melting of the liquid film, the interface which was mechanical in nature on the first cycle is now metallurgical. This results in the much lower baseline shift observed in additional solidification and re-melt peaks.

The effect of this phenomenon is even more profound in the multi-thickness results discussed in § 4.3.2. The thickness of the different interlayers was created by stacking the foils; which in turn, resulted in more mechanical interfaces between the diffusion couple stack-up and the crucible. When additional foil layers are added at the interface of a type-2 diffusion couple experiment, the magnitude of the baseline shift increases. The number of mechanical interfaces increases the contact resistance between the base metal and the sensor, which has the effect of increasing the value of R in Equation 2-117. Therefore, it can be concluded that the large baseline shift that is observed on the first heating segment is indeed due to the effect of thermal coupling between the sample and the crucible; this induces error in the measurement of the melting endotherm and may contribute to the apparent fraction of liquid lost in the DSC results of Figure 4-7.

Accurate integration of the melting endotherms in the presence of the baseline shift is difficult. The integration method shown in Figure 3-10 uses a linear interpolation of the baseline; however, the actual baseline profile is unknown and must be expected to deviate significantly. The endotherm on the first cycle of the DSC trace in Figure 4-18 is measured considerably higher than the endotherm on the second cycle. The process kinetics of isothermal solidification can be considered sufficiently slow that during the time between the first and second melting events, the amount of liquid lost to isothermal solidification will be small. Thus, the reason for the higher enthalpy measured on the first cycle can be attributed to measurement error induced by baseline shift across the melting endotherm.

An overestimation in the value of ΔH_m due to baseline shift on the first heating segment will have the effect of decreasing the fraction of liquid remaining calculated using Equation 4-6. Hence, along with the effects of the base metal presence in the sample crucible and the effect of primary solidification that is not measured by the DSC, the effect of baseline shift contributes to the apparent loss of liquid at t_o and the general underestimation of the fraction of liquid remaining during isothermal solidification in Figure 4-5. Results of additional DSC experiments can be exploited to quantify these effects and ultimately correct the calculated interface kinetics.

4.4. Correction Methodology

4.4.1. Modified Temperature Program

To quantify and correct the effects of primary solidification and baseline shift, a modified temperature program has been developed. The solid/liquid diffusion couples produced using the modified temperature program have been termed type-3 DSC experiments (Table 3-1). As shown in Figure 3-6 (c) the type-3 DSC diffusion couple experiment uses a preliminary

thermal cycle before the isothermal hold cycle. The sample is heated to the peak temperature (T_b, i.e. 800°C for the eutectic foil), then immediately cooled before it is heated again to the isothermal hold temperature. The preliminary cycle is designed to remove the effects of baseline shift during melting by establishing an interface with a stable thermal conductivity without having a significant effect on the process kinetics. Since the interface kinetics in the Ag-Cu experiments are relatively slow, the effect of the preliminary cycle are minimal. This is supported by the results.

An additional thermal cycle was appended to the heating schedule after the isothermal hold time in order to provide more data. This third cycle, which gives a total of 6 enthalpy measurements, is valuable because it adds a heating segment after the isothermal hold period. Thus, the enthalpy of the eutectic melting endotherm can be measured before and after the isothermal hold period. A DSC trace with the corresponding temperature program for a typical type-3 DSC experiment is shown in Figure 4-20. The eutectic foil composition was used for the interlayer to be consistent with the results from Table 4-4.

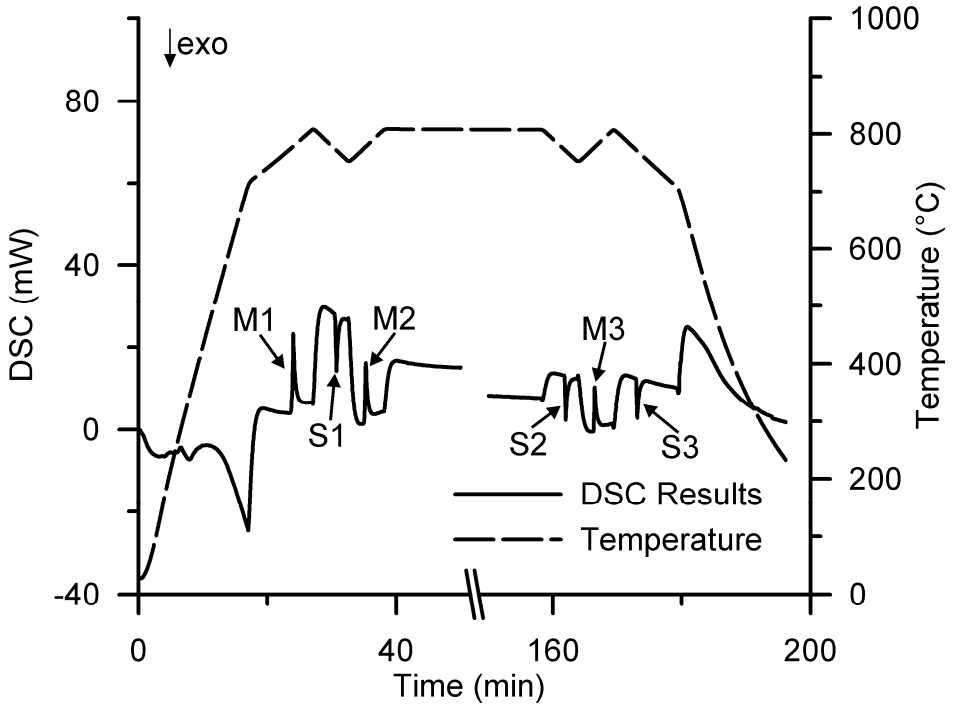

Figure 4-20: Modified DSC temperature program with preliminary and ensuing heating cycles [57].

Table 4-6 gives the results of the type-3 diffusion couple DSC experiments. The values *M1* and *S1* refer to the melting and solidification enthalpies, respectively, for the preliminary heating cycle. Likewise, *M2* and *S2* are the measured melting and solidification enthalpies for

the isothermal hold cycle. Finally, *M3* and *S3* represent the enthalpies of the appended thermal cycle. These peaks are labelled in Figure 4-20.

Table 4-6: Enthalpy measurements for type-3 diffusion couple DSC results (enthalpies are in mJ).

$\sqrt{t}$ ($hr^{1/2}$)	M1	S1	M2	S2	M3	S3	M1/M2	S2/M3
0.0	430	318	340	310	326	290	1.26	0.95
0.5	446	317	364	297	322	274	1.22	0.92
0.5	430	310	338	286	309	293	1.27	0.93
1.0	474	332	382	273	290	271	1.24	0.94
1.4	501	331	368	246	257	229	1.36	0.96
2.0	433	331	363	170	198	168	1.19	0.86
2.5	454	341	359	123	139	120	1.26	0.89
3.0	440	338	382	73	83	68	1.15	0.87

4.4.2. Correcting Baseline Shift

The effect of baseline shift can be quantified by comparing the initial and secondary melting enthalpies (*M1* and *M2* respectively). Examination of the data shows that the initial endotherm (*M1*) is consistently measured larger than the second melting endotherm (*M2*). Since the amount of liquid formed during each heating segment is assumed constant because the process kinetics are slow, the value given by *M2* is considered more correct.

To quantify the baseline shift effect, the data from Table 4-6 can be exploited. The average change in measured enthalpy (*M1-M2*) is 89 mJ. A ratio of the initial melting endotherm to the secondary melting endotherm can by found by *M1/M2*, which is shown in Table 4-6. This ratio considers the effect that different base metal configurations may have on the DSC results. The average *M1/M2* ratio is 1.24, thus, the baseline shift across the melting endotherm due to interface development increases the enthalpy measured by an average 24%.

4.4.3. Correcting Primary Solidification

The effects of primary solidification can be interpreted from the data by comparing endotherms with adjacent exotherms. For example, *S1* is adjacent to *M2*, and *M3* is adjacent to both *S2* and *S3*. The initial endotherm (*M1*) is neglected because of baseline shift effects. In Table 4-6 the solidification enthalpy is consistently less than the adjacent melting enthalpy. Again, it is assumed that the total liquid formed in contiguous segments is equal because the interface kinetics are sufficiently slow. The effect of primary solidification can be quantified

by taking a ratio of solidification enthalpy to an adjacent melting enthalpy (e.g. *S1/M2*, *S3/M3*, or *S2/M3*).

The average ratio values (*S/M*) are calculated from Table 4-6 to be 0.90, 0.88, and 0.91 for *S1/M2*, *S3/M3*, and *S2/M3*, respectively. The ratios *S1/M2* and *S2/M3* can be considered more accurate because they compare the melting endotherm with the previous solidification exotherm. In this sense, there is no liquid loss due to isothermal solidification during the period between peaks because there is no liquid. The extent of isothermal solidification between cycles can be approximated by comparing the two solidification exotherms after the isothermal hold period. Taking a ratio of *S2/S3* gives an average value of 1.04. Multiplying this ratio with *S3/M3* gives an average value of 0.92, which is very close to the average value measured for *S2/M3*, or 0.91. This is expected since *S2/S3*×*S3/M3* gives *S2/M3*. Thus, the average value for the ratio, *S/M*, is 0.91.

From this data it can be deduced that the amount of liquid as measured by the solidification exotherm is about 9% less than that measured by the melting endotherm for a given amount of liquid. The epitaxial primary solidification which is not observable on the DSC has a significant effect; however, a fraction of base metal dissolution is also excluded. To correct for these effects, the measured solidification enthalpy must be adjusted by a factor of 1.10 (*M/S*, or 1/0.91) when compared to the enthalpy of melting.

4.4.4. Corrected Results

By quantifying the effects of baseline shift and primary solidification, the original diffusion couple interface kinetics in Figure 4-7 can be corrected. Multiplication of the original as measured enthalpy ratio (Table 4-4) by the average initial shift (e.g. *M1/M2*, or 1.24) and the ratio *M/S* (e.g. 1.10) adjusts the data to account for the experimental artefacts of baseline shift and primary solidification. The correction factor (ψ) is found to be 1.36. This correction can then be applied to the original DSC results (Equation 4-8) from Figure 4-7 giving the fraction of liquid remaining as a function of root time in Figure 4-21. The corrected data can be fit to a line which has the form of Equation 4-9. This corrected fraction of liquid remaining extrapolates close to unity at the ordinate axis, crossing at 99.4%.

$$\text{fraction of liquid remaining} = \psi \frac{\Delta H_s}{\Delta H_f} \qquad \text{Equation 4-8}$$

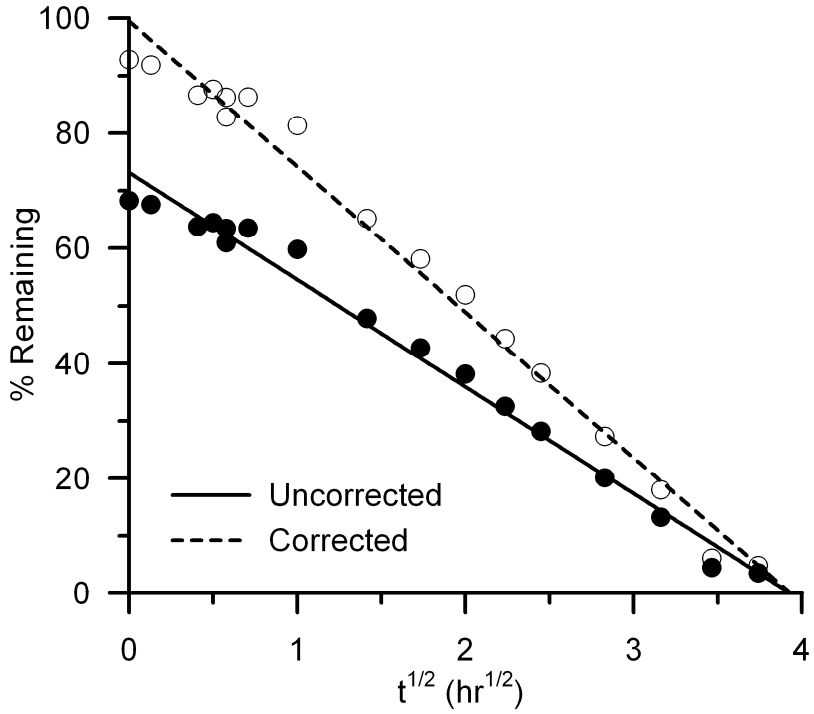

Figure 4-21: Effect of applying a correction factor to the diffusion couple interface kinetics (28%Cu interlayer, 25 μm thick, T_b = 800°C) [57].

$$\%LR = -25.3 \cdot \sqrt{t} + 99.4 \qquad \text{Equation 4-9}$$

The corrected data matches the expected interface kinetics (Figure 4-5) exceptionally well. The correction has been applied in a logical sense and the results appear intuitively correct. Now that the interface kinetics have been accurately characterized, they can be compared to other experimental setups such as different temperatures, foil thickness, or material systems. Furthermore, the results can be compared to the predictions generated by analytical models, which assume 100% liquid remaining at t_o.

In addition to the corrected data in Figure 4-21, the data from the type-3 experiments in Table 4-6 can be used to characterize interface kinetics and confirm the validity of the correction. The dataset *S2/M1* is comparable to the original experimental results; however, the ratio *S2/M2* eliminates the baseline shift effect, and shows only the effect of primary solidification (i.e. underestimate the fraction of liquid remaining). Furthermore, similar types of peaks can be compared. The ratios *S2/S1* and *M3/M2* are the fractions of liquid remaining, taken from the solidification exotherms and melting endotherms respectively, before and after the isothermal hold period.

All of the results for the fraction of liquid remaining can be interpreted to give a time required for the completion of isothermal solidification (t_s), and a corresponding interface rate constant (ξ). This data can then be used along with analytical modeling to predict the

isothermal solidification kinetics when one or more parameter in the system is changed, such as foil thickness, etc.

4.5. Summary

An experimental approach for quantifying the kinetics of interface motion in a solid/liquid diffusion couple using DSC has been developed. Experimental results show that a number of factors affect the enthalpy measurements. The initial interlayer composition, the heating rate, the reference crucible contents, and the base metal coating must be considered in development of the experiment parameters. The process kinetics of isothermal solidification can be calculated from the experimental DSC results. The presence of base metal in the sample crucible has a profound effect on the enthalpy measurements. First, conduction of heat into the base metal reduces the enthalpy measured upon both melting and solidification. Second, the combined effects of base metal dissolution during melting and epitaxial primary solidification upon cooling result in a systematic underestimation of the fraction of liquid remaining. Finally, baseline shift upon initial melting of the interlayer causes an overestimation in measurement of the melting endotherm. These effects can be quantified by appending a heating cycle before and after the isothermal hold period. A resulting factor (ψ) can be applied to the calculated fraction of liquid remaining to correct the experimental artefacts.

5. Analysis of Diffusion Couple Interface Kinetics

5.1. DSC Results

The additional enthalpy peaks provided by the modified temperature program allow for a number of different ways to analyze and interpret the DSC data in order to characterize the interface kinetics of the solid/liquid diffusion couple.

The original results, shown with the correction applied in Figure 4-21 can be compared to the DSC results obtained by taking the ratio *S2/M1* from the data in Table 4-6. The value of *S2/M1* gives the closest result to the original DSC results since it is a ratio of the solidification exotherm taken after the isothermal hold period to the initial melting endotherm; the fraction of liquid remaining using *S2/M1* is shown in Figure 5-1, along with a correction factor, ψ, of 1.36 using Equation 5-1. A comparison of the fraction of liquid remaining after an isothermal hold period as calculated using the type-2 results and *S2/M1* from the type-3 results is shown in Figure 5-2.

$$\text{fraction of liquid remaining} = \psi \frac{S2}{M1} \qquad \text{Equation 5-1}$$

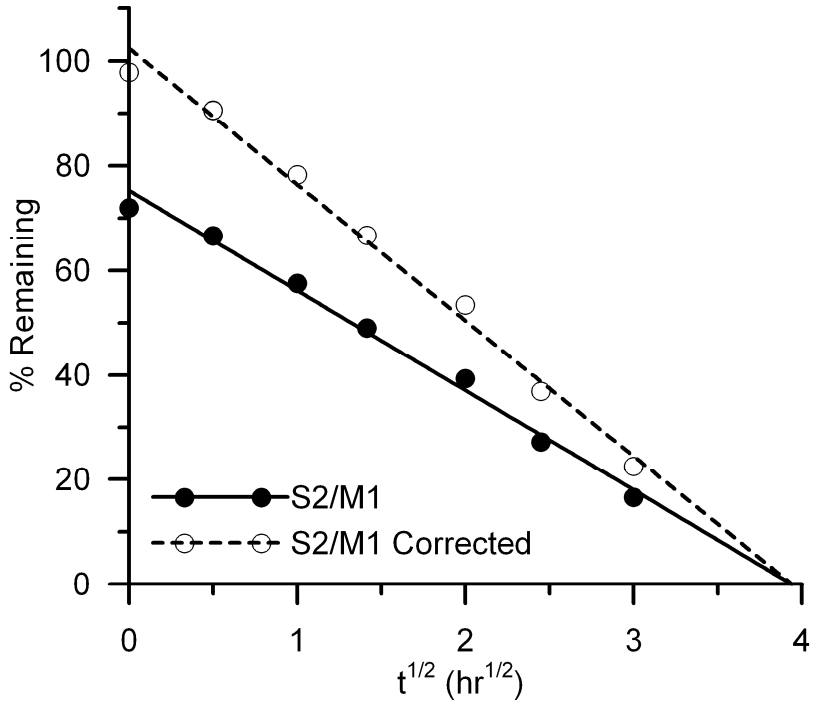

Figure 5-1: Modified temperature program type-3 DSC results with correction (28%Cu interlayer, 25 μm thick, T_b = 800°C).

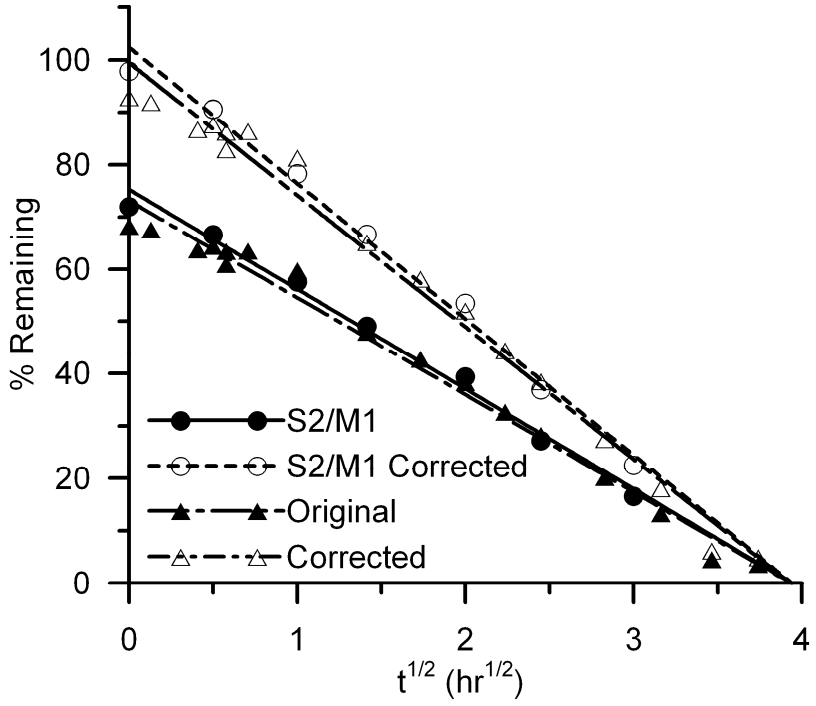

Figure 5-2: Comparison of interface kinetics as determined from the fraction of liquid remaining using the original type-2 DSC results and modified temperature program type-3 DSC results, both are corrected using ψ=1.36 (28%Cu interlayer, 25 μm thick, T_b = 800°C).

Inspection of Figure 5-2 shows that the interface kinetics measured using comparable peaks in the type-2 and type-3 solid/liquid diffusion couple experiments are similar. The linear trend applied to the data shows similar characteristics. The time required for the completion of isothermal solidification (t_s) is the same for both methods. Both corrected fits cross the vertical axis at approximately 100%. The interface kinetics indicated by the slope of the line are comparable. There is no significant discernable difference between the results of the type-2 and type-3 experiments.

The result in Figure 5-2 is important because it confirms that the effect of adding a thermal cycle before the isothermal hold period is negligible. The interface kinetics for similar solid/liquid diffusion couples are not affected by the modification. Thus, it is appropriate to utilize the additional data provided by the added thermal cycles to interpret the DSC results.

The DSC results in Figure 5-1 give the fraction of liquid remaining after an isothermal hold time as calculated using the ratio *S2/M1*, where *M1* is the initial melting endotherm. As described in § 4.3.4, there is a baseline shift that occurs across the endotherm as a result of interface development in the diffusion couple. It has been shown § 4.4.2 that the baseline shift has the effect of increasing the measured endothermic enthalpy and reducing the calculated fraction of liquid remaining. Figure 4-18 shows that the baseline shift occurs only on the first heating cycle, a result of the development of a metallurgical interface; thus, the second melting endotherm (*M2*) does not have the inherent effect of baseline shift. In the same manner as Figure 5-1, the fraction of liquid remaining can be calculated by taking the ratio *S2/M2*. In this sense the effect of baseline shift is expected to be removed from the measurement system.

The fraction of liquid remaining calculated using *S2/M2* from the data in Table 4-6 is shown in Figure 5-3. The interface kinetics calculated using the ratio *S2/M1* are also given in Figure 5-3 for comparison.

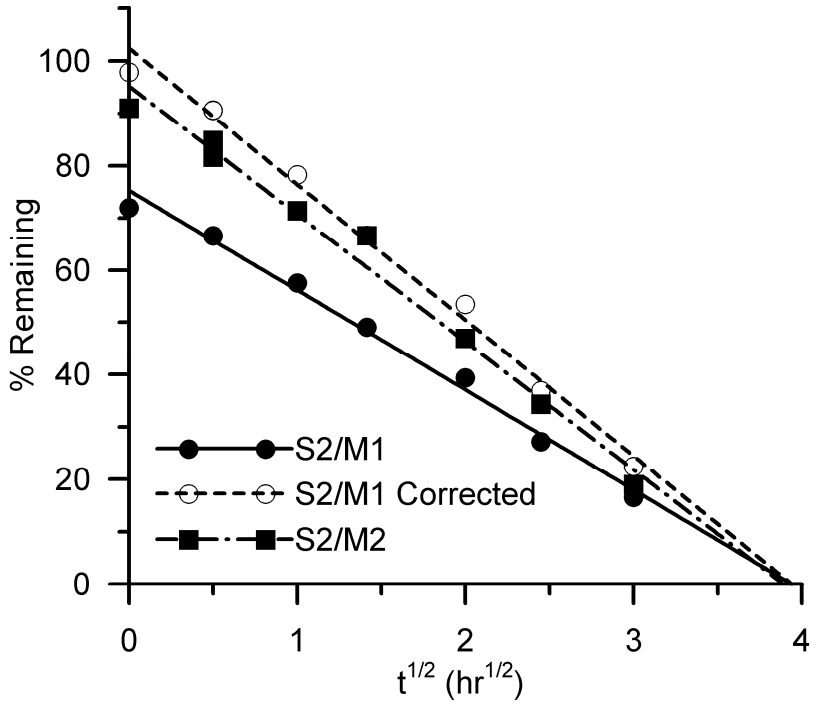

Figure 5-3: Comparison of interface kinetics calculated using the ratio *S2/M1* and *S2/M2* (28%Cu interlayer, 25 μm thick, T_b = 800°C) [57].

The fitted least squares regression trend line for the *S2/M2* dataset crosses the ordinate axis at 95%. The effect of baseline shift has been removed from the results; however, the effect of primary solidification during cooling to the eutectic temperature persists. The fit line lies lower than the corrected line in Figure 5-3 as a result of this effect. The predicted t_s is the same since all lines converge at the abscissa. A correction for the primary solidification effect would remedy this problem.

In addition to comparing dissimilar peaks (i.e. endotherms and exotherms); like peaks can be analyzed to give an indication of interface kinetics. The type-3 modified temperature program provides 6 peaks, 3 endotherms and 3 exotherms which can be exploited. The similar peaks can be compared with each other before and after the isothermal hold period. To find the fraction of liquid remaining using the endotherms, the ratio *M3/M2* can be used to compare melting before and after the isothermal hold. Likewise, the ratio *S2/S1* can be used to evaluate the interface kinetics using the solidification exotherms. Figure 5-4 shows the results of this analysis using the data from Table 4-6. The fitted lines compare well with each other with a slight difference in slope and intercept with the vertical axis. The t_s predicted by extrapolation of both the *M3/M2* and *S2/S1* lines to the abscissa compares very well with that predicted by the uncorrected *S2/M1* data.

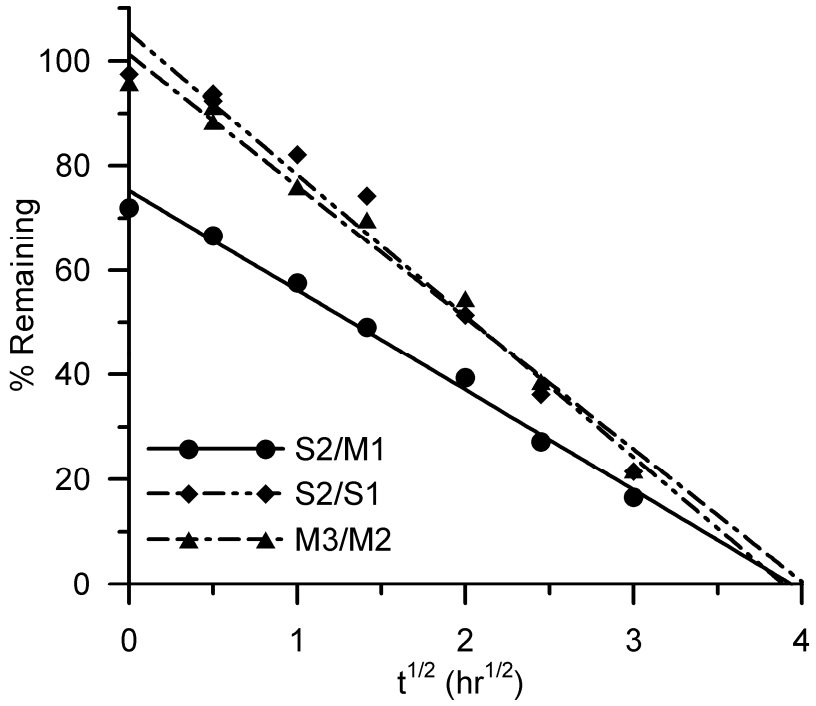

Figure 5-4: Comparison of interface kinetics using similar peaks (*S2/S1* and *M3/M2*) compared to *S2/M1* (28%Cu interlayer, 25 μm thick, T_b = 800°C) [57].

The interface kinetics found using similar peaks are also compared to the *S2/M2* and corrected *S2/M1* lines in Figure 5-5 and Figure 5-6. As expected the *S2/M2* line lies below both the *M3/M2* and *S2/S1* lines. By using the similar peaks, the effects of baseline shift and primary solidification have been neutralized. The initial melting endotherm, across which the baseline shift occurs is not considered in this analysis. Furthermore, since like peaks are used, the differences in dissolution and primary solidification between the endotherms and exotherms are not manifested in the results. Thus, the interface kinetics, as measured, should compare well with the corrected results using *S2/M1*. This is shown in Figure 5-6, the results from the similar peaks, *M3/M2* and *S2/S1* do in fact agree very well with the corrected *S2/M1* line. The difference between the individual lines is difficult to distinguish and the t_s values predicted by each line are reasonably close enough to be considered the same.

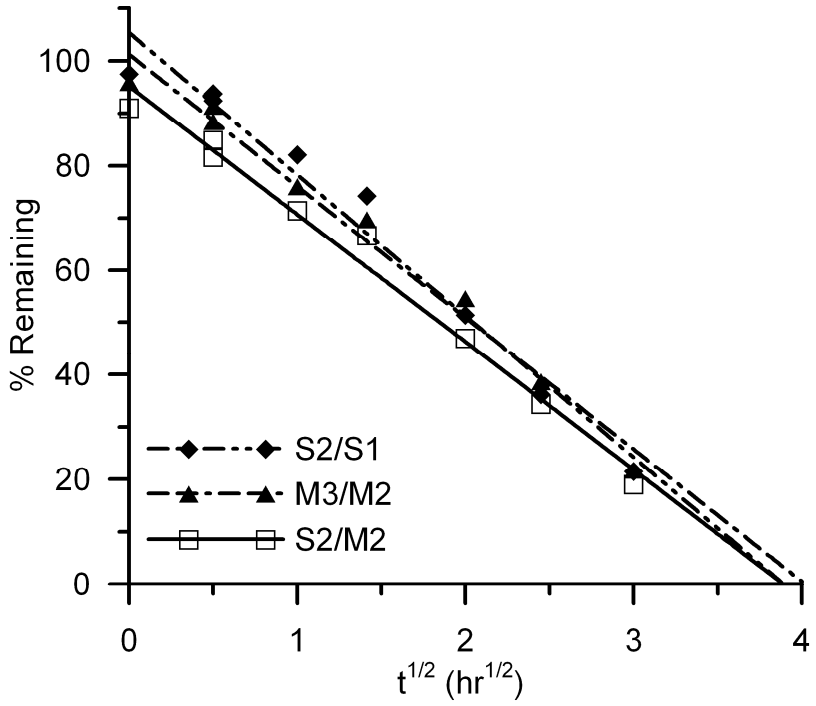

Figure 5-5: Comparison of interface kinetics using similar peaks and *S2/M2* (28%Cu interlayer, 25 μm thick, T_b = 800°C).

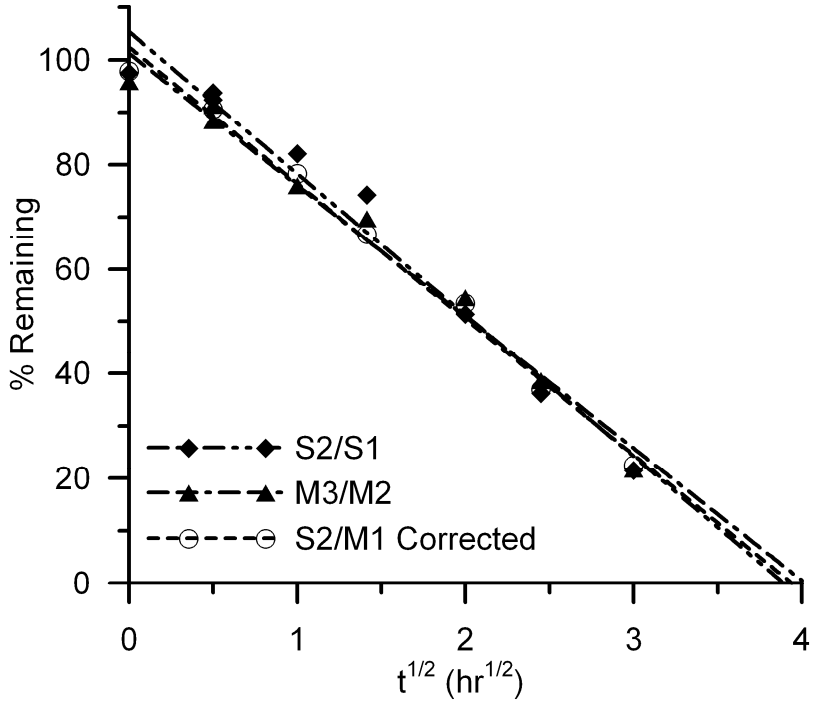

Figure 5-6: Comparison of interface kinetics using similar peaks and corrected *S2/M1* (28%Cu interlayer, 25 μm thick, T_b = 800°C).

There are a number of datasets that can be used to quantify the interface kinetics. The corrected type-2 and type-3 results from dissimilar peaks, as well as the uncorrected results obtained using similar peaks.

If the fraction of liquid remaining at a time t is given by χ, the corrected DSC results given in the form of Equation 4-9 can be written as Equation 5-2:

$$\chi = \beta\sqrt{t} + \chi_o \qquad \text{Equation 5-2}$$

where β is the slope of the line and χ_o is the initial liquid fraction which is normally unity; however, in some results the fitted line does not pass through exactly 100% liquid remaining at t_o.

The position of the solid/liquid interface can be found by Equation 5-3.

$$X(t) = (\chi_o - \chi)\cdot\frac{W_{max}}{2} \qquad \text{Equation 5-3}$$

Rearranging Equation 5-3 and combining with Equation 5-2 gives Equation 5-4.

$$\frac{2}{W_{max}}\cdot\frac{X(t)}{\sqrt{t}} = \beta \qquad \text{Equation 5-4}$$

By definition, ξ is given by Equation 5-5. This can be substituted into Equation 5-4.

$$\xi = \frac{X(t)}{\sqrt{t}} \qquad \text{Equation 5-5}$$

Thus, the interface rate constant, ξ, can be determined from the experimental results (i.e. slope of the fitted line) through Equation 5-6.

$$\xi = \beta\cdot\frac{W_{max}}{2} \qquad \text{Equation 5-6}$$

Alternatively, at the completion of isothermal solidification (i.e. t_s), χ is 0 and Equation 5-2 can be rewritten as Equation 5-7.

$$\beta = -\frac{\chi_o}{\sqrt{t_s}} \qquad \text{Equation 5-7}$$

Intuitively, χ_o is 1; however, slight deviations from this are observed in the experimental results due to experimental error. Assuming that χ_o is 1 and substituting into Equation 5-6 gives a solution for the experimental rate constant from the experimentally measured value of t_s (Equation 5-8).

$$\xi = -\frac{W_{max}}{2\cdot\sqrt{t_s}} \qquad \text{Equation 5-8}$$

The predicted t_s is determined by extrapolating the regression line to the abscissa, where the fraction of liquid remaining is zero. The time is found through Equation 5-9.

$$t_s = \left(\frac{\chi_o}{\beta} \right)^2 \qquad \text{Equation 5-9}$$

Results from the original type-2 experiments are $\chi_o = 0.994$, and $\beta = -0.235/\sqrt{\text{hr}}$, as given by Equation 4-9. The t_s predicted from these results is 15.5 hours given a maximum liquid width of 59.5 μm (Equation 2-56). This gives a measured interface rate constant of $\xi = -0.126$ μm/√s using Equation 5-8.

The measured interface rate constants for the entire series of experimental results, is given in Table 5-1. The values range from -0.124 μm/√s to -0.129 μm/√s, with one outlying value of -0.134 μm/√s. The average value for the interface rate constant is -0.126 μm/√s.

Table 5-1: Summary of interface kinetics.

Results	χ_o	β (1/√hrs)	t_s (hrs)	ξ (μm/√s) (Equation 5-6)	ξ (μm/√s) (Equation 5-8)
Type-2 corrected	0.994	-0.253	15.5	-0.125	-0.126
S2/M1 corrected	1.02	-0.260	15.4	-0.129	-0.126
M3/M2	1.01	-0.252	16.1	-0.125	-0.124
S2/S1	1.05	-0.270	15.1	-0.134	-0.128

5.2. Modeling

The isothermal solidification kinetics generated from the DSC results can be compared to the predictions produced from the analytical models derived in § 2.2. The time required for the completion of isothermal solidification (t_s) and the interface rate constant (ξ) are the specific output parameters of interest.

The model input is determined by the experimental setup. At 800°C, $C_{\alpha L}$ is 12.6 at.% (7.8 wt.%) and $C_{L\alpha}$ is 34.9 at.% (24 wt.%).

Selection of an appropriate diffusion coefficient is difficult as published chemical diffusion data in this composition range is unavailable. The diffusivity in Ag with a range of 0 - 2 at. % Cu at 800°C is reported to be 5.9×10^{-10} cm^2/s [111]. Homogeneous diffusion data, however, shows that diffusivity is enhanced with increasing concentration of Cu in Ag [112]. Agreement with the models is very good if a published diffusion coefficient of 7.0×10^{-10} cm^2/s (for a 6.56 at. % Cu homogeneous solution [112]) is selected.

5.3. Moving Interface Solution

Using the moving interface solution, the interface rate constant, ξ, is calculated as -0.126 μm/√s (Equation 2-93) and isothermal solidification is predicted to take 15.5 hours to complete (Equation 2-94). This agrees exactly with the isothermal solidification kinetics measured using DSC. It should be noted that if a lower diffusivity value was selected, the interface kinetics would be slower, for example if $D = 5.9 \times 10^{-10}$ cm^2/s the calculated $\xi = -0.116$ μm/√s, and the predicted isothermal solidification time would be 18.4 hours. However, the value of $D = 7.0 \times 10^{-10}$ cm^2/s will be used here because: first, it is based on sound scientific knowledge; and second, it supports the experimental results.

It has been widely reported that grain boundaries provide an enhanced solute diffusion path that results in faster diffusion rates and irrigation of the base metal [2,68,76]. This effect has been shown to be negligible in the Ag-Cu system at temperatures above 700°C in a coarse grained base metal where there are few grain boundaries to enhance diffusion [111]. Furthermore, the effect of grain boundaries on the process kinetics becomes less significant at long isothermal hold times.

5.4. Stationary Interface Solution

Using Equation 2-48 for the stationary interface solution, isothermal solidification is predicted to require 21.3 hours. Zhou reported that the assumption of a stationary solid/liquid interface results in an overestimation that is largely dependent on the liquidus and initial base metal solute compositions [59]. Following the method developed by Zhou for the estimation error, Equation 5-10, derived from Equation 2-48 and Equation 2-94, shows that the estimation error in the stationary solution gets large when C_o or $C_{\alpha L}$ is large, or when $C_{L\alpha}$ gets relatively small [59]. The effect of the $C_{\alpha L}$ and $C_{L\alpha}$ compositions on the estimation error associated with using the stationary solution over the moving interface solution is shown graphically in Figure 5-7. In this study, the error associated with using the stationary interface is found to be 38%, as pointed out by the arrow. These results show that the stationary solution can only be used under specific conditions if a minimal amount of estimation error is expected; solutions that assume a moving interface are much more accurate.

$$\text{Error} = \left[\frac{\pi \cdot \xi^2}{4D} \cdot \left(\frac{C_{L\alpha}}{C_{\alpha L} - C_o} \right)^2 - 1 \right] \times 100\% \qquad \text{Equation 5-10}$$

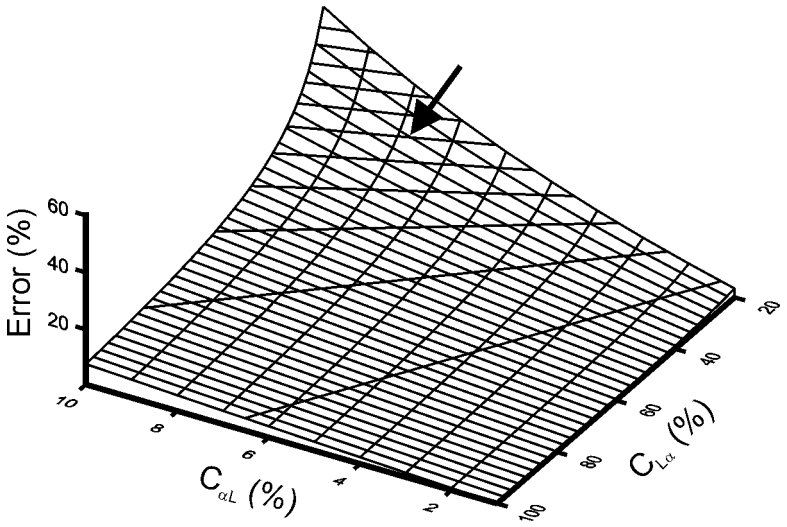

Figure 5-7: Effect of solidus and liquidus concentrations on estimation error, C_o=0 [100].

5.5. Nakao et al. Solution

Finally, the predicted isothermal solidification time using the Nakao et al. solution is 8.7 hours (Equation 2-58). This treatment, however, is not theoretically accurate on a physical basis since it assumes a stationary solution with a shifting reference frame and does not account for increased solute build up in the base metal as a result of the sweeping action of the solid/liquid interface. The resulting composition profile of the solute in the base metal after 15 hours of isothermal hold time is shown in Figure 5-8. The shape of the Nakao et al. profile is identical to that of the stationary interface profile with a shift from the original solid/liquid interface position. This assumption virtually enhances flux at the solid/liquid interface and results in an overestimation of the isothermal solidification kinetics as shown in the results.

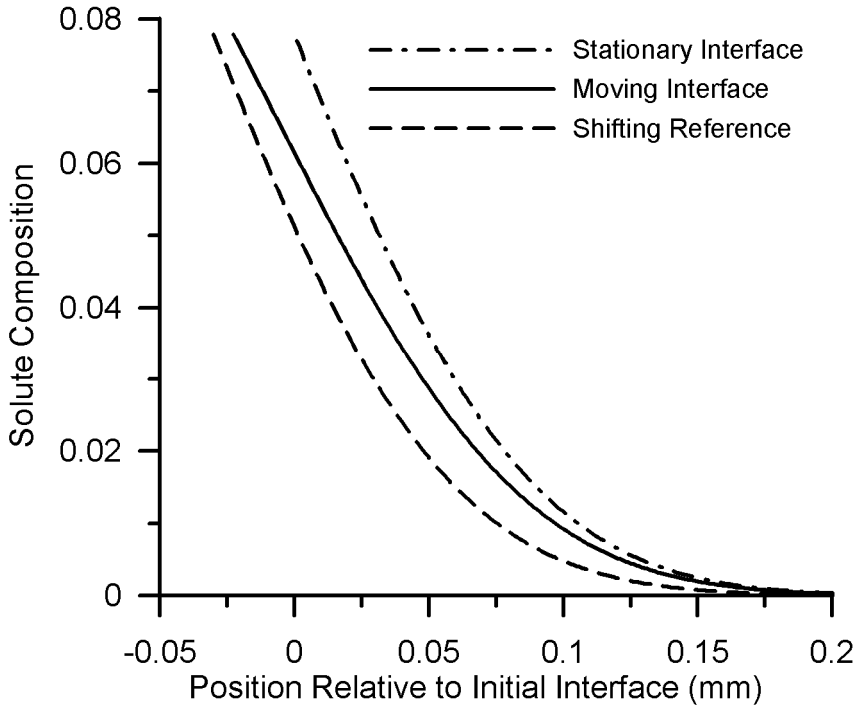

Figure 5-8: Composition profile of solute in the base material [100].

5.6. Comparison of Results

The model results are compared to the experimental DSC results in Figure 5-9. As shown, the best analytical model for predicting the isothermal solidification process kinetics in TLP bonding is the moving interface prediction (ξ = -0.126 μm/√s). As noted, the selected value for the solute diffusivity has a profound effect on the accuracy of the predicted isothermal solidification kinetics. The interface rate constant for the stationary solution as calculated using Equation 2-93 is ξ = -0.107 μm/√s. Similarly, the interface rate constant using the Nakao et al. solution is ξ = -0.168 μm/√s. Examination of Figure 5-9 shows how the stationary solution underestimates the interface kinetics, while the shifting reference frame solution of Nakao et al. overestimates.

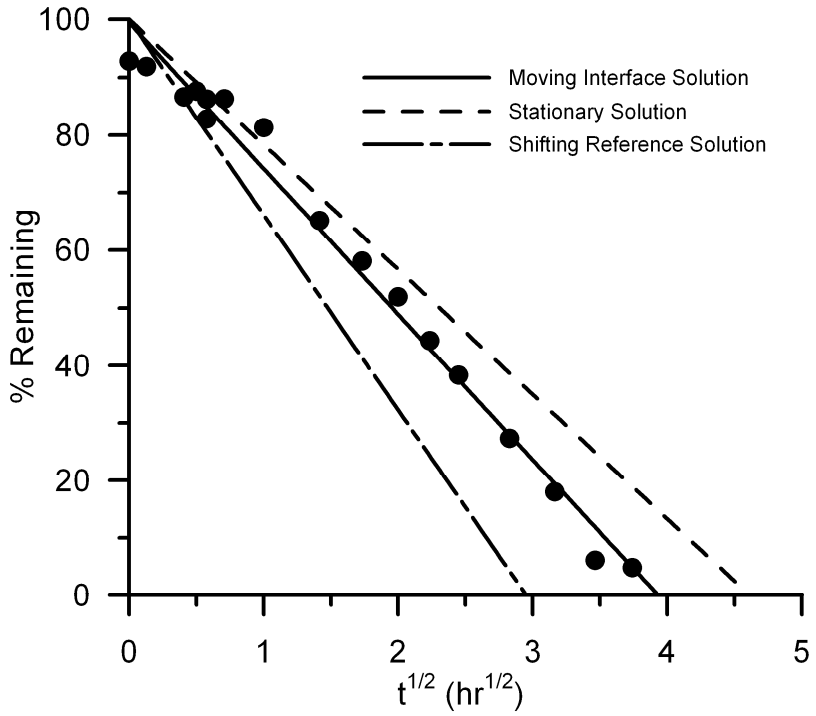

Figure 5-9: Comparison of experimental and modeling results (28%Cu interlayer, 25 μm thick, T_b = 800°C).

The DSC results can also be compared to interface kinetics reported in the literature. Tuah-Poku et al. [39] measured isothermal solidification kinetics for TLP bonds at 820°C with pure Ag base metal and an 80 μm thick pure Cu interlayer and reported extreme inaccuracy with the analytical models. From their experimental results, which were collected using visual inspection of metallurgically prepared samples, an interface rate constant, ξ, was found to be -0.290 μm/√s [39]. Since these experiments were conducted at a higher temperature than the DSC trials (820°C vs. 800°C), the interface kinetics are expected to differ somewhat. If the diffusivity value used earlier is corrected for the increase in temperature, the constant becomes: $D = 10 \times 10^{-10}$ cm^2/s. With $C_{\alpha L} = 11.3$ at.% (7.0 wt.%) and $C_{L\alpha} = 29.8$ at.% (20 wt.%), the predicted interface rate constant is -0.160 μm/√s, which is significantly slower than the measured value. There is a marked difference between the results collected by Tuah-Poku et al. using visual inspection and the results collected using DSC under similar experimental conditions, even when the small difference in temperature is considered.

Tuah-Poku et al. repeated their experiment using a 75 μm thick Ag-20 wt.% Cu foil interlayer at the same bonding temperature [39]. Isothermal solidification was reported to be complete, except for some liquid trapped at the grain boundaries after 8 hours, for which ξ = -0.221 μm/√s. The predicted interface rate constant (which is assumed to be unaffected by changes in interlayer thickness or composition) gives a time of 15.2 hours for completion of

isothermal solidification. It is predicted that 27% of the liquid remains after 8 hours. According to Tuah-Poku et al., the non-planar characteristics of the interface make it difficult to accurately make a quantitative measure of the isothermal solidification kinetics because at some areas liquid is trapped at the grain boundaries, while at others isothermal solidification is complete. The DSC results, however, provide an accurate representation of the process kinetics as they are not prone to measurement error of this nature.

In the present study, the DSC experiment was repeated using a Ag-24 wt.% Cu foil interlayer at 800°C. The results are shown in Figure 5-10 by the solid line. In this case, the interlayer composition is the same as the liquidus composition at T_b and there is not expected to be any base metal dissolution. The interlayer consists of eutectic and pro-eutectic α-Ag. The eutectic melts first followed by dissolution of the pro-eutectic phase; however, the kinetics of dissolution are expected to differ somewhat from the case of the eutectic interlayer. The α-phase is dispersed throughout the interlayer in the 24%Cu interlayer so dissolution does not occur on a planar interface but throughout the liquid layer. As a result, the correction factor, ψ, that is applied to the results has to be adjusted (i.e. 1.25 vs. 1.36 for the eutectic interlayer). The value of ψ is determined by fitting the data to pass through 100% rather than determining it experimentally (i.e. type 3 experiment).

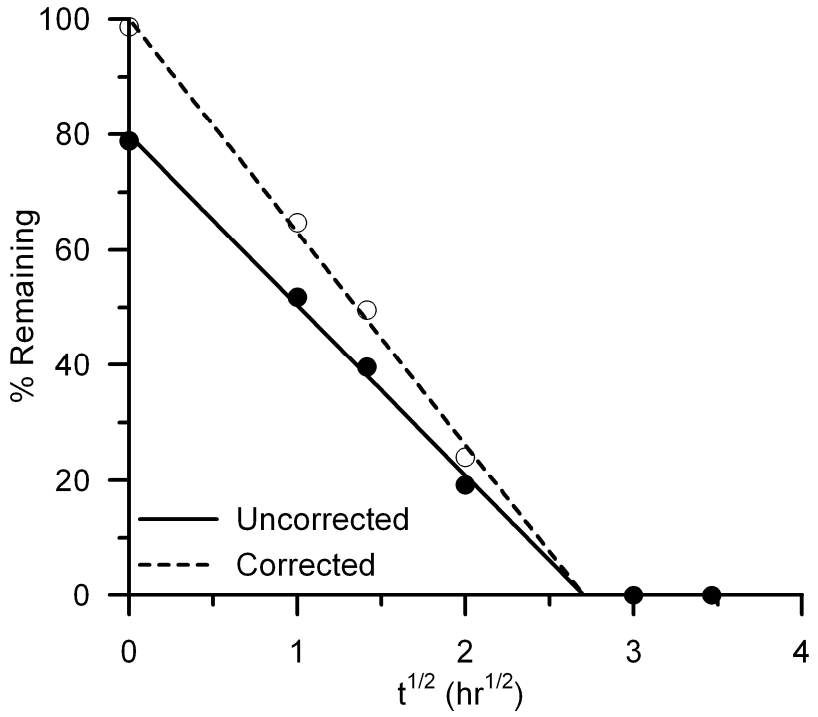

Figure 5-10: Results of isothermal solidification for Ag base metal and Ag-24%Cu interlayer (T_b = 800°C).

Since the temperature has not changed, the interface rate constant should be the same as the original conditions (eutectic interlayer), which was ξ = -0.126 μm/√s. The results give a measured ξ of -0.128 μm/√s, which is very close to the original results for the eutectic interlayer. The DSC method consistently produces accurate results.

The isothermal solidifications kinetics for the Ag-10%Cu interlayer are given in Figure 5-11. The isothermal hold temperature, T_b, was 880°C, at which temperature the liquidus composition is 10% Cu, the same as the interlayer. Thus, as in case of the 24% Cu interlayer, there will be no base metal dissolution upon heating to the bonding temperature. Examination of a typical DSC trace for the Ag-10%Cu interlayer (i.e. Figure 4-14) shows that only a small portion of the interlayer melts as eutectic. The resulting endotherm and exotherm for eutectic melting and solidification, respectively, is small and there is no indication of dissolution or primary solidification in the DSC trace. The small magnitude of the peak makes accurate enthalpy measurement difficult; however, the results in Figure 5-11 agree well with the expected square root interface motion. The uncorrected results intersect the ordinate axis near unity; thus, only a small correction is applied to the results. Once again, the correction is determined by fitting the data to pass through 100%.

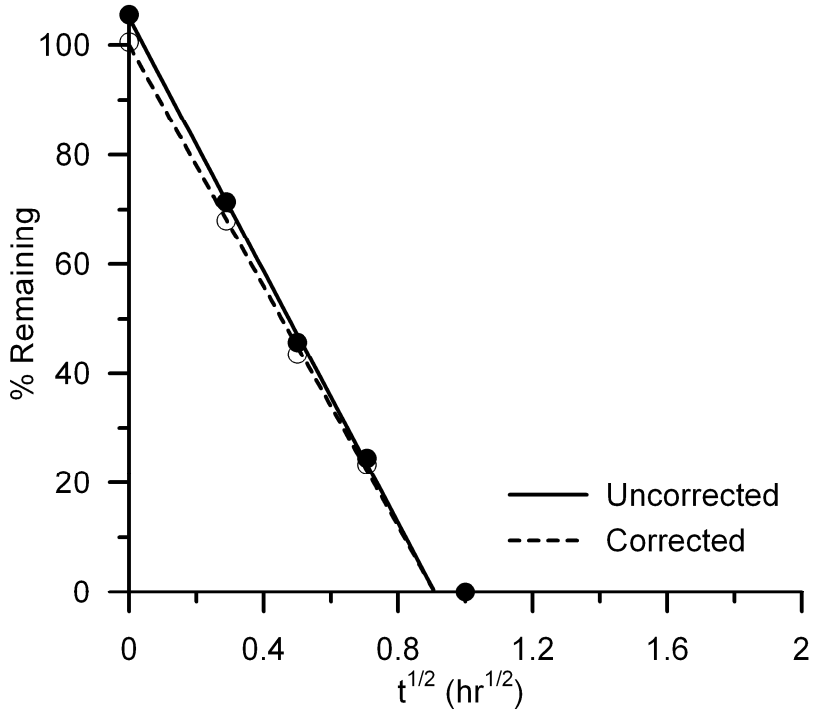

Figure 5-11: Results of isothermal solidification for Ag base metal and Ag-10%Cu interlayer (T_b = 880°C).

Inspection of the DSC trace in Figure 4-14 shows that baseline shift on the heating cycle is not significant. This is likely due to the progressive formation of the solid/liquid interface as

the interlayer is dissolved. The large difference in correction between the 10% Cu results and the eutectic/24%Cu results can be attributed to the lack of baseline shift as well as the kinetics of dissolution.

The interface rate constant for isothermal solidification as measured from the results in Figure 5-11 is $\xi = -0.452$ μm/√s. The interface velocity is significantly higher for the 10%Cu interlayer held at 880°C than for the diffusion couples conducted at 800°C. Assuming that the partition coefficient is constant for all temperatures, the change in the interface rate constant is due solely to an increase in diffusivity according to Equation 2-93. This result is intuitive since the diffusivity is expected to increase with increasing temperature. The effective diffusivity for this system is determined to be $D = 6.4 \times 10^{-9}$ cm^2/s by fitting to the kinetic measurements. This is an entire order of magnitude higher than the effective diffusivity found for the diffusion couples held at 800°C, which is reasonable given the increase in T_b from 800°C to 880°C.

Due to the small magnitude of the eutectic endotherm and exotherm in the DSC trace of the solid/liquid diffusion couple for the 10%Cu case, it is apparent that the DSC method is at the process limits. Since there are no peaks to measure in the DSC trace for the 5%Cu interlayer diffusion couple shown in Figure 4-15, it in not possible to quantify the isothermal solidification kinetics. The temperature, T_b, is also limited as shown by the results in Figure 4-16 for a eutectic diffusion couple heating to 920°C where there is no eutectic solidification upon cooling.

If Cu is substituted for the base metal using a Ag-Cu eutectic interlayer and an 800°C isothermal hold temperature, the resulting isothermal solidification kinetics are shown in Figure 5-12. As in the Ag base metal case with the eutectic interlayer a correction of $\psi = 1.31$ is needed. The resulting interface kinetics give an interface rate constant of $\xi = -0.019$ μm/√s and an effective diffusivity of $D = 3.3 \times 10^{-10}$ cm^2/s. The interface kinetics with the Cu base metal and eutectic interlayer are significantly lower than that measured with the Ag base metal. This is due in part to the lower effective diffusivity, but more to the significantly higher partition coefficient (i.e. 11.1 compared to 2.4) at the Cu rich end of the phase diagram. It is obvious why this experiment was not carried out to completion since the predicted time required for completion of isothermal solidification is 574 hours.

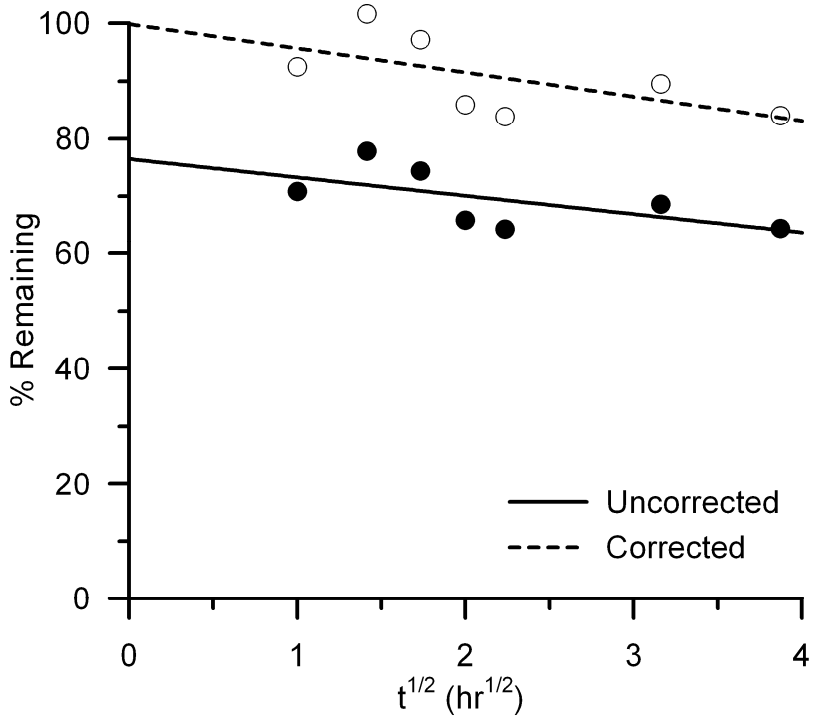

Figure 5-12: Results of isothermal solidification for Cu base metal and Ag-Cu eutectic interlayer (T_b = 800°C).

5.7. Metallurgical Analysis

A cross-section of a TLP half-sample shows a eutectic region, a two-phase region, and the single phase base metal (Figure 4-8). The eutectic region (dark) is clearly shown in the backscatter electron image in Figure 5-13. The interface between the eutectic and the two-phase region is scalloped with a cusp that penetrates into the two-phase region of the base metal. Previous work has shown that during cooling from the bonding temperature to the eutectic temperature, primary solidification of α-phase occurs epitaxially at the solid/liquid interface. The scalloped eutectic/base metal interface is evidence of a cellular solidification mode. The precipitates in the two-phase region, which have grown after solidification is complete, have obscured the primary solidification structure making it impossible to measure the original eutectic liquid width using visual inspection.

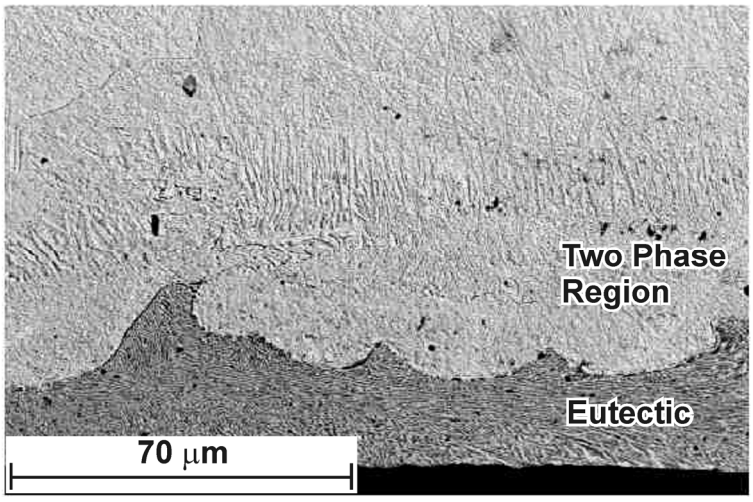

Figure 5-13: Backscatter electron image of interface region.

The two-phase region in Figure 4-8 clearly shows a discontinuous structure known as cellular precipitation because the boundary of the region moves with the advancing tips of the precipitates [102]. A gradient of solute exists in the base metal with decreasing Cu concentration from the solid/liquid interface. During cooling, the saturated band of material at the eutectic/base metal interface will become supersaturated. Cellular precipitation is known to initiate at a number of different sites including grain boundaries and eutectic/supersaturated solid solution interfaces [110]. The reaction front, shown clearly in Figure 5-14, is a migrating grain boundary that facilitates growth of the precipitates by providing a diffusion path for solute partitioning [102]. The supersaturated α' phase is decomposed into the α (Ag) and β (Cu) phases, where α has the same structure as α' but is depleted in solute and β is the equilibrium precipitate [102]. Upon further cooling, the cellular precipitation reaction front will advance as the decreasing solubility limit follows the compositional gradient. The microstructure is undesirable since the precipitates are too coarse to improve the mechanical properties of the joint. This illustrates the importance of a suitable homogenization stage after the completion of isothermal solidification to decrease the solute peak below the solubility limit and avoid potentially harmful precipitation.

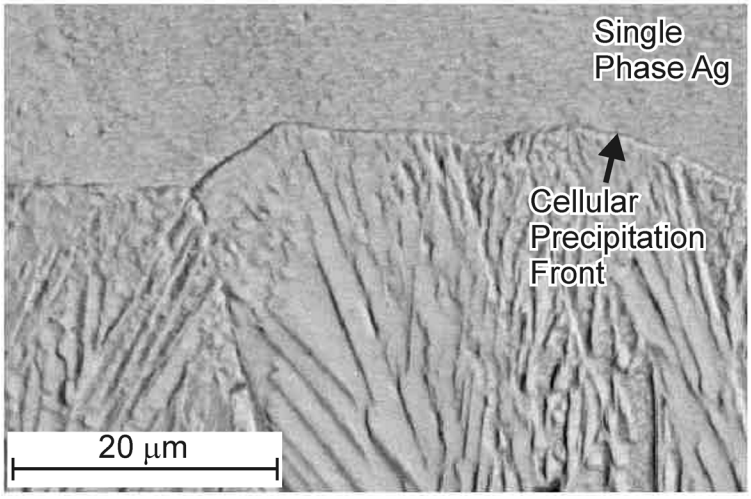

Figure 5-14: Solid-state transformation region/base metal interface.

The concentration of Cu was measured at intervals perpendicularly into the base metal from the interface of the eutectic microstructure. Upon cooling from T_b there is some primary α-phase solidification and the location of the solid/liquid interface (before cooling) has become obscured by cellular precipitation. To account for this, the concentration data has been shifted by some amount to get better agreement with the predicted profile. The actual distance that the data was shifted depends on the extent of primary solidification and the reference point that was chosen along the eutectic interface. Since this interface was scalloped, there is no uniform distance from the reference point to the original solid/liquid interface. A diagram showing why the origin shift is required is shown in Figure 5-15. The shifted concentration profiles are shown graphically in Figure 5-16 and agree well with those predicted by the moving interface model, perhaps lying slightly above the prediction. At shorter distances from the interface there is significant noise in the measurements caused by the cellular precipitation microstructure. As the distance from the interface increases past the cellular precipitation reaction front, the measured concentration profile becomes smooth and shows good agreement with the prediction.

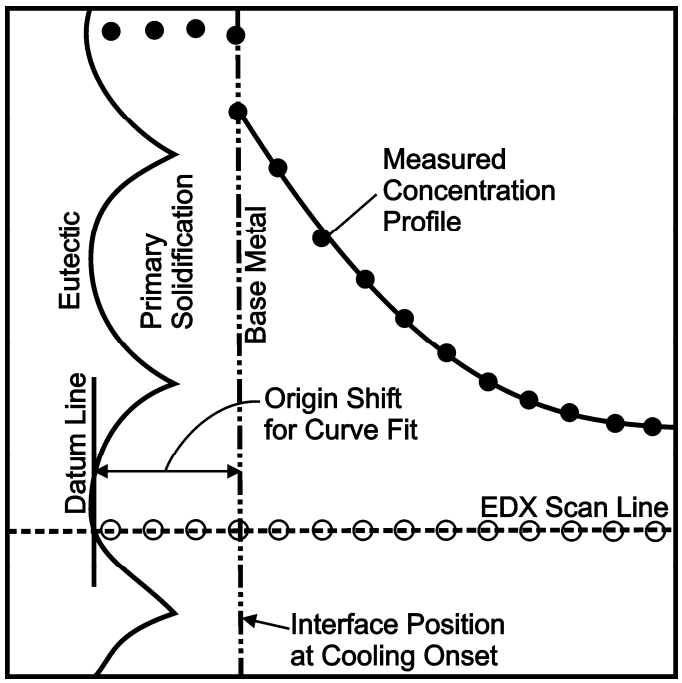

Figure 5-15: Schematic showing the effect of primary solidification on the measured concentration profile. The origin for the concentration profile must be shifted by some amount so that it is in the position of the solid/liquid interface at the onset of cooling.

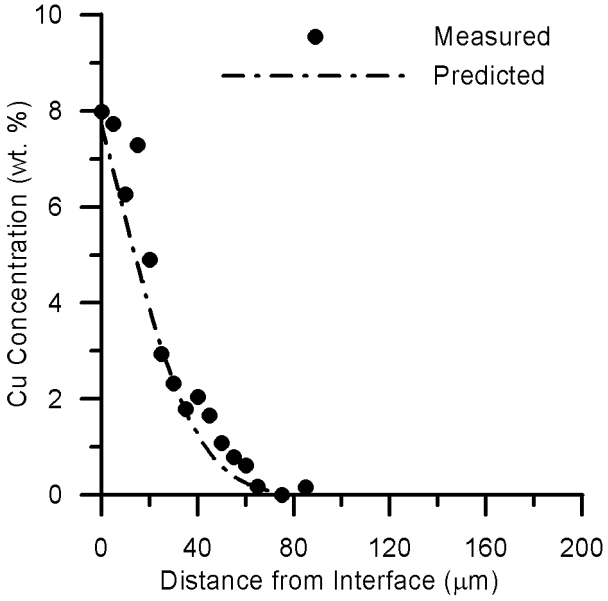

(a)

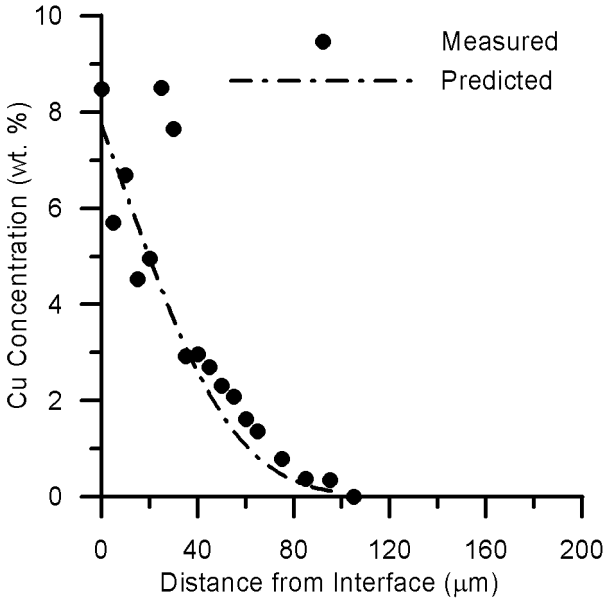
Measured
Predicted
Cu Concentration (wt. %)
Distance from Interface (μm)
0
2
4
6
8
10
0
40
80
120
160
200

(b)

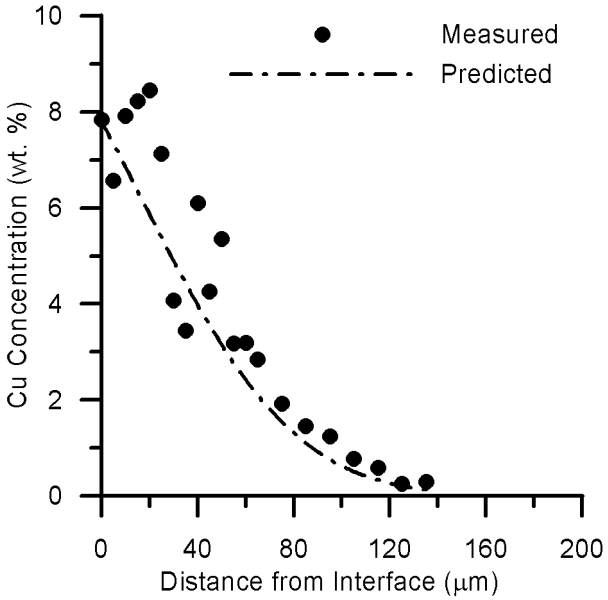
Measured
Predicted
Cu Concentration (wt. %)
Distance from Interface (μm)
0
2
4
6
8
10
0
40
80
120
160
200

(c)

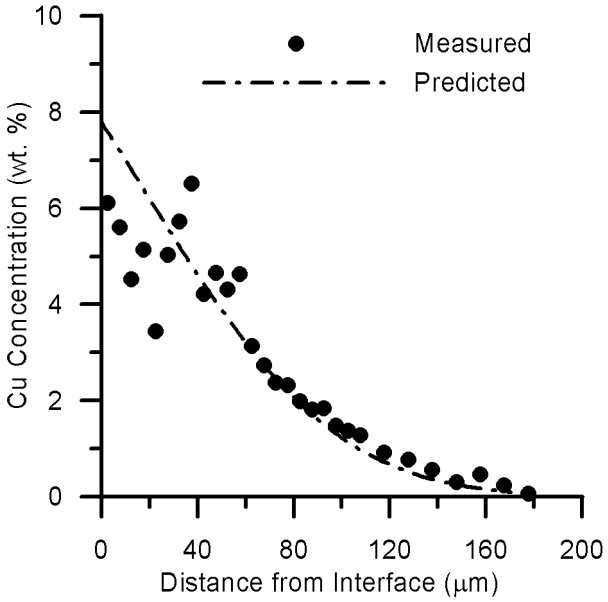

(d)

Figure 5-16: Cu concentration profiles measured after (a) 2 hours, (b) 4 hours, (c) 8 hours, (d) 12 hours [100].

5.8. TLP Full-Samples

TLP full-sample joints were produced with a 25 μm thick Ag-28 wt.% Cu foil interlayer. The joints were prepared in a similar manner to the DSC experiment TLP half-samples. The DSC traces of these samples are not of interest since the thick base metal between the joint and the measuring thermocouples dampens heat flow to the point that it cannot be measured. Cross-sections of the TLP bonds with increasing isothermal hold times are shown in Figure 5-17. After one hour at the bonding temperature a uniform layer of eutectic remains at the joint interface. Increasing the hold time to two hours results in a thin and broken eutectic layer. The eutectic region is reduced to sparse and irregular pockets after three hours and has completely disappeared after four hours. Based on rate constant experimentally measured with the DSC, i.e. $\xi = -0.126$, the expected time required for completion is 3.9 hours. Thus, the rate constant predicted by the DSC shows good agreement with the metallographic results. It would be very difficult, however, to accurately measure the process kinetics using visual inspection to estimate the liquid width, especially if isothermal solidification was not taken to completion. This elucidates that the DSC method provides an accurate quantification of the interface kinetics during isothermal solidification where traditional metallographic techniques have failed.

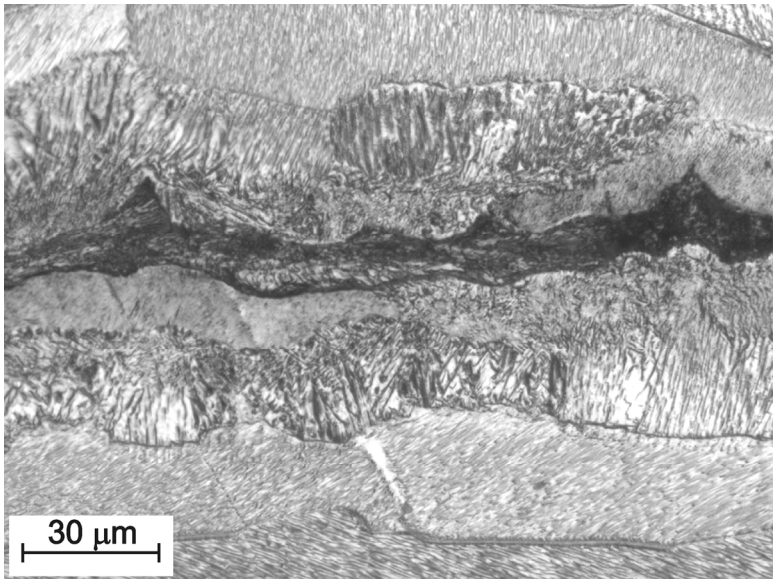

(a)

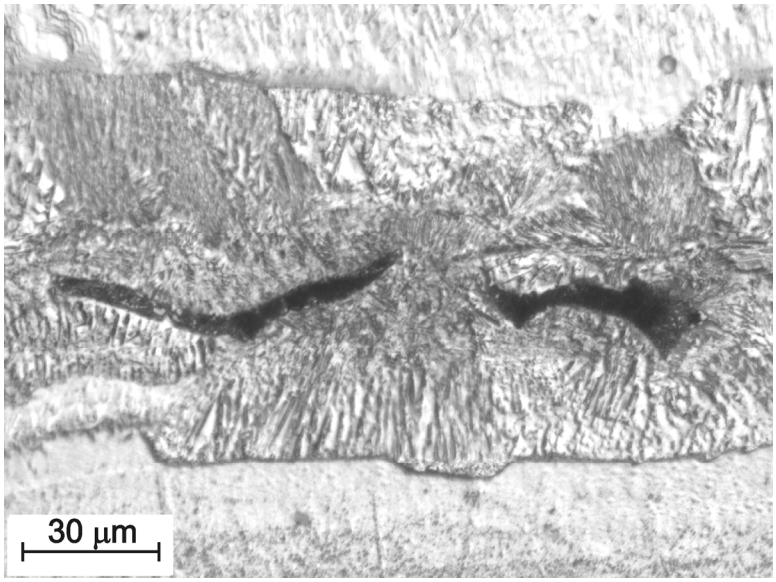

(b)

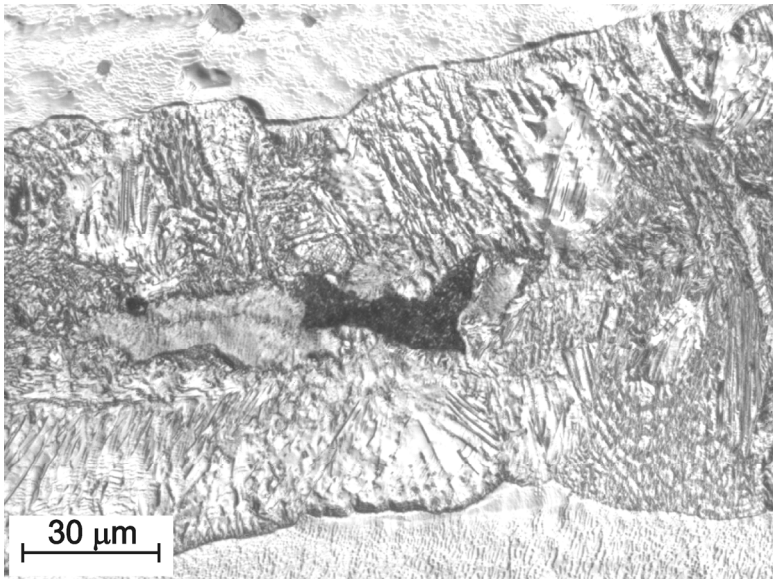

(c)

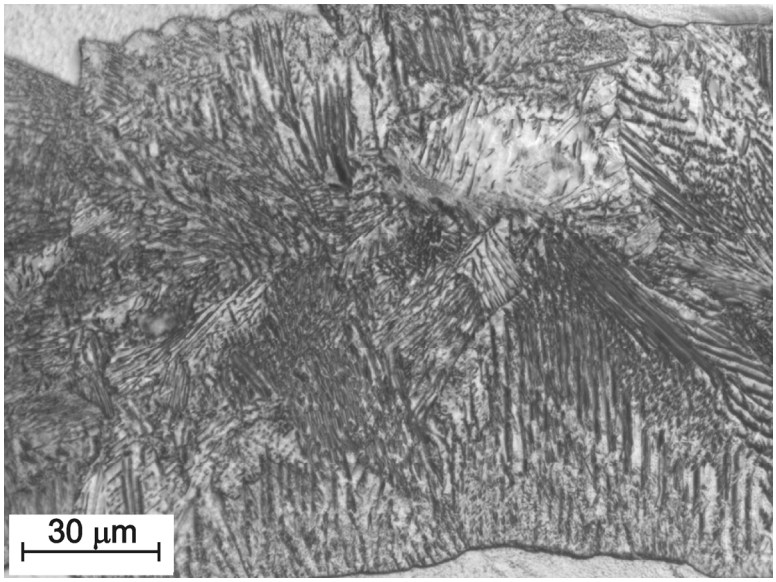

(d)

Figure 5-17: TLP bonded samples after (a) 1 hour, (b) 2 hours, (c) 3 hours, (d) 4 hours. As expected, the width of the cellular precipitation region increases with time due to increasing penetration of solute in the base metal [100].

5.9. Summary

An interface rate constant for isothermal solidification can be determined from the experimental results and compared to the predictions of analytical models. The additional

enthalpy data from the modified temperature program can also be used to quantify the interface kinetics using similar peaks. The measured interface rate constant is similar regardless of the analysis method. Compared to analytical model predictions, the experimentally measured interface kinetics agree well with the solution that assumes a moving solid/liquid interface.

6. Analysis of Ternary Diffusion Couples

6.1. Development and Results of DSC Experiments in Ternary System

In the isothermal solidification process characteristic of TLP bonding, the addition of a second solute to the liquid increases the complexity of the material system. In consideration of the increased complication with a ternary system, it is desirable to limit the difficulty of interpreting the interface kinetics by selecting a material system that is simple in nature. Observation of the liquidus projection in Figure 6-1 shows that the addition of Au to the Ag-Cu binary system results in a system with a single ternary eutectic. The eutectic occurs at a composition of Ag - 27 wt.% Au - 27 wt.% Cu. The eutectic trough extends from the Ag-Cu binary eutectic (Figure 6-2) along a line of nearly constant Cu composition.

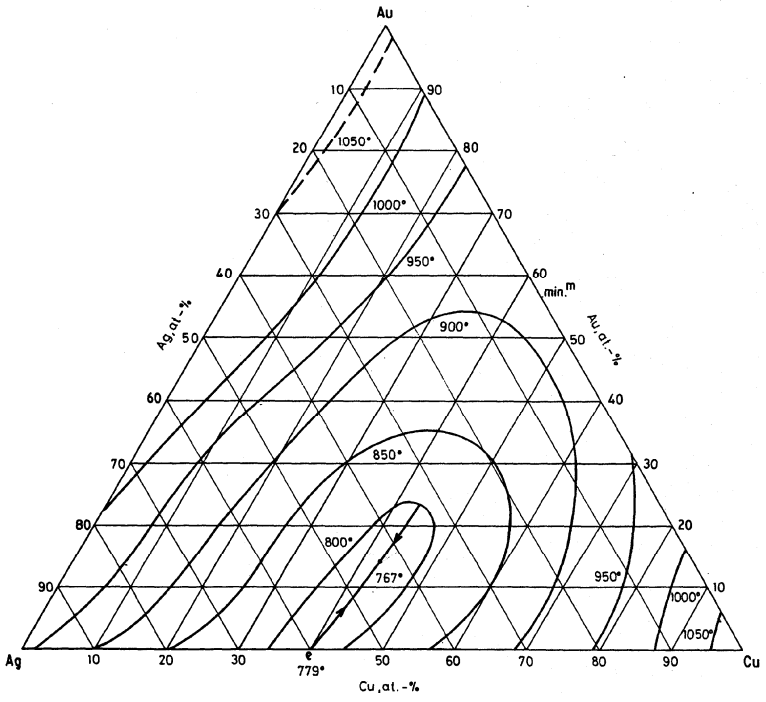

Figure 6-1: Ag-Au-Cu liquidus projection [104].

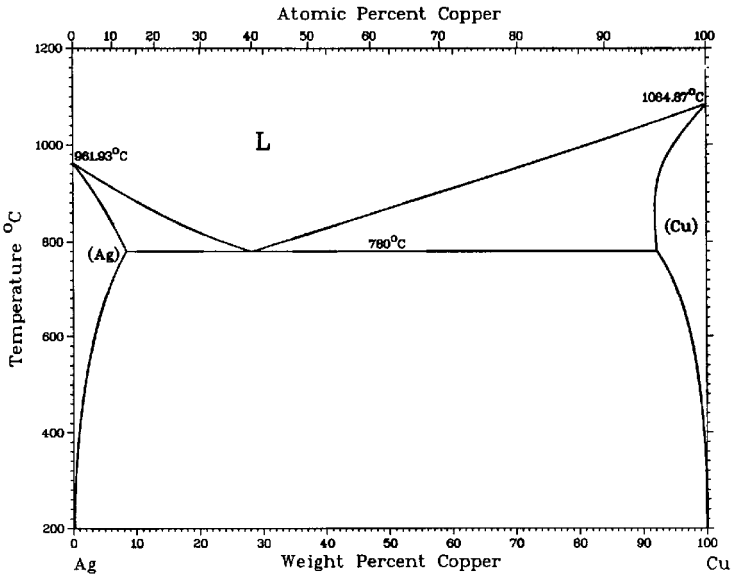

Figure 6-2: Ag-Cu phase diagram [103].

According to the liquidus projection (Figure 6-1), the ternary eutectic temperature is 767°C, which is lower than the Ag-Cu eutectic at 780°C. The eutectic trough extends in a direction of increasing Au and terminates at a temperature near 800°C. The Au-Cu binary phase diagram (Figure 6-3) is isomorphous at higher temperatures with incomplete solubility at lower temperatures. Similarly, the Ag-Au binary phase diagram (Figure 6-4) is isomorphous. The Ag-rich corner of the Ag-Au-Cu Gibbs' isotherm at 800°C is shown in Figure 6-5. A liquid loop is defined by a liquidus line that runs from the Ag-Cu binary up to the terminal point of the eutectic trough, and back to the Ag-Cu binary. Accordingly, the solidus line on the Ag-rich side runs up to the eutectic trough terminus and back to the Cu-rich side. The two phase region is surrounded by an isomorphous solid region which corresponds with what is seen in the binary Ag-Au and Au-Cu systems.

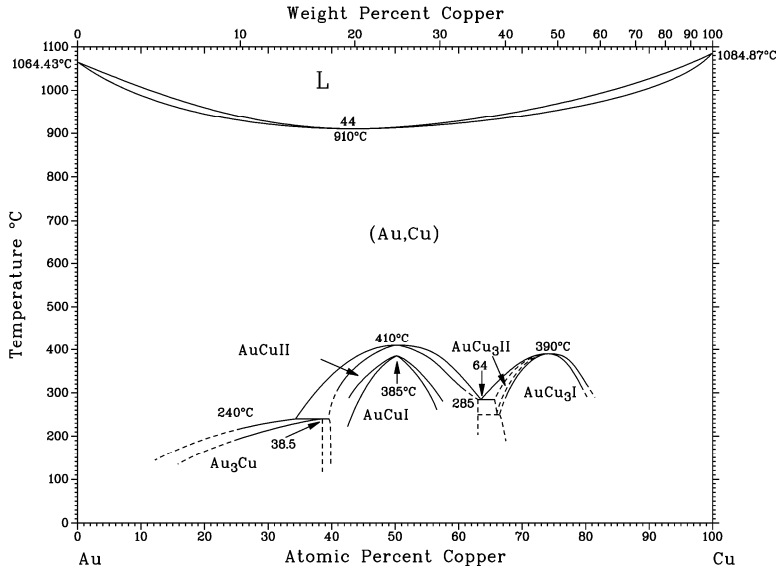

Figure 6-3: Au-Cu phase diagram [113].

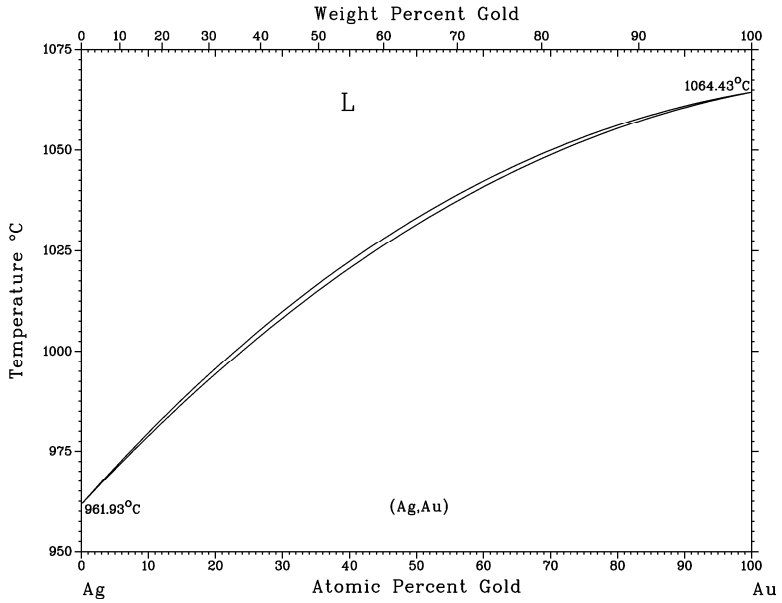

Figure 6-4: Ag-Au phase diagram [114].

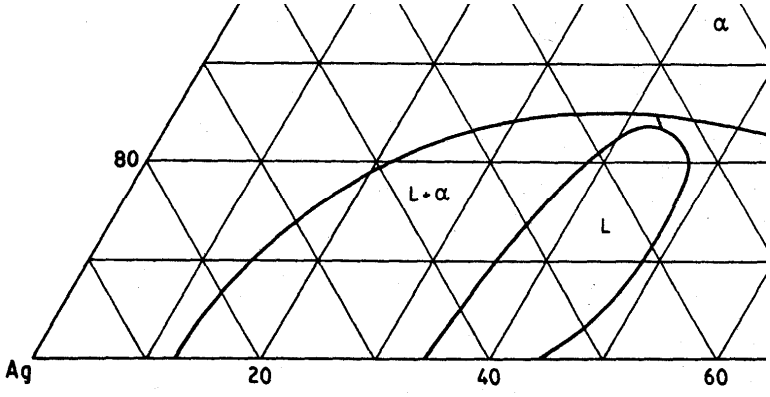

Figure 6-5: Ag-rich corner of Gibbs' isotherm at 800°C [104].

From examination of the Gibbs' isotherm in Figure 6-5, it is apparent that this ternary system lends itself to TLP bonding. As in the binary case, pure Ag was selected for the base metal. This is a model selection since oxides of Ag are reduced at the bonding temperature and no intermetallics are formed along any possible diffusion paths in the solid. The resulting analysis is simplified because the system is ideal.

Observations from the binary case show that in order to quantify the isothermal solidification kinetics using DSC, the isothermal hold temperature must be sufficiently higher than the eutectic temperature to fully resolve the DSC peaks. In this case, the eutectic temperature is 767°C and an isothermal hold temperature of 800°C was selected. This represents a superheat of 33°C, which is larger than that used in the Ag-Cu binary case (800°C - 780°C = 20°C). The bonding temperature was selected because the Gibbs' isotherm for Ag-Au-Cu at 800°C is available; furthermore, this temperature allows comparison with the binary Ag-Cu isothermal solidification kinetics. Increasing the superheat has been shown to increase the dissolution of the interlayer and increase the amount of primary solidification that occurs upon cooling, which is expected to have a minor effect on the uncorrected DSC results.

The interlayer composition for the solid/liquid diffusion couples was the ternary composition (Ag – 27 wt.% Au – 27 wt.% Cu). The interlayer foils were prepared by melting a mixture of pure metal powders and rolling the cast ingot to a thin foil. The foils were then punched into circular discs. A result of the manual foil preparation method is that each heat had a different nominal thickness. In this case, there were 3 different heats: one thick and two thin, resulting in foils with the following nominal thicknesses: 21.3 μm, 25.4 μm, and 40.6 μm. Only interlayer foils from the same heat were used to compare isothermal solidification kinetics in solid/liquid diffusion couple experiments.

Similar to the binary DSC experiments, two different temperature programs were used for the solid/liquid diffusion couples. Both type-2 (basic, see Table 3-1) and type-3 (modified) temperature programs were used. Typical DSC traces for the ternary solid/liquid diffusion

couples are shown in Figure 6-6 and Figure 6-7 for the type-2 and type-3 temperature programs, respectively. Examination of the DSC traces show results that are similar to the binary case. A single peak exists for both melting (endotherm) and solidification (exotherm). It is apparent that the peak corresponds to the eutectic in both cases.

The melting endotherm for a ternary solid/liquid diffusion couple in Figure 6-8 shows a shift in the baseline across the endotherm that is typical of what was observed in the binary case. Similarly, in the type-3 modified temperature program (Figure 6-9), the baseline shift occurs only on the first heating cycle and not on subsequent melting endotherms. This may be easier to observe by separating the peaks in Figure 6-10 with the DSC trace plotted as a function of time. Note that significant baseline shift occurs across the first endotherm.

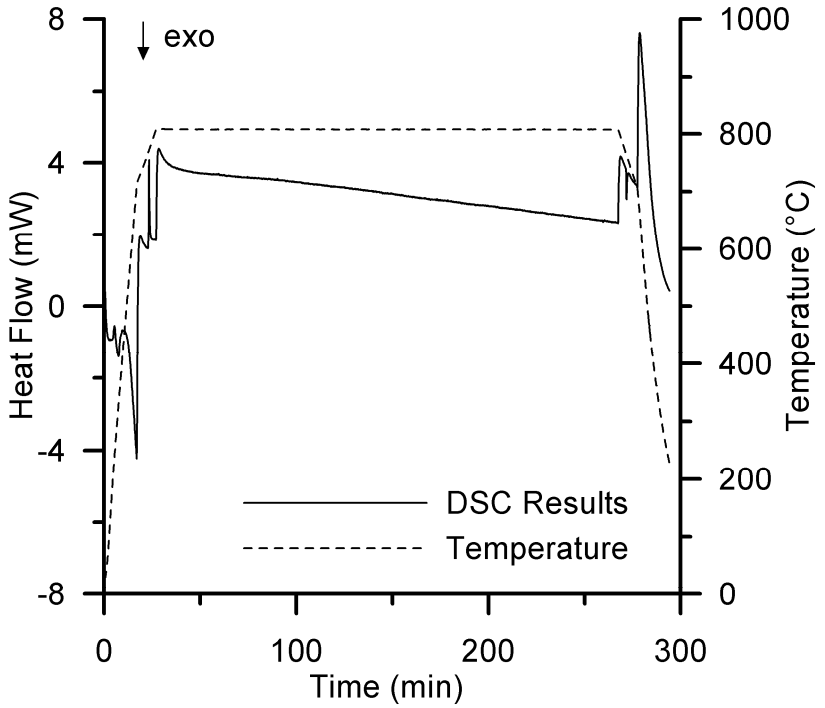

Figure 6-6: Typical DSC trace for a Ag-Au-Cu solid/liquid diffusion couple.

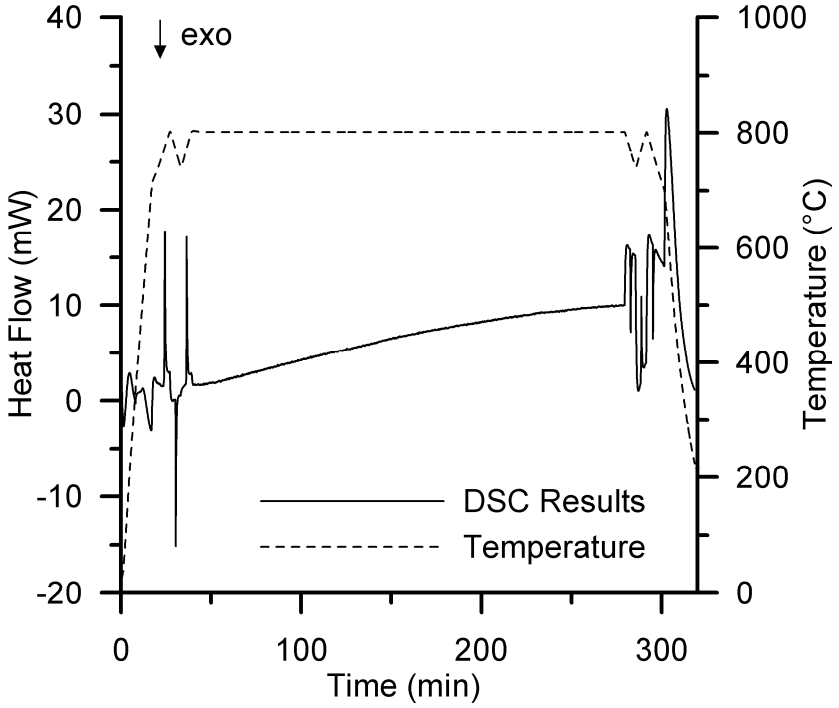

Figure 6-7: Typical DSC trace for a Ag-Au-Cu solid/liquid diffusion couple using a type-3 temperature program.

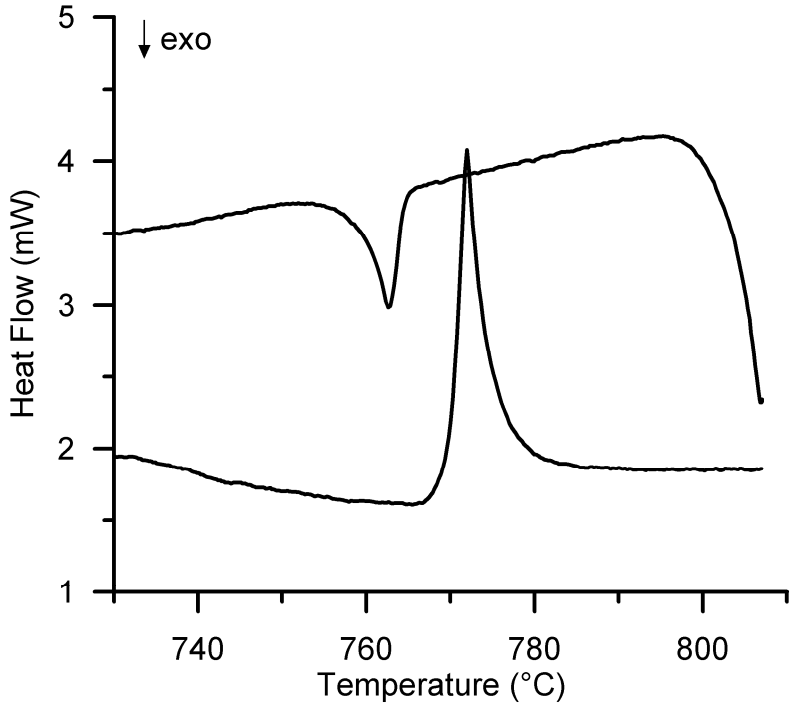

Figure 6-8: Typical DSC trace as a function of temperature for type-2 temperature program.

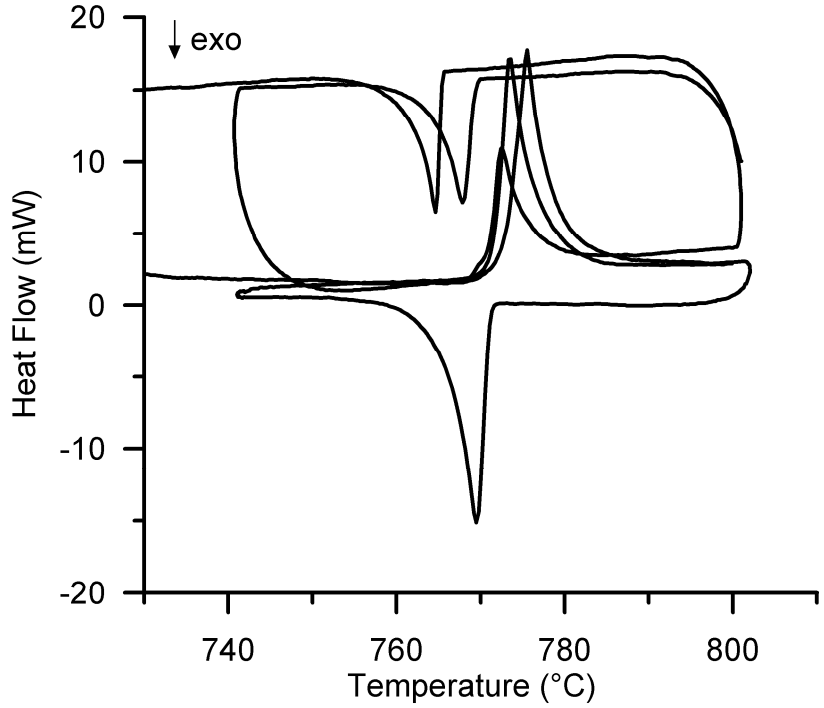

Figure 6-9: Typical DSC trace as a function of temperature for type-3 temperature program.

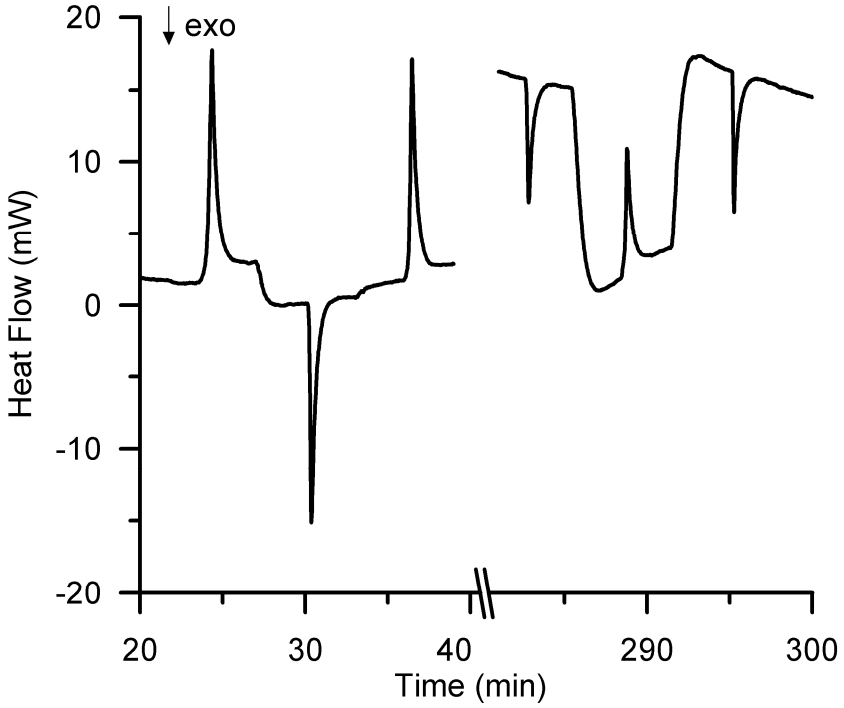

Figure 6-10: Typical DSC trace as a function of time for type-3 temperature program.

The DSC results for the ternary solid/liquid diffusion couples agree with the observations from the binary experiments. Primary solidification, which is expected to occur upon cooling from the isothermal hold temperature, does not appear as a solidification exotherm on the DSC trace; and, this is expected to influence the DSC results. Baseline shift upon melting of the interlayer is observed and is expected to result in an increase in the measurement of the endotherm. With increasing isothermal hold time, the magnitude of the solidification exotherm is expected to decrease as the liquid width decreases. Thus, analysis of the isothermal solidification kinetics in the solid/liquid diffusion couples can be performed using a similar method to the binary case by taking a ratio of the solidification exotherm to the melting endotherm (i.e. Equation 4-6). The type-2 DSC results for the 40.6 μm (thick) Ag-Au-Cu interlayer are shown in Table 6-1. Similarly, the type-2 DSC results for the 21.3 μm (thin) are given in Table 6-2. As expected, examination of the fraction of liquid remaining shows a systematic decrease with increased isothermal hold time in both the thick and thin foils.

Table 6-1: Type-2 DSC results for thick Ag-Au-Cu solid/liquid diffusion couples.

Isothermal Hold Time (hrs)	Square Root Time ($hrs^{1/2}$)	Final Enthalpy (mJ), ΔH_s	Initial Enthalpy (mJ), ΔH_m	% Liquid Remaining (%)
0.00	0.00	509	605	84.2
1.00	1.00	639	903	70.8
2.00	1.41	476	738	64.5
4.00	2.00	496	806	61.5
9.00	3.00	397	779	50.9
16.0	4.00	295	780	37.8
25.0	5.00	208	820	25.3
36.0	6.00	111	700	15.9
64.0	8.00	67.9	823	8.25
81.0	9.00	31.8	859	3.70
81.0	9.00	35.1	799	4.40

Table 6-2: Type-2 DSC results for thin Ag-Au-Cu solid/liquid diffusion couples.

Isothermal Hold Time (hrs)	Square Root Time ($hrs^{1/2}$)	Final Enthalpy (mJ), ΔH_s	Initial Enthalpy (mJ), ΔH_m	% Liquid Remaining (%)
0.00	0.00	195	275	71.1
0.25	0.50	198	297	66.6
1.00	1.00	199	318	62.6
2.25	1.50	143	315	45.2
4.00	2.00	97.0	302	32.1
4.00	2.00	140	370	37.9
6.25	2.50	90.2	319	28.3
9.00	3.00	56.6	329	17.2
12.0	3.46	0.0	329	0.00
16.0	4.00	0.0	367	0.00

6.2. Ag-Au-Cu Solid/Liquid Diffusion Couple Results

The results of Table 6-1 are plotted in Figure 6-11. The percentage of liquid remaining in the solid/liquid diffusion couple as calculated by Equation 4-6 is shown as a function of the square root of the isothermal hold time. As in the binary case, the liquid width is shown to decrease with a linear trend throughout most of the isothermal solidification period. Another similarity with the binary case is that the linear trend line does not intersect the ordinate axis at unity, but instead shows an apparent loss of liquid at short isothermal hold times. In the binary DSC experiments, this was shown to be an experimental artefact which was revealed by use of the type-3 temperature program.

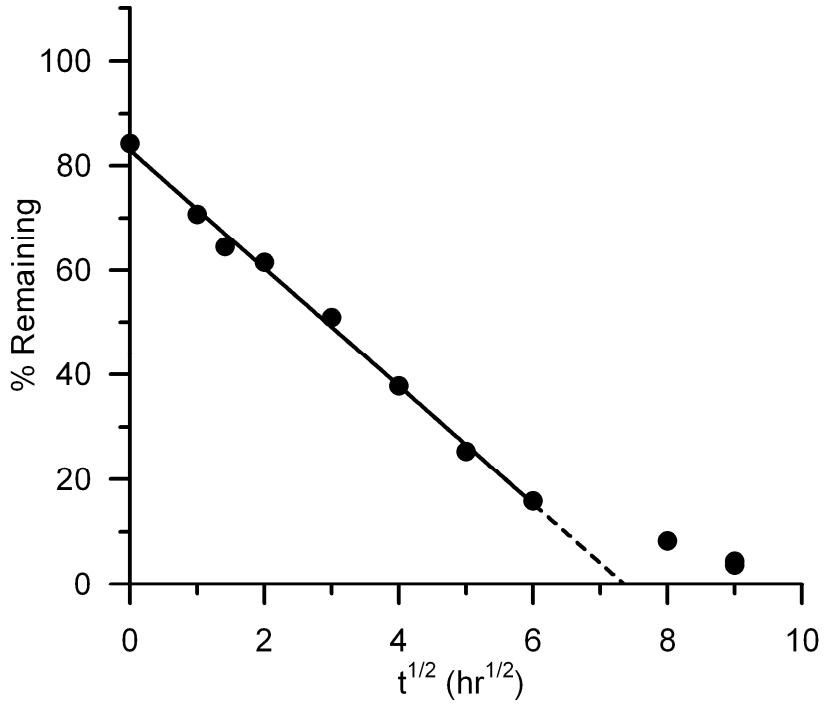

Figure 6-11: DSC results for thick foil Ag-Au-Cu diffusion couples.

At longer isothermal hold times, the interface kinetics appear to decrease. This is apparent after 36 hours at the bonding temperature. The linear regression trend line shown in Figure 6-11 is fit only to the data from 0 to 36 hours. The extrapolation to the abscissa is shown by the broken line. The data that lies above the fit line deviates from the linear trend and is excluded from the fit. Time for the completion of isothermal solidification is predicted in the binary case by extrapolating the linear trend line to the abscissa, where the fraction of liquid remaining is zero. In Figure 6-11 the two outlying points are excluded from the analysis; hence, the uncertain extrapolation given by the broken line is not an accurate prediction of the isothermal solidification time. A second fit could be applied to the points from 36 hours onward to give a good prediction of the time at which the liquid phase is eliminated.

The deviation from the linear relationship between the interface position and the root of time is a possible indication of the existence of a second regime of interface kinetics as suggested by the literature. This follows the theory of isothermal solidification in a ternary system.

The type-2 solid/liquid diffusion couple interface kinetics for the thin foil from Table 6-2 are plotted in Figure 6-12. Again, the fit line does not approach unity at zero isothermal hold time and is consistent with the previous results.

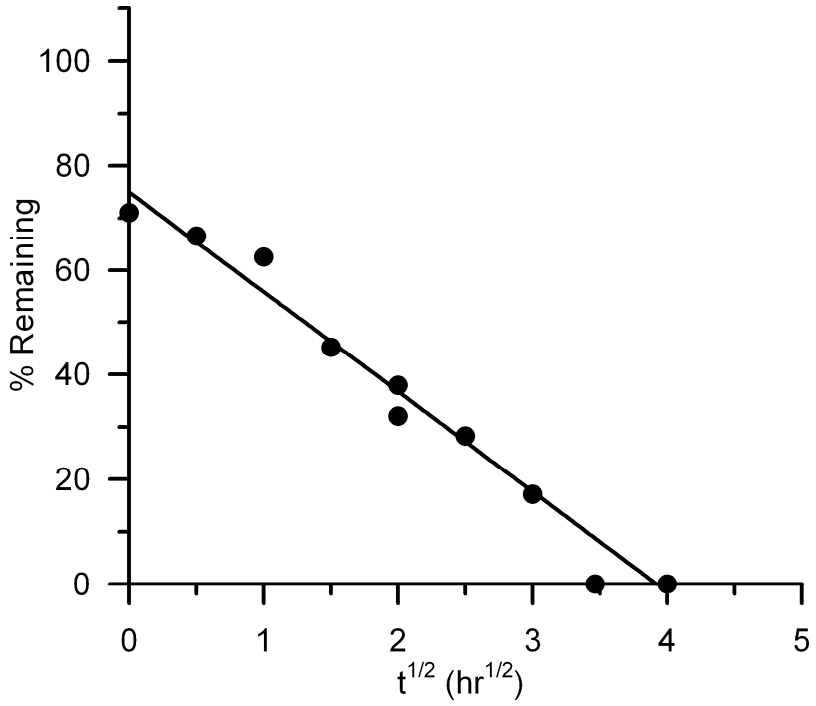

Figure 6-12: DSC results for thin foil Ag-Au-Cu diffusion couples.

The apparent shift in interface kinetics that was observed with the thick foil in Figure 6-11 is not clear in the thin foil results (Figure 6-12). Instead, a linear fit applied to the non-zero points in Figure 6-12 correlates with the data over the entire range.

In both Figure 6-11 and Figure 6-12, the characteristic deviation of the abscissa intercept indicates that, like in binary isothermal solidification, the artefacts of the DSC experiments must be corrected. It has already been shown that a set of type-3 modified temperature program DSC experiments can be used to correct the interface kinetics measured using type-2 experiments, as well as collect additional data that can be utilized to characterize isothermal solidification. The results of the type-3 solid/liquid diffusion couple DSC experiments are summarized in Table 6-3.

Table 6-3: Type-3 DSC results for thin Ag-Au-Cu solid/liquid diffusion couples.

$\sqrt{t}$ ($hr^{1/2}$)	M1	S1	M2	S2	M3	S3	M2/M1	S2/M3
0.50	469	366	394	323	361	331	0.84	0.90
1.00	459	338	362	265	286	274	0.79	0.93
2.00	453	351	375	197	214	190	0.83	0.92
3.00	449	361	392	121	137	118	0.87	0.88
4.00	450	358	389	27.0	33.0	24	0.87	0.81

The results of Table 6-3 are summarized in Figure 6-13. The interface kinetics as measured using S2/M1 shows similar results to those measured using the type-2 temperature program for a thin foil (Figure 6-12) with slight differences attributed to variation in initial thickness between the two heats of foil used for each set of diffusion couples. The nature of the ternary diffusion couple results in Figure 6-13 compares very well with the binary results shown in Figure 5-3 and Figure 5-4. Using the data, there are a number of additional methods which can be used to interpret the results.

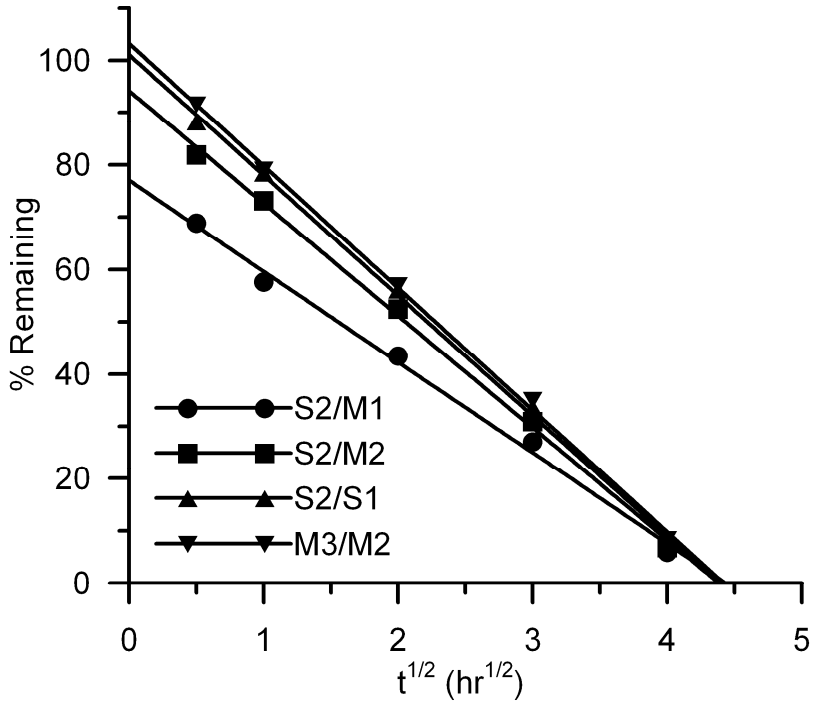

Figure 6-13: Ag-Au-Cu diffusion couple modified temperature program results.

From the results in Table 6-3, an average value for the effect of baseline shift on the initial heating cycle can be found (see § 4.4.2). This value is given by the average *M1/M2* and is found to be 1.19, compared to 1.24 for the binary Ag-Cu results. The effect of primary solidification and dissolution can be found (see § 4.4.3) using the average *M/S* ratio, which is found to be 1.13, compared to 1.10 for the binary results. Following the methodology from § 4.4.4, the correction factor (ψ) for the ternary DSC measurements is found to 1.34. This compares to the value of $\psi = 1.36$ for the binary results.

The correction factor is applied to the *S2/M1* data from Table 6-3 with the results given in Figure 6-14. Similarly, the correction is applied to the type-2 results for both thin (i.e. Figure 6-12) and thick (i.e. Figure 6-11) foils in Figure 6-15 and Figure 6-16, respectively. The corrected fraction of liquid remaining for both of the thin foils (Figure 6-14 and Figure 6-15)

passes through nearly 100% at zero isothermal hold time. The corrected results for the thick foil case, however, deviate by over 10%. This is likely a result of the different initial foil thickness and suggests that the effect of baseline shift could be dependent on the thickness of the foil.

As in the binary case, the solid/liquid diffusion couple interface kinetics can be quantified using the similar peak data in Table 6-3. Figure 6-17 shows a comparison of the corrected results using the ratio of solidification exotherm to melting endotherm (*S/M*) and the results using similar peaks (i.e. *M3/M2* and *S2/S1*). The measured process kinetics are related to the slope of the fit line. Examination of Figure 6-17 shows that there is good agreement between the techniques. This agrees with the binary case in Figure 5-5. Either of the methods can be used to quantify interface kinetics with the same result.

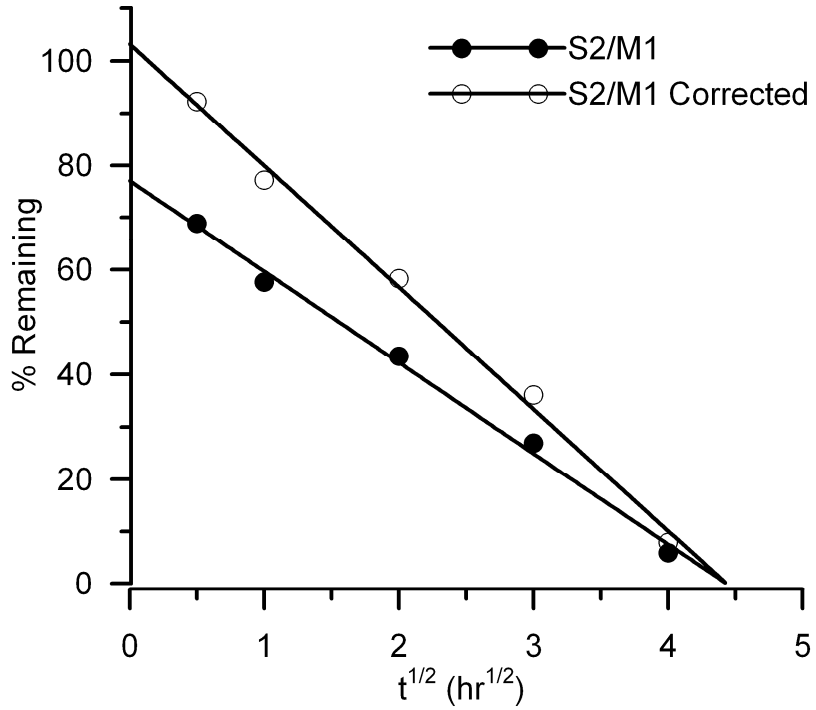

Figure 6-14: Modified temperature program results corrected.

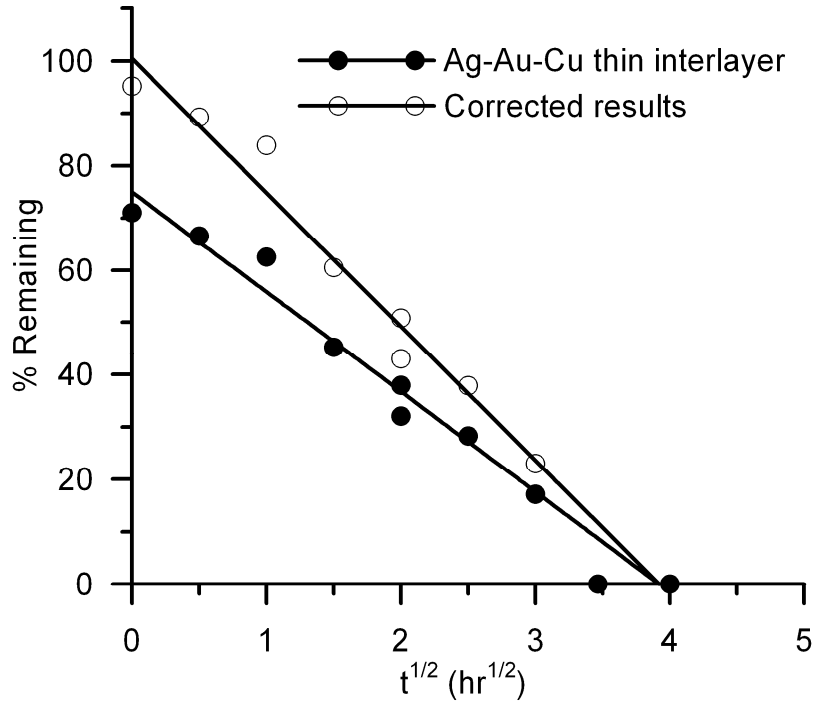

Figure 6-15: Thin foil results corrected.

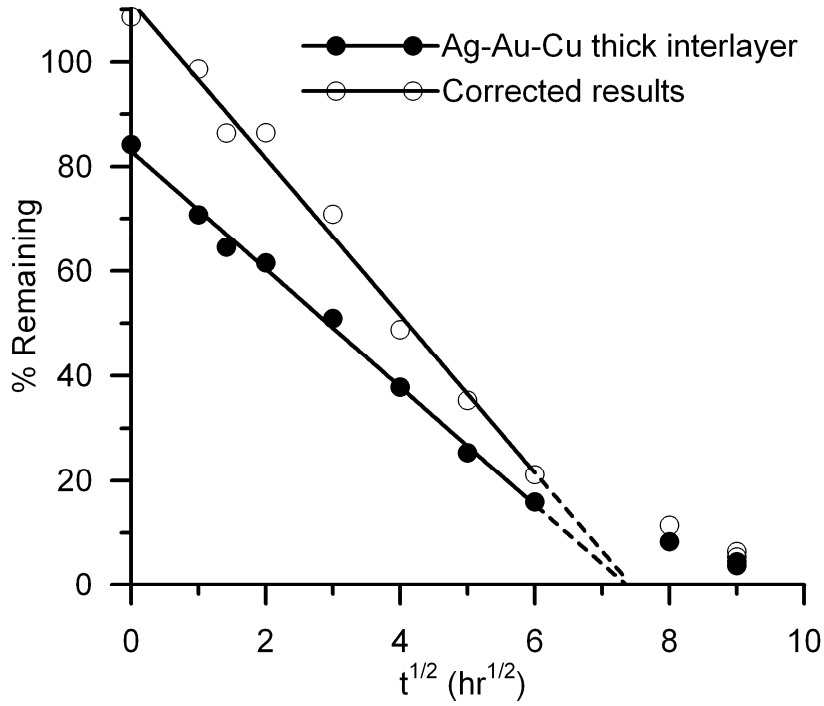

Figure 6-16: Thick foil results corrected.

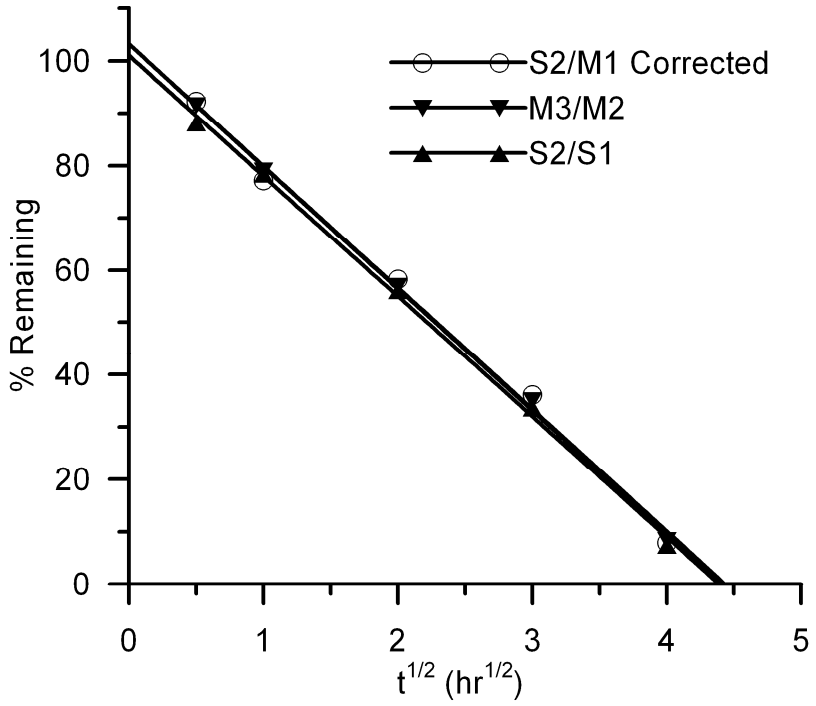

Figure 6-17: Comparison of corrected results vs. similar peaks.

The corrected line in Figure 6-17 is derived on the application of a constant correction factor, ψ. The assumption that ψ is constant may not be valid throughout isothermal solidification in ternary systems. In theory, isothermal solidification proceeds with a shifting liquid composition. Any change in the liquid composition is likely to have an effect on the fraction of liquid that solidifies as eutectic during cooling from the isothermal hold temperature. The distance of the liquidus composition from the eutectic composition will influence the extent of primary solidification; thus, any tie line shift on the Gibbs' isotherm could affect the relationship between the solidification exotherm and melting endotherm. In binary isothermal solidification, the composition of the liquid remains constant throughout isothermal solidification. The ratio of adjacent melting and solidification peaks can be considered constant with time. In the ternary case, however, the assumption that the liquid composition is shifting throughout isothermal solidification is an indication that the assumption of a constant ψ may not be valid.

Closer examination of the endotherms and exotherms in Table 6-3 shows that the effect of primary solidification on the enthalpy measurements varies with isothermal hold time. The ratio of adjacent solidification exotherms to melting endotherms (see Figure 6-10) is plotted as a function of isothermal hold time in Figure 6-18. The value *S1/M2* is the exotherm to endotherm ratio before the isothermal hold period. The values *S2/M3* and *S3/M3* are the exotherm to endotherm ratios after the isothermal hold period. Observation of Figure 6-18 shows that the exotherm to endotherm ratio before isothermal solidification remains constant

as the isothermal hold time for the solid/liquid diffusion couple increases. This is expected because these enthalpies are measured before the isothermal hold period and the fraction of eutectic melting and solidification is constant. The enthalpy ratios after the isothermal hold time, however, show a systematic decrease with increasing progression of isothermal solidification.

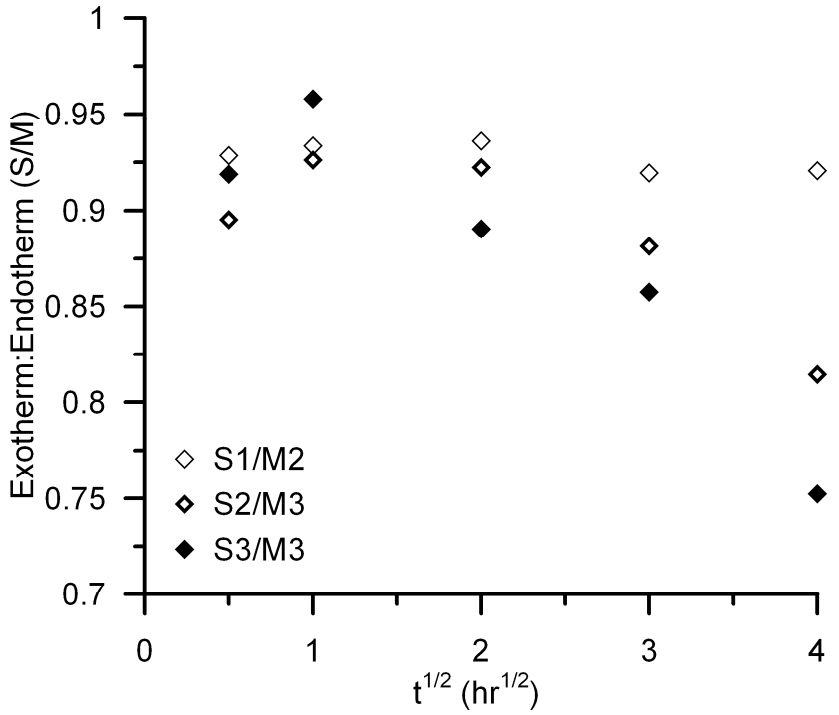

Figure 6-18: Observation of changing effect of primary solidification during isothermal solidification in the DSC results.

The average value for the pre-hold enthalpy ratio *S1/M2* is 0.93. The post-isothermal hold enthalpy ratio *S2/M3* increases initially from 0.90 at 0.25 hrs to 0.93 at 1 hr, and then decreases to 0.81 at 16 hrs. Likewise, the enthalpy ratio *S3/M3* initially increases from 0.92 to 0.96 between 0.25 and 1 hrs, and decreases to 0.75 after 16 hours of isothermal hold time. The shift in the post-hold enthalpy ratios are an indication of changing interface conditions during isothermal solidification when compared to the constant pre-hold ratio. These changing conditions relate to the tie line shift occurring as isothermal solidification proceeds. The solidus and liquidus concentrations at the interface influence the fraction of eutectic solidifying upon cooling.

The slight increase, followed by the systematic decrease in the exotherm to endotherm enthalpy ratio supports the theory that isothermal solidification proceeds in ternary systems by means of a shifting tie line on the Gibbs' isotherm. The results indicate that the liquid

composition initially shifts closer to the eutectic (up to one hour) and then moves away from the eutectic until the completion of isothermal solidification.

The implication of the shifting tie line and change in enthalpy ratio (i.e. change in primary solidification effect) is that ψ is shifting throughout isothermal solidification. If the correction factor is obtained at each data point by multiplying the average baseline correction factor (i.e. average *M1/M2*) by the local primary solidification factor (i.e. *M3/S2*), a shifting correction factor can be obtained. This correction factor is plotted as a function of the square root of time in Figure 6-19. The individual data points in Figure 6-13 (*S2/M1*) are corrected using the shifting values of ψ and plotted in Figure 6-20.

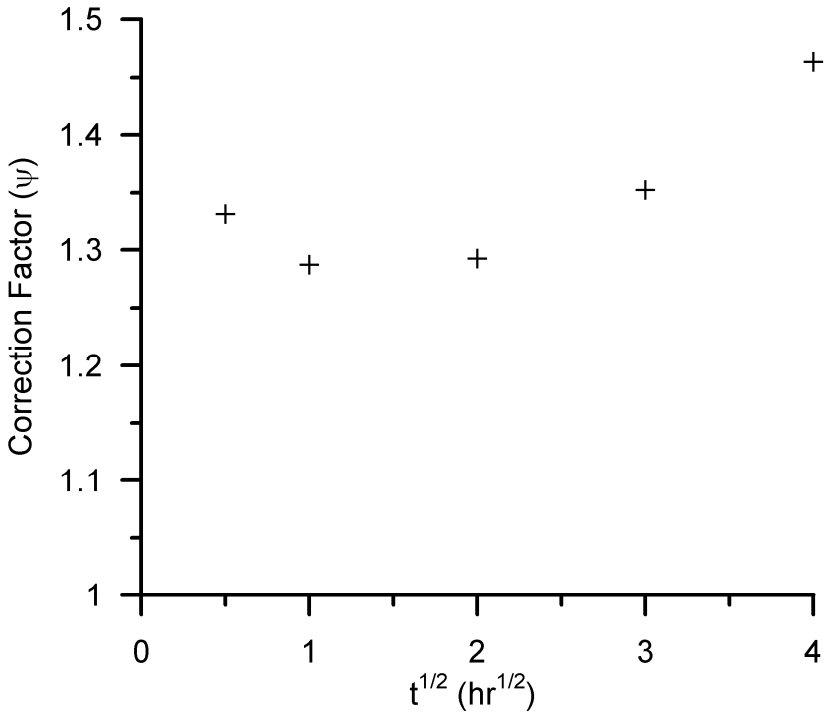

Figure 6-19: Shifting correction factor for Ag-Au-Cu solid/liquid diffusion couples.

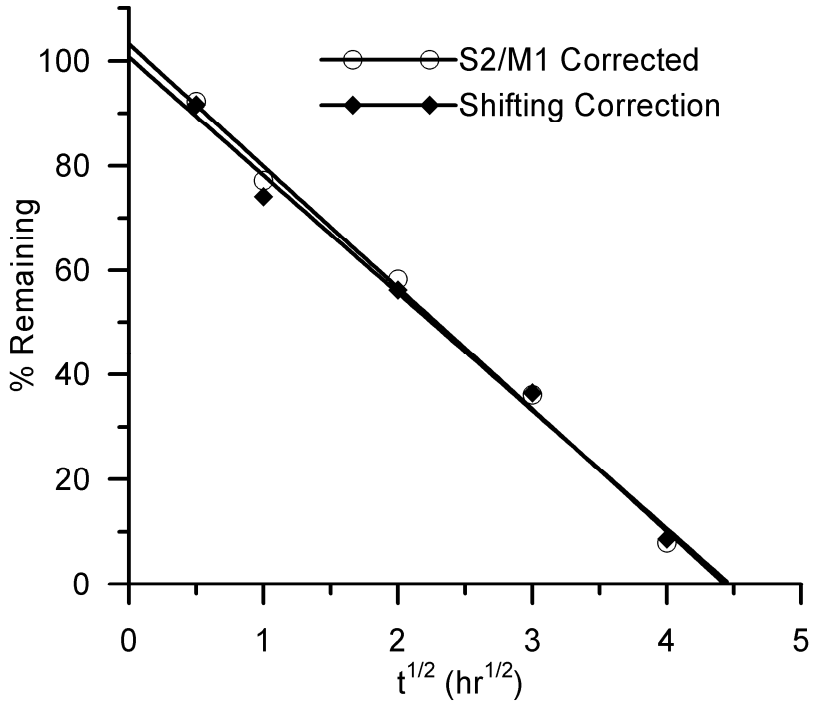

Figure 6-20: Ag-Au-Cu solid/liquid diffusion couple results, average correction factor and shifting correction factor.

A comparison of the data correction methods is shown in Figure 6-20. There is a slight difference between the interface kinetics obtained using the average correction and the shifting correction as shown by slopes of the lines. The results obtained with the shifting correction come slightly closer to 100% liquid remaining at zero isothermal hold time; however, the results between the two are insignificant.

At longer isothermal hold times when the correction factor value increases well above the average value, the fraction of liquid remaining decreases such that the magnitude of the net change in value becomes quite small. Hence, any influence of the shifting correction is minor. Based on these results, the use of an average correction factor compares very well with the use of a unique value of ψ for each data point. Thus, for the type-2 Ag-Au-Cu DSC experiments, the results can be corrected with an average factor with acceptable results. This allows comparison of results for different initial conditions with the same factor and is useful when local correction data from a type-3 experiment is not available.

In this way, any of the three methods can be used to accurately quantify the solid/liquid interface kinetics. Taking a ratio of similar peaks, such as *S2/S1* or *M3/M2* yields results that are similar to the ratio of exothermic enthalpy after isothermal hold time to endothermic enthalpy before (i.e. *S2/M1* corrected).

Using the average correction, and a normalization procedure for comparing solid/liquid diffusion couples with different initial foil thicknesses, the results from Figure 6-14 (type-3

thin foil), Figure 6-15 (type-2 thin foil), and Figure 6-16 (type-2 thick foil) can be compared. The normalized time is given by Equation 6-1. This comparison is shown in Figure 6-21. The process kinetics described by each of the lines are similar and compare well with each other.

$$\sqrt{t^*} = \frac{2 \cdot \sqrt{t}}{W_{max}} \qquad \text{Equation 6-1}$$

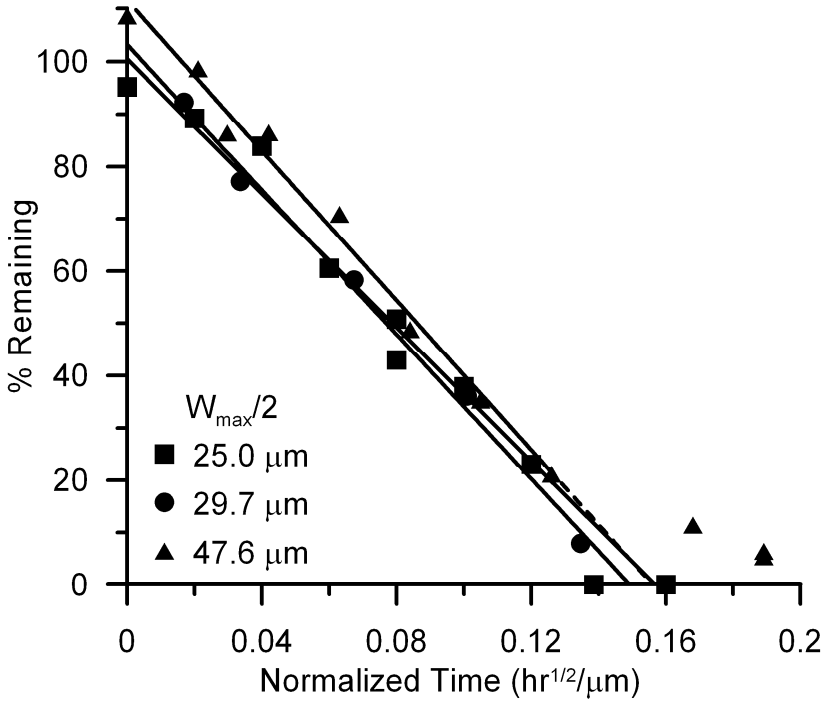

Figure 6-21: Normalized Ag-Au-Cu diffusion couple results.

Direct comparison of the interface kinetics in Figure 6-21 allows examination of the apparent change in interface kinetics for the thick foil first shown in Figure 6-11. The shift in interface kinetics does not appear in the results for the thin foil cases. It is unclear why the second kinetic regime occurs in only the thick foil case; one possibility is that the measurement resolution is not high enough to observe the slight decrease in the interface velocity.

Figure 6-22 shows how the absolute final enthalpy of solidification (ΔH_s) decreases with isothermal hold time for both the thick and thin foil interlayers (i.e. a comparison of Table 6-1 and Table 6-2). It is clear that the absolute ΔH_s is significantly larger for the thicker case, as expected. At longer isothermal hold times, the interface velocity decreases is a way that would suggest saturation of the base metal; however, this is not expected (based on modeling results).

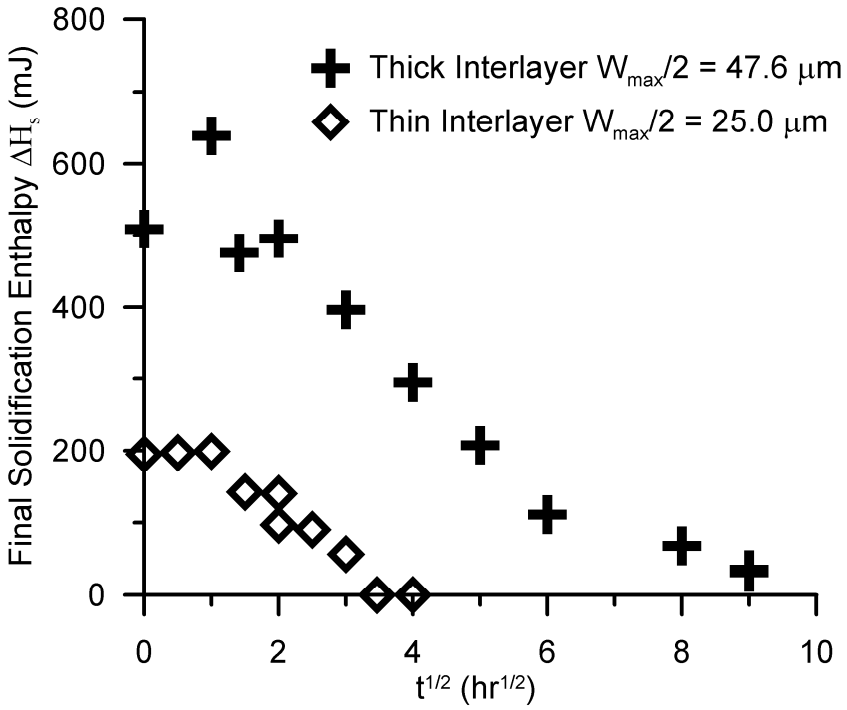

Figure 6-22: Comparison of the absolute final solidification enthalpy, ΔH_s, for thick and thin interlayers.

The kinetics of isothermal solidification in binary systems can be compared to those in ternary systems. The results can be normalized for interlayer thickness; however, it is not possible to normalize for the chemical difference in liquid composition. Nevertheless, the ternary Ag-Au-Cu results can be compared with the binary Ag-Cu results as both experiments were completed at the same isothermal hold temperature of 800°C. The comparison, shown in Figure 6-23, reveals that the process kinetics for the binary Ag-Cu solid/liquid diffusion couple with a eutectic interlayer are slightly faster than the interface kinetics for the ternary eutectic Ag-Au-Cu system at the same temperature.

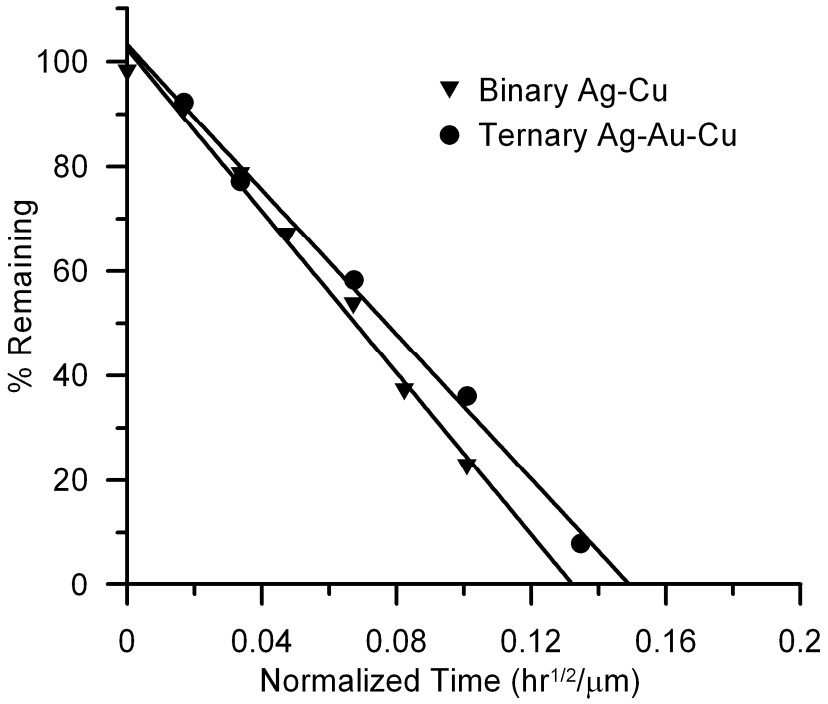

Figure 6-23: Comparison of normalized (for W_{max}) interface kinetics in binary and ternary diffusion couples.

6.3. Modeling Isothermal Solidification in Ternary Diffusion Couples

A comprehensive analysis of the interface kinetics can be compared to the results of analytical and numerical models. An analytical analysis of ternary biphase diffusion couples was first given by Coates and Kirkaldy [115]. They found that for an infinite diffusion couple with fixed boundaries and constitutive conditions, multiple interface velocities can exist. Maugis et al. [116] used analytical solutions to determine that for certain compositions, up to three solutions for the interface velocity can exist. The existence of one, two, or three solutions for the interface depends on the diffusion couple endpoints.

To find the solution, the phase boundary and tie lines on the Gibbs' isotherm at 800°C must be defined. To simplify the analysis, the phase boundaries are assumed linear, as shown in Figure 6-24. Using the linear assumption, the relation between the tie lines are defined using the relationship given in Equation 6-2. Furthermore, a parameter, ζ, is introduced to define the tie line position. The parameters of Equation 6-2 are defined in Figure 6-24 and Table 6-4.

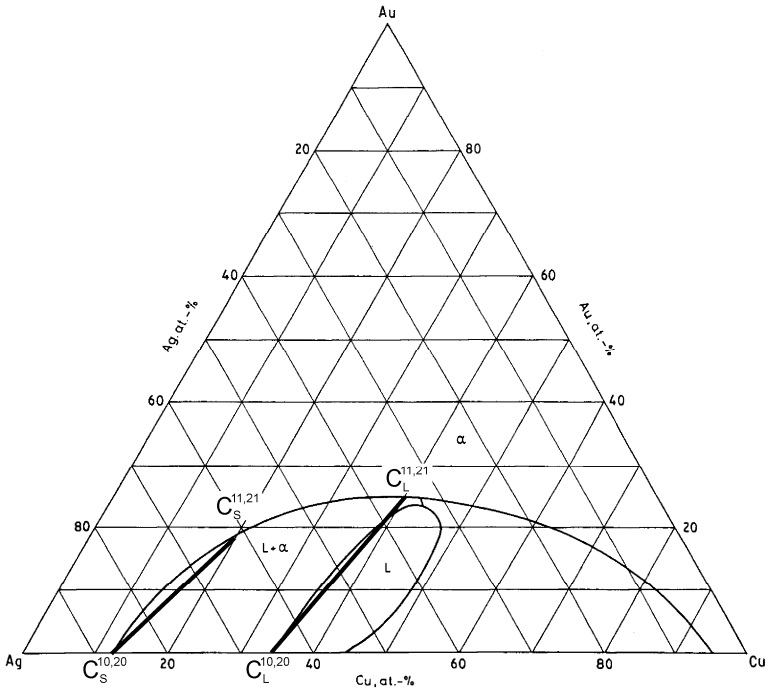

Figure 6-24: Linearization of phase boundaries.

Table 6-4: Values for phase boundary endpoints defined in Figure 6-24.

C_S^{10}	12.5 %	C_S^{20}	0 %
C_S^{11}	17 %	C_S^{21}	20 %
C_L^{10}	34 %	C_L^{20}	0 %
C_L^{11}	40 %	C_L^{21}	25 %

$$\frac{C_S^1 - C_S^{10}}{C_S^{11} - C_S^{10}} = \frac{C_L^1 - C_L^{10}}{C_L^{11} - C_L^{10}} = \frac{C_S^2 - C_S^{20}}{C_S^{21} - C_S^{20}} = \frac{C_L^2 - C_L^{20}}{C_L^{21} - C_L^{20}} = \zeta \qquad \text{Equation 6-2}$$

Functions for the tie line compositions (Equation 6-3 through Equation 6-6) can then be found by rearranging Equation 6-2, and substituting the simplifying functions defined by Equation 6-7 through Equation 6-10.

$$C_L^1 = \zeta \cdot \Delta C_L^1 + C_L^{10} \qquad \text{Equation 6-3}$$

$$C_S^1 = \zeta \cdot \Delta C_S^1 + C_S^{10} \qquad \text{Equation 6-4}$$

$$C_L^2 = \zeta \cdot \Delta C_L^2 + C_L^{20} \qquad \text{Equation 6-5}$$

$$C_S^2 = \zeta \cdot \Delta C_S^2 + C_S^{20} \qquad \text{Equation 6-6}$$

$$\Delta C_L^1 = C_L^{11} - C_L^{10} \qquad \text{Equation 6-7}$$

$$\Delta C_S^1 = C_S^{11} - C_S^{10} \qquad \text{Equation 6-8}$$

$$\Delta C_L^2 = C_L^{21} - C_L^{20} \qquad \text{Equation 6-9}$$

$$\Delta C_S^2 = C_S^{21} - C_S^{20} \qquad \text{Equation 6-10}$$

This gives four equations and four variables, so the tie line can be defined at any point.

The solution for the interface rate constant (e.g. Equation 2-93) can be found from the mass balance for each solute. If the effects of cross diffusion can be neglected, the mass balance solutions are given by Equation 6-11 and Equation 6-12, where D_{11} and D_{22} are the diffusivities of Cu and Au in Ag, respectively.

$$\xi = -\left(\frac{C_S^1}{C_L^1 - C_S^1}\right) \cdot 2 \cdot \sqrt{\frac{D_{11}}{\pi}} \cdot \frac{\exp\left(\frac{-\xi^2}{4 \cdot D_{11}}\right)}{\operatorname{erfc}\left(\frac{\xi}{2\sqrt{D_{11}}}\right)} \qquad \text{Equation 6-11}$$

$$\xi = -\left(\frac{C_S^2}{C_L^2 - C_S^2}\right) \cdot 2 \cdot \sqrt{\frac{D_{22}}{\pi}} \cdot \frac{\exp\left(\frac{-\xi^2}{4 \cdot D_{22}}\right)}{\operatorname{erfc}\left(\frac{\xi}{2\sqrt{D_{22}}}\right)} \qquad \text{Equation 6-12}$$

If a transcendental function, u, is defined by Equation 6-13 and Equation 6-14, then Equation 6-11 and Equation 6-12 can be rewritten as Equation 6-15 and Equation 6-16, respectively.

$$u_1 = -2 \cdot \sqrt{\frac{D_{11}}{\pi}} \cdot \frac{\exp\left(\frac{-\xi^2}{4 \cdot D_{11}}\right)}{\operatorname{erfc}\left(\frac{\xi}{2\sqrt{D_{11}}}\right)} \qquad \text{Equation 6-13}$$

$$u_2 = -2 \cdot \sqrt{\frac{D_{22}}{\pi}} \cdot \frac{\exp\left(\frac{-\xi^2}{4 \cdot D_{22}}\right)}{\operatorname{erfc}\left(\frac{\xi}{2\sqrt{D_{22}}}\right)} \qquad \text{Equation 6-14}$$

$$\xi = \left(\frac{C_S^1}{C_L^1 - C_S^1}\right) \cdot u_1 \qquad \text{Equation 6-15}$$

$$\xi = \left(\frac{C_S^2}{C_L^2 - C_S^2} \right) \cdot u_2 \qquad \text{Equation 6-16}$$

To ensure the full solution set of ξ is found, Equation 6-15 and Equation 6-16 cannot simply be set equal to each other and solved. The tie line definitions, Equation 6-3 to Equation 6-6, can be substituted for the tie line compositions in Equation 6-15 and Equation 6-16.

$$-\zeta = \frac{\left(C_L^{10} - C_S^{10}\right) \cdot \xi - C_S^{10} \cdot u_1}{\left(\Delta C_L^1 - \Delta C_S^1\right) \cdot \xi - \Delta C_S^1 \cdot u_1} \qquad \text{Equation 6-17}$$

$$-\zeta = \frac{\left(C_L^{20} - C_S^{20}\right) \cdot \xi - C_S^{20} \cdot u_2}{\left(\Delta C_L^2 - \Delta C_S^2\right) \cdot \xi - \Delta C_S^2 \cdot u_2} \qquad \text{Equation 6-18}$$

The mass balances, Equation 6-17 and Equation 6-18 can then be set equal to each other and solved. The solution is thus given by the roots of the equation: *w(ξ)*.

$$\frac{\left(C_L^{10} - C_S^{10}\right) \cdot \xi - C_S^{10} \cdot u_1}{\left(\Delta C_L^1 - \Delta C_S^1\right) \cdot \xi - \Delta C_S^1 \cdot u_1} - \frac{\left(C_L^{20} - C_S^{20}\right) \cdot \xi - C_S^{20} \cdot u_2}{\left(\Delta C_L^2 - \Delta C_S^2\right) \cdot \xi - \Delta C_S^2 \cdot u_2} = w(\xi) \qquad \text{Equation 6-19}$$

$$w(\xi) = 0 \qquad \text{Equation 6-20}$$

Maugis et al. [116] found that up to three roots to *w(ξ)* could exist for diffusion couples, depending on the terminal compositions. The existence of multiple interface velocities could lead to a breakdown of the planar interface between the phases, especially if the diffusion path established by the tie line position (ζ) crosses into the two phase region on the isotherm.

In the present study, the solution is simplified by the assumption of no concentration gradient in the liquid phase, such that the terminal liquid composition of the solid/liquid diffusion couple exists on the liquidus phase boundary. Using the tie line definitions established by Figure 6-24, only the solute diffusivities for Cu and Au in Ag are required to find a solution. From the literature, the value of $D_{11} = 1.1 \times 10^{-10}$ cm^2/s and $D_{22} = 2.3 \times 10^{-10}$ cm^2/s [117], can be used for the diffusivity of Cu and Au, respectively. Note that this is for a temperature of 725°C, and is the only data available in the literature. Substituting the diffusivities into the transcendental functions, Equation 6-13 and Equation 6-14, the function *w(ξ)* can be plotted in Figure 6-25.

From Figure 6-25, it can be seen that *w(ξ)* is a discontinuous function with one root. The solution, as shown in Figure 6-26 is found at $\xi = -0.051$ μm/√s. The corresponding value of ζ is 1.038×10^{-15}, which approaches 0. This tie line position corresponds to $C_L^1 = 0.34$, $C_L^2 = 0$, and $C_S^1 = 0.125$, $C_S^2 = 0$. This solution lies on the Ag-Cu binary, and thus is not valid. Therefore, no solution exists for a single tie line and isothermal solidification must proceed by a shifting tie line as described in § 2.5.2.

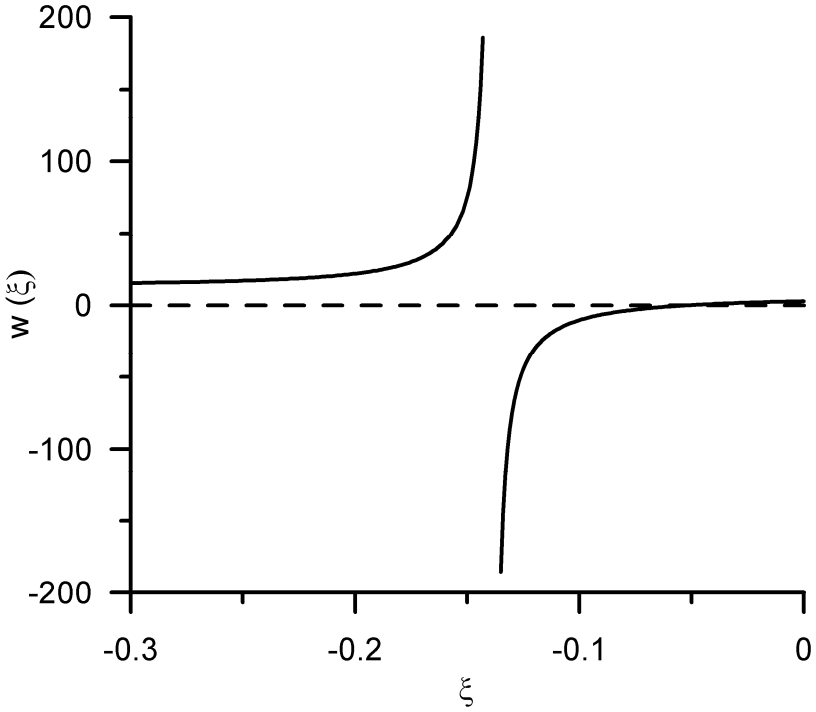

Figure 6-25: Solution set of function w(ξ).

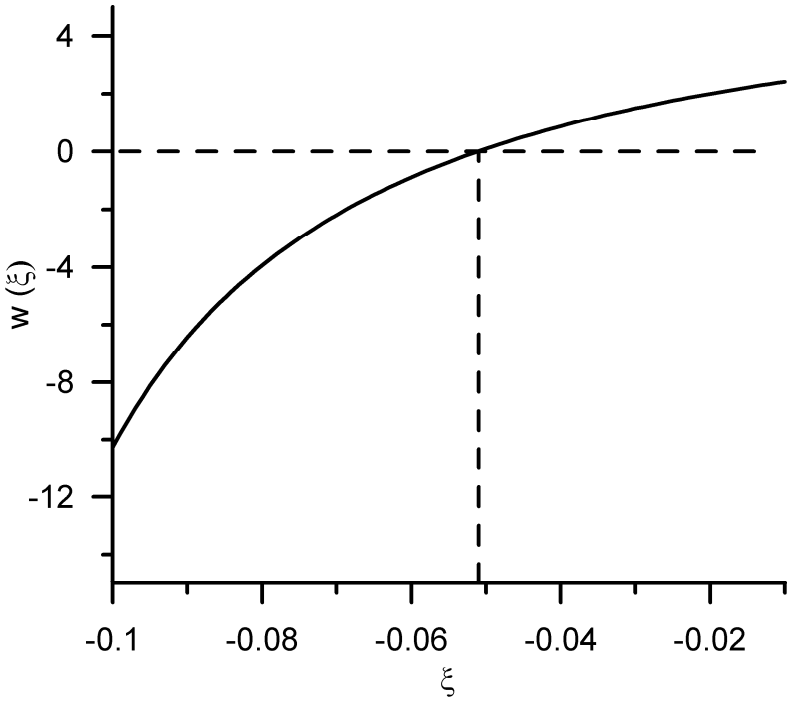

Figure 6-26: Roots to the solution of function w(ξ).

Two different approaches are proposed for modeling isothermal solidification in ternary solid/liquid diffusion couples. A stepwise solution assuming a linear Zener diffusion profile in the base metal can be developed (see Equation 2-109) by a mass balance for each liquid width. The solution is stepped with small incremental changes in the concentration of the solutes, which are related by the tie line definitions, given by Equation 6-3 to Equation 6-6. The mass balances that are solved simultaneously are given by Equation 6-21 and Equation 6-22.

$$\left[C_S^1\right]_{j+1}\sqrt{D_{11}t_{j+1}}-\left[C_S^1\right]_j\sqrt{D_{11}t_j}=\left[C_L^1\right]_j w_j-\left[C_L^1\right]_{j+1}w_{j+1} \qquad \text{Equation 6-21}$$

$$\left[C_S^2\right]_{j+1}\sqrt{D_{22}t_{j+1}}-\left[C_S^2\right]_j\sqrt{D_{22}t_j}=\left[C_L^2\right]_j w_j-\left[C_L^2\right]_{j+1}w_{j+1} \qquad \text{Equation 6-22}$$

The assumption of a linear solute profile in the stepwise solution is predicted to significantly affect the accuracy of the solution. Hence, a more accurate approach is desired.

The second approach is the finite difference method. In this study, an explicit finite difference solution is developed following the approach used by Zhou et al. [88]. In the present solution, the simplifying assumption of no concentration gradient in the liquid (i.e. uniform liquid composition) is applied. Furthermore, the effects of cross diffusion are ignored. Other assumptions follow the analytical solutions for analytical solutions in binary systems.

The length of the sample (L) is set to 1 mm, and is divided by H elements, such that the element length (Δx) given by L/H is 10 μm. The nodal position is given by $x_j = (j - 1)\cdot\Delta x$, for $j = 1, 2, \ldots, H + 1$. The solid/liquid interface lies between $j = k$ and $k + 1$, where k is given by Equation 6-23. The interface position is defined by p (Equation 6-24), where $0 \le p \le 1$. The time step, Δt, was initially 6 s, and increased by 3 s after each time step up to a maximum of $\Delta x^2/2\cdot D_{max}$ to ensure stability of the solution.

$$k = 1+\frac{X(t+1)}{\Delta x} \qquad \text{Equation 6-23}$$

$$p = \frac{X(t+1)-(k-1)\cdot\Delta x}{\Delta x} \qquad \text{Equation 6-24}$$

If $p \le 0.5$, the solution near the solid/liquid interface, $j = k + 1$ is given by:

$$C_{k+1}^i(t+1)=C_{k+1}^i(t)+\frac{D_{ii}\cdot\Delta t}{\Delta x^2}\cdot 2\cdot\left[\frac{C_S^i}{(1-p)\cdot(2-p)}-\frac{C_{k+1}^i(t)}{1-p}+\frac{C_{k+2}^i(t)}{2-p}\right] \qquad \text{Equation 6-25}$$

And, for $j = k + 2, k + 3, \ldots, H$:

$$C_j^i(t+1)=C_j^i(t)+\frac{D_{ii}\cdot\Delta t}{\Delta x^2}\left(C_{j+1}^i(t)-2\cdot C_j^i(t)+C_{j-1}^i(t)\right) \qquad \text{Equation 6-26}$$

At the boundary node, the solution is given by:

$$C^i_{H+1}(t+1) = C^i_{H+1}(t) + \frac{D_{ii}\cdot\Delta t}{\Delta x^2}\cdot 2\cdot\left(C^i_H(t) - C^i_{H+1}(t)\right) \qquad \text{Equation 6-27}$$

If $p > 0.5$, the solution set is given by Equation 6-28 for $j = k + 2$:

$$C^i_{k+2}(t+1) = C^i_{k+2}(t) + \frac{D_{ii}\cdot\Delta t}{\Delta x^2}\cdot 2\cdot\left[\frac{C^i_S}{(2-p)\cdot(3-p)} - \frac{C^i_{k+2}(t)}{2-p} + \frac{C^i_{k+3}(t)}{3-p}\right] \qquad \text{Equation 6-28}$$

And Equation 6-29 for $j = \underline{k} + 3, k + 4, \ldots, H$:

$$C^i_j(t+1) = C^i_j(t) + \frac{D_{ii}\cdot\Delta t}{\Delta x^2}\cdot\left(C^i_{j+1}(t) - 2\cdot C^i_j(t) + C^i_{j-1}(t)\right) \qquad \text{Equation 6-29}$$

The solution near the solid/liquid interface and at the boundary node is given by Equation 6-30 and Equation 6-31, respectively.

$$C^i_{k+1}(t+1) = \frac{2\cdot C^i_S}{(2-p)\cdot(3-p)} + \frac{2\cdot(1-p)\cdot C^i_{k+2}(t+1)}{2-p} - \frac{(1-p)\cdot C^i_{k+3}(t+1)}{3-p} \qquad \text{Equation 6-30}$$

$$C^i_{H+1}(t+1) = C^i_{H+1}(t) + \frac{D_{ii}\cdot\Delta t}{\Delta x^2}\cdot 2\cdot\left(C^i_H(t) - C^i_{H+1}(t)\right) \qquad \text{Equation 6-31}$$

The composition gradient at the solid/liquid interface is given by Equation 6-32 if $p \le 0.5$.

$$\frac{\partial C^i}{\partial x} = \frac{1}{\Delta x}\cdot\left[\frac{(2\cdot p-3)\cdot C^i_S}{(1-p)\cdot(2-p)} + \frac{(2-p)\cdot C^i_{k+2}(t)}{1-p} - \frac{(1-p)\cdot C^i_{k+3}(t)}{2-p}\right] \qquad \text{Equation 6-32}$$

If $p > 0.5$, the composition gradient is:

$$\frac{\partial C^i}{\partial x} = \frac{1}{\Delta x}\cdot\left[\frac{(2\cdot p-5)\cdot C^i_S}{(2-p)\cdot(3-p)} + \frac{(3-p)\cdot C^i_{k+2}(t)}{2-p} - \frac{(2-p)\cdot C^i_{k+3}(t)}{3-p}\right] \qquad \text{Equation 6-33}$$

The mass balance for each solute is given by Equation 6-34. The mass balances are solved simultaneously. If no solution can be found to satisfy both mass balances, the solution that minimizes the error between them is used.

$$D_{ii}\cdot\frac{\partial C^i}{\partial x}\cdot\Delta t = C^i_L(t+\Delta t)\cdot X(t+\Delta t) + C^i_S(t+\Delta t)\cdot\left[X(t+\Delta t) - X(t)\right] - C^i_L(t)\cdot X(t) \qquad \text{Equation 6-34}$$

The initial width of the liquid phase is denoted by $W_{max}/2$ because the system is modeled as a TLP half sample symmetric about the joint centerline. Assuming no solute is lost from the interlayer during initial heating to the eutectic temperature, and diffusion into the base metal during dissolution can be neglected, the maximum liquid width can be found using conservation of mass in the liquid. Thus, dissolution will occur along a straight line from the initial interlayer composition (i.e. Ag-Au-Cu eutectic) to the base metal composition (e.g. pure

Ag). The composition of the liquid after dissolution will lie on the liquidus phase boundary (Figure 6-27). In this study the liquid composition at the start of isothermal solidification is taken as Ag - 37.6 at.% Cu - 15.0 at.% Au for modeling purposes. Using this composition, the maximum liquid width, $W_{max} = 1.17 \cdot W_o$, where W_o is the interlayer width.

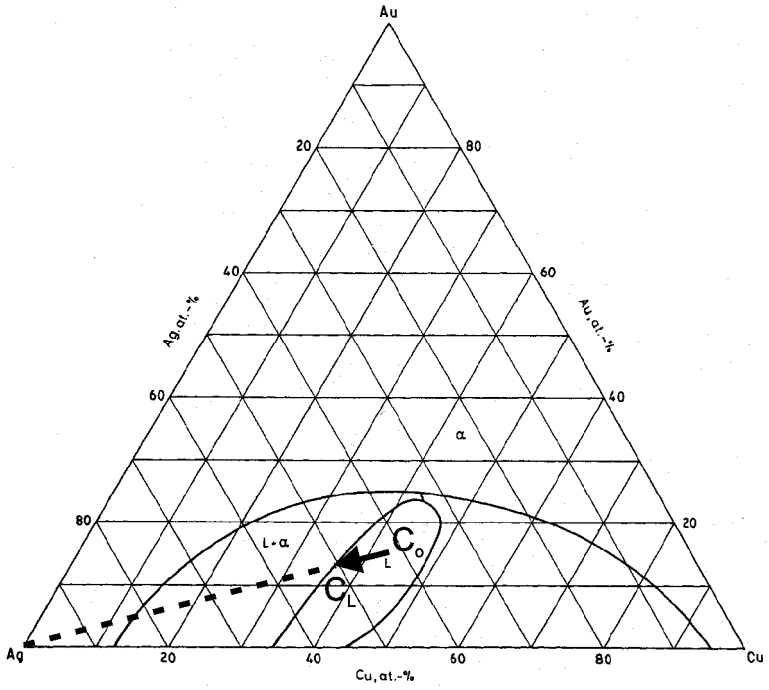

Figure 6-27: Dissolution of base metal [104].

6.4. Modeling Results

The isothermal solidification process in the solid/liquid diffusion couples used for the DSC experiments was modeled using both the finite difference and stepwise approaches described above. The modeled output is then compared with the experimental results. The modeling approach requires appropriate selection of solute diffusivities. This is difficult in ternary systems where accurate diffusion data is rarely available.

Published values for diffusion in the Ag-Au-Cu ternary system were determined experimentally by Ziebold and Ogilvie [117], who used diffusion couple sandwiches. From these results, the diffusivity of Cu (D_{11}) is found to be 1.1×10^{-10} cm^2/s, and the diffusivity of Au (D_{22}) is found to be 2.3×10^{-10} cm^2/s at 725°C for a composition of Ag - 16.9 at.% Au - 11.2 at.% Cu. These results indicate that the diffusivity of Au is enhanced with increasing Cu in the matrix. The diffusion study has shown that the effects of cross diffusion are nearly negligible within the composition range of interest [117]. Cross diffusional effects are neglected in the numerical models.

Using an initial liquid width ($W_{max}/2$) of 29.7 μm and solute diffusivities described above, the results of finite difference modeling are shown in Figure 6-28. The composition of both solutes, Cu and Au are given as a function of position from the joint centerline at the completion of isothermal solidification (i.e. the liquid width is zero).

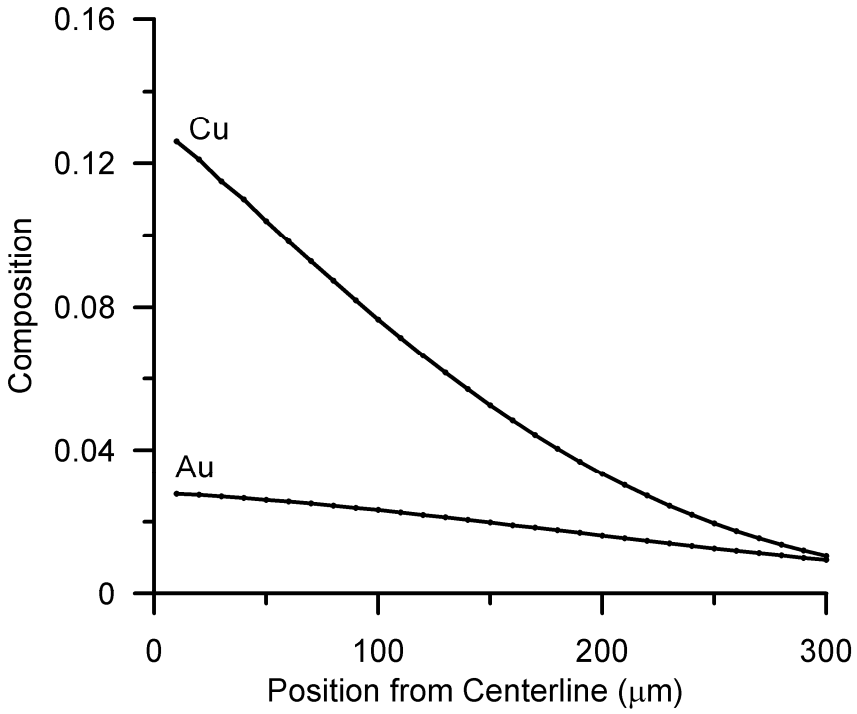

Figure 6-28: Composition profile of Cu and Au solutes at the end of isothermal solidification. $D_{11} = 1.1 \times 10^{-10}$ cm^2/s, $D_{22} = 2.3 \times 10^{-10}$ cm^2/s.

The process kinetics predicted by the modeling results can be plotted by the fraction of liquid remaining as a function of the square root of the isothermal hold time. The results are given in Figure 6-29. The results are nearly linear indicating that the interface rate constant remains steady throughout the duration of the isothermal solidification process. A linear regression fit line is applied to the modeled results and shows very good agreement. From the linear fit, an effective interface rate constant for isothermal solidification can be found. The experimentally measured process kinetics for the DSC type-3 corrected results (e.g. Figure 6-14) are also given in Figure 6-29 for comparison. Comparison of the results show that the finite difference prediction does not agree well with the interface kinetics measured experimentally.

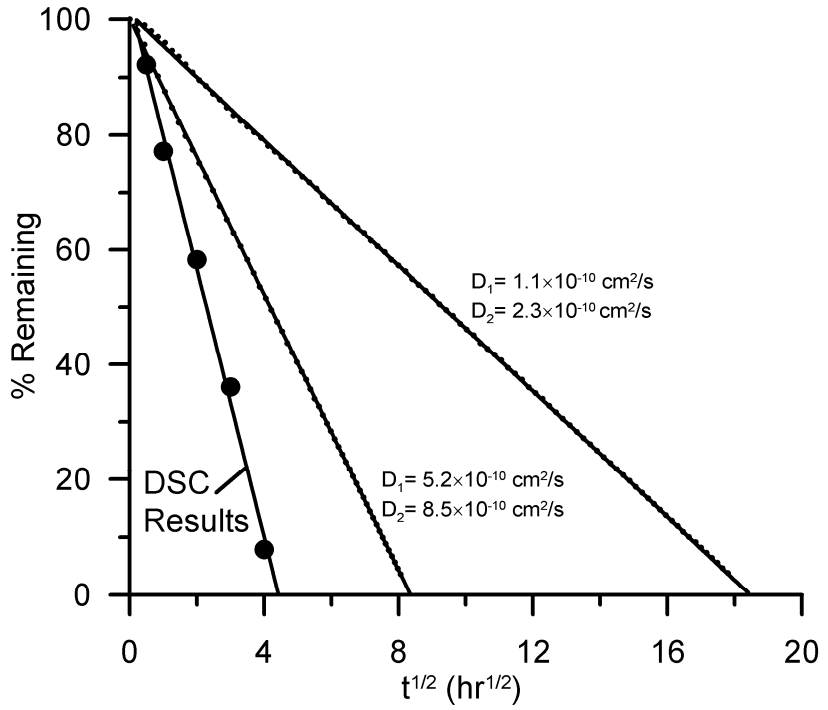

Figure 6-29: Comparison of interface kinetics, $W_{max}/2 = 29.7$ μm. Experimentally measured and finite difference predictions: $D_{11} = 1.1 \times 10^{-10}$ cm^2/s, $D_{22} = 2.3 \times 10^{-10}$ cm^2/s, and $D_{11} = 5.2 \times 10^{-10}$ cm^2/s, $D_{22} = 8.5 \times 10^{-10}$ cm^2/s.

Clearly, the published diffusivities for 725°C are too slow. The isothermal hold temperature is 800°C but the only temperature for which diffusion data is available is 725°C and no activation energies were given in the literature. Thus, correction for the increased diffusivities with increasing temperature is difficult; however, the effect is expected to be significant with the increase of 75°C. Given the lack of available diffusion data at the temperature of interest, the solute diffusivity was corrected using activation energies for Cu and Au in binary Ag systems. The activation energy (Q) of 184 kJ/mol was taken for Cu in Ag, and 155 kJ/mol for Au in Ag. Using Equation 6-35, the diffusivity of Cu in Ag (D_{11}) was found to be 5.2×10^{-10} cm^2/s, and the diffusivity of Au in Ag (D_{22}) was found to be 8.5×10^{-10} cm^2/s.

$$D_{800} = D_{725} \cdot \exp\left(\frac{-Q}{R \cdot 1073K} + \frac{Q}{R \cdot 998K}\right) \qquad \text{Equation 6-35}$$

The finite difference prediction results using $D_{11} = 5.2 \times 10^{-10}$ cm^2/s and $D_{22} = 8.5 \times 10^{-10}$ cm^2/s are given in Figure 6-30. The predicted interface kinetics for the temperature adjusted diffusivities are shown in Figure 6-29. As in the previous case, the liquid width decreases almost linearly with the root time, suggesting that the interface rate constant is steady during isothermal solidification. The comparison shows that increasing the diffusivity

results in an increase in the interface rate constant; however, the kinetics are still significantly slower than the experimentally measured results.

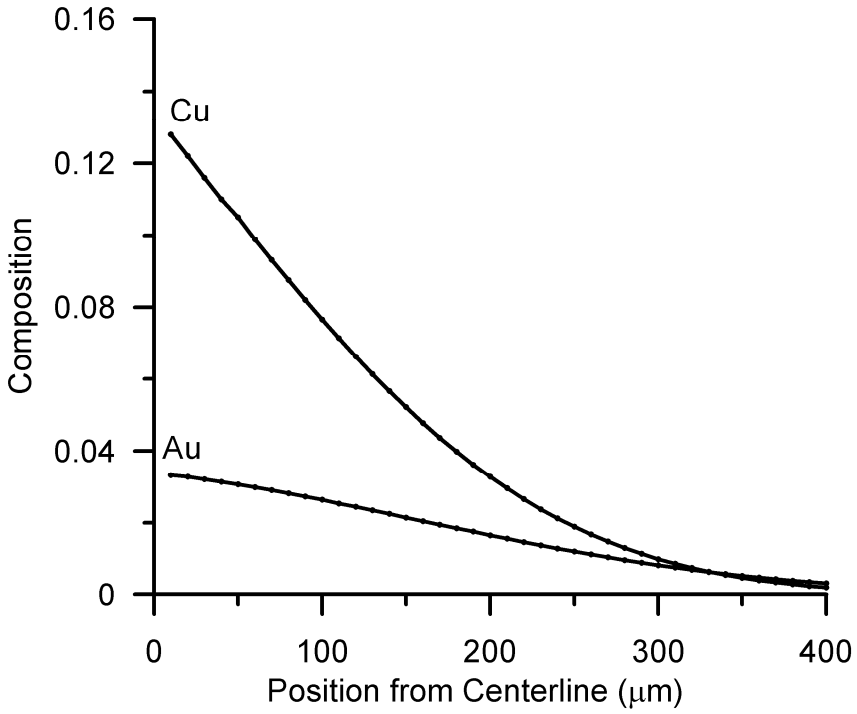

Figure 6-30: Composition profile of Cu and Au solutes at the end of isothermal solidification. $D_{11} = 5.2 \times 10^{-10}$ cm^2/s, $D_{22} = 8.5 \times 10^{-10}$ cm^2/s.

The poor agreement between the measured and predicted results is likely due to inaccuracies in the available diffusion data in the Ag-Au-Cu system at 800°C along with the assumptions made during derivation of the models. From Figure 6-31, the interface kinetics predicted using the finite difference model are faster than those given by the stepwise solution that assumes a Zener solute diffusion profile in the solid (Equation 6-21 and Equation 6-22). In this case, the linear diffusion profile on the solid results in an overestimation of the time required for the completion of isothermal solidification.

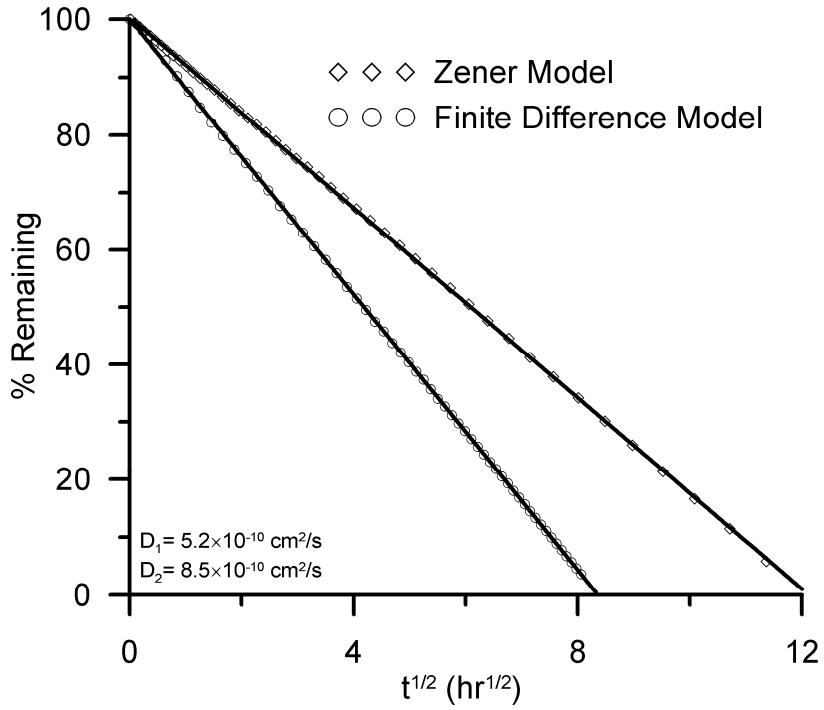

Figure 6-31: Comparison of interface kinetics predicted by the stepwise solution assuming a Zener diffusion profile and the finite difference method for $D_{11} = 5.2 \times 10^{-10}$ cm^2/s and $D_{22} = 8.5 \times 10^{-10}$ cm^2/s.

Agreement between the measured and predicted results can be improved by adjusting the value of the solute diffusivities. Figure 6-32 shows the effect of increasing the Cu diffusivity (D_{11}). The interface rate constant increases with increased D_{11} when D_{22} is held constant. In Figure 6-32, the interface rate constant decreases with increasing Au diffusivity (D_{22}). Figure 6-33 shows the interface rate constant as a function of D_{22}. The effect of increasing D_{22} is to slightly decrease the magnitude of the interface velocity, but the effect is not as strong as that of D_{11}. For example, doubling D_{22} from 7×10^{-10} cm^2/s to 14×10^{-10} cm^2/s has little effect on the interface rate constant, whereas doubling D_{11} has a profound effect.

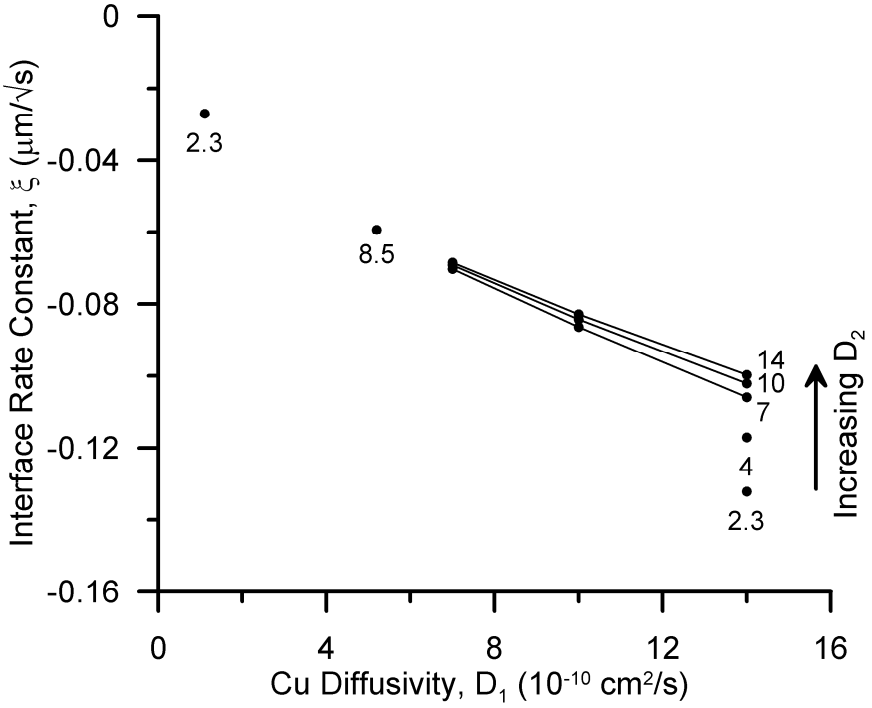

Figure 6-32: Effect of D_{11} on the interface rate constant, ξ.

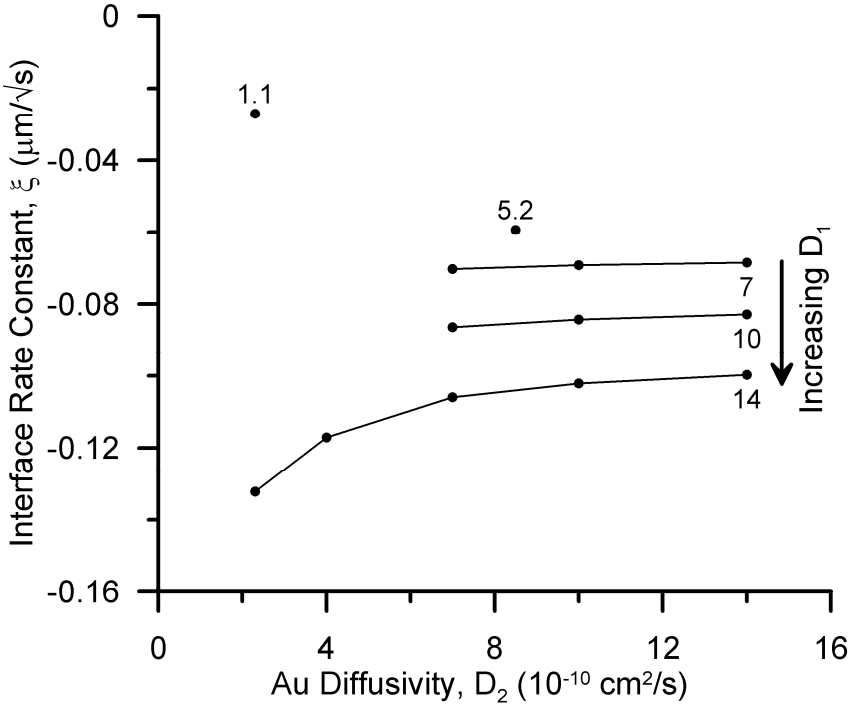

Figure 6-33: Effect of D_{22} on the interface rate constant, ξ.

The data in Figure 6-32 and Figure 6-33 suggests that for higher values of D_{11} and lower values of D_{22}, the interface rate constant approaches that of the experimental results. Figure 6-34 shows that increasing the value of D_{11} gives closer agreement with the interface kinetics observed with the DSC experiments. If the value of D_{22} is decreased to 2.3×10^{-10} cm^2/s, the interface kinetics increase beyond that observed experimentally.

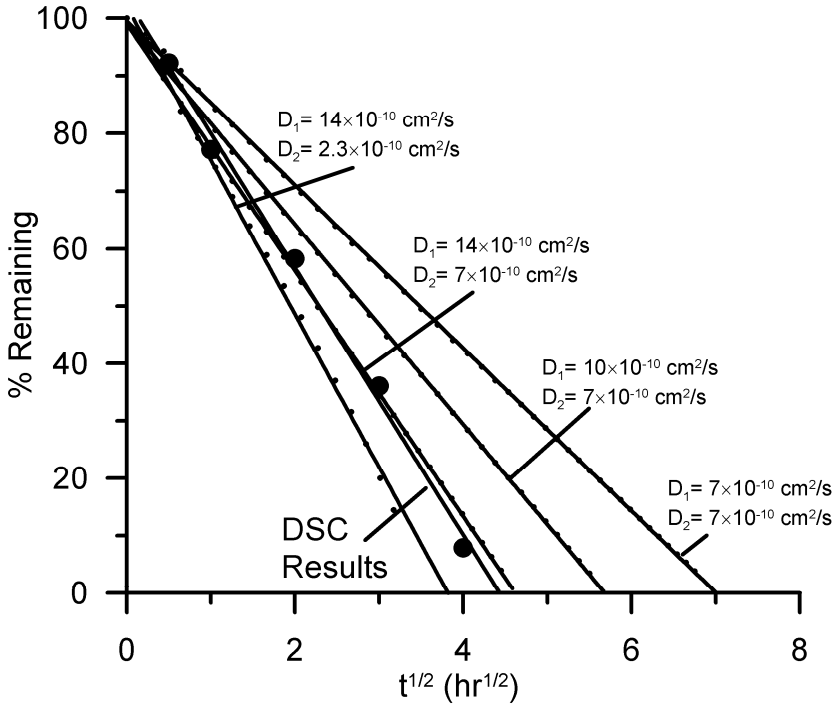

Figure 6-34: Comparison of experimentally measured interface kinetics with finite difference predictions.

The solid/liquid interface tie line compositions shift as isothermal solidification proceeds. This can be observed in the finite difference model output. Figure 6-35 shows the liquid Au composition at the solid/liquid interface as a function of isothermal hold time for different values of D_{11} and D_{22}. Examination of the results in Figure 6-35 shows that both the magnitude and rate of change in composition depends on the diffusivity values. With increasing interface velocity and decreasing D_{22}, the magnitude of the shift in liquid Au composition decreases. The corresponding result for the solid Au composition at the solid/liquid interface is given in Figure 6-36.

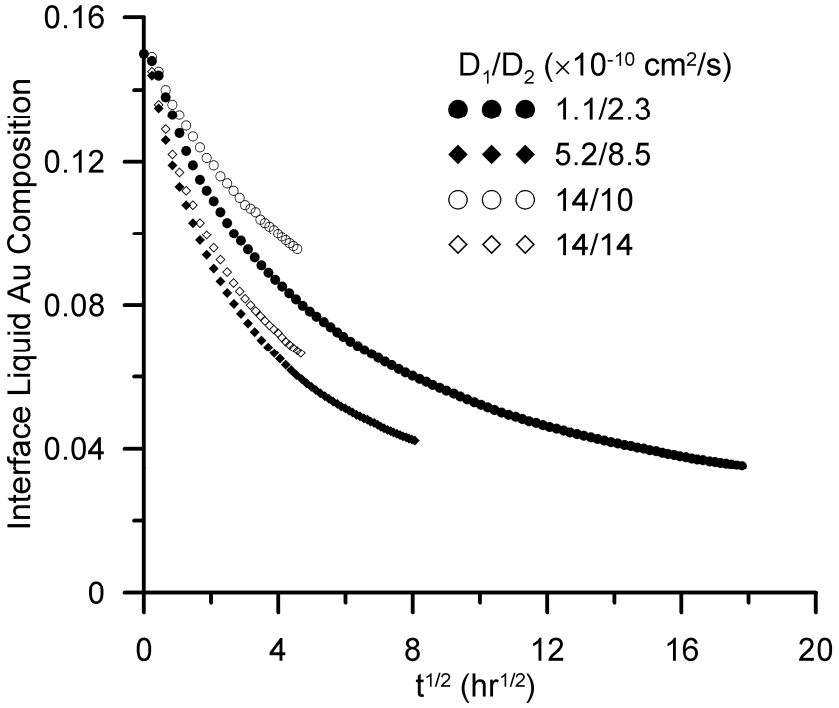

Figure 6-35: Liquid Au composition at the solid/liquid interface as a function of root time.

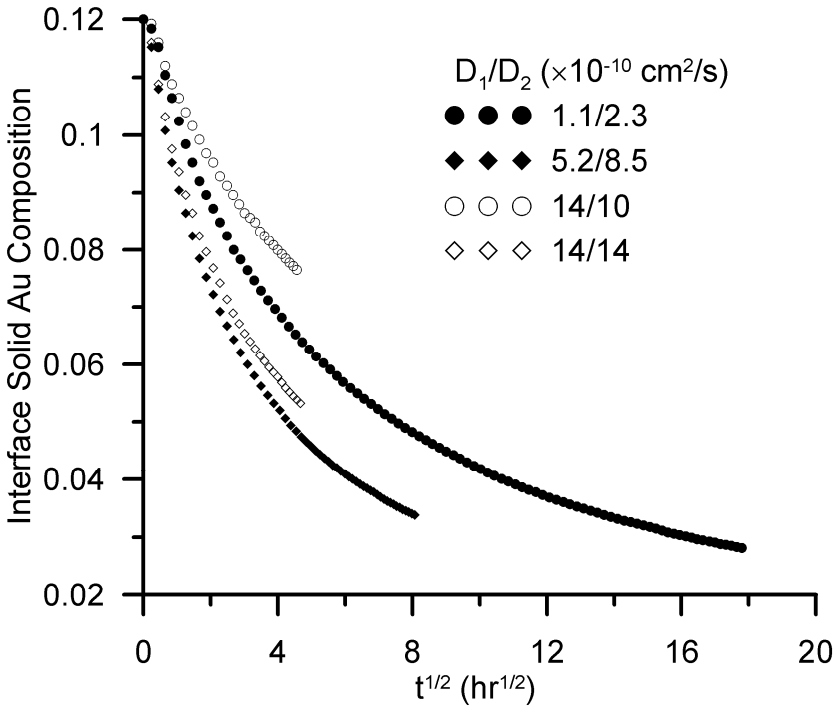

Figure 6-36: Solid Au composition at the solid/liquid interface as a function of root time.

Figure 6-35 and Figure 6-36 show the predicted Au interface compositions for different assumed diffusivity values of Au and Cu. The individual plots show the shifting composition with increasing hold time until the end of isothermal solidification. Thus, from these figures, the process kinetics as well as the nature of tie line shift can be observed. The hollow symbol plots for constant D_{11} show that increasing the Au diffusivity, D_{22}, has little effect on the time for completion of isothermal solidification; however, there is a noticeable increase in tie line shift. Decreasing the assumed diffusivity value of Cu, D_{11}, results in an increase in the time required for isothermal solidification.

The corresponding plots for the liquid and solid Cu compositions at the solid/liquid interface are shown in Figure 6-37 and Figure 6-38, respectively. The magnitude of the composition shift during isothermal solidification is significantly less than that for Au. This is expected since the phase boundaries run nearly parallel to the lines of equal Cu on the phase diagram. The decreasing magnitude in tie line shift corresponds with an increase in the interface kinetics. From Figure 6-32, the interface kinetics increase as D_{11} increases and D_{22} decreases. For high values of D_{11} and low values of D_{22}, the predicted direction of tie line shift changes. Figure 6-39and Figure 6-40 show the effect of decreasing D_{22} on the direction and magnitude of Au interface composition shift in liquid and solid, respectively.

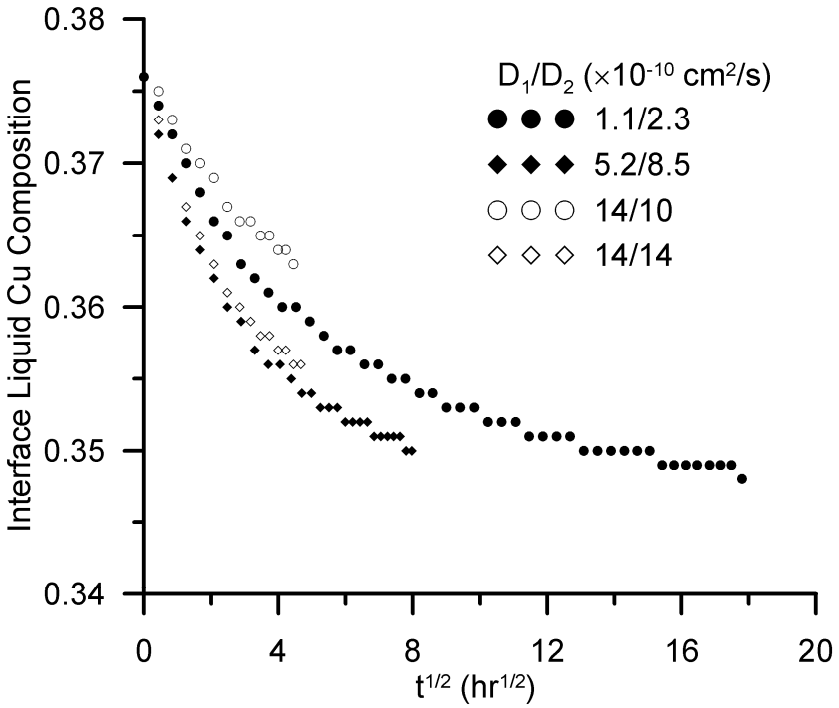

Figure 6-37: Liquid Cu composition at the solid/liquid interface as a function of root time.

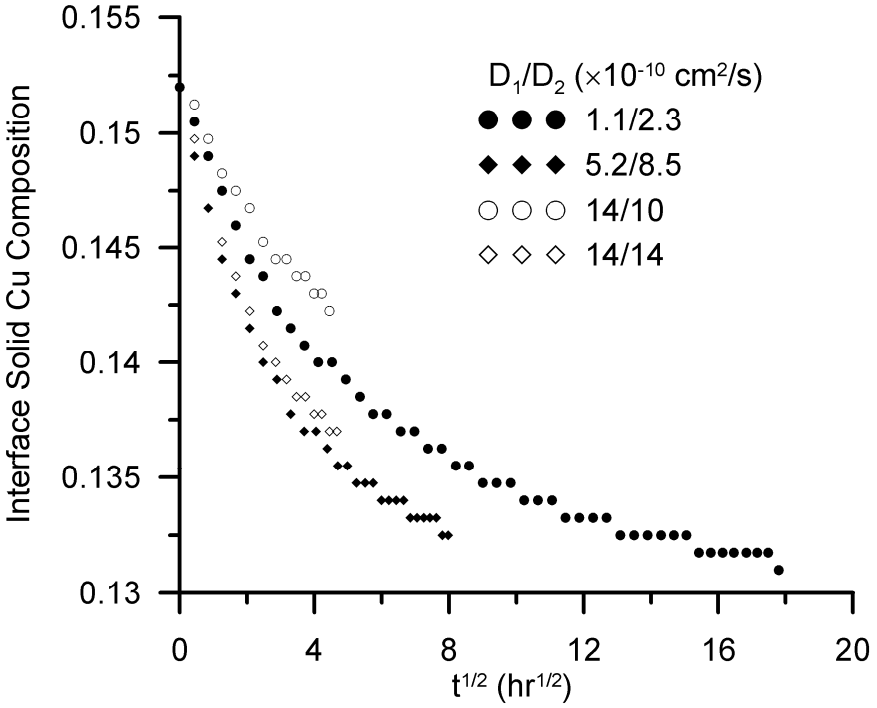

Figure 6-38: Solid Cu composition at the solid/liquid interface as a function of root time.

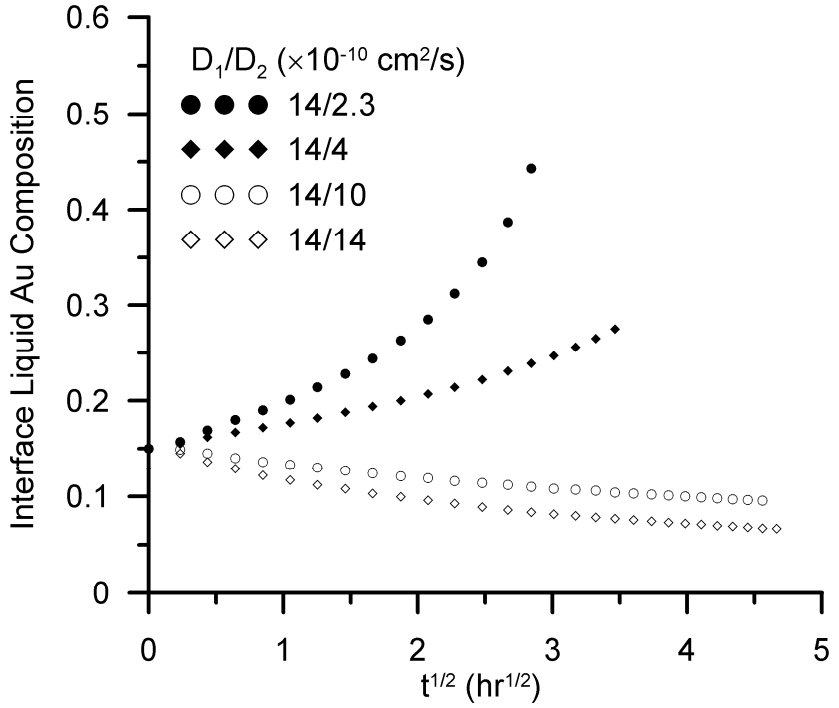

Figure 6-39: Shifting Au liquid composition at the solid/liquid interface with decreasing values of D_{22}.

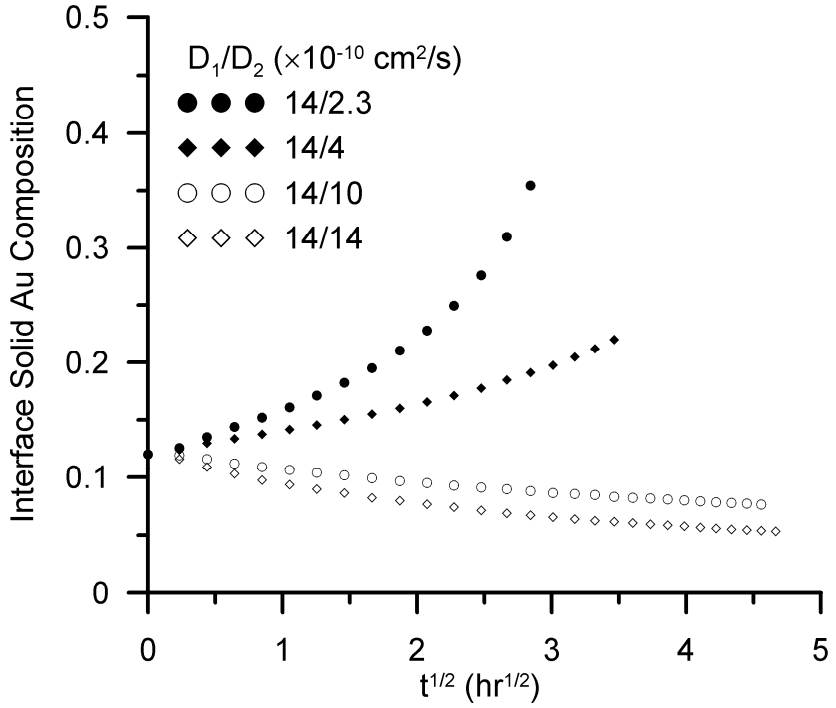

Figure 6-40: Shifting Au solid composition at the solid/liquid interface with decreasing values of D_{22}.

The increase in interface kinetics observed with increasing Cu diffusivity is intuitive since faster diffusion supports a higher interface velocity. Furthermore, the tie line shift in a direction of decreasing Au content with increasing Au diffusivity is a result of the increased solute flux but little change in interface velocity, thus the composition of the liquid shifts in a direction of decreasing solute content to satisfy the mass balance at the solid/liquid interface.

The nature of the phase boundaries in the Ag-Au-Cu ternary system at 800°C plays a significant role in determining the characteristics of isothermal solidification. With a tie line shift in the direction of decreased Au content, the Cu content also decreases slightly. The mass balance at the solid/liquid interface must always be satisfied; hence, with increasing tie line shift, the interface velocity decreases to enable the decrease in liquid Cu content through solute flux. It is through this mechanism that the interface kinetics decrease with increasing Au diffusivity.

At lower Au diffusivities and higher Cu diffusivities, the tie line shifts to higher Au concentrations. In this sense, the solute flux at the interface is not great enough to satisfy the mass balance and the Au is repartitioned back into the liquid as the interface advances. This is coupled with an increase in Cu content, which in turn supports a higher interface velocity as Cu is repartitioned back into the liquid instead of diffusing into the solid through interface flux.

In the Ag-Au-Cu system, isothermal solidification kinetics seems to be mainly controlled by the diffusivity of Cu. There is little freedom in the liquid Cu concentration because the phase

boundaries run nearly parallel to Cu isopleths, or lines of equal Cu concentration, thus the interface kinetics are established to satisfy the mass balance. With little shift in the Cu liquid concentration, diffusive solute flux drives the solid liquid interface as there is no build up or decrease of solute in the liquid phase.

By the nature of the phase boundaries, the Au concentration in the liquid can change with relatively little change in the Cu concentration. Due to the greater freedom in the Au concentration, the direction and magnitude of tie line shift appears to be controlled by the Au diffusivity. In this sense, if the Au diffusivity results in a solute flux that is faster than the solid/liquid interface velocity can support (which is established by the Cu diffusivity), then the tie line shifts in a direction of decreasing Au concentration. Likewise, if the Au diffusivity is relatively low compared to the interface velocity determined by Cu diffusivity, then the tie line shifts in a direction of increasing Au concentration.

The composition profiles of solute in the base metal were measured experimentally using energy dispersive x-ray spectrometry. The results are shown in Figure 6-41 for Au and Figure 6-42 for Cu. These measurements were conducted for the type-2 DSC experiments with a maximum liquid width of $W_{max}/2 = 46.7$ μm (i.e. thicker interlayer). The experimental results show that the tie line shifts in a direction of decreasing Au and Cu concentration. In Figure 6-41, the position of the interface between the solidified eutectic phase and the Ag base metal is given by position "0". The composition of the Au solute goes from approximately 12% after 0 hours of isothermal hold time to approximately 6% after 81 hours at 800°C. The Cu composition profiles shown in Figure 6-42 also show a decrease in the interfacial base metal Cu concentration with increasing isothermal hold time; however, the magnitude of the shift is considerably less than change in Au observed in Figure 6-41. The observed compositions can be plotted on the Gibbs' isotherm at 800°C in Figure 6-43. The approximate liquid compositions are also plotted to establish the initial and final tie lines as observed experimentally. The tie line shift during isothermal solidification is easily seen in this figure, shifting in a direction of decreasing Au and Cu concentrations.

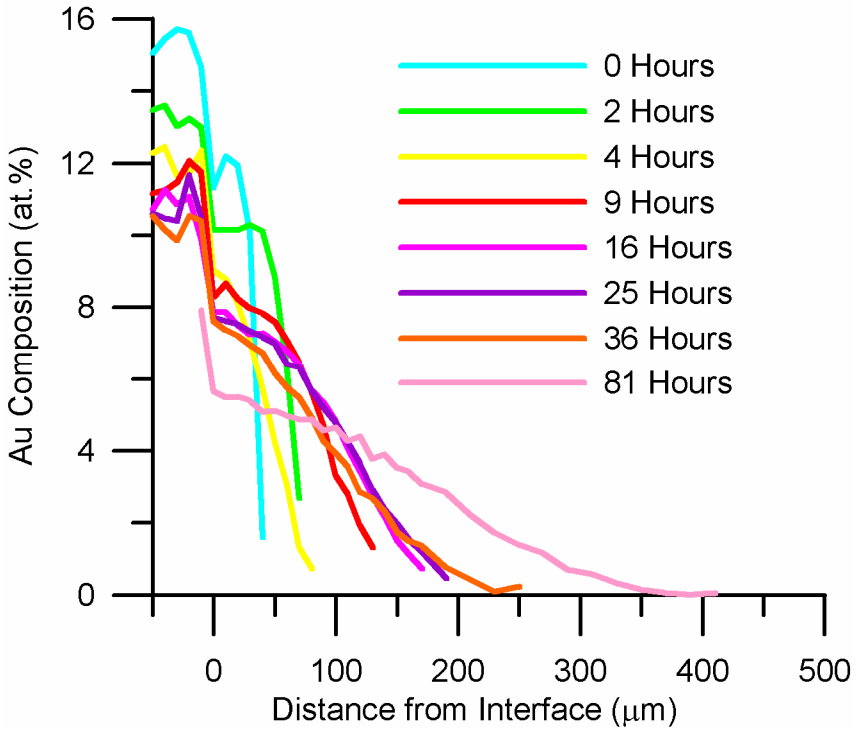

Figure 6-41: Au composition profile measured using EDS for a maximum liquid width of $W_{max}/2$ = 47.6 μm.

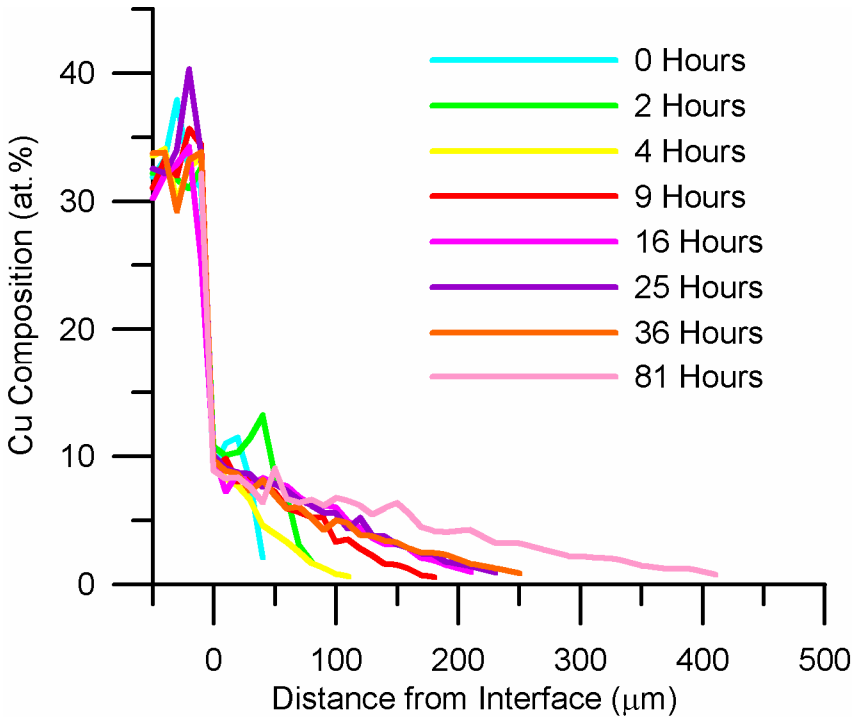

Figure 6-42: Cu composition profile measured using EDS for a maximum liquid width of $W_{max}/2$ = 47.6 μm.

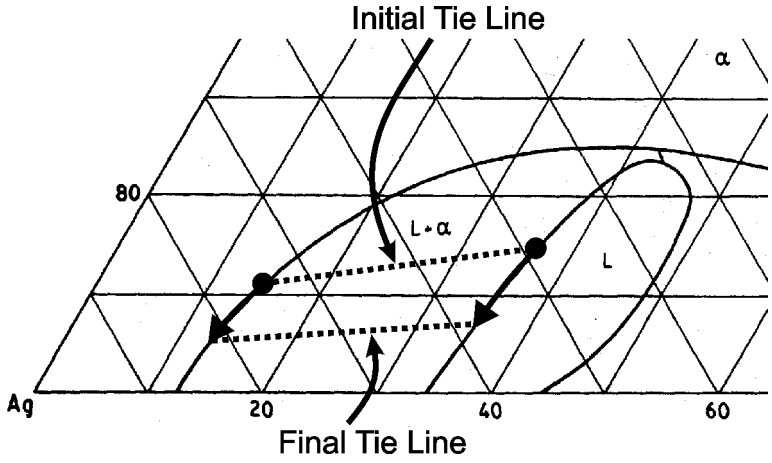

Figure 6-43: Measured shifting tie lines.

The experimental results for tie line shift are most closely matched by the prediction given using a Cu diffusivity, $D_{11} = 14 \times 10^{-10}$ cm^2/s and a Au diffusivity, $D_{22} = 10 \times 10^{-10}$ cm^2/s. The interface kinetics predicted using this combination are shown in Figure 6-44, the prediction agrees fairly well with the measured results. The results of the finite difference prediction for this combination of diffusivities is shown in Figure 6-45. The prediction for interface kinetics given by the finite difference approach is compared to that of the stepwise solution in Figure 6-46.

Figure 6-46 shows that the interface velocity is under predicted by the stepwise solution that assumes a linear diffusion profile. As in Figure 6-31, the predicted time required for completion of isothermal solidification is much higher with the stepwise solution compared to the finite difference approach. This finite difference approach gives a better representation of the mechanics of isothermal solidification, compared to the stepwise solution, which can only be used to effectively develop a basic understanding of isothermal solidification in ternary systems.

The effect of varying the liquid width at the beginning of isothermal solidification in the solid/liquid diffusion couples can also be observed using the finite difference approach. Figure 6-47 shows the interface kinetics modeled for two different experimental initial liquid widths. The results are normalized for time based on the liquid width. The interface kinetics for the different liquid widths are in good agreement with each other, the difference can be attributed to numerical error. Similarly, the shifting interface liquid Au composition can be normalized for the maximum liquid width, as shown in Figure 6-48. The results of the simulation show that the magnitude of the shift is independent of the maximum liquid width.

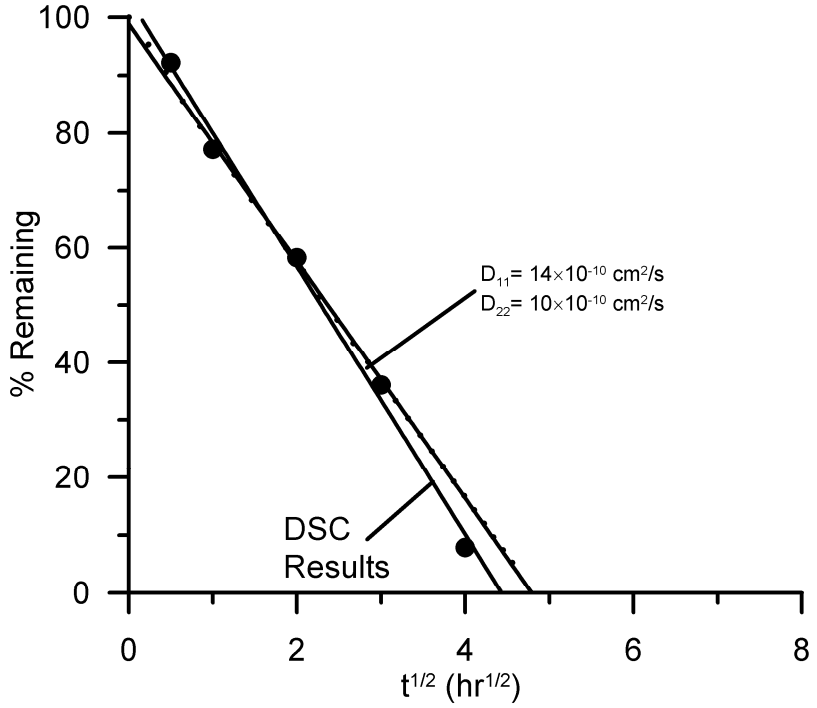

Figure 6-44: Comparison of experimentally measured interface kinetics with finite difference predictions, $D_{11} = 14 \times 10^{-10}$ cm^2/s and $D_{22} = 10 \times 10^{-10}$ cm^2/s.

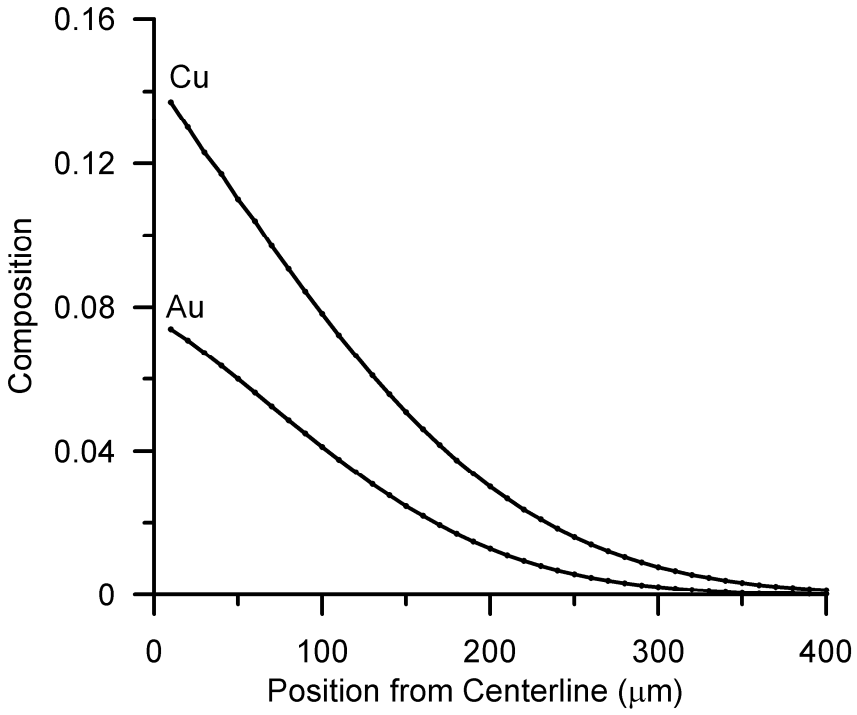

Figure 6-45: Composition profile of Cu and Au solutes at the end of isothermal solidification. $D_{11} = 14 \times 10^{-10}$ cm^2/s, $D_{22} = 10 \times 10^{-10}$ cm^2/s.

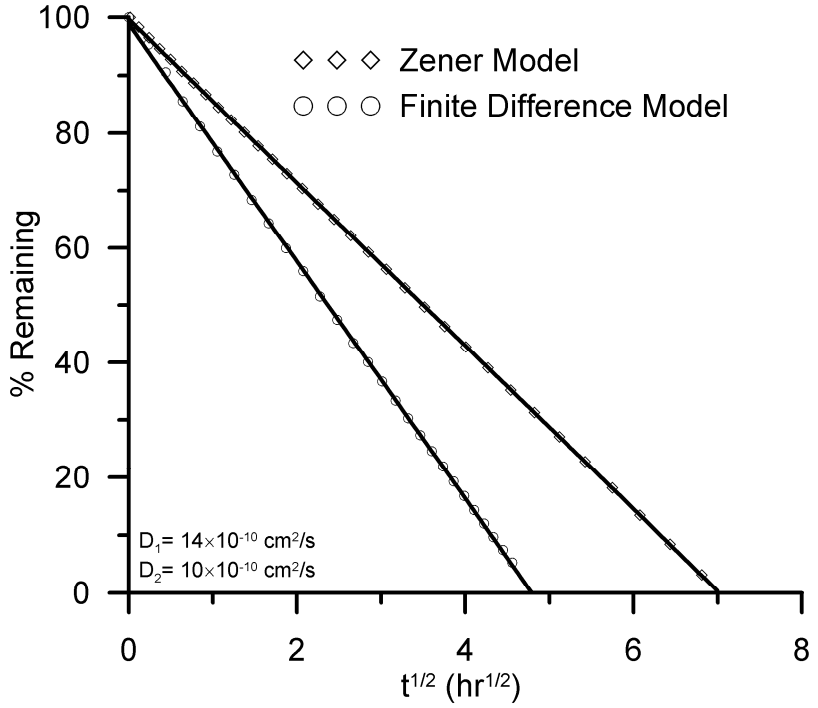

Figure 6-46: Comparison of interface kinetics predicted by the stepwise solution assuming a Zener diffusion profile and the finite difference method for $D_{11} = 14 \times 10^{-10}$ cm^2/s and $D_{22} = 10 \times 10^{-10}$ cm^2/s.

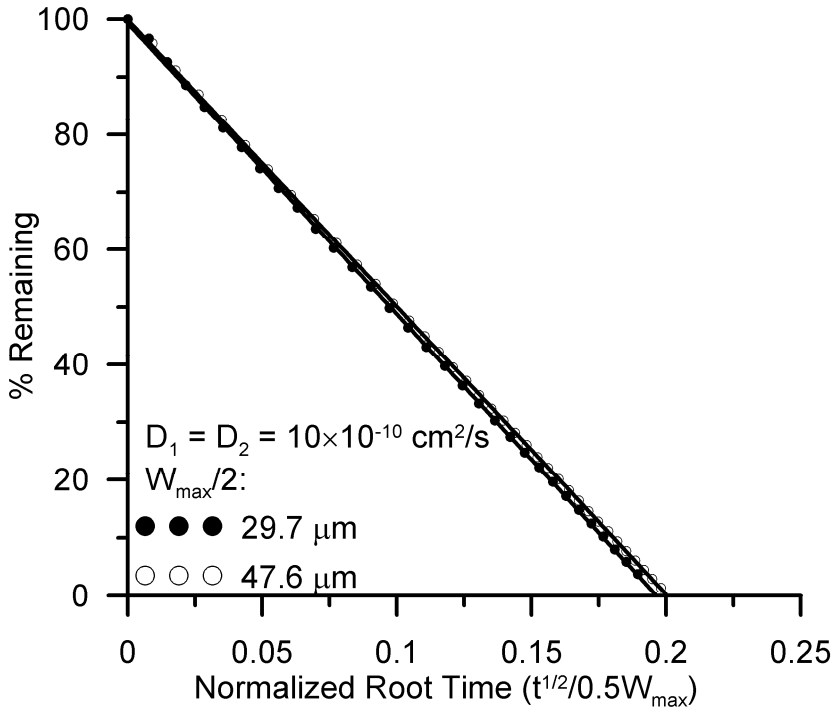

Figure 6-47: Comparison of finite difference prediction results for a thin vs. thick interlayer.

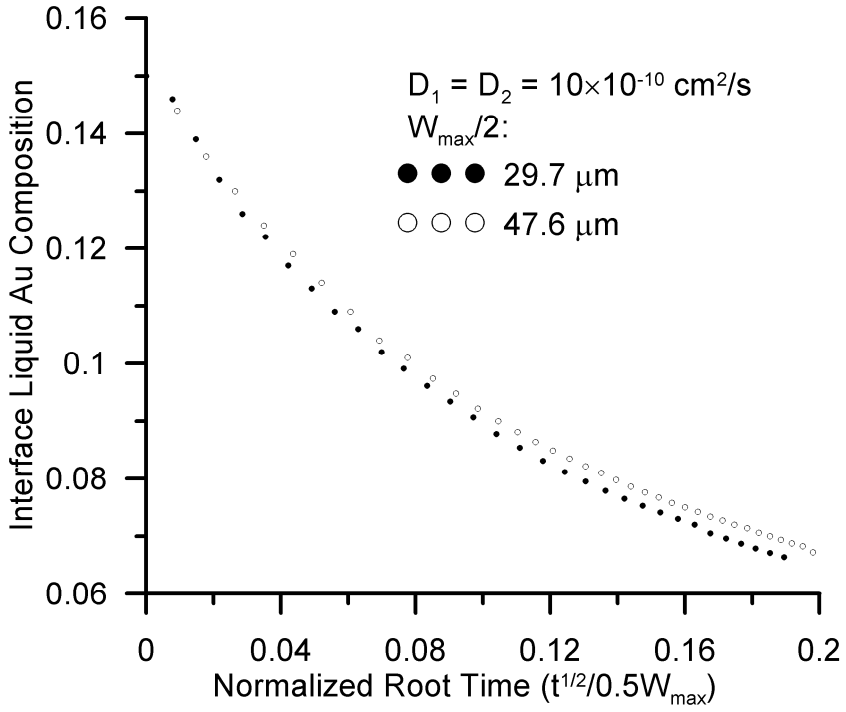

Figure 6-48: Comparison of the liquid Au composition at the solid/liquid interface for thick and thin interlayers.

The modeled and experimental results for the shifting tie line observation support the DSC results plotted in Figure 6-18. The liquidus composition is shifting farther away from the eutectic, which is expected to increase the fraction of the liquid that will solidify to the primary phase upon cooling from the isothermal hold temperature. This is shown in the DSC results as a decrease in the ratio of the solidification exotherm to melting endotherm in adjacent peaks as isothermal solidification proceeds, and the tie line shifts farther from the eutectic. Following this logic, the DSC results could possibly be used to identify the direction of tie line shift during isothermal solidification.

Control of the final liquid composition is important when harmful microstructures may form upon cooling through solid-state transformations. For example, in the Ag-Au-Cu system, the Cu_3Au phase can be avoided if the Au content is controlled. Thus, the shifting tie line towards the Ag-Cu binary system can reduce the need for homogenization heat treatments after isothermal solidification is complete.

The modeled and experimental results both show an interface rate constant that remains nearly constant throughout isothermal solidification. This does not help explain the deviation from linear interface kinetics observed at longer isothermal hold times in Figure 6-16 for the thick foil. In this material system, a change in the kinetic regime is not observed due to the nature of the phase boundaries. With the concentration of both solutes decreasing as isothermal solidification proceeds, there is no accumulation of a species that would eventually

lead to a change in the interface kinetics. Therefore, the interface kinetics remain constant, which is similar to the binary case.

It is acknowledged that the diffusivities that are required to give good agreement between the experimental and modeled results seem excessively high. Furthermore, it should be noted that a number of combinations of D_{11} and D_{22} could give good agreement with the experimental results, and the solid/liquid diffusion couple interface kinetics cannot be used to determine the effective solute diffusivities in ternary systems as in binary systems. A complete analysis of composition profiles in the solid would be required to experimentally determine the actual diffusivities. The lack of accurate diffusion and phase diagram (e.g. tie line) data for the experimental system contributes to the uncertainty in the finite difference predictions. With experimental tie line compositional information, the accuracy of the model could be improved with realistic diffusivity values. Additionally, the assumption that cross-diffusional effects can be neglected simplifies the model derivation but may increase the prediction error.

6.5. Summary

The DSC method for quantifying solid/liquid interface kinetics during isothermal solidification has been applied to ternary alloy solid/liquid diffusion couples. Eutectic Ag-Au-Cu foil interlayers were coupled with pure Ag base metal to study the effects of an additional solute on interface motion. As in the binary case, experimental artefacts including baseline shift and primary solidification contribute to a systematic underestimation of the fraction of liquid remaining. A modified temperature program has been employed to quantify and correct these effects. The experimental results show a linear relationship between the interface position and the square root of the isothermal hold time. The shifting tie line composition at the interface has been shown to affect the DSC results; however, the impact on the calculated interface kinetics has been shown to be minimal in this case.

The experimental results have been compared to predictions generated using the finite difference approach; however, the lack of accurate thermodynamic data for the Ag-Au-Cu ternary system has limited agreement. Numerical modeling results can be used to further develop the theoretical understanding of isothermal solidification in ternary systems. Results show that the mechanism governing interface motion is related to the nature of the phase boundaries on the Gibbs' isotherm. In this case, the liquidus boundary runs nearly parallel to the Cu isopleths and as a result the solid/liquid interface is driven by the diffusion of Cu. Tie line shift is a function of Au diffusion since there is a greater degree of freedom in the liquidus composition. The experimentally measured interface composition shift agrees well with the modeling prediction.

7. Conclusions

The objectives of this work were to:

1. Develop a technique for quantifying interface kinetics during isothermal solidification using DSC, and characterize the effects of sample geometry on the results.
2. Compare the experimental results with the predictions of various analytical methods for isothermal solidification.
3. Quantify the process kinetics of isothermal solidification in a ternary alloy system, and compare to the results of predictive models for interface motion with two solutes to evaluate the validity of the simulations and improve the fundamental theoretical understanding of the process.
4. Compare the predictions for compositional shift at the solid/liquid interface with experimentally measured results to determine if tie line shift can be observed with DSC, and further understand the driving force behind the direction of change.

To accomplish the stated objectives, carefully planned experiments using TLP half-samples analogous to solid/liquid diffusion couples were carried out. The progress of isothermal solidification was calculated by measuring the solidification enthalpy of the remaining liquid upon cooling the sample after an isothermal hold period. The length of the isothermal hold period was varied to show the solid/liquid interface kinetics as a fraction of the original quantity of liquid. The Ag-Cu binary eutectic system was selected for experimental work.

7.1. Using DSC to Measure Isothermal Solidification Kinetics

7.1.1. DSC Process Parameters and Effects on the DSC Results

The effects of a number of variables on the resulting DSC trace were investigated, including the initial interlayer composition, the heating rate, the reference crucible contents, and the base metal coating. In some cases, the variables were found to have an effect on the shape of the DSC trace. The direct comparison of two interlayers with dissimilar compositions was made with a pure Cu (i.e. Type-I) and a eutectic Ag-Cu (i.e. Type-II) foil. The onset of melting on the DSC trace is shifted to a higher temperature with the pure foil, a result of the longer time required for dissolution of the interlayer as solute transport from the interlayer to the base metal occurs. The melting endotherm for the pure foil is shifted to a higher temperature than the eutectic, and as a result, increased heating above the eutectic temperature is required to resolve the peak where the DSC trace returns to the baseline.

Similarly, the heating rate also affects the shape of the melting endotherm. Higher heating rates result in a broadening of the peak. The time required for dissolution and thermal lag in the measurement system combine to increase the temperature range over which the peak is plotted. The resulting superheat above the eutectic temperature that is required for the DSC trace to return to baseline is also increased with higher heating rates. To reduce broadening of the melting endotherm, the heating rate around the temperature of interest must be controlled.

Other factors that have been discussed include the contents of the reference crucible and the presence of a coating on the base metal. Including a mass of base metal in the reference crucible helps to keep the heat capacity of the sample and reference cells similar and remove the base metal effects from the DSC trace. The resulting DSC trace has less noise and lower hysteresis. The alumina coating is applied to the base metal in the solid/liquid diffusion couples. The coating is applied to all surfaces, except the faying surface, to prevent liquid from wetting the sides of the sample to maintain the assumption of a planar interface and keep liquid near the DSC measurement thermocouple.

7.1.2. Calculating Interface Kinetics

The progression of isothermal solidification was determined from the solid/liquid diffusion couple DSC results. The fraction of liquid remaining can be calculated by comparing the exothermic enthalpy measured during solidification to the known heat of formation for eutectic Ag-Cu. The effect of base metal in the solid/liquid diffusion couple is to act as a heat sink with a relatively large inertia. Some of the enthalpy released during solidification is conducted away from the interface into the base metal as a temperature gradient is established. In Ag-Cu solid/liquid diffusion couples, the enthalpy measurements were reduced by an average of 26%. The phenomena of base metal effects on DSC results has been simulated for emulsions [105,106], supporting the experimental observations. Although variation in the mass of base metal in the solid/liquid diffusion couple was not found to affect enthalpy measurements; the best results were achieved by comparing the melting endotherm with solidification exotherm for each diffusion couple. Rather than adjusting the exotherm values by some common factor, this method considers the thermal properties of each sample individually as they are constant during the experiment.

Plotting fraction of liquid remaining as a function of the square root of the isothermal hold time shows a linear relationship, as expected. However, the linear trend does not agree with phenomenological expectations that the fraction of liquid remaining at the initiation of the isothermal solidification stage should be unity (i.e. 100% liquid remaining at zero isothermal hold time). This deviation was observed in the results presented by Venkatraman et al. [77] in the literature but could not be explained. Two fundamental causes for this discrepancy have been observed and the mechanisms for propagation of this error in the DSC measurements

have been proposed. The underestimation by DSC measurement of the fraction of liquid remaining in solid/liquid diffusion couples can be attributed to baseline shift occurring upon initial melting of the interlayer; and exclusion of the primary component in the solidification exotherm.

7.1.3. Effect of Primary Solidification on the DSC Trace in Solid/Liquid Diffusion Couples

Upon cooling from the isothermal hold temperature, primary solidification has been shown to occur epitaxially at the solid/liquid interface [74,97]. The fraction of primary liquid solidification in the Ag-Cu solid/liquid diffusion couple DSC experiments could not be determined through metallographic techniques because a solid state precipitation reaction has obscured the underlying solidification microstructure. Primary solidification has a remarkable effect on the DSC trace, and is a significant contributor to the overall underestimation of the fraction of liquid remaining.

The solidification exotherm for a solid/liquid diffusion couple shows no indication of primary solidification. In a similar composition of liquid without base metal interaction, the DSC trace shows two exothermic peaks on the cooling segment. There is a characteristic eutectic exotherm, and an additional peak for the fraction of primary solidification. When interaction is enabled in a solid/liquid diffusion couple, only the characteristic eutectic peak is observed. Due to the epitaxial mechanism of primary solidification upon cooling, the enthalpy is not quantifiable using DSC.

DSC results show that the fraction of primary solidification increases with increasing isothermal hold temperature. The absence of the primary component of liquid solidifying athermally after the isothermal hold period decreases the measured enthalpy. The resulting calculated fraction of liquid remaining underestimates the actual residual. This effect is muted by the corollary for dissolution, which is not as easily quantified.

Dissolution of the base metal upon heating past the eutectic temperature is a continuous process and as a result, there is no clearly defined peak that can be quantified. Some dissolution may be included in the endothermic melting peak; in this sense, a fraction of base metal dissolution is also excluded from the enthalpy measurements.

In this study, the effect of primary solidification is to systematically underestimate the fraction of liquid remaining. For example, in the Ag-Cu binary case with an isothermal hold temperature of 800°C, the amount of liquid as measured on solidification is on average 9% lower than that for a given amount of liquid measured on melting. This is quantified by comparing adjacent melting endotherms and solidification exotherms when additional heating cycles are appended to the beginning or end of the temperature program.

7.1.4. Baseline Shift in DSC Trace on Initial Melting of the Interlayer

A baseline shift has been shown to occur across the melting endotherm of a solid/liquid diffusion couple DSC trace upon initial melting of the interlayer. This shift is only found to occur on the first heating cycle when additional thermal cycles are appended to the temperature program. The baseline shift experienced upon initial interlayer melting is greater than that expected for any reason found in the literature (i.e. variations in specific heat with phase change).

The baseline shift across the melting endotherm is attributed to the changing nature of the interface between the interlayer and the base metal. Before melting, the interface is mechanical; however, after melting the liquid wets the base metal resulting in a metallurgical interface with good thermal coupling. The improved thermal coupling results in a shift in the baseline as the contact resistance between the large thermal mass of base metal and the DSC measurement head decreases. Any baseline shift observed on subsequent cycles can be attributed to change of specific heat with change of phase.

Baseline shift has been shown to overestimate the melting enthalpy on the first cycle. Comparison of melting endotherms of adjacent heating cycles for Ag-Cu diffusion couples gives an initial melting enthalpy that is on average 24% higher than an endotherm where no baseline shift occurs. The increase in the melting enthalpy measurement due to baseline shift has the effect of decreasing the calculated fraction of liquid remaining, underestimating the actual value.

7.1.5. Correcting the Measured Interface Kinetics

A methodology for quantifying the effects of baseline shift and primary solidification by use of a modified temperature program has been developed which enables correction of the original interface kinetics. When the interface kinetics measured using DSC are corrected, the results agree well with intuitively expected results, the fraction of liquid remaining at the start of the isothermal hold period is near unity. The fraction of liquid remaining decreases linearly with the square root of the isothermal hold time.

The time required for completion of isothermal solidification for a solid/liquid diffusion couple can be found when no liquid remains. The slope of the linear relationship is related to the process kinetics of isothermal solidification by the initial width of the liquid phase. An interface rate constant can be found from the experimental results, which is an indication of the solid/liquid interface velocity. When the DSC results are corrected, the process kinetics can be compared to predictions of analytical and numerical models.

The modified temperature program enables analysis of the isothermal solidification kinetics through two additional methods. The fraction of liquid remaining can be determined by comparing similar types of peaks, before and after isothermal solidification. By comparing

similar peaks, the effects of baseline shift and primary solidification are effectively removed from the analysis. Process kinetics, whether measured from a basic temperature program or through a modified temperature program using similar peaks, agree well with each other.

7.2. Isothermal Solidification Kinetics in the Binary Ag-Cu System

7.2.1. Experimentally Measured Process Kinetics

The interface rate constant for the Ag-Cu binary system with pure Ag base metal was found to be -0.126 μm/√s using the experimental DSC approach with an isothermal hold temperature of 800°C. Increasing the isothermal hold temperature has been shown to increase the interface rate constant. The ability to quantify isothermal solidification kinetics using the DSC method is limited by the formation of eutectic. In the Ag-Cu system, if the isothermal hold temperature was increased to 920°C, there was no measurable eutectic formed upon cooling. All of the liquid solidifies to the primary phase and there is no solidification exotherm to measure and compare. If the initial interlayer composition is greater than the solubility limit and shows some eutectic melting, the apparent fraction of liquid remaining will be zero for all times.

TLP full samples were examined to confirm the results of the solid/liquid diffusion couples (i.e. TLP half samples). The results show that the value for the interface rate constant determined experimentally using DSC is accurate for the process kinetics of TLP bonding; however, finding an interface rate constant from the TLP full samples is difficult. Measurement of the irregular eutectic width using metallographic techniques is prone to significant measurement error. Compared to experimental results in the literature for Ag-Cu at 820°C found using metallographic techniques [39], the interface kinetics determined using DSC are much slower. The DSC method for quantifying interface kinetics has been shown to give an accurate measure of the solid/liquid interface velocity.

7.2.2. Analytical Modeling of Isothermal Solidification Kinetics in Binary Alloy Systems

Three analytical models for isothermal solidification in TLP bonding have been applied to the experimental Ag-Cu system. The difference between the models is the treatment of the solid/liquid interface: stationary, moving, or attached to a shifting frame of reference. The results have been compared to experimental interface kinetics. Selection of an appropriate solute diffusivity has been shown to have a profound impact on the accuracy of the predictions.

In this study, an assumption of a stationary solid/liquid interface has been shown to underestimate the interface velocity. The assumption of a stationary interface with a shifting

frame of reference has been shown to overestimate the interface velocity. The best agreement with experimental results was found with the assumption of a moving interface. The predicted interface kinetics could be matched exactly with the measured results; however, it must also be noted that an exact prediction can be obtained with any of the simulations if a specific diffusivity is selected. When realistic values for solute diffusion are selected, the moving interface solution gives the best results.

Analytical solutions are appropriate for simulating isothermal solidification kinetics so long as the effects of grain boundary diffusion can be neglected, or can be included in an effective diffusivity. The simulation results agree very well with measured results if a diffusivity of $D = 7.0 \times 10^{-10}$ cm^2/s is used (at 800°C), thus, a constant chemical diffusion coefficient is suitable. Measured solute profiles in the base metal agree well with model output.

Several reports have claimed that simple analytical solutions do not accurately predict the process kinetics of isothermal solidification; however, in many cases the discrepancy is due to either experimental error, or inaccurate thermodynamic data. The results of this study have shown that DSC is capable of accurately quantifying interface kinetics in a solid/liquid diffusion couple, and that when compared to predictions of analytical solutions, the accurate experimental results compare well.

7.3. Isothermal Solidification Kinetics in the Ternary Ag-Au-Cu System

7.3.1. Experimentally Measured Process Kinetics

The DSC method for quantifying solid/liquid interface kinetics during isothermal solidification has been applied to ternary alloy solid/liquid diffusion couples. Eutectic Ag-Au-Cu foil interlayers were coupled with pure Ag base metal to study the effects of an additional solute on interface motion. As in the binary case, experimental artefacts including baseline shift and primary solidification contribute to a systematic underestimation of the fraction of liquid remaining. A modified temperature program has been employed to quantify and correct these effects.

The corrected results, as well as those obtained using similar peaks, show a fraction of liquid remaining that decreases linearly with the square root of time. This infers that a single interface rate constant can be applied to the results over the entire duration of isothermal solidification. The measured interface kinetics are independent of the measurement method, whether it is a corrected ratio of exotherm to endotherm, or a ratio of similar peaks. The interface kinetics are also independent of the initial interlayer thickness as normalized results show a similar interface rate constant.

The application of a constant correction factor to the DSC results is made under the assumption that the experimental artefact of primary solidification is not changing as isothermal solidification progresses. Isothermal solidification when more than one solute is present occurs via shifting tie line compositions at the solid/liquid interface. The DSC results show that the fraction of liquid solidifying in the primary phase changes with isothermal hold time. As isothermal solidification progresses, the effect of primary solidification on the DSC results increases. Application of a correction factor that changes according to the effect of primary solidification may be appropriate; however, in the Ag-Au-Cu results, the difference in interface kinetics with a static correction factor is minimal. By comparing similar peaks, the experimental artefacts can be removed from the measurement. The results show no difference between the measurement methods. Thus, in this case, all methods are suitable.

7.3.2. Modeling Isothermal Solidification in the Ternary Ag-Au-Cu System

Using analytical methods, it has been shown that no solution for isothermal solidification exists at a single tie line composition. Thus, isothermal solidification proceeds by a shifting tie line and numerical methods must be employed. A finite difference approach has been taken to model the process. Some thermodynamic data for the Ag-Au-Cu system is available, including a Gibbs' isotherm at the isothermal hold temperature showing the phase boundaries. The phase boundaries were linearized and the tie lines were defined. Diffusivity data is available, however, the data is not valid for the temperature of interest.

Given the lack of accurate thermodynamic data, accurate predictions of the process kinetics are difficult. The finite difference model can be used to better understand the fundamental theoretical mechanism of isothermal solidification.

Inspection of the phase boundaries on the Gibbs' isotherm for Ag-Au-Cu at 800°C shows that the liquidus line runs nearly parallel to Cu isopleths. Thus, there is little freedom in the liquid Cu composition and as a result, the interface velocity is mostly driven by the diffusion of Cu into the base metal.

On the other hand, there is greater freedom in the liquid concentration of Au. A decrease in Cu corresponds with a relatively large decrease in Au, and vice-versa. By nature of the greater freedom in the Au composition, the shifting tie line is driven by diffusion of Au into the base metal. Modeling results show that the direction of tie line shift depends on the diffusivity of Au, if the diffusivity is high the tie line shifts in a direction of decreasing Au.

The modeling results support the experimental observations. Though accurate predictions of interface kinetics cannot be found given the published diffusivities, the direction of compositional change at the solid/liquid interface is correctly predicted over the range of realistic diffusivity values.

Theory of isothermal solidification developed in this study agrees with the current state of research. However, the Ag-Au-Cu ternary system does not fit into the paradigm for phase boundaries that have been considered thus far. When the concentration of one solute decreases at the expense of the other, the second solute will accumulate in the liquid such that it can limit interface velocity and result in a second kinetic regime. The results of this study have developed the fundamental theoretical understanding of isothermal solidification in ternary systems, and confirmed that the finite difference approach can be used to simulate interface motion. It is suggested that simulation accuracy could be improved with the availability of accurate thermodynamic data. It is recognized that very often this data is unavailable for complicated ternary or higher order systems. Accurate experimental methods, such as that using DSC, are valuable in the development of parameters for processes employing isothermal solidification, such as TLP bonding.

7.4. Recommendations for Further Research

Opportunities for additional work exist in developing a comprehensive understanding of the baseline shift observed during initial interlayer melting. Modeling the thermodynamics of interface development and heat flow within the sample cell could provide insight into the mechanism of baseline shift across the melting endotherm. If the nature of enthalpy change and characteristics of heat flow within the cell are better understood, it may be possible to quantify the enthalpy accurately, without empirically derived corrections or additional thermal cycles appended to the temperature program.

It is recommended that the DSC method for measuring the kinetics of isothermal solidification is extended to more complicated systems. For example, preliminary tests have been conducted in the Ag-Cu-P system, which has industrial applications, especially for joining Cu-alloys since this interlayer exhibits self-cleaning properties. The interlayer composition was near eutectic, Ag - 18 wt.% Cu - 7.5 wt.% P and the isothermal hold temperature was 665°C.

The preliminary results shown in Figure 7-1 are for pure Ag base metal. There is a clear shift in the interface kinetics after approximately 9 hours of isothermal hold time. It is unclear if the change in kinetics is due to interfacial phenomena, or if interface motion is arrested due to saturation of the base metal (P has low solubility in Ag). On the other hand, if the intermetallic Cu_3P is formed, diffusion of P into the base metal will continue; however, the situation is more complicated. When Cu is used for the base metal the alumina stop-off is insufficient to prevent liquid from spreading away from the faying surface. P is a deoxidizer for Cu and as a result the liquid aggressively wets the Cu base metal and infiltrates the coating causing erroneous enthalpy measurements. It is recommended that another coating material, such as Cr, is used to prevent spreading away from the joint.

Accurate phase boundary and diffusion data for the Ag-Cu-P ternary system is not available in the literature. Using pseudo-binary phase diagrams, a composite Gibbs' isotherm at 665°C is approximated in Figure 7-2. From the complexity of the isotherm it is clear that the tie line cannot be easily approximated. Additional thermodynamic data would be required to successfully simulate isothermal solidification using the finite difference method.

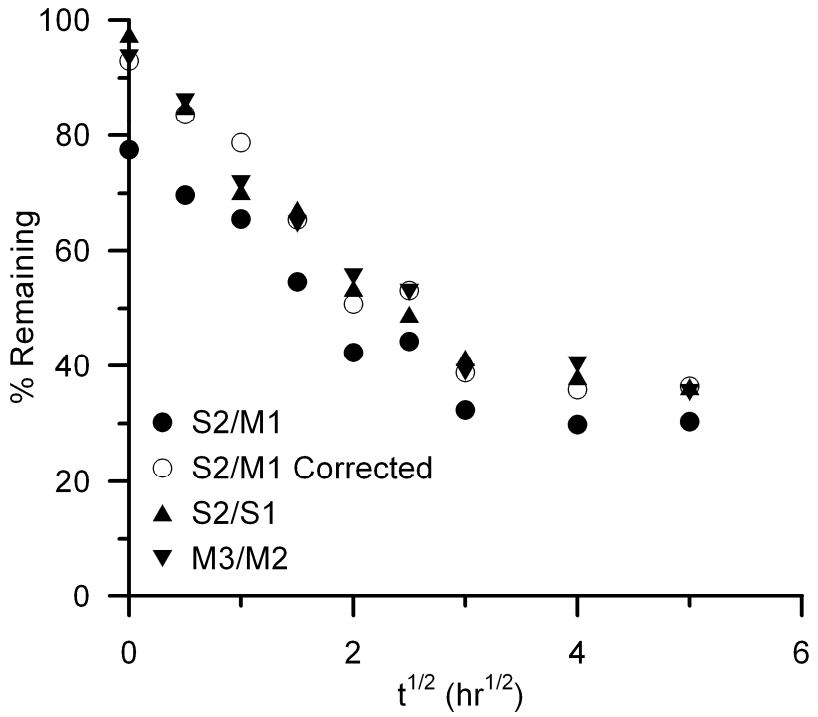

Figure 7-1: Ag-Cu-P with Ag-base metal DSC results.

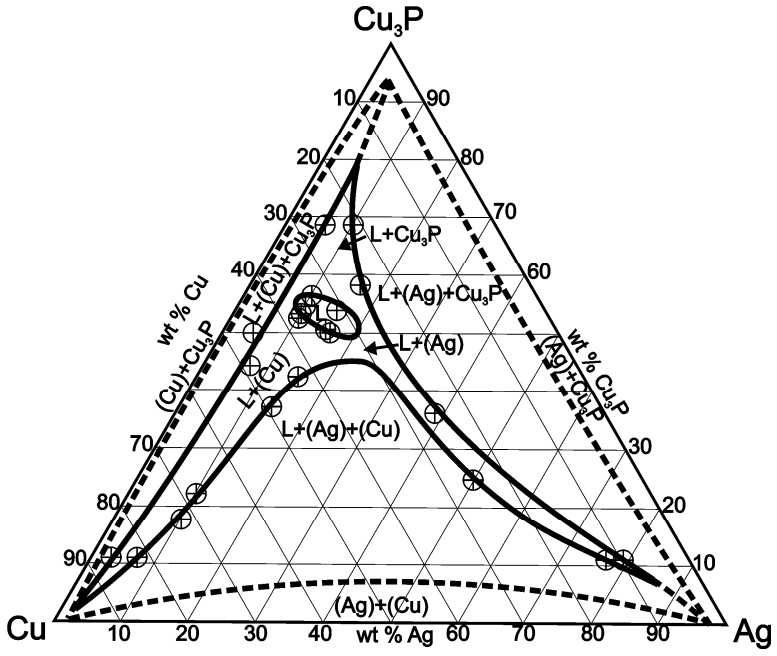

Figure 7-2: Composite Ag-Cu-P ternary isotherm at 665°C.

8. References

1. D.S. Duvall, W.A. Owczarski, and D.F. Paulonis, *Welding Journal*, 53, 203-214 (1974).
2. Y. Zhou, W.F. Gale, and T.H. North, *Int. mater. rev.*, 40, 5, 181-196 (1995).
3. L.P. Connor (Ed.) *Welding Handbook*, Eighth edition, Volume 1, American Welding Society, Miami FL (1989).
4. K. Nishimoto, K. Saida, D. Kim, Y. Nakao, *ISIJ Int.*, 35, 10, 1298-1306 (1995).
5. M.S. Yeh, and T.H. Chuang, *Welding Journal*, 76, 12, 517s-521s (1997).
6. J.P. Jung, C.S. Kang, *Mater. Trans., JIM.*, 37, 5, 1008-1013 (1996).
7. W.D. MacDonald, and T.W. Eagar, *The Metal Science of Joining (Ed M.J. Cieslak, J.H. Perepezko, S. Kang, and M.E. Glicksman),* p. 93-100, The Minerals, Metals & Materials Society (1992).
8. J.E. Ramirez and S. Liu, *Welding Journal,* 365s-375s (1992).
9. W.M. Miglietti and R.C. Pennefather, *Proceedings from Materials Solutions '97 on Joining and Repair of Gas Turbine Components,* 15-18 September 1997, Indianapolis, Indiana, 61-77 (1997).
10. L. Bernstein and H. Bartholomew, *Trans. AIME,* 236, 405-412 (1966).
11. J.T. Niemann, and R.A. Garrett, *Welding Journal*, 53, 4, 175s-184s (1974).
12. Z. Li, Y. Zhou, and T.H. North, *Canadian Association for Composite Structures and Materials,* Proceedings of Cancom 93, Second Canadian International Composites Conference and Exposition, Ottawa, Canada, 1017-1027 (1993).
13. J.M. Gomez de Salazar, F.J. Mendez, A. Urena, J.M. Guilemany, and B.G. Mellor, *Scripta Mater.*, 37, 6, 861-867 (1997).
14. W.F. Gale and Y. Guan, *Journal of Materials Science,* 32, 357-364 (1997).
15. S.F. Corbin and P. Lucier, *Metall. mater. trans. A,* 32A, 971-978 (2001).
16. W.D. MacDonald, and T.W. Eagar, *Annu. rev. mater. sci.*, 22, 23-46 (1992).
17. C.S. Smith, *A Search for Structure,* Cambridge, Mass.; MIT Press, pp. 92-94.
18. J.G. Hawthorne, C.S. Smith, *Mappae Clavicula. Trans. Am. Philos. Soc.*, 64, 3-128 (1974).
19. J.G. Hawthorne, C.S. Smith, *On Divers Arts, The Treatise of Theophilus,* University of Chicago Press, Chicago (1963).
20. B. Cellini, *Due Trattati, uno intorno alle otto principali arti del l'oreficiera. L'altro in material dell'arte della scultura*, Florence (1568).
21. H.A.P. Littledale, *Brit. Patent no. 415,181,* 1933.
22. E. Misiorowski, *Granulation, reviving an ancient technique* in *Heritage*, May 1995.
23. W.F. Gale and D.A. Butts, *Sci. Technol. Weld. Joi.,* 9, 4, 283-300 (2004).
24. J.F. Lynch, L. Feinstein and R.A. Huggins, *Welding Journal,* 38, 2, 85s-89s (1959).
25. W.A. Owczarski, *Welding Journal*, 42, 2, 78s-83s (1962).
26. L. Bernstein, *Journal of the Electrochemical Soc.,* 113, 12, 1282-1288 (1966).
27. G.S. Hoppin III and T.F. Berry, *Welding Journal,* 49, 1, 505s-509s (1970).

28. K.C. Wu, *Welding Journal*, 50, 9, 386s-393s (1971).
29. R.R. Wells and E.B. Mikus, *US patent no. 3,417,461*, (1968).
30. J.T. Niemann and R.A. Garrett, *Welding Journal,* 53, 8, 351s-360s (1974).
31. W.A. Owczarski, W.H. King, and D.F. Paulonis, *US patent no. 3,530,568*, (1970).
32. D.S. Duvall, W.A. Owczarski, D.F. Paulonis, and W.H. King, *Welding Journal*, 51, 2, 41s-49s (1972).
33. B. Norris, *Designing with Titanium, Proceedings of the Institute of Metals Conference*, Bristol 83-86 (1986).
34. Y. Nakao, K Nishimoto, K. Shinozaki, and C. Kang, *Trans. Japan Welding Soc.*, 20, 1, 60-65 (1989).
35. Y. Nakao, K. Nishimoto, K. Shinozaki, and C. Kang, in "*Superalloys 1988,"* Metallurgical Society of AIME, Warrendale PA (1989).
36. Y. Nakao et al., *The 5th International Symposium of the Japan Welding Soc.,* 139-144 (1990).
37. A.A. Shirzadi and E.R. Wallach, *Science and Technology of Welding and Joining*, 2, 3, 89-94 (1997).
38. A.A. Shirzadi, *Welding in the World*, 41, 435-442 (1998).
39. I. Tuah-Poku, M. Dollar, and T.B. Massalski, *Metall. trans., A., Phys. metal. mater. sci.*, 19A, 3, 675-686 (1988).
40. W.D. Zhuang and T.W. Eagar, *Welding Journal*, April 1997, 157s-162s (1997).
41. E. Lugscheider, Th. Schittny and E. Halmoy, *Welding Journal*, 68, 1, 9s-13s (1989).
42. T.I. Khan and E.R. Wallach, *Materials Science and Technology,* 12, 603-607 (1996).
43. Z. Li, W. Fearis, and T.H. North, *Mater. Sci. Technol.*, 11, 4, 363-369 (1995).
44. H. Nakagawa, C.H. Lee and T.H. North, *Metall. Trans. A.*, 22A, 543-555 (1991).
45. T.H. North, K. Ikeuchi, Y.Zhou, and H. Kokawa, *The Metal Science of Joining (Ed M.J. Cieslak, J.H. Perepezko, S. Kang, and M.E. Glicksman),* p. 83-91, The Minerals, Metals & Materials Society (1992).
46. A.A. Shirzadi and E.R. Wallach, *US Patent No. 6,257,481*.
47. H. Assadi, A.A. Shirzadi, and E.R. Wallach, *Acta mater.*, 49, 31-39 (2001).
48. A.A. Shirzadi and E.R. Wallach, *Acta mater.,* 47, 13, 3551-3560 (1999).
49. J. Crank, *The Mathematics of Diffusion*, Oxford University Press, Oxford (1975).
50. L.S. Darken and R.W. Gurry, *Physical Chemistry of Metals*, pp. 445-57, McGraw-Hill, New York (1953).
51. P. Shewmon, *Diffusion in Solids, 2nd ed.*, pp. 37-39. Metall. Soc., Warrendale, Penn (1989).
52. W.D. MacDonald and T.W. Eagar, *Proc. TMS Symp. Mater. Sci. Joining,* (1992).
53. G. Lesoult, *Center for Joining of Materials Report*, Carnegie Mellon University, Pittsburgh, PA, Sept. 1976.
54. E.A. Moelwyn-Hughes, *Kinetics of Reaction in Solution*, pp. 374-77, Oxford, Clarendon (1947)
55. S. Liu, D.L. Olsen, G.P. Martin, and G.R. Edwards, *Weld. J.*, 70, 8, 207s-15s (1991).
56. Y. Zhou and T.H. North, *Z. Metallkd.,* 85, 775-780 (1994).
57. M.L. Kuntz, S.F. Corbin, Y. Zhou, *Acta Mater.,* 53, 3071-3082 (2005).
58. M.R. Spiegel, *Applied Differential Equations*, 3rd edition, p. 260, Prentice Hall (1958).
59. Y. Zhou, *J. Mater. Sci. Lett.*, 20, p. 841-844 (2001).

60. H. Ikawa, Y. Nakao, T. Isai, *Trans. Jpn. Weld. Soc.,* 10, 1, 25-29 (1979).

61. Y. Nakao, K. Nishimoto, K. Shinozaki, C.Y. Kang, *Joining of Advanced Materials (Ed T.H. North),* p. 129-144, Chapman and Hall (1990).

62. S. R. Cain, J.R. Wilcox, and R. Venkatraman, *Acta mater.,* 45, 2, 701-707 (1997).

63. P.V. Dankwerts, *Trans. Faraday Soc.,* 46, 701-712 (1950).

64. A. Sakamoto, C. Fujiwara, T. Hattori, and S. Sakai, *Weld. J.,* 68, 63-71 (1989)

65. A. LeBlanc and P. Mevrel: *in Proc. Conf. "High temperature materials for power engineering", Ed. E. Bachelet et al.*, 1451-1460, Dordrecht, The Netherlands (1990).

66. R.F. Sekerka, *'Physical Metallurgy of Metal Joining' Ed. R. Kossowsky and M.E. Glicksman,* Met-Soc AIME, Warrendale, PA. 1-3 (1980).

67. J.P. Jung and C.S. Kang, *Mater. Trans., JIM,* 38, 10, 886-891 (1997).

68. W.D. MacDonald, and T.W. Eagar, *Metall. mater. trans., A Phys. metall. mater. sci.*, 29A, 1, 315-325 (1998).

69. P. Maugis, W.D. Hopfe, J.E. Morral and J.S. Kirkaldy, *Acta Mater.,* 45, 5, 1941-1954 (1997).

70. C.W. Sinclair, *J. Phase Equilibria*, 20, 4, 361-369 (1999).

71. C.W. Sinclair, G.R. Purdy, and J.E. Morral, *Metall. Trans. A.*, 31A, 1187-1192 (2001).

72. J.S. Langer and R.F. Sekerka, *Acta Metall.*, 23, 1225-1237 (1975).

73. T. Shinmura, K. Ohsasa, and T. Narita, *Mater. Trans.,* 42, 2, 292-297 (2001).

74. K. Saida, Y. Zhou, and T.H. North, *J. Japan Inst. Metals,* 58, 7, 810-818 (1994).

75. K. Saida, Y. Zhou and T.H. North, *Journal of Materials Science*, 28, 6427-6432 (1993).

76. Y. Zhou, and T.H. North, *Acta. Metall. Mater.*, 42, 3, p. 1025-1029 (1994).

77. R. Venkatraman, J.R. Wilcox, and S.R. Cain, *Metall. mater. trans., A Phys. metall. mater. sci.*, 28A, 699-706 (1997).

78. H. Kokawa, C.H. Lee, and T.H. North, *Metall. Trans. A*, 22A, 1627-1631 (1991).

79. D-U. Kim, C-Y. Kang, and W-J. Lee, *Metals and Materials*, 5, 5, 477-484 (1999).

80. E.W. Hart, *Acta Metall.*, 5, 597 (1957).

81. K. Ikeuchi, Y. Zhou, H. Kokawa, and T.H. North, *Metall. Trans. A,* 23A, 2905-2915 (1992).

82. Y. Takahashi, K. Morimoto, and K. Inoue, *Trans. JWRI*, 30, 535-541 (2001).

83. R.A. Tanzilli and R.W. Heckel, *Trans. AIME,* 242, 2313-21 (1968).

84. R.W. Heckel, A.J. Hickl, R.J. Zaehring, and R.A. Tanzilli, *Metall. Trans.,* 3, 2565-9 (1972).

85. S.K. Pabi, *Phys. Status Solidi,* 51, 281-9 (1979).

86. R.D. Lanam, and R.W. Heckel, *Metall. Trans.,* 2, 2255-66 (1971).

87. B. Karlsson and L.E. Larsson, *Mater. Sci. Eng.,* 20, 161-70 (1975).

88. Y. Zhou, and T.H. North, *Model. Simul. Mater. Sci. Eng.,* 1, 505-516 (1993).

89. T-C Jen and Y. Jiao, *Numerical Heat Transfer, Part A,* 39, 123-138 (2001).

90. J.S. Kirkaldy and D.J. Young, *Diffusion in the Condensed State*, The Institute of Metals, (1987).

91. J.S. Kirkaldy, J.E. Lane, and G.R. Mason, *Can. J. Phys.,* 41, 2174 (1963).

92. T.O. Ziebold and R.E. Ogilvie, *Trans. AIME,* 239, 942 (1967).

93. H. Fujita, and L.J. Gosting, *J. Am. Chem. Soc.,* 78, 1099 (1956).

94. C. Zener, *J. Appl. Phys.*, 20, 950-953 (1949).

95. G.R. Purdy, D.V. Malakhov, and A. Guha, *J. Phase Equilibria,* 22, 4, 439-450 (2001).

96. K. Ohsasa, T. Shinmura, T. Narita, *J. Phase Equilibria,* 20/3, 199-206 (1999).

97. C.E. Campbell, W.J. Boettinger, *Metall. Trans. A*, 31A, 2835-2847 (2000).

98. K. Nishimoto and K. Saida, *IBSC 2000: International Brazing & Soldering Conference*, Albuquerque NM, 2-5 Apr. 2000, 398-405 (2000).

99. M.E. Brown, *Introduction to Thermal Analysis,* Chapman and Hall, New York (1988).

100. Y. Zhou, M.L. Kuntz, S.F. Corbin, In: *Joining of Advanced and Specialty Materials V*, Materials Solutions '02. Materials Park (OH): ASM International, 2003. p.75.

101. K. Easterling, *Introduction to the Physical Metallurgy of Welding,* Butterworths & Co., London (1983).

102. D.A. Porter, and K.E. Easterling, *Phase Transformations in Metals and Alloys,* 2nd Edition, Chapman and Hall.

103. P.R. Subramanian and J.H. Perepezko. *Ag–Cu binary alloy phase diagram. In: Baker H, editor. ASM handbook. Alloy phase diagrams, vol. 3.*, Materials Park (OH): ASM International; p. 228.(1992).

104. A. Prince, *Int. Mater. Rev.,* 33, 6, 314-338 (1988).

105. J.-P. Dumas, Y. Zeraouli, and M. Strub, *Thermochimica Acta,* 236, 227-237 (1994).

106. J.-P. Dumas, Y. Zeraouli, and M. Strub, *Thermochimica Acta,* 236, 239-248 (1994).

107. Y. Zeraouli, A.J. Ehmimed, and J.-P. Dumas, *Int. J. Therm. Sci.,* 39, 780-796 (2000).

108. A.J. Ehmimed, Y. Zeraouli, J.-P. Dumas, and A. Mimet, *Int. J. Therm. Sci.,* 42, 33-46 (2003).

109. A. Jamil, T. Kousksou, Y. Zeraouli, and J.-P. Dumas, *Thermochimica Acta,* In print.

110. D. Hamana, and Z. Boumerzoug, *Materials Science Forum*, 294-296, p. 593-596 (1999).

111. J.R. Cahoon and W.V. Youdelis, *AIME Met. Soc. Trans.,* 239, 1, 127-129 (1967).

112. E. A. Brandes, *Smithells Metals Reference Book, 6th Ed.,* Butterworths, London (1983).

113. H. Okamoto, D.J. Chakrabarti, D.E. Laughlin, and T.B. Massalski *Au–Cu binary alloy phase diagram. In: Okamoto, H. and Massalski, T.B., editors. Phase Diagrams of Binary Gold Alloys*, Materials Park (OH): ASM International; (1987).

114. H. Okamoto, and T.B. Massalski *Ag–Au binary alloy phase diagram. In: Okamoto, H. and Massalski, T.B., editors. Phase Diagrams of Binary Gold Alloys*, Materials Park (OH): ASM International; (1987).

115. D.E. Coates and J.S. Kirkaldy, *Metall. Trans.* 2, 3467 (1971).

116. P. Maugis, W.D. Hopfe, J.E. Morral, and J.S. Kirkaldy, *Acta Mater.* 45, 5, 1941-1945 (1997).

117. T.O. Ziebold, and R.E. Ogilvie, *Trans. Met. Soc. AIME*, 239, 942-953 (1967).